STUDIES ON PHOTOVOLTAIC DEVICES DEVELOPED BY ORGANIC DYES AND IODINE BASED PEROVSKITE

By

POOJA AGARWALA

UNIVERSITY OF PETROLEUM AND ENERGY STUDIES

Under the Guidance of

DR. RAJNISH GARG, PROFESSOR
CENTRE FOR NANOTECHNOLOGY AND DEPT. OF MECHANICAL ENGINEERING
UPES, DEHRADUN, INDIA

And

DR. K. R. JUSTIN THOMAS, ASSOCIATE PROFESSOR
CENTRE FOR NANOTECHNOLOGY AND DEPT. OF CHEMISTRY
IIT, ROORKEE, INDIA

Submitted

IN PARTIAL FULFILLMENT OF THE REQUIREMENT OF THE DEGREE OF DOCTOR OF PHILOSOPHY

TO

UNIVERSITY OF PETROLEUM AND ENERGY STUDIES
DEHRADUN
February, 2015

UNIVERSITY OF PETROLEUM AND ENERGY STUDIES DEHRADUN
INDIAN INSTITUTE OF TECHNOLOGY ROORKEE

ACKNOWLEDGMENT

I would like to convey my deepest gratitude to my supervisor Dr. Rajnish Garg, Professor, Department of Mechanical Engineering,, UPES, Dehradun, India, for his constant support, the trust he kept in my abilities, encouragement and judicious interventions made this thesis to come into picture. It gives me great pleasure to express my profound regards and sincere gratitude to Dr. K. R. Justin Thomas, Associate Professor, Centre for Nanotechnology and Dept. of Chemistry, IIT, Roorkee, India, for his guidance and encouragement during the synthesis of organic sensitizers. I am thankful for his time, attempt, constant support and faith in me during period of my research work.

I am grateful to Prof. Subodh G. Mhaisalkar, Director, at Energy Research Institute at Nanyang Technological University (ERI@N), Singapore, for providing me an excellent opportunity to explore the world of energy. His valuable supervision, support and motivation throughout the project has been of utmost substance during the solar device fabrication. I express my deep regards to him for providing me with a prospect of using the device fabrication and characterization facilities at ERI@N. I extend my thanks to the whole Perovskite group at ERI@N for their support in some way or other and for keeping a healthy working environment.

I voice my gratefulness to Dr. Sanket Goel, VP (R&D) and Associate Professor at University of Petroleum and Energy Studies, Dehradun, India, for his constant moral support and guidance during my research course work.

I want to express my gratitude to Dr. Ritu Barthwal, Professor, Department of Biosciences and Biotechnology, IIT Roorkee for providing me NMR facility as the essential characterization unit for my compounds.

My sincere feelings to respectable Head of Department, Department of Chemistry, IIT, Roorkee, for providing the necessary environment and facilities of research in the department and lab.

I am thankful to central characterization facility at IIT, Roorkee for providing me XRD, FESEM, AFM units as essential characterization of my solar cell device films.

Thank goes to all members of our research group for their help and providing fruitful environment in the lab during my PhD tenure.

Last but not the least I wish to avail this opportunity to express my sense of gratitude and love to my mother, my parent-in-laws and my husband for keeping a faith in me and for their never ending encouragement and to all my family members and friends for their affection and support in all respect.

I dedicate this thesis to both my daughters, Shivalika and Vedika, who believed in me and stood by me with their unconditional love and support. They have been the pillars of strength throughout my PhD work and made it possible.

Pooja Agarwala

CERTIFICATE

This is to certify that the thesis entitled **"Studies on Photovoltaic Devices Developed by Organic Dyes and Iodine Based Perovskite"** submitted by Pooja Agarwala to University of Petroleum and Energy Studies, for the award of the degree of Doctor of Philosophy is a bonafide record of the research work carried out by her under our joint supervision and guidance. The content of the thesis, in full or parts have not been submitted to any other institute or university for the award of any other degree or diploma.

Internal Guide : **Dr.Rajnish Garg**
Professor,
Department of Mechanical Engineering,
University of Petroleum and Energy Studies,Dehradun
Uttarakhand, India.

External Guide : **Dr.K.R. Justin Thomas**
Associate Professor,
Centre for Nanotechnology and Dept. of Chemistry,
Indian Institute of Technology, Roorkee
Uttarakhand, India.

Place:

Date:

SUMMERY

Traditionally silicon solar cells have been in wide use as a device to convert the solar energy directly to electrical energy. For past two decades researchers had been exploring more efficient and economically sound way to harvest solar energy. The replacement of silicon with metallic and non metallic conjugated polymers has attracted the researchers owing to their synthetic and structural flexibility. Due to their vast applicability in photovoltaic devices, conjugated organic materials have been attracting wide interest among academicians and industrialists. Fluorine, tri phenyl amine, phenothiazine, anthracene, thiophene and carbazole-based conjugated compounds have been increasingly explored in this field. Synthesis and characterization of carbazole based functional materials has been undertaken in this study. Although carbazole in a weak donor in comparison with some of the most used donor moieties, its merit of easy functionalization at multiple nucleus positions (C1, C2, C3, C6, C7 and N9) make it easy to tune its photophysical and electrochemical properties. Suitable substitution via thiophene and bithiophene linkage changes the conformation of the molecule which in turn affects the charge transfer characteristics of the material.

Substitution of silicon with conjugated polymers has enforced the use of a charge transporter in the device which would be a semiconductor. In this study TiO_2 nanoparticles are used as semiconductor which is made by sol-gel method. Different particle size gives different film morphology which affects the charge transportation in the device interphase.

Recently, perovskite based solar cells have shown the highest efficiency with the advantage of even much cheaper ensemble as in comparison with conjugated polymer based

dye sensitized solar cells. Due to its enticing characteristic of being an ambipolar material and being able to generate as well as transfer the electrons of its own, perovskite material has also been explored in this work.

The thesis is divided into seven chapters. First chapter presents the background of photovolaics, aim and scope of the work undertaken. Chapter 2 reviews the literature available on the synthesis and application of conjugated polymers i.e., sensitizers and hole transporting materials. It discusses the working principle of DSSCs based on liquid as well as solid electrolyte. Recent progress in the DSSCs and introduction of perovskite material as sensitizers is also been discussed. The synthetic methods of TiO_2 nanoparticles and their structural merits are discussed in detail. Based on this chapter, the research gap has been identified and defined in chapter 3. Chapter 4 describes the general procedures involved in synthesis of organic dyes and TiO_2 nanoparticles. Steps involved in fabrication of DSSCs based on organic dyes in conjunction with liquid electrolyte and perovskite based ssDSSCs are described. This chapter also elaborates the characterization techniques used in the whole research work for material and device characterizations.

Results and discussions are explained in Chapter 5 and chapter 6. Since dye molecules and semiconductor, both the elements contribute majorly to the performance of DSSCs, a detailed discussion is conceived in these chapters focusing on both the materials. In chapter 5 the synthesis and application of a series of carbazole based tetra-anchoring cruciform organic dyes (P1-P5) is discussed (chart-1). Elongation of π-bridge has a significant influence on optical and photovoltaic properties of these materials. HOMO and LUMO levels of the all synthesized dyes (P1, P2, P3, P4 and P5) are observed well aligned for efficient electron injection and charge transportation in DSSCs. The effect of some of the

aspects of device engineering such as, photoanode thickness, dye loading time and additives, are also explored. This chapter evidently reveals that the excessive thickness of the TiO_2 film is unfavorable for the DSSC performance owing of the electron recombination. Longer dye loading time can cause the formation of over layer of dye molecules which hinders the proper electron generation. Charge recombination and aggregation of dye on TiO_2 film are found to be restrained in the presence of binary additive and enhanced efficiency is achieved. Therefore, optimizing the cell efficiency requires optimization of every component within the DSSC system.

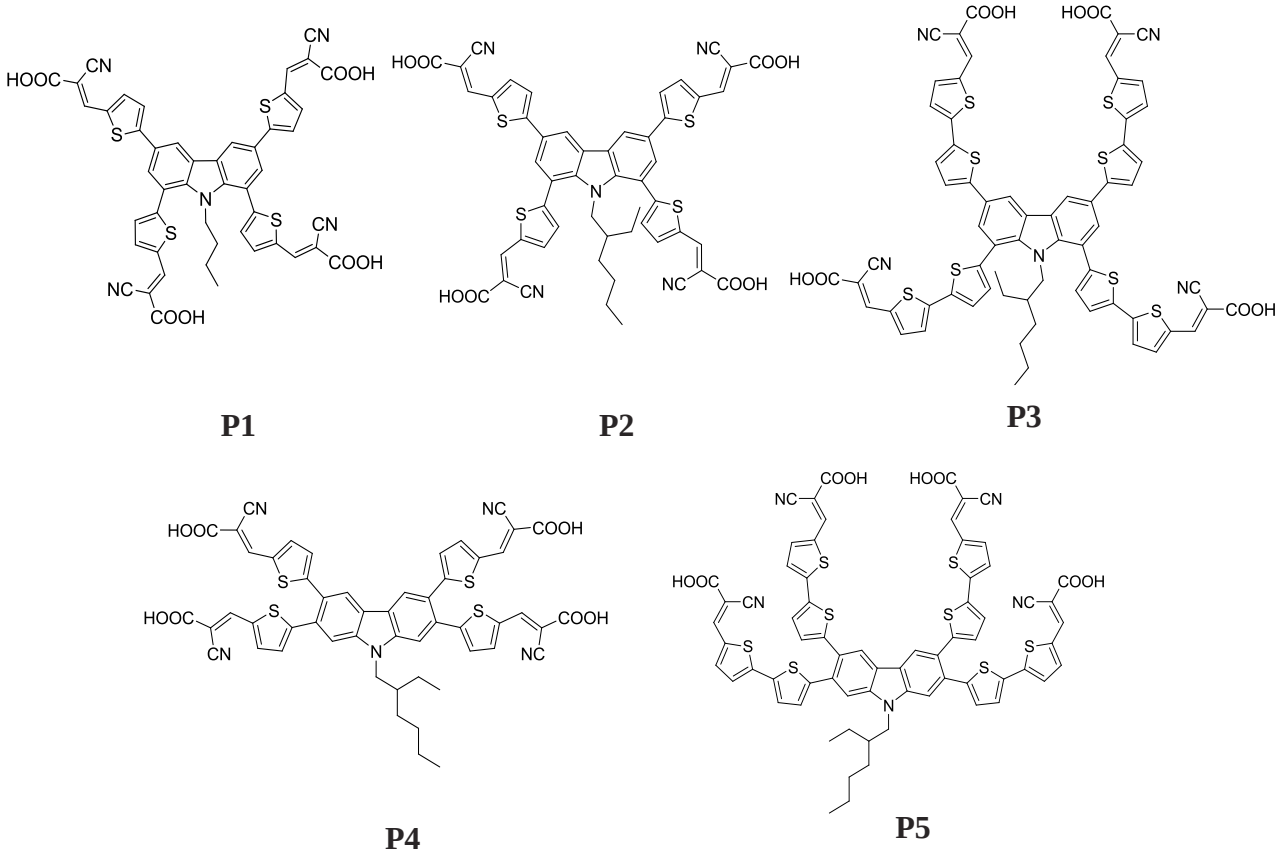

Chart-1: Structures of a series of novel D-(π-A)$_4$ carbazole based conjugated organic polymers.

This chapter also includes the effect of cosensitization on optical properties and photovoltaic performance of the DSSCs. In this study five of the tetraanchoring organic dyes are used as principal dyes in conjunction with indoline dye D-205. It is observed that cosensitization caused reduction of aggregates in all the films is the major influential factor for higher packing density of the dyes on the film surface which is responsible for the enhanced efficiencies of DSSCs. Later part of the chapter focuses on the photovoltaic properties of low band gap TiO_2 nano-composites consisting of different proportions of anatase and rutile phases. This chapter also reveals the significance of different firing temperatures on the phase composition of TiO_2 NPs, effect of different composition of phases in bi phase semiconductor's optical band gap and consequent influence on the photovoltaic performance of DSSCs. The presence of rutile NPs is proved favorable in reducing the band gap of semiconductor.

Chapter 6 is focused on the study of thin film solid state solar cells based on perovskite and elaborate the results and discussions of the work done on perovskite based solar cells during the research duration. Two types of titanium dioxide (TiO_2) nanoparticles are synthesized by non-hydrolytic sol-gel method. The effect of variation of annealing temperatures along with the presence of different organic solvents during the synthesis is studied in respect with particle size, absorption in visible range and band gap. The organic solvents used in this study were ethanol and benzyl alcohol. The effect of different surface area and pore size has been further studied on the percolation of PbI_2, formation of perovskite and overall performance in perovskite based solar cells. The influence of graphene oxide (GO) and different annealing temperatures of TiO_2/GO composite on the morphology and optical properties of photoanode are also considered in this chapter. The devices are studied

to analyze the effect of TiO_2/GO composite on the electron generation and transportation in perovskite based solar cells.Chapter 7 gives the conclusion of the study.

TABLE OF CONTENT

LIST OF SYMBOLS

hv	Photon energy
h	Planck's Constant (6.62×10^{-34} W.s)
c	The speed of light (3×10^{8} ms^{-1})
q	Charge constant of an electron (1.6021×10^{-19} C)
V_{oc}	Open-circuit photovoltage
I_{sc}	Short-circuit current
J_{sc}	Short-circuit current density
FF	Fill factor
E_f	Fermi level
P_{in}	Intensity of incident light
P_{max}	Maximum power
α	Absorption coefficient
η	Overall solar-to-electrical-energy conversion efficiency
E_g	Band gap of semiconductor
τ_d	Electron transport or collection time
τ_n	Electron lifetime
R_t	Charge transport resistance
R_{ct}	Charge transfer (recombination) resistance
C_μ	Chemical capacitance
δ	Chemical shift
eV	Electron volt

LIST OF ABBREVIATIONS

FTO	Flourine doped tin oxide
DSSC	Dye-sensitized solar cell
HTM	Hole Transport Material
NMR	Nuclear magnetic resonance
MS	Mass spectroscopy
DPV	Diffrential pulse voltammetry
EDX	Energy dispersive X-ray
AFM	Atomic force microscopy
SEM	Scanning electron microscope
TEM	Tunneling electron microscope
IPCE	Incident photon-to-current conversion efficiency
EIS	Electrochemical impedance spectroscopy
BET	Brunauer-Emmett-Teller measurement
HOMO	Highest occupied molecular orbital
LUMO	Lowest unoccupied molecular orbital
FTIR	Fourier Transform Infrared
XRD	X-ray Diffraction
1D	One dimensional
3D	Three dimensional
TPA	Tri phenyl amine
DMSO	Di methyl sulfoxide

DMF	Di methyl formamide
ACN	Acetonitrile
DI	De-ionized
TW	Terawatt

LIST OF FIGURES

LIST OF TABLES

SUPPORTING INFORMATION

BRIEF CURRICULUM VITAE

ACHIEVEMENTS

A project entitled "**Synthesis of photovoltaic materials and fabrication of photovoltaic device - Dye-sensitized solar cell**" is sanctioned under WOS-A scheme by Department of Science and Technology, New Delhi. **2013**

Received "**Young Scientist Award**" for **best oral presentation**, under the discipline of "**Engineering Science and Technology**" in 7th Uttarkhand State Science and Technology Congress-2012. Presented a paper entitled, "Fabrication of Dye-Sensitized Solar Cells Based On Carbazole-Cruciform As An Organic Sensitizer". **2012**

PUBLICATIONS

1. Sarika Sharma, Sulaxna Sharma, **Pooja Agarwala**, Rajneesh Garg and P. Gopinath, 'A study on Ni-P and Ni-P-ZnO composite coatings developed by electroless technique', *Advanced Materials Research Vol. 585 (2012) pp 512-516.*

2. Pooja Agarwala, Preeti Makkar, Sarika Sharma , Rajnish Garg, '**The Effect of Heat Treatment of TiO_2 Nano Particles on Photovoltaic Performance of fabricated DSSCs'**,Journal of Materials Engineering & Performance(2014), Vol. 23 Issue 10, pp 3703.

3. Effect of different organic solvents and annealing temperatures on optical property of TiO_2 nanoparticles, Pooja Agarwala[1,2], Vijaya Agarwala[1],Rajnish Garg[2]

[1]Centre of Nanotechnology , Indian Institute of Technology Roorkee , Roorkee, India

[2]CentreforNanotechnology-MaterialsEngineeringUniversity of Petroleum and Energy Studies, Dehradun, India

Accepted in International Journal of Technical Research & Application (IJTRA) with article ID: GIC14369 and e-ISSN no. 2320-8163.

4. Dye-sensitized solar cells based on novel carbazole- cruciform dye with D-(π-A)$_4$ skeleton

Pooja Agarwala[a], K. R. Justin Thomas[b], Rajnish Garg[a], Kulkarni Sneha Avinash[c]

[a]University of Petroleum and Energy Studies,Dehradun ,[b]Organic Materials Laboratory, Department of Chemistry, Indian Institute of Technology Roorkee, [c]Energy Research Institute, Nanyang Technological University, Singapore.

Communicated in 2014.

5. Study of electronic and photovoltaic properties of organic sensitizers based on D-(π-A)$_4$

molecular frame containing varying length and position of π-bridge in dye sensitized solar cells, Pooja Agarwala[a], K. R. Justin Thomas[b], Pablo P. Boix[c]

[a]University of Petroleum and Energy Studies, Dehradun ,[b]Organic Materials Laboratory, Department of Chemistry, Indian Institute of Technology Roorkee, [c]Energy Research Institute, Nanyang Technological University, Singapore.

Communicated in 2014.

6. Cosensitization generated molecular rearrangement of novel tetra anchoring organic dyes using indoline dye as filler.

Pooja Agarwala[a], K. R. Justin Thomas[b], Rajnish garg[a]

[a]University of Petroleum and Energy Studies, Dehradun ,[b]Organic Materials Laboratory, Department of Chemistry, Indian Institute of Technology Roorkee.

Under review.

7. Effect of surface area of TiO_2 nanoparticles on perovskite based solar cell performance

Pooja Agarwala[1,2], Vijaya Agarwala[1],Rajnish Garg[2]

[1]Centre of Nanotechnology , Indian Institute of Technology Roorkee , Roorkee, India

[2]CentreforNanotechnology-MaterialsEngineeringUniversity of Petroleum and Energy Studies, Dehradun, India.

Under review.

CONFERENCE PROCEEDINGS

- **National conference** conducted by Department of Applied Science and Humanities, Faculty of Engineering and Technology, Jamia Millia Islamia, New Delhi. Presented a paper entitled "**The Effect of Heat Treatment of TiO_2 Nano Particles on Photovoltaic Performance of fabricated DSSCs**" by **Pooja Agarwala[a]**, Preeti Makkar[b], Sarika Sharma[b], Rajnish Garg[a].[a]University of Petroleum and Energy Studies,Dehradun, [b] Surface Engineering lab.,MMED, IIT Roorkee. **2014**
- **International conference** conducted by University of Hyderabad (UoH), Gachibowli, Hyderabad, INDIA, Indian National Academy of Engineering., INDIA and Royal Academy of Engineering, United Kingdom on **Functional and energy materials, manufacturing and structures (FAEMMS-2013).** **2013**
- **National conference** conducted by Department of Science and Technology, Govt. of Uttarakhand in 7th Uttarakhand State Science and Technology Congress-2012, during 21st-23rd Nov. 2012 in Dehradun, India. Presented a paper entitled "Fabrication of Dye-Sensitized Solar Cells Based On Carbazole-Cruciform As An Organic Sensitizer"by **Pooja Agarwala**, K. R. Justin Thomas, Rajnish Garg, Kulkarni Sneha Avinash, Subodh G. **2012**

Mhaisalkar.

- **International Conference** on Advance Materials and Processing: Challenges and Opportunities (AMPCO 2012), Nov. 2-4, 2012, IIT, Roorkee,INDIA. Paper entitled "**A study on Ni-P and Ni-P-ZnO composite coatings developed by electroless technique**" by Sarika Sharma, Sulaxna Sharma, **Pooja Agarwala**, R.C. Agarwala, V.Agarwala and G.Nath. **2012**

- **International Conference** of Young Researchers on Advanced Materials (ICYRAM 2012), 1 to 6 July 2012, Singapore. Poster entitled "**Bactericidal Activity of Synthesized ZnO Nanorods Towards Gram-negative and Gram-positive Bacterial Species**" by Sulaxna Sharma,**Pooja Agarwala (presenting author),**Devendra Naik, Rajneesh Garg. **2012**

Chapter 1: INTRODUCTION

1.1 MOTIVATION AND OVERVIEW

The modern world utilization of electric energy is approximately 12-13 TW and the earth receives more solar energy in one hour than the energy used globally in one year, considering the solar constant 1.7×10^5 TW at the top of the earth's atmosphere [1].However the solar energy incidence is quite less thus a vast area of energy converters would be required to meet the world's energy consumption and a high efficiency solar energy conversion is the key to the success. Solar cells have been recognized as an important alternative power source especially since Three Mile Island disaster in 1979 and Chernobyl disaster in 1986 when scientists and environmentalists were enforced to focus more on clean, safe and renewable sources of energy. Traditional fossil energy is also exhausted at an unprecedented rate in past few decades. In order to accomplish with the escalating energy needs and casting off the serious problem of global warming, alternative clean and sustainable source of energy are being explored. Among the existing renewable energy sources, solar energy is one of the most promising due to the abundant solar radiations. A lot of work has been done to convert sun light into electricity by using solar cell. Solar Cells are optoelectronic devices that convert solar energy directly to electrical energy by photovoltaic effect i.e. the creation of a voltage in an illuminated junction [2].

Based on the material employed there are mainly three types of solar cells: inorganic, organic and hybrid i.e. Dye Sensitized Solar Cells. As hybrid solar cells merge the merits of both organic as well as inorganic materials, it had been aimed to prevail over the drawbacks of inorganic and organic solar cells in DSSCs. The typical DSSC is composed of a

photoanode and a counter electrode (cathode) sandwiching a redox mediator. It consists of five materials: (1) a fluorine-doped SnO_2 (FTO) glass substrate, (2) a nanocrystalline TiO_2 thin film as a semiconductor, (3) a dye sensitizer, (4) an electrolyte (redox mediator), and (5) a platinum-coated glass substrate [3]. Among all components, the semiconductor, dye and electrolyte are considered to be the most vital components in a dye sensitized solar cell.In spite of cost effectiveness and simple fabrication of DSSCs, these cells are yet to enter the market due to less efficiency and instability in comparison with inorganic i.e. silicon solar cells. Stability of such cells has been improved by replacing liquid electrolyte by hole transporting material in Solid state DSSCs but with the compromized photovoltaic efficiency. Very recently one more category of hybrid solar cells has shown promising results i.e. perovskite solar cells in which organic sensitizers are being replaced by perovskite sensitizers in layered architecture. It comprises of TiO_2, with $CH_3NH_3PbI_3$ perovskite as light harvester and a polymeric hole conducting material. It is anticipated to overcome with the downsides of traditional DSSCs in perovskite based hybrid solar cells.

This chapter discusses the motivation and objective of the work along with the brief discussion on hybrid solar cells based on dye and perovskite. It also gives overview of thesis in chapter scheme briefing about all the chapters of thesis.

1.2 DYE SENSITIZED SOLAR CELLSTO PEROVSKITE SOLAR CELLS

1.2.1 Dye sensitized solar cells

A dye is an organic chromophore that absorbs visible light and its excited state has an oxidation potential which permits electron injection into the conduction band of the semiconductor. This way sensitization of semiconductor allows broadening of absorption spectrum useable for free carrier generation within a semiconductor. Gerischer [4] and

Tsubomura [5] first materialized the concept of dye sensitization of wide band gap semiconductors in 1960s where ZnO semiconductor was sensitized by dyes such as rose Bengal. Since a planar surface covered with a monolayer of a strongly absorbing sensitizer cannot absorb more than 1% of the light [5], the efficiencies remained low for many years [6]. A breakthrough for these cells was constituted by replacement of planar electrode by a mesoporous nanocrystalline semiconductor film, possessing a high surface area [7].Michael Grätzel and Brian O'Regan presented their work in 1991 with an impressive overall efficiency higher than 7%, using a ruthenium based sensitizer and a porous TiO_2 layer as the semiconductor material [8]. This drastic increase in performance of DSSCs could take place due to the increased surface area allowing for a sensitizer to bind on the surface three times more than the geometric area of the sample.

Being a dominant part of DSSC, sensitizer contributes key role towards commercialization. Metal complexed dyes have always been very popular in DSSC. Among these, Ru complexes have shown the best photovoltaic properties so far [9-12]. In spite of showing good photovoltaic performance, purification and structural tuning during synthesis of Ru based dyes is cumbersome. Lately the sensitizer development was mainly focused on organic compounds owing to easy structural modification and fast purification.

1.2.2 ss Dye sensitized solar cells

The DSSCs are economic photovoltaic device in terms of simple manufacturing process and cheap materials used which does not require high quality purification. But issues related to stability are very critical for commercializing these devices. The dye and the electrolyte are two components in a DSSC which gets degraded with time. For dyes, lack of adequate and fast regeneration leads to dye decay through side reactions [13]. The structural

modification of dye molecule has been studied to suppress the issue of instability of dye [14]. In case of liquid electrolyte, the solvents used for the preparation are highly volatile and liable to evaporate on prolonged exposure to heat and light. It has been researched to replace liquid electrolyte with polymer electrolyte, ionic liquids, p-type semiconductors such as CuI or CuSCN and organic hole conductors in order to evade the problems related to leakage and evaporation [15-23].

Recently, the conversion efficiency of the ssDSSC based on an organic hole conductor have achieved over 7 % PCE [24]. These interesting results have stimulated research on the ssDSSCs. The solid system adaptation of DSSCs requires a complete change in the traditional cell design owing to different mechanisms of charge transport in liquid charge-transporting medium, i.e. electrolyte than in a solid one (hole transporting material).

1.2.3 Perovskite based solar cells

There is another type of hybrid solar cell in which organometal halide perovskites are used as light absorbers. In a very short period of time these cells have exceeded organic solar cells and traditional ssDSSCs in regards of efficiency as well as cost effectiveness. Recently reported efficiency of such cells is around 15 % [25-34] in solid state geometry with hole transport material,which is beyond best obtained by DSSCs based on Ru dyes [35]. The active layers of perovskite photovoltaic devices are often similar to that of a classical hybrid solar cell in which a mesoporous [36] metal-oxide scaffold is infiltrated with the perovskite instead of dye. The efficiency to convert light to electricity in any solar cell can be determined by the energy gap of the absorber material. It was ascertained that mixed halide $CH_3NH_3PbI_2X$ with X representing I, Br, or Cl offers the smallest gap in the electronic density of states and is the most efficient perovskite-based absorber till date [37]. The

organometal halide perovskite is one of the key components leading to the proper functioning of a solar cell. It is demonstrated very recently that perovskite absorbers can function at the highest efficiencies in simplified device architectures, where the perovskite film is sandwiched between the two electrodes, surpassing the need for a nanostructured acceptor [38]. However, it's poor reproducibility issues result in very large efficiency fluctuations observed between nominally identical samples [39]. With the past results the correlation of performance of such solar cells with the nanostructured semiconductors cannot be overlooked. Due to more promising stability and well known structure-property relationship, different morphologies and different particle sized nanostructure semiconductors have been studied with perovskite material [31, 40]. It is desirable to focus on both the materials, i.e. perovskite and TiO_2, to lead these hybrid solar cells towards commercialization.

1.3 OBJECTIVE OF THE WORK

The research work covers the synthesis of photovoltaic materials for solar devices and fabrication of DSSCs as well as Perovskite solar cells. There is a significant role of photoanode in both types of solar cells. A photoanode is composed of two components; semiconductor and sensitizer. The essential focus of this thesis is on the photoanode. The enhancement in properties of semiconductors and sensitizers are route to improved photovoltaic performance. The modulation and synthesis of novel organic sensitizers is carried out for the purpose of DSSC applications. The idea of modifying the dye molecule is there for decades. It is chosen to design and synthesize multi anchoring novel organic sensitizers with the variation in π-bridge length and position at core moiety. In present study all the synthesized dyes are used for the purpose of DSSC fabrication. For perovskite solar

cell fabrication, the focus has been to synthesize TiO_2 nanoparticles in different particle size by chemical route. Halide perovskites are used as light harvester.

Being key components of the solar devices TiO_2 nanoparticles and organic sensitizers are the focal point of the study. Hence, the objective of the research can be highlighted in following points:

- Synthesis of novel organic dye molecules by different organic synthetic methods.
- Synthesis of TiO_2 nano particles by different chemical routes.
- Study of synthesized organic dye molecules on DSSCs.
- Study of synthesized TiO_2 nanoparticles on Perovskite solar cells.

1.4 CHAPTER SCHEME

The outline of this thesis is as follows:

Chapter1 presents a brief background of photovolaics, motivation and the main objective of the study.

Chapter 2 is related to the literature survey. It discusses photovoltaic effect and various types of photovoltaics. It explains components and working principle of DSSCs based on liquid as well as solid electrolyte (hole transport material). Recent progress in the DSSCs and introduction of perovskite material as sensitizers is also been discussed. Work undertaken in past in the field of clean energy with detailed description on each component of DSSC is also described here in this chapter. Some metal complex dyes and metal free organic dyes are discussed in order to find out the scope of the work. The synthetic methods of TiO_2 nanoparticles and their structural merits are discussed in detail.

Chapter 3 defines the research gap identified by which the need of current work is defensible.This chapter briefs about the challenges in DSSCs. The design of whole research work undertaken is outlined with the aid of a flow diagram.

Chapter 4 describes various chracterization techniques used in this work with their main principle of operation. The materials used are discussed briefly. The general procedures involved in synthesis of organic dyes and TiO_2 nanoparticles are depicted through schematic diagrams. Steps involved in fabrication of DSSCsbased on organic dyes in conjunction with liquid electrolyte are described. Perovskite based ssDSSCsfabrication is explained in the form of schematic diagrams with short description.

Chapter 5 discusses the results and discussions of the work carried out during the PhD research which concentrates on dye sensitized solar cells (DSSCs). Since dye molecules and semiconductor, both the elements contribute to the performance of DSSCs, adetaileddiscussion is conceived in this chapter focusing on these two. The chapter is divided in to two sections, i.e., study of Carbazole based tetra anchoring organic dyes for DSSC and study of low band gap semiconductor for DSSC. In former section the synthesis and application of a series of carbazole based tetra-anchoring cruciform organic dyes (P1-P5) is discussed. It also includes the effect of cosensitization on photovoltaic performance of the DSSCs. Later part of the chapter focuses on the photovoltaic properties of low band gap TiO_2 nano-composites consisting of different proportions of anatase and rutile phases.

Chapter 6 is focused on the study of thin film solid state solar cells based on perovskite and elaborate the results and discussions of the work done on perovskite based solar cells during the PhD research. The chapter is classified in two parts, i.e., effect of surface area of TiO_2 nanoparticles on perovskite based device performance and effect of

graphene oxide (GO) on charge transfer in perovskite based solar cells. Former part of the chapter explains the effect of boiling point of solvent on the nucleation and growth of TiO_2 nanoparticles. The effect of variation of annealing temperatures along with the presence of different organic solvents during the synthesis is studied in respect with particle size, absorption in visible range and band gap. Later part of chapter reveals the influence of graphene oxide (GO) and different annealing temperatures of TiO_2/GO composite on the morphology and optical properties of photoanode. The devices are studied to analyze the effect of TiO_2/GO composite on the electron generation and transportation in perovskite based solar cells.

Chapter 7 gives the conclusion of the study.

References

1. Nozik, A. J., (2005), “Exciton Multiplication and Relaxation Dynamics in Quantum Dots: Applications to Ultrahigh-Efficiency Solar Photon Conversion”, Inorg. Chem. 2005, vol. 44, pp. 6893-6899.

2. Hu, C., (2010), "Modern Semiconductor Devices for Integrated Circuits", 1st ed, Berkeley: Pearson, USA, 351 pages.

3. Ooyama, Y., Harima, Y., (2009), “Molecular Designs and Syntheses of Organic Dyes for Dye-Sensitized Solar Cells”,Eur. J. Org. Chem., vol. 18, pp. 2903-2934.

4. Gerischer, H., Michel-Beyerle, M. E., Rebentrost, F., Tributsch, H., (1968), “Electrochim. Acta”, vol. 136, pp. 1509-1515.

5. Tsubomura, H., Matsumura, M., Nomura, Y., Amamiya, T., (1976), “Dye Sensitised Zinc Oxide: Aqueous Electrolyte: Platinum Photocell”, Nature, vol. 261 (5559), pp. 402-403.

6. Ardo, S., Meyer, G.J., (2009), “Photodriven Heterogeneous Charge Transfer With Transition-Metal Compounds Anchored to TiO_2Semiconductor Surfaces”,Chem. Soc. Rev., vol. 38 (1), pp. 115-164.

7. Silvestro, D., J., Grätzel, M., Kavan, L., Moser, J., Augustynski, J., (1985), “Highly Efficient Sensitization of Titanium Dioxide”, J. Am. Chem. Soc.,vol. 107 (10), pp. 2988-2990.

8. O’Regan, B.C., Moser, J. E., Anderson, M. and Grätzel, M., (1990), “Vectorial Electron Injection into Transparent Semiconductor Membranes and Electric-Field Effects on the Dynamics of Light-Induced Charge Separation”, J. Phys. Chem-Us, vol. 94, pp. 8720-8726.

9. O'Regan, B. and Grätzel, M., (1991), “A Low-Cost, High-Efficiency Solar-Cell Based on Dye Sensitized Colloidal TiO_2 Films”, Nature, vol. 353, pp. 737-740.

10. Haque, S.A., Handa, S., Peter, K., Palomares, E., Thelakkat, M., Durrant, J. R., (2005), "Supermolecular Control of Charge Transfer in Dye-Sensitized Nanocrystalline TiO_2 Films: Towards A Quantitative Structure-Function Relationship", Angew. Chem., Int. Ed., vol. 44, pp. 5740-5744.

11. Klein, C., Nazeeruddin, M. K., Liska, P., Di Censo, D. , Hirata, N., Palomares, E., Durrant, J. R. and Grätzel, M., (2005), "Engineering of ANovel Ruthenium Sensitizer and Its Application In Dye-Sensitized Solar Cells For Conversion Of Sunlight Into Electricity", Inorg. Chem., vol. 44, pp. 178-180.

12. Chen, K. S, Liu, W. H., Wang, Y. H. , Lai, C. H., Chou, P. T., Lee, G. H., Chen, K., Chen, H. Y., Chi, Y. and Tung, F.C., (2007), "New Family Of Ruthenium-Dye-Sensitized Nanocrystalline TiO_2 Solar Cells With A High Solar-Energy-Conversion Efficiency", Adv. Funct. Mater, vol. 17, pp. 2964-2974.

13. Faiz, J., Philippopoulos, A. I., Kontos, A. G., Falaras, P., Pikramenou, Z., (2007), "Functional Supramolecular Ruthenium Cyclodextrin Dyes For Nanocrystalline Solar Cells", Adv. Funct. Mater, vol. 17, pp. 54-58.

14. Grunwald, R., Tributsch, H., (1997), "Mechanisms of instability in Ru-Based Dye Sensitization Solar Cells", J. Phys. Chem. B, vol. 101, pp. 2564-2575.

15. Yen, Y. S., Chou, H. H., Chen, Y. C., Hsu, C. Y., Lin, J. T., (2012), "Recent Developments in Molecule-Based Organic Materials For Dye-Sensitized Solar Cells", J. Mater. Chem., vol. 22, pp. 8734-8747.

16. Bach, U., Lupo, D., Comte, P., Moser, J. E., Weissortel, F., Salbeck, J., Spreitzer, H., Grätzel, M., (1998), "Solid-State Dye-Sensitized Mesoporous TiO_2 Solar Cells With High Photon-to-Electron Conversion Efficiencies", Nature 395, 6702, pp. 583-585.

17. Bandara, J. and Weerasinghe, H., (2005), "Solid-State Dye-Sensitized Solar Cell with p-Type NiO as a Hole Collector", Solar Energy Materials and Solar Cells, 85 (3), pp. 385-390.

18. Hagen, J., Schaffrath, W., Otschik, P., Fink, R., Bacher, A., Schmidt, H. W., Haarer, D., (1997), "Novel Hybrid Solar Cells Consisting Of Inorganic Nanoparticles and An Organic Hole Transport Material", Synth. Met., 89 (3), pp. 215-220.

19. Konno, A., Kitagawa, T., Kida, H., Kumara, G. R. A., Tennakone, K., (2005), "The Effect of Particle Size and The Conductivity of CuI Layer on The Performance of Solid-State Dye sensitized photovoltaic cells", Curr. Appl. Phys., vol 5 (2), pp.149-151.

20. O'Regan and Schwartz, D. T., (1996), "Efficient Dye-Sensitized Charge Separation In AWide-Band-Gap p-n Heterojunction", J. Appl. Phys., vol 80 (8), pp. 4749-4754.

21. Senadeera, R., Fukuri, N., Saito, Y., Kitamura,T., Wada,Y. and Yanagida,S., (2005), "Volatile Solvent Free Solid State Polymer Sensitized TiO_2Solar Cells With Poly(3,4-ethylenedioxythiophene) As AHole Transporting Medium", Chem. Commun., vol 17, pp. 2259-2261.

22. Tennakone, K., Kumara, G. R. R. A., Kumarasinghe, A. R., Wijayantha, K. G. U., Sirimanne, P. M., (1995), "A Dye-Sensitized Nano-Porous Solid-State Photovoltaic Cell", Semicond. Sci. Technol., vol. 10 (12), pp. 1689-1693.

23. Wang, B. Li, L., Kang, B., Wang, P. and Qiu, Y., (2006), "Review Of Recent Progress In Solid-State Dye-Sensitized Solar Cells", Solar Energy Materials and Solar Cells, vol. 90 (5), pp. 549-573.

24. Nogueira, A. F., Longo, C. and De Paoli, M. A., (2004), "Polymers in Dye Sensitized Solar Cells: Overview and Perspectives", Coordination Chemistry Reviews, vol. 248 (13-14), pp. 1455-1468.

25. Hsu, C. Y., Chen, Y. C., Lin, R. Y. Y, Hob, K. C., Jiann, T., (2012), "Solid-State Dye-sensitized solar cells based on spirofluorene (spiro-OMeTAD) and arylamines as hole transporting materials", Phys. Chem. Chem. Phys., vol 14, pp. 14099-14109.

26. Kojima, A., Teshima, K., Shirai, Y., Miyasaka, T., (2009), "Organometal halide perovskites as visible-light sensitizers for photovoltaic cells", J. Am. Chem. Soc., vol 131, pp 6050-6051.

27. Etgar, L., Gao, P., Xue, Z., Peng, Q., Chandiran A.K. , Liu,B., Nazeeruddin, M. K. and Grätzel,M., (2012), "Mesoscopic $CH_3NH_3PbI_3/TiO_2$ heterojunction solar cells", J. Am. Chem. Soc., vol. 134 , pp. 17396-17399.

28. Kim, H. S., Lee, C. R., Im, J. H., Lee, K. B., Moehl, T., Marchioro, A., Moon, S. J., Humphry-Baker, R., Yum, J. H., Moser, J. E., Grätzel, M. and Park, N. G. (2012), "Lead iodide perovskite sensitized all-solid-state submicron thin film mesoscopic solar cell with efficiency exceeding 9 %." Sci. Rep., vol. 2 (591), pp. 1-7.

29. Qiu, J., Qiu, Y., Yan, K., Zhong, M., Mu, C., Yan, H. and Yang, S., (2013), "All-solid-state hybrid solar cells based on a new organometal halide perovskite sensitizer and one-dimensional TiO_2 nanowire arrays", Nanoscale, vol. 5, pp. 3245-3248.

30. Lee, M. M., Teuscher, J., Miyasak, T., Murakami, T. N.and Snaith, H. J. (2012), "Efficient hybrid solar cells based on meso-superstructured organometal halide perovskites", Science 2012, vol. 338, pp. 643-647.

31. Kim, H.S., Lee, J.W., Yantara, N., Boix, P. P., Kulkarni, S. A., Mhaisalkar, S., Grätzel, M. and Park, N.G., (2013), "High Efficiency Solid-State Sensitized Solar Cell-Based on Submicrometer Rutile TiO_2 Nanorod and $CH_3NH_3PbI_3$ Perovskite Sensitizer", Nano Lett. 2013, vol. 13, pp. 2412-2417.

32. Abrusci, A., Stranks, S. D., Docampo, P., Yip, H.L., Jen, A. K. Y. and Snaith, H. J., (2013), "High-performance perovskite-polymer hybrid solar cells via electronic coupling with fullerene monolayers", Nano Lett., vol. 13, pp. 3124-3128.

33. Cai, B., Xing, Y., Yang, Z., Zhang, W.H. and Qiu, J., (2013), "High performance hybrid solar cells sensitized by organolead halide perovskites", Energy Environ. Sci., vol. 6, pp. 1480-1485.

34. Burschka, J., Pellet, N., Moon, S. J., Baker, R. H., Gao, P., Nazeeruddin, M. K. and Grätzel, M., (2013), "Sequential deposition as a route to high-performance perovskite-sensitized solar cells",Nature, vol. 499, pp. 316-319.

35. Liu, M., Johnston, M. B., Snaith, H. J., (2013), "Efficient planar heterojunction perovskite solar cells by vapour deposition", Nature, vol. 501, pp. 395-398.

36. Yella, A., Lee, H. W., Tsao, H. N., Yi. C., Chandiran, A. K., Nazeeruddin, M. K., Diau, E. W. G., Yeh, C.Y., Zakeeruddin, S. M., Grätzel, M., (2011), "Porphyrin-Sensitized Solar Cells with Cobalt (II/III)-Based Redox Electrolyte Exceed 12 Percent Efficiency", Science, Vol. 334 (6056), pp. 629-634.

37. Lee, M. M., Teuscher, J., Miyasaka, T., Murakami, T. N. and Snaith, H. J., (2012), "Efficient hybrid solar cells based on meso-superstructured organometal halide perovskites", Science, vol. 338, pp. 643-647.

38. Mosconi, E., Amat, A., Nazeeruddin, M. K., Grätzel, M., De Angelis, F., (2013), "First-Principles Modeling of Mixed Halide Organometal Perovskites for Photovoltaic Applications", J. Phys. Chem. C, vol. 117, pp. 13902-13913.

39. Liu, M., Johnston, M. B. and Snaith, H. J., (2013), "Efficient planar heterojunction perovskite solar cells by vapour deposition", Nature, vol. 501, pp. 395-398.

40. Eperon, G. E., Burlakov, V. M., Docampo, P., Goriely, A., Snaith, H. J., (2013), "Morphological Control for High Performance, Solution-Processed Planar Heterojunction Perovskite Solar Cells", Adv. Funct. Mater., Vol. 24, pp. 151-157.

Chapter 2: LITERATURE REVIEW

2.1 CHAPTER OVERVIEW

In this chapter almost all the aspects based on previous work related to the prime focus of this research study, are put together. A detailed literature survey has been carried out in order to compile information regarding the earlier research conducted in the field of photovoltaics and described in the subsequent section. It consists of theoretical, practical and application based suppositions as a consequence of the past work done by researchers in the area of clean energy. On the basis of sequential data gathered the scope of the work is ascertained at the end of the chapter. The chapter discusses the fabrication, working principle and performance of dye sensitized solar cell (DSSC) as well as perovskite solar cells. It makes a detailed description on each component of DSSC like semiconductor, dye, electrolyte and electrode. Various designs of metal complex dyes and metal free organic dyes are discussed in the chapter in order to find out the scope of refinement in the dye molecular structures. Different morphologies of nanoparticles and their structural influence on the performance of solar cells is also described alongwith the synthesis methods.

2.2 PHOTOVOLTAIC EFFECT

In general, basic concept behind the conversion of solar energy directly to electrical energy in a photovoltaic device is termed as photovoltaic effect. A potential difference is created at the junction of two different materials in response to the solar radiations. The basic processes behind the photovoltaic effect are:

1. The absorption of photons resulting in generation of the charge carriers followed by formation of a junction,

2. Separation of photo-generated charge carriers at the junction,

3. Collection of the separated charge carriers at the terminals of the junction.

2.2.1 Potential barrier in solar cell

Sunlight is composed of photons which contain energy corresponding to different wavelengths. When illuminated on a PV cell, these photons are absorbed and their energy is transferred to the electrons in an atom of the semiconductor. With its newfound energy, electron from valence band of the semiconductor jumps to the conduction band and leaves a hole behind. An electric field is generated inside the cell which provides the voltage needed to drive the current through an external load. This potential voltage is termed as barrier which is created by keeping two opposite electric charges adjacent. It keeps electrons and holes separated by sending more electrons on one side and holes at the other side of the cell, setting up a voltage difference between either ends of the cell. This voltage difference is subsequently used to drive an electric current in external circuit. The excited electron-hole pair tries to recombine spontaneously as the system prefers to be electrically neutral. So, it is difficult yet vital to keep electron-hole separated in a PV cell.

2.2.2 p-type and n-type semiconductor

There are several ways to form a potential barrier in a solar cell. One is to slightly change the crystal i.e. making p-type and n-type semiconductor so that the structure on either side of the separating line is different. The p-type and n-type corresponds to positive and negative semiconductors due to profusion of holes or electrons. When the p-type and n-type semiconductors are sandwiched together, the excess electrons in the n-type material flow to the p-type, and the holes thereby vacated during this process flow to the n-type. This way the two semiconductors create an electric field at the junction and act as a battery. The electric field generated this way causes the electrons to jump from the semiconductor out toward the

surface and make them available for the electrical circuit. At the same time, the holes move in the opposite direction, toward the positive surface, where they await incoming electrons.

2.2.3 The electric current

When n-type side is connected to p-type side of the cell by means of an external electric circuit, current flows through the circuit in order to reduce the charge imbalance induced by light. Electrons flow out of the electrode on n-type side, through a load and flow into the p-type side, where they recombine with holes. Therefore, the light energy initially absorbed by the electrons is worn up while the electrons power the external circuit. Thus, equilibrium is maintained. More the incident light creates electron-hole pairs, more charge imbalance occur which is relieved in the form of current, giving up energy in performing work.

2.3 PHOTOVOLTAIC DEVICE

A photovoltaic device is an arrangement composed of different components designed to provide electric power using the sun as the power resource. As the light energy is absorbed in the process in order to generate the output of electricity, it does not release any greenhouse gases into atmosphere. Therefore, it is considered to be the cleanest source of electric power.

2.3.1 Historic background of photovoltaics

In 1839, Nineteen-year-old Edmund Becquerel, a French experimental physicist, first discovered the phenomenon of the conversion of light to electricity, known as the photovoltaic effect while experimenting with an electrolytic cell made up of two metal electrodes [1]. Willoughby Smith later discovered the photovoltaic effect in selenium in 1873 [2]. In 1876 William G. Adams and Day observed the photovoltaic effect in solid selenium [3]. It was 1883 when an American inventor, Charles Fritts, described the first solar cells

made from selenium wafers. In 1904, Albert Einstein theoretically explained the photovoltaic effect [4] and later received Nobel Prize for his work in1923. The existence of a barrier layer in PV devices was reported in1914. In 1918, Polish scientist Czochralski developed a way to grow single-crystal silicon. Major steps toward commercializing photovoltaic cells began in the 1940s and early 1950s, when the Czochralski process was developed for producing highly pure crystalline silicon [5]. In 1954, scientists at Bell Laboratories depended on the Czochralski process to develop a crystalline silicon photovoltaic cell, with an efficiency of 6%. Chapin, Fuller, Pearson (AT&T) submitted their results to the Journal of Applied Physics [6].

Hoffman Electronics achieved 8% efficient cells in 1957 and "Solar Energy Converting Apparatus," patent #2,780,765, was issued to Chapin, Fuller, and Pearson, AT&T in the same year. A year later Hoffman Electronics achieved 9% efficient PV cells which was raised to 10% efficient in 1959. Hoffman Electronics demonstrated the use of a grid contact to significantly reduce series resistance which raised efficiency up to 14% by 1960. In 1974, the Japanese Sunshine project commenced, which was followed by establishment of Solec International and Solar Technology International in 1975. Many important events in the field of photovoltaics came into sight in 1980. Researchers of the University of New South Wales in Australia constructed a solar cell with more than 20% efficiency in 1985. In 1990 Siemens bought ARCO Solar and established Siemens Solar Industries, which is now one of the biggest photovoltaic companies in the world. In 1977 Solar Energy Research Institute (SERI) was founded and later renamed as National Renewable Energy Laboratory (NREL). During 2000 and 2001 production of Japanese producers increased significantly. Companies like Sharp, Sanyo and Kyocera produced solar modules with peak power, which is equivalent to

the annual consumption of Germany. In 2002 NASA successfully conducted two tests of a solar-powered, remote-controlled aircraft called Pathfinder Plus. In the first test, researchers demonstrated the aircraft's use as a high-altitude platform for telecommunications technologies.

2.3.2 Classification of solar cells

2.3.2.1 Silicon, III-V solar cells

Since the research in the field of photovoltaics, three types of cells are worked upon which constitute different materials. Inorganic solar cells are usually made from silicon. Silicon is "doped" so that when light strikes on it, electrons are released and generate an electric current. There are three basic types of Si solar cells.Monocrystalline cells are cut from a silicon ingot grown from a single large crystal of silicon while polycrystalline cells are cut from an ingot made up of many smaller crystals. Third type is the amorphous or thin-film solar cell. They are made by depositing a thin film of silicon onto a sheet of another material such as steel. Today the photovoltaic market is dominated by silicon solar cells that utilize silicon in multicrystalline and monocrystalline forms. Silicon solar cell research is mainly concentrated on using thin-film crystalline silicon, which avoids the costly crystal growing and sawing processes. Thin film technologies reduce the amount of silicon used and hence the cost per watt of power output. Thin cells also allow the use of poorer-quality material for a given efficiency [7]. Silicon solar cells have some limitations as they require good crystal quality, have low light absorption and are not compatible with flexible substrates, a step towards amorphous silicon had been taken. Amorphous solids, like common glass, are materials in which the atoms are not arranged in any particular order. The efficiency of amorphous solar panel is not as high as those made from individual solar cells

because amorphous materials contain large numbers of structural and bonding defects. The efficiency has improved over recent years to the point where they can be seen as a practical alternative to crystalline cells. Their great advantage lies in their relatively low cost of power generation. Today, amorphous silicon is commonly used for solar-powered consumer devices that have low power requirements (e.g., wrist watches and calculators). Crystalline cells generally have a longer lifetime than the amorphous variety. It was in 1954 when a crystalline silicon photovoltaic cell, with an efficiencyof 6% was first developed [8]. Recently, silicon nanostructure (SNS)-based solar cells have attracted considerable interest because of their excellent anti-reflection properties [9]. Multiple scattering incidents in these solar cells result in strong light trapping properties which, in turn, result in near-zero optical reflection [10].

In view of the physical limitation of silicon being highly pure and well crystalline to be an efficient material for solar cells, the search for new materials began and multi-junction III-V cells were developed in 1960. Multi-junction (Tandem) solar cells have the potential for achieving high conversion efficiencies of over 50% and are promising for space and terrestrial applications [11]. III-V semiconductor compound materials have advantages including the bandgap tunability by elemental compositions, higher photon absorption by direct bandgap energies, higher resistivity against high-energy rays in space, and smaller efficiency degradation by heat than Si solar cells [12]. The energy conversion efficiencies of III-V solar cells have been steadily increasing year-to-year and are approaching 40% for the laboratory-scale cells [13]. One of the major factors of energy loss in a solar cell is the gap between the photon energy and the bandgap energy Eg of the photovoltaic material. No absorption would occur if the photon energy was smaller than the bandgap energy and

merely the part equal to the bandgap energy out of the photon energy could be extracted as electric power leaving the other part wasted as heat if larger. Multi-stacking of photovoltaic materials of different bandgap energies is, therefore, commonly used for high efficiency III-V solar cells to reduce this energy loss and absorb the photon energy from the sunlight spectrum more widely and efficiently. The cells made by this strategy takes advantage of tunable band gap energies and lattice constants with the compositions of III-V semiconductor compounds and called multijunction or tandem cells. These cells have single junction to multijunction architecture i.e. 1J, 2J, 3J and 4J. 4J exhibits significantly higher efficiency represented by the spectral coverage relative to single-junction solar cells.

One of the most common and highest efficiency two 2J cells consists of a combination of In0.49Ga0.51P and GaAs with the same lattice constant of 5.64 Å and the bandgap energy of 1.86 eV and 1.42 eV, respectively [14]. For 3J cells, the most common so far, a Ge bottom cell is added to the InGaP/GaAs 2J cell to form an InGaP/GaAs/Ge structure for Ge's lattice constant of 5.66 Å nearly equal to that of InGaP/GaAs. This 3J structure is grown on a Ge substrate and an advantage is that, Ge is a cheaper and mechanically stronger material than GaAs relative to cells grown on GaAs substrates. Spectrolab, a leading manufacturer of high performance III-V cells, presented a lattice-matched In0.495Ga0.505P/In0.01Ga0.99As/Ge 3J cell with a 39.0% efficiency at 236 suns under AM1.5D in 2005 [15, 16] followed by a metamorphic (i.e., slightly lattice-mismatched) In0.56Ga0.44P/In0.08Ga0.92As/Ge with 40.7% at 240 suns in 2007 [17, 18]. Higher indium content in top InGaP and middle InGaAs subcells pulls their bandgap energies down and increases photocurrent in those subcells to obtain a better current-matching to the bottom Ge

subcell. Fraunhofer Institute has achieved a 41.1% efficiency at 454 suns under AM 1.5D with a metamorphic In0.65Ga0.35P/In0.17Ga0.83As/Ge (3J) cell in 2009 [19].

Solar cell efficiency records have been generated mostly with InGaP/(In)GaAs/Ge (3J) and its derivative InGaP/(In)GaAs/InGaAs. Specifically for the space use, very thin, light and flexible InGaP/GaAs (2J) and InGaP/GaAs/Ge (3J) cells are being developed recently [20-22]. For further improvement of the cell efficiency, cells with more junctions are being proposed such as an InGaP/GaAs/InGaAsN/Ge four-junction (4J) structure [23]. Recently an (Al)InGaP/InGaP/Al(In)GaAs/(In)GaAs/InGaAsN/Ge (6J) cell has been demonstrated [24]. The efficiency of this 6J cell was 23.6% under AM 0 at 1 sun (135 mW cm^{-2}). This efficiency is much lower than the highest efficiency 3J cell regardless of more number of junctions presumably due to the current-limiting InGaAsN layer with low quantum efficiency. Open circuit voltage (V_{oc}) of this 6J cell was however 5.33 V, significantly higher than the 3.09 V of the highest efficiency 3J cell, simply because of the series connection of six semiconductor materials.

2.3.2.2 Organic solar cells (OSCs)

Organic photovoltaics (OPVs) are based on organic semiconductors. It is one of the most promising technologies for the low cost energy production with the advantages of being flexible, semi-transparent and solution processable [25]. The materials used in these PVs are the organic molecules and polymers which are chemically tunable to adjust physical properties, such as band gap, valance and conduction energies, charge transport, solubility and morphological properties [26]. From economic point of view the need of very small quantity of organic material in comparison with inorganic materials for the application on large scale production makes their use more tempting. Due to these beneficial and attractive

features, a great deal of attention was given to research and development for higher OPV efficiency over the last few years. Recently the efficiency of 10% has been achieved by OSCs [27]. Typical Organic solar cells are based on a charge transfer occurring at the interface between two distinct materials named Donor and Acceptor, respectively. To allow the separation of the excitons diffusing to this interface, the energy difference between the lower unoccupied molecular orbital (LUMO) levels of the two materials has to be larger than the exciton binding energy [28]. Charge transfer in organic materials used in these solar cells takes place intermolecularly from molecule to molecule in case of small organic molecules and intramolecularly along the polymer chain in case of large organic molecules. Besides the substrate (usually PET foil) and conductive electrodes (usually Al and indium doped tin oxide (ITO)), an OPV cell comprises two main layers, active layer and interlayer. Active layer is composed of both n- and p-type semiconductors. Photons are converted into electrical current in this layer. Interlayer is usually made up of conducting polymer PEDOT:PSS. It serves to smooth ITO surface and increases its work function. When the energy from the photon is absorbed, electrons and holes slightly decouple to form excitons. These excitons then diffuse to the interface between n-type and p-type semiconductors (active layer), where electrons and holes fully separate from each other, producing direct current (DC). So far, in the field of organic solar cells, a vast variation in designs which combine two or more individual single cells as a tandem structure have been considered.

In the beginning of development of organic photovoltaics, single layers of an organic semiconductor were deposited between electrodes made up of two different metals. The efficiency observed from such devices was as low as ~0.01% [29]. In 1986 when Tang *et.al.* introduced a thin film organic solar cell composed of a donor-acceptor (DA) heterojunction,

the efficiency improved dramatically to ~0.95% [30]. The DA interface allows for efficient dissociation of excitons in comparison to a single organic layer. The most studied donor materials are the polyacenes [31-33] such as pentacene and tetracene, and the metal phthalocyanines (MePc), such as CuPc or ZnPc. For acceptors, perylene compounds like perylenetetracarboxylic bis-benzimidazole (PTCBI) and C_{60} are generally used [34-36]. One more promising combination for organic solar cells is poly (3-hexylthiophene) (P3HT) and [6,6]-phenyl C_{61}-butyric acid methylester (PCBM) blend. It is the most efficient fullerene derivate-based donor-acceptor copolymer, which can give solar conversion efficiencies up to 6% [37, 38].

2.3.2.3 Hybrid solar cells

Hybrid solar cells merge advantages of both organic and inorganic semiconductors. Organic material consists of conjugated polymers and acts as a donor. It absorbs light and considered as hole transporter. Inorganic materials in hybrid cells are used as the acceptor and electron transporter. The acceptor material needs a suitable energy offset to the binding energy of the exciton to the absorber. The energy required to separate the exciton is provided by the energy offset between the LUMOs or conduction bands of the donor and acceptor [39]. After dissociation, the carriers are transported to the particular electrodes through a percolation system. Structural modifications in organic polymers and morphological improvement in inorganic materials top up the tuning of the band gaps and coordination of energy levels in desired manner. Therefore, the hybrid photovoltaic devices have a potential for not only low-cost by processing but also for scalable solar power conversion.

Controlling the interface of inorganic-organic hybrid solar cells affects the efficiency of the cells. An increased efficiency can be achieved by increasing the interfacial surface area

between the organic and the inorganic materials for facile charge separation and transportation towards the appropriate electrode without recombining. In such solar cells efficiency depends upon three factors. First, the band gap should be reduced to absorb red photons, second, contact resistance between each layer in the device should be minimized to offer higher fill factor and third, charge-carrier mobility should be increased while minimizing carrier recombination and keeping the series resistance of the device low.

Nano crystals (NCs) are supposed to be an ideal component for hybrid solar cells owing to the tunable bandgap, solution-processability, large dielectric constants and tunability of the NC shape could further promote charge transportation. In 1996 Greenham *et.al.* used CdSe nanodots as acceptor and MEH-PPV as donor for making the first polymer: NC hybrid solar cell [40]. The power conversion efficiency (PCE) of the device was low, which was attributed to poor charge transport through CdSe nanodots. Afterwards, much effort has been devoted to improve the charge transport by tuning the NC shape as well as controlling the nanomorphology [41, 42]. A steady improvement in the device efficiency was achieved due to ongoing engineering work on the NCs, with PCE reaching 2.6% in 2006 [43]. In 2010 Dayal *et.al.* used a low bandgap polymer (PCPDTBT) as the donor, and attained efficiency over 3% [44]. As the data of earlier studies on hybrid solar cells suggested that few hybrid solar cells based on NCs other than CdSe could show efficiencies over 2%, CdSe was the only option for efficient hybrid PVs. In 2011, Ren *et.al.* reported a high efficiency of 4.1%, using P3HT and CdS NCs, which is currently the record efficiency for hybrid PVs [45]. The recent developments are helpful to reconsider the strengths and limitations of hybrid PVs, aiming for further improvement of the device performance.

2.4 DYE SENSITIZED SOLAR CELLS (DSSCs)

The phenomenon of sensitisation of wide band gap semiconductors using dyes was worked upon in the early days of photography in the 19th century. Those were the fundamental studies about electron-transfer processes involving valence and conduction bands of a semiconductor wrapped up in a redox electrolyte. Gerischer first combined the stability of large band gap semiconductors with the photosensitivity to light in the visible region by dye adsorption onto semiconductor surface [46]. Later a lot of work was undertaken on all the aspects including the chemisorption of sensitizers [47-49], electrolyte redox chemistry and the judicious selection of photoelectrode materials [49-51]. Most semiconductors such as CdS, CdSe, GaP and Si experienced serious photocorrosion or even normal corrosion in the dark. Being stable, wide band-gap semiconductor TiO_2 became the material of choice. TiO_2 having a mesoporous structure with high surface area causing a drastic enhancement of the amount of adsorbed dye led to a breakthrough of dye-sensitized devices as solar cell.

In 1991 O'Regan and Grätzel developed the most well known and low cost solar cells i.e. dye-sensitized solar cell [52]. Till date, record efficiencies up to 12 % have been achieved for these devices [53] which are much lower than that of silicon solar cell. As it is highly expensive to acquire crystalline silicon with high purity and difficult to sustain the supply of such soaring cost material, researchers started looking for new low cost materials and devices. Although DSSCs suffer from a number of issues related to stability, it's main advantages of low cost, cheap materials and ease of fabrication, has forced the researchers to focus on the lacking aspects of the DSSCs much carefully. The key difference between DSSC and silicon solar cells is that the light absorption and charge transportation are done

separately by sensitizer and semiconductor in DSSC, whereas both procedures are carried out by same semiconductor in the conventional cell. Secondly, in the *p-n* junction cell an electric field is necessary for charge separation which is done via diffusion in DSSCs. Lastly, in conventional cell both minority and majority charge carriers coexist in a *p-n* junction making these cells sensitive to any trap impurities that may lead to recombination. But in DSSC the electron transport occurs in the semiconductor film and the regeneration of dye occurs through ions in the electrolyte, minimizing the chances for recombination.

2.4.1 Structure and working principle of DSSCs

In 1961, Shockley and Queisser evaluated the thermodynamical limitation of the energy conversion efficiency of a solar cell based on simple calculations and derived two basic phenomena. Firstly, only photons possessing energy larger than the band gap of the photoactive materials can be absorbed and take part in the photovoltaic conversion. Secondly, hot charge carriers created upon photon absorption relax down to the conduction band of the photoactive materials, giving rise to the so-called ‘‘thermalization’’. The main events to take place in any solar cell are: light absorption, charge separation and charge transportation.

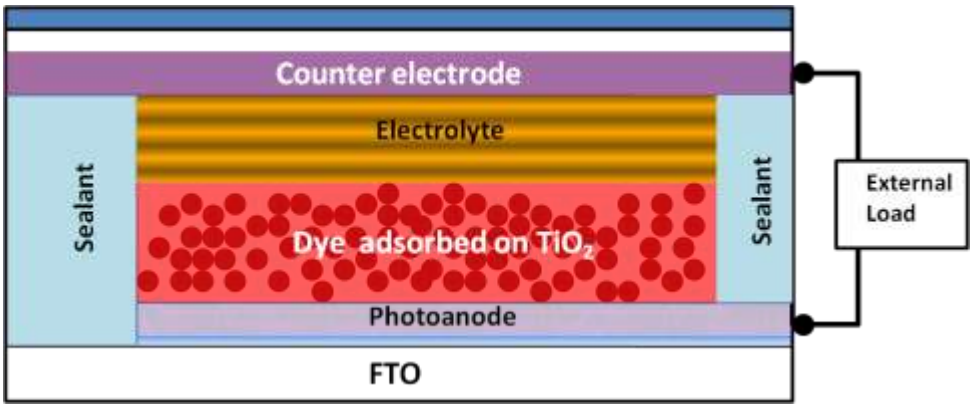

Figure 2.1: Schematic diagram of DSSC.

In the simplest configuration (Figure 2.1), the DSSC is composed of a transparent conducting glass electrode coated with porous nanocrystalline TiO_2 with dye molecules anchored on its surface. An electrolyte containing a reduction-oxidation couple such as I^-/I_3^- and a catalyst coated counter-electrode in conjunction completes the cell. On illumination the cell produces voltage over and current through an external load connected to the electrodes. The photon absorption takes place in a layer of organic dye which causes the excited electrons to jump from the highest occupied molecular orbital (HOMO) to the lowest unoccupied molecular orbital (LUMO) of the dye molecule followed by injection into the conduction band of the semiconductor [54]. These electrons travel through the semiconductor film to the fluorine doped tin oxide (FTO) back electrode where they are collected and directed towards the external circuit. The regeneration of the oxidized dye molecule takes place subsequently through electron transfer via redox couple to the HOMO of dye molecule. In DSSC, the nanoporous network of metal oxide semiconductor film on a conducting glass is sensitized with a monolayer of visible light absorbing dye. This structure is termed as Photoanode where the electricity is generated by triggering the electrons to travel through the external circuit to the counter electrode. The counter electrode is a platinum coated FTO which remains in contact with photoanode by a layer of redox electrolyte. The electrons reduce triiodide (I_3^-) back to iodide (I^-), which regenerates the dye molecule and the whole cycle is repeated.

Anode: $S + h\nu \rightarrow S^* Absorption$ (2.1)

$S^* \rightarrow S^+ + e^-(TiO_2) Electron\ injection$ (2.2)

$2S^+ + 3I^- \rightarrow 2S + I_3^- Regeneration$ (2.3)

Cathode: $I_3^- + 2e^-(Pt) \rightarrow 3I^-$ (2.4)

Cell: $e^-(Pt) + h\nu \rightarrow e^-(TiO_2)$ (2.5)

As visualized in the cell reaction (2.5) the function of the cell is regenerative in nature and no chemical substances are consumed or produced during the working cycle.

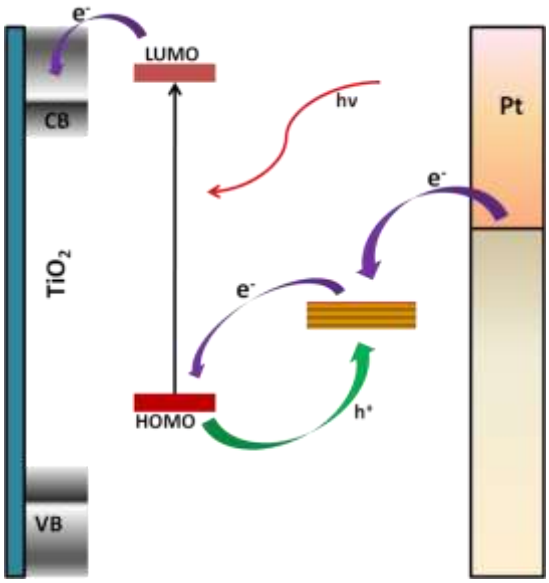

Figure 2.2: Energy level diagram of DSSC.

Figure 2.2, energy level diagram shows the DSSC in which the energy level position of the system shows that the cell is capable of producing voltage between its electrodes and across the external load. The potential difference between the conduction band edge of TiO_2 and the redox potential of I^-/I_3^- pair in the electrolyte decides the photovoltage in open circuit condition. There are variety of parameters to influence the rate of electron injection, such as the length of the π-bridge between electron donor and acceptor [55], the density of acceptor states [56], and the electronic coupling between the dye and the semiconductor. [57]. Moser

et.al. has shown that the quantum yield of the electron injection is controlled by the incident wavelength [58]. Since the NPs are too small to contain significant band bending the major mechanism for electron transport through the NP film is diffusion. In order to develop an efficient DSSC electron diffusion through the NP film should be much faster than the electron recombination with oxidized dyes on the TiO_2 surface or I_3^- in the electrolyte. However, the rate of electron transportation is deeply affected by multiple trapping/detrapping events occurring within grain boundaries [59]. It has been observed that the diffusion coefficient of an electron in the anatase TiO_2 NP film is several orders of magnitude lower than that in single-crystal anatase TiO_2 [60]. The fabrication of one-dimensional TiO_2 related DSSCs, such as nanorod (NR) DSSCs and nanowire (NW)/NP composite DSSCs, have recently been reported for improving the electron transport rate in anodes [61-64] which is attributed to the single-crystalline anatase nanorods [63].

The structures of a dye molecule have a profound effect on efficient charge transfer in DSSCs. For efficient electron injection into the anode, the lowest unoccupied molecular orbital (LUMO) of the dye should be localized near the anchoring group and above the conduction band edge of TiO_2. The HOMO of the dye should lie below the energy level of the redox mediator to allow efficient regeneration of the oxidized dye. The positive charge resulting after electron injection should be localized on the donor part, which is further away from the TiO_2 surface to minimize charge recombination between the injected electrons and the resulting oxidized dye [65]. The dye aggregation on the surface should be avoided in order to shun the non-radiative decay of the excited state to the ground state [66].

2.5 SOLID STATE DYE SENSITIZED SOLAR CELLS (ssDSSC)

Liquid electrolyte has been the main reason behind the instability of DSSCs, due to which it was thought to replace the liquid electrolyte with some solid polymer. This can rectify the problems related to the liquid electrolyte and at the same time it can play a part in current flow in DSSCs. This replacement has various consequences on all the aspects of a cell. The whole geometry needs to be modified for adaptation of solid state arrangement. Since late 90's many inorganic p-type semiconductorsand organic materials have been tested in this regard, but in all cases the incident monochromatic photon-to-electron conversion efficiency remained low. A dye-sensitized heterojunction of TiO_2 with amorphous organic hole-transport material 2, 2', 7, 7'-tetrakis(*N*,*N*-di-*p*-methoxyphenyl-amine)9, 9'-spirobifluorene (OMeTAD) was found to be very efficient in photoinduced charge-carrier generation in 1998 by U. Bach *et.al.* [67]. It was learnt that solar cell based on OMeTAD converts photons to electric current with a yield of 33%. Interfacial charge recombination processes have been identified as the main loss mechanism in this type of cell. For further development of the ssDSSC based on spiro-MeOTAD it is essential to find strategies to suppress interface charge recombination and to identify the differences in charge transport compared to the high efficiency electrolyte solar cell. A better understanding of the electronic processes in the ssDSSC and the optimization of the inorganic/organic interpenetrating network promises further improvement of the device performance. The key issue related to the replacement of the liquid electrolyte by solid charge transport material is the relatively low hole mobility in organic semiconductors originated by less efficient hole transport in the solid medium. Slow charge transport generates concentration gradients in the hole conductor

matrix which leads to a charging of the interface which will considerably increase the interfacial recombination.

The basic ground of the generation of interface charging is the imperfect penetration of the hole conductor into the colloidal film. This is easily avoided in case of liquid electrolyte where the penetration is full and a semiconductor/electrolyte junction occurs at each nanocrystal. It gives an intimate contact which causes high mobility of electroactive species. It has been established that electron transport in nanocrystalline TiO_2 films is dominated by electron trapping in intra-bandgap defect states causing the immobilization of electrons [68]. Therefore, it is suggested that a decrease of layer thickness should enhance the charge transport. Thinning of TiO_2 film ensures efficient collection even for low electron diffusion length, which is a direct evaluation for the charge recombination. However, thin TiO_2 layers offer less active surface area for dye adsorption and consequently lower light harvesting capability. Therefore, it is important to have a dye with very fine optical properties which inhibits a high molar extinction coefficient to increase the optical density of the dye-sensitised thin film. Thus, it is suggested that efficiency enhancement of solid-state dye-sensitized solar cells requires optimization of all components, such as the sensitizer, mesoporous TiO_2 film, hole-transport material and the blocking layer.

2.5.1 Structure and working principle of ssDSSC

A solid state dye sensitized solar cell is shown in Figure 2.3. ssDSSCs possess a monolithic structure in contrast to the sandwich design of the liquid electrolyte based DSSCs. A TiO_2 mesoporous thin film is coated on the conducting side of flourin doped tin oxide glass which consists of a monolayer of sensitizer and makes the photoelectrode. It is placed

in contact with a solid state hole conductor, a p-type semiconductor which is connected to the counter electrode.

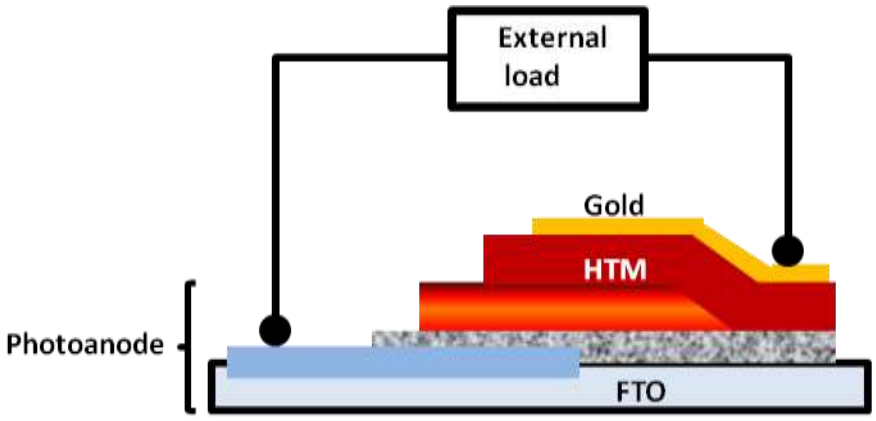

Figure 2.3: Schemetic diagram of ssDSSC.

Working of the ssDSSC is almost same as it is in DSSC based on liquid electrolyte (Figure 2.4). All the other processes such as photoexcitation of dye, electron injection and dye regeneration are same in both type of DSSCs, the only difference is the direct hole transportation from dye to the HTM, and then to the counter electrode via hopping in case of ssDSSC. Therefore, the kind of transportation which is electronic in ssDSSCs and ionic in photoelectrochemical cells is the main difference in the working of both types of cells. The most important reactions involved in a DSSC using a hole transporting material are shown in equations (2.6-2.10);

$$S^* \rightarrow S^+ + e^-(TiO_2) \quad (2.6)$$

$$S^+ + HTM \rightarrow S + HTM^+ \quad (2.7)$$

$$HTM^+ + e^-(Au) \rightarrow HTM \quad (2.8)$$

$$S^+ + e^-(TiO_2) \rightarrow S \quad (2.9)$$

$$e^-(TiO_2) + HTM^+ \rightarrow HTM \quad (2.10)$$

After the photoexcitation of the dye, electron injection into the conduction band of TiO_2 takes place. The oxidised dye molecule is reduced by electron donation from the hole conductor. The regeneration of hole conductor occurs at the counter electrode, and the circuit is completed via electron migration through the external circuit [69]. In this process the recapture of the conduction band electron by the oxidized dye in interrupted by regeneration of the dye by the hole conductor. In the ssDSSC, the charge transfer reactions between the dye sensitized TiO_2 and hole transporting material (HTM) is considered to be the most critical step in determining the overall solar cell efficiency [70].

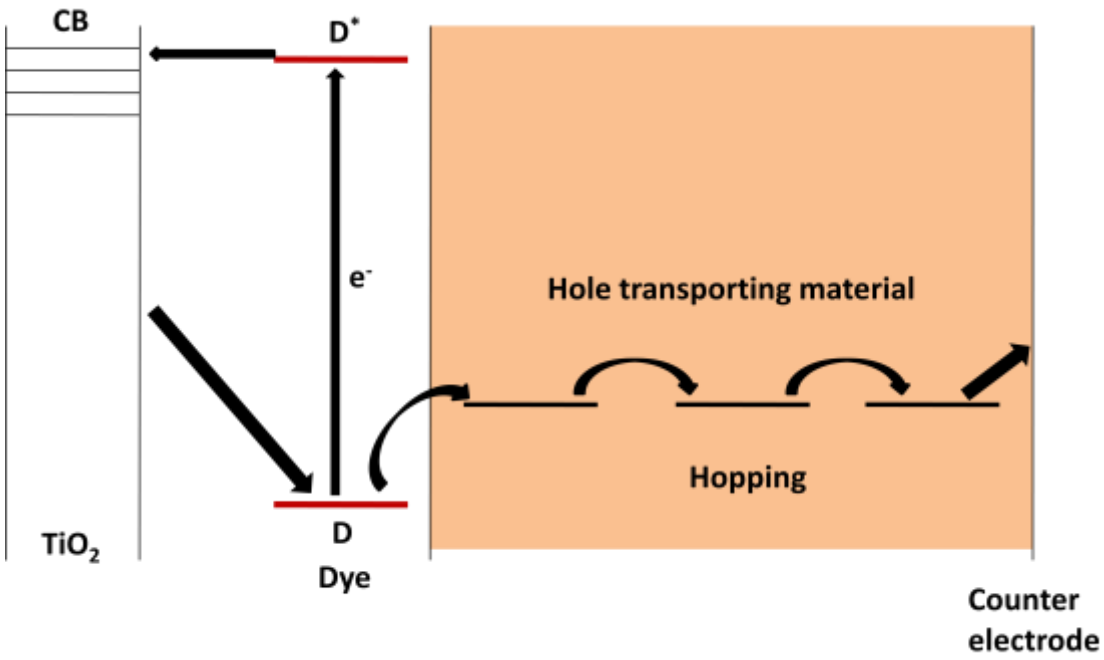

Figure 2.4: Schematic description of a solid state dye sensitized solar cell.

2.6 PARAMETERS IN DSSC

In order to evaluate and establish the performance of various solar cells, a few parameters are defined. Various mechanisms and overall performance of the device can be explained on the basis of the calculation of these parameters.

2.6.1 Current-voltage characteristics

The measurement of a *J-V* curve is an efficient way to estimate the photovoltaic performance of a DSSC. From the *J-V* curve (Figure 2.5), the following parameters can be obtained: V_{oc}, J_{sc}, *ff* and η.

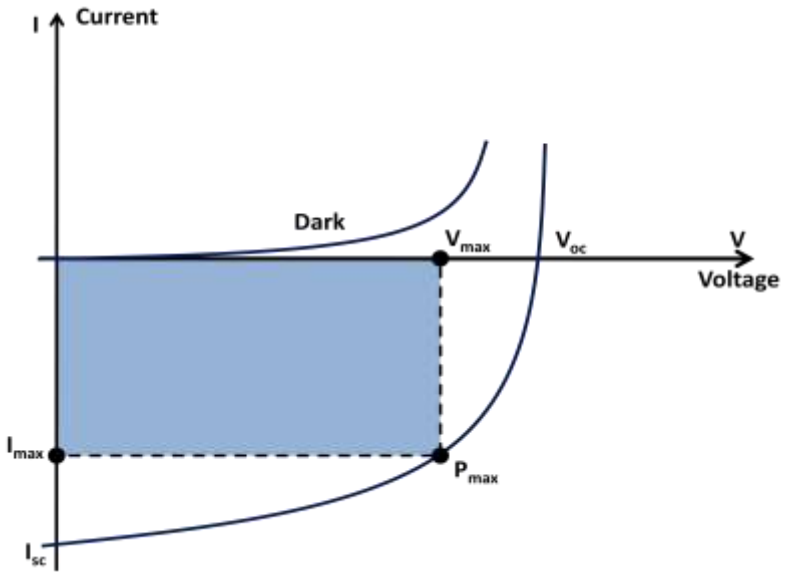

Figure 2.5: *J-V* graph of a DSSC showing various parameters of performance.

The V_{oc} of a DSSC corresponds to the difference between the Fermi level of the semiconductor and the redox potential of the electrolyte. The position of the Fermi level is in the band gap, close to the valence band of p-type semiconductor. When the electrons are injected from dye HOMO level into the conduction band of TiO_2, the electron density

increases which raises the Fermi level towards the conduction band edge. This shift in the Fermi level is the reason behind the generation of the photovoltage in the external circuit. J_{sc} is the photocurrent per unit area under short-circuits condition. It is related to the optical properties of the dye, as well as to different dynamic processes in the cell. The *FF* of a solar cell is defined as the maximum power output divided by the product of J_{sc} and V_{oc}, denoted by P_{max} in equation (2.11). The *FF* can assume values between 0 and 1. The fill factor measures the ideality of the device. The recombination of conduction band electrons with the acceptor species of the electrolyte influences the *FF* unfavorably [54]:

$$FF = \frac{P_{max}}{J_{sc}V_{oc}} \tag{2.11}$$

From the parameters discussed above, the η equation (2.12) of a solar cell can be calculated by the ratio of the maximum output electrical power to the energy of incident sunlight (I_s).

$$\eta = \frac{J_{sc}V_{oc}FF}{P_{in}} \tag{2.12}$$

2.6.2 Incedent photon to current conversion efficiency (IPCE)

"The IPCE value corresponds to the photocurrent density produced in the external circuit under monochromatic illumination of the cell divided by the photon flux that strikes the cell" [71]. It can be obtained by equation 2.13:

$$IPCE = 1240\frac{J_{sc}\,(\lambda)}{\lambda P_{in}(\lambda)} \tag{2.13}$$

J_{sc} is the short-circuit photocurrent density generated by the monochromatic light, λ and P_{in} are the wavelength and intensity of the monochromatic light. It depends on various factors related to the dye such as the light intensity, light absorption, injection efficiency and regeneration of the oxidized dye. It is associated to IPCE and theoretical values of J_{sc} can be calculated from the IPCE spectrum. The IPCE can also be expressed as the product of the light harvesting efficiency (LHE), the quantum yield of hole injection (Φ_{inj}), and the efficiency of collecting (η_{coll}) the holes at the FTO substrate.

$$IPCE(\lambda) = LHE(\lambda)\phi_{inj}\eta_{coll} \tag{2.14}$$

The absorbed photon-to-current conversion efficiency (APCE) can be estimated from the ratio of IPCE and LHE. It is a better measure of the intrinsic light conversion efficiency.

$$APCE(\lambda) = \frac{\text{IPCE}\,(\lambda)}{\text{LHE}\,(\lambda)} \tag{2.15}$$

2.7 COMPONENTS OF DSSC

In both types of DSSCs required components are same i.e. sensitizer, photoelectrode, electrolyte and counter electrode but their assembly is different which totally depends upon the type of electrolyte used. In this section all the components are described briefly.

2.7.1 Photoelectrode

The main photoconversion takes place at photoelectrode, hence it is considered as the soul of a DSSC. A photoelectrode consists of three components, i.e. substrate, metal oxide semiconductor and sensitizer. Each of them has a specific role but the combined performance of these elements decides the efficiency of the DSSCs.

2.7.1.1 Substrate

In a standard DSSC the cell is assembled in between the conducting coated glass substrates which work as a current collector, a support structure to the cell and as a sealing layer between the cell and the ambient air. The coating of transparent conducting oxide (TCO) is done for the purpose of making a non conducting surface as conducting. The most frequently used TCOs in thin film photovoltaic cells are fluorine-doped tin oxide (SnO_2:F) and indium tin oxide (In_2O_3:Sn or ITO). The primary requirement for being a good TCO is to be completely transparent and stable at the temperature at which cell processing is done i.e., sintering of the deposited TiO_2 film at 450-500°C. Being the only TCO coating, stable at high temperatures, the SnO_2:F has been the material of choice for DSSCs [72]. The technology of the production of SnO_2:F coated glass plates is well established and these are commercially available with several commercial manufacturers.

From the application point of view it has been considered to replace the glass substrate by flexible transparent plastic substrate which provides a vast range of applicability at lower cost. The other benefits associated with the plastic substrate based DSSCs are the easy handling and transportation, light weight and reduction in the total cell area which makes it more versatile in use. Since polymers cannot withstand high temperature, SnO_2: F is replaced by In_2O_3:Sn to be used as TCO coating on plastic foils. In 2000 Sommeling *et.al.*

found out that ITO can be deposited by room temperature sputtering which is suitable for plastic substrates. For same reason the sintering of the nanostructured TiO_2 films has to be subsituted by a low-temperature sintering method.

Currently the polymer substrate used in DSSCs in recent studies has been ITO-coated polyethylene terepthalate (PET). However, there are some issues in using polymers as substrate material in DSSC such as polymer permeability to oxygen and water vapor and instability of polymer itself in the presence of electrolyte [73]. Due to these problems the stability and durability of the DSSCs based on plastic substrates is questionable. In 2001 a new method for making nanostructured electrodes on plastic substrates had been invented by Lindström *et.al.* in which TiO_2 powder suspension was compressed by a static or dynamic (roller mill) compression for working electrodes in DSSC. Once compressed no heat treatment is required for the films.

2.7.1.2 Metal oxide semiconductor

On the conducting substrates metal oxide semiconductor film is deposited which is the centre for initializing the process of electron transportation in DSSC. These are wide band gap materials which are porous and exhibit a high surface area. Since they absorb only ultraviolet light, leaving the rest of the visible region of solar spectrum, they are sensitized by a dye adsorbed on its surface for the visible spectrum coverage and effective light harvesting. The primary requirements for being a good semiconductor film are high surface area and good transparency [74]. Many other metal oxides, such as zinc oxide (ZnO) [75], niobium oxide (Nb_2O_5) [76], tin oxide (SnO_2) [77], have been studied on DSSCs, but it was observed that only TiO_2 and ZnO perform the best in terms of efficiency. It is studied that electron density and electron injection is influenced by the band structure of semiconductor. In case of

Nb_2O_5 and TiO_2, both have the same band gap energies i.e. 3.2 eV but Nb_2O_5 was not found to be as efficient as TiO_2 for DSSC applications. The reason could be different band structure of Nb_2O_5 which has its conduction band more negative by approximately 0.2-0.3 eV and above the LUMO of the dye. Thus, electron injection from dye does not take place in the conduction band of Nb_2O_5 [76]. The conduction band edge must lie slightly below the excited state energy level of dye for efficient electron injection and this condition is fulfilled by TiO_2. Since ZnO has a drawback of being chemically unstable in presence of electrolyte, TiO_2 leads the main role as metal oxide semiconductor in solar cells. Some mixed oxides like strontium titanate ($SrTiO_3$) [78] and zinc stannate (Zn_2SnO_4) [79] have also been investigated but no other semiconductor could have as high efficiency as titanium dioxide [80].

2.7.1.3 Sensitizers

A sensitizer is the photoactive component used in a photovoltaic device in order to harvest the incident light for photon-to-electron conversion. Two types of sensitizers have been in use for the purpose of photosensitization of TiO_2 mesoporous film, i.e. metal complexes and metal free organic compounds. For the realization of effective absorption of incident light, dye molecules are positioned at the semiconductor film surface. Being one of the most vital elements of DSSC, all sensitizers should posses some basic qualities.

One of the foremost requirements is that a dye should absorb light at wave lengths up to approximately 920 nm [81]. However, the difference in the energy levels of the HOMO and the LUMO is decreased by broadening of the absorption spectra. This consequently hinders the driving force for electron injection into the conduction band of semiconductor or regeneration of the dye from the electrolyte. It is desired to have the LUMO of the adsorbed dye molecule to be above the conduction band edge of TiO_2 for the efficient electron

transition provided the distance should be just enough to minimize the energy losses and maximize the photovoltage. HOMO of the dye molecule should be somewhat below the redox potential of electrolyte for proficient dye regeneration [82]. The electron injection from the excited state of the dye molecule to the conduction band of TiO_2 should be fast enough to overcome the process of unwanted recombination and relaxation. The sensitizer should be electrochemically and thermally stable to sustain working environment for long period. Dye molecule should consist of anchoring groups to get attached to the surface of TiO_2 mesoporous film, so that it can be well adsorbed to the semiconductor surface.

2.7.1.4 Electrolyte

The conducting medium in which the flow of current takes place in the form of ions in a DSSC is called elecrolyte. Since the central functioning in a DSSC is based on the injection of electrons from the photoexcited state of the sensitizer into the conduction band of TiO_2, an electrolyte plays very crucial role of being the intermediate for the electron transportation. In this process the dye is regenerated by electron donation from iodide in the electrolyte which is simultaneously restored by the reduction of triiodide at the counter electrode. This way the power generation from sun light occurs without any permanent chemical transformation [83]. Several features are essential for any electrolytes in a DSSC [84].

The electrolyte must be able to transport the charge carrier between photoanode and counter electrode. The oxidized dye must be reduced to its ground state rapidly after the dye injects electrons into the conduction band of TiO_2. Thus, the electrolyte must be chosen as per the dye redox potential. The electrolyte should facilitate a good interfacial contact between the mesoporous TiO_2 layer and the counter electrode. An electrolyte must permit

rapid diffusion of charge carriers in order to achieve higher conductivity. It should be chemically, thermally, optically and electrochemically stable for long duration. Interfacial stability of an electrolyte is also a major point of concern so that the possibilities of dye desorption and degradation at the oxide surface can be evaded. For the device fabrication point of view the electrolyte solvent should be chosen wisely as it should not be very viscous which causes poor pore filling yet not too volatile to evaporate fast. It should also have a good compatibility with the sealing material used for the sealing of the DSSCs. Since I_3^- reduces the visible light absorption by the dye as a result of reacting with the injected electrons and in turn produces the dark current, the concentration of I^-/I_3^- must be optimized carefully. Three different types of electrolytes are usually used in DSSC- liquid, quasi-solid and solid electrolytes.

2.7.1.4.1 Liquid electrolyte

Liquid electrolytes consist of organic solvent, redox couple, and additive. Many types of liquid electrolytes containing iodide/triiodide redox couple and high dielectric constant organic solvents such as acetonitrile (AcN), ethylene carbonate (EC), 3-methoxypropionitrile (MePN), propylenecarbonate (PC), γ-butyrolactone (GBL), and *N*-methylpyrrolidone (NMP) have been studied for years [85-87]. The results indicate that each component of liquid electrolyte plays a specific role in the photovoltaic performance of DSSCs.

So far the most efficient redox system is iodide/triiodide [52]. Although other systems have also been implemented in DSSC such as quinone/hydroquinone [88], ferrocenium/ferrocene [89], Br_3^- / Br^- [90] and Co^{III}/Co^{II} [91], only iodide-triiodide redox couple gives the highest power conversion efficiency among the ruthenium polypyridyl dyes.

This is one of the reasons which is why practically liquid or quasi-solid DSSC are based on iodine.

In liquid electrolytes basic component is the organic solvent which gives an environment for iodide/triiodide ions for dissolution and diffusion. The photovoltaic performance of DSSC is highly influenced by the physical characteristics of organic solvent which includes donor number, dielectric constants, viscosity etc. The investigations showed that the donor number of the solvent foretells the extent of transformation from iodide to triiodide ions in a given solvent [83] which influences the open circuit voltage (V_{oc}) positively and short-circuit current density (J_{sc}) negatively [85]. Consequently the overall conversion efficiency is swayed in presence of different solvents in electrolytes. As per the electron donor-acceptor reaction between organic solvent and triiodide (2.16) [83], it is important for the reaction equilibrium to incline towards the right so that the concentration of triiodide can be controlled leading to less dark reaction to take place. The higher donor number of solvent can be correlated with V_{oc} via reaction (2.16) [92].

$$Solvent + I_3^- \leftrightarrow Solvent \ldots . I_3^- \leftrightarrow Solvent \ldots . I_2 + I^- \quad (2.16)$$

Several solvents have been tested for the electrolyte system. The main solvents used for DSSC are nitriles like acetonitrile, acetomethoxypropio-, valero-, or butyronitrile or mixture of carbonates like ethylene/propylenecarbonate. An example of a typical electrolyte composition is 0.5 M LiI, 0.05 M I_2 and 0.5 M TBP in 3-methoxypropionitrile. There is a significant role of cations in liquid electrolytes in the process of light-to-electricity conversion process of DSSCs. Particularly small cations such as protons (Li^+, etc.) play an

important role in the photoelectric performance of DSSCs. The electron diffusion in the conduction band of TiO_2 takes place via an ambipolar diffusion mechanism [93]. Due to the small radius, Li^+ deeply penetrates into dye-coated mesoporous TiO_2 film and creates an ambipolar Li^+-e^- with the electrons in the conduction band of TiO_2. In this way the transport speed of electrons takes a plunge which in turn enhances the J_{sc} of DSSCs [94].

In spite of being proven the most efficient redox couple for regeneration of the oxidized dye, issues with iodide/triiodide related to severe corrosion for many sealing materials, especially metals and poor long-term stability of DSSC cannot be ignored. Therefore, other kinds of redox couples such as Br^-/Br_2, SCN^-/SCN_2, $SeCN^-/SeCN_2$ bipyridine cobalt (III/II) complexes were also explored. But these redox couples show lower light-to-electricity conversion efficiencies than the iodide/triiodide redox couple does [95-97] owing to their unmatchable energy with sensitized dyes.

Electric additive is an important component in liquid electrolytes which can hugely enhance the photovoltaic performance even with addition in a small quantity to the electrolyte. Nitrogen-containing heterocyclic additives have been investigated on the photovoltaic performance of DSSCs and it was observed [98, 99] that electric additives such as 4-*tert*-butylpyridine, pyridine could enhance V_{oc} but decrease J_{sc}. The negative influence of ambipolar Li^+ on DSSCs such as decrease of V_{oc}, due to its easy combination with triiodide [100, 101] can also be overcome by adding cations with larger ionic radii. An imidazole cation is used for this purpose as additive in liquid electrolyte which forms a Helmholtz layer on the surface of TiO_2 film and blocks the direct contact of triiodide with ambipolar Li^+-e^- and enhances the V_{oc} of the DSSC [101].

Due to the issues related to stability with organic solvents in liquid electrolytes, ionic liquids (ILs) have been developed in recent years as solvents or components of liquid and quasi-solid electrolytes for DSSCs [102-104]. The main advantages of ILs over organic solvents are their reduced volatility as a result of negligible vapor pressure, electrochemical stability, thermal stability, and high ionic conductivity, which leads to a better long-term stability in solar cells. The main disadvantage of ILs is the usually lowering of performance in devices because of their high viscosity, which results in mass-transfer limitations of the photocurrent under full illumination [105].

In recent studies the focus has been on the substitution of liquid electrolyte by polymer electrolyte [106, 107], gel electrolytes [108, 109], organic or inorganic hole conductors [110, 111] and less volatile ionic liquids [112, 113]. In order to beat the problem of solvent leakage a unique approach has been adopted in which the gelation of the organic solvents by adding polymeric agents, called fillers, transforms the electrolyte into a quasi solid electrolyte. Scrosati and co-workers [114] invented that the addition of TiO_2 and other nanoparticles improves the ionic conductivity of polymer electrolytes. It is deduced that incorporation of nanoscale inorganic fillers in the electrolyte improves the mechanical, interfacial, and conductivity properties of the gel polymer electrolytes. The drawback of adding these materials is the reduced electrolyte penetration results in less conversion efficiency. Addition of TiO_2 nanoparticles to the polymer matrix is the most used approach [115, 116].

A different approach of plasticizing electrolyte by using γ-butyrolactone (GBL) as plasticizer is developed for the application in batteries. GBL is well known for contributing in the coordination of Li^+ ions and the suspension of lithium salts in polymer systems [117].

Both gelated and hole-conducting electrolytes have been studied by De Paoli and co-workers in detail [118].

2.7.1.4.2. Hole transporting material (HTM)

After the electrons are injected into the conduction band of TiO_2 it leaves the hole behind in the ground state of the dye which is carried to cathode by HTM. For being a good HTM some conditions are to be fulfilled as its upper edge of valance band must be located above the ground state level of the dye for efficient dye regeneration. A good contact of HTM with porous TiO_2 layer is of prime importance and finally it should not absorb the visible spectrum and should not interfere in the electron transport by dye. There are two types of HTMs i.e. inorganic and organic HTM. Several inorganic HTMs have been investigated but CuI [119, 120] and CuSCN [121, 122] are the representative inorganic HTMs among all. The hole conducting ability is facilitated by the high conductivity of around 10^{-2} S/cm of these inorganic materials. To form a complete layer during the device fabrication, copper-based materials can be either solution or vacuum deposited on TiO_2 film. The efficiency showed by ssDSSCs fabricated by inorganic HTMs is considerably fine but they have issues such as instability, crystallization on TiO_2 film surface before penetrating into the pores causing insufficient pore-filling. These drawbacks of inorganic HTMs are surmounted in organic HTMs as they possess the advantages of low crystallinity, easy film formation and plentiful sources. Organic HTMs have already been widely used in organic solar cells [123], organic thin film transistors [124], and organic light-emitting diodes [125].

In 1998 the first efficient ssDSSC using organic HTM, 2, 2’, 7, 7’-tetrakis(N,N-di-p-methoxyphenylamine) 9,9’-spirobifluorene (spiro-OMeTAD) (Figure 2.6 (a)) was reported by Udo *et.al*. which became the pioneer for the current ssDSSCs [126]. Initially the

efficiency obtained was very low which enhanced by utilization of additives, like $Li(CF_3SO_2)_2N$ and 4-*tert*-butylpyridine. The presence of these additives in spiro-OMeTAD

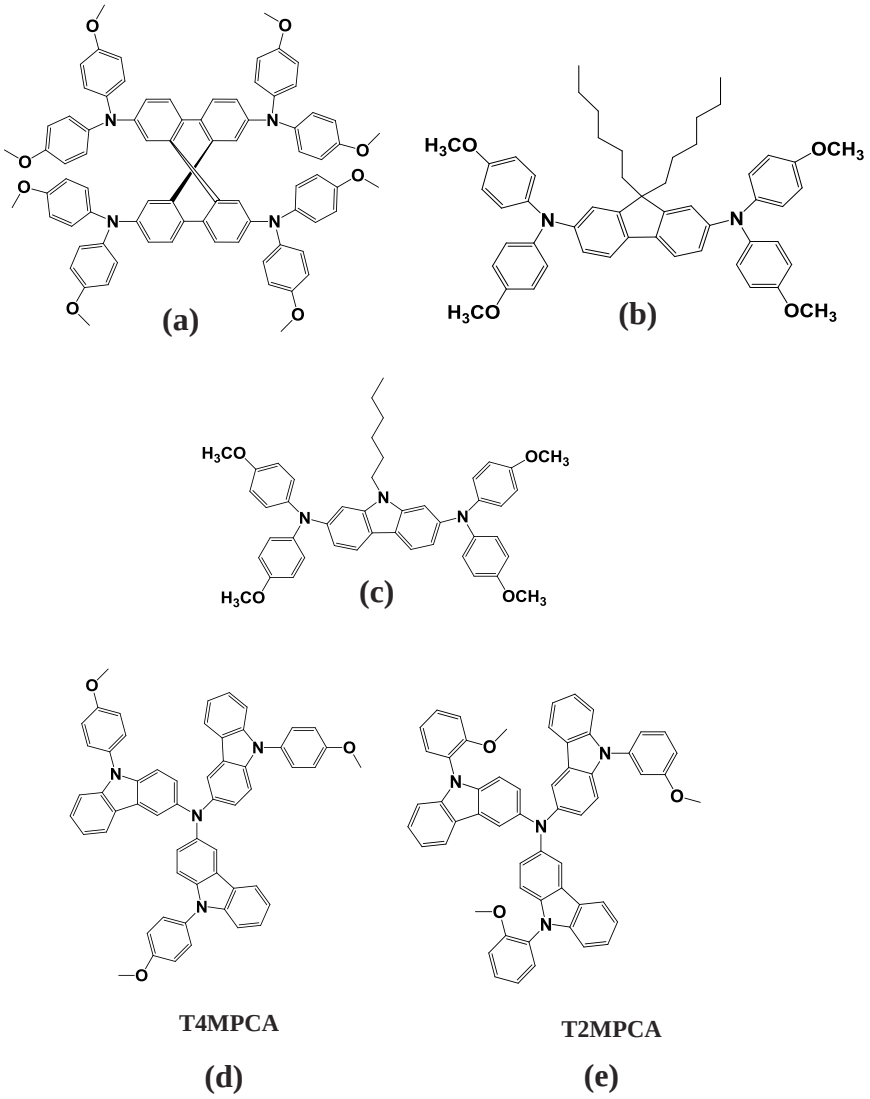

Figure 2.6: Molecular structure of some well studied HTMs (a-e).

solution increased the short circuit current and the open circuit voltage and led to an enhancement of the power conversion efficiency in ssDSSCs [127]. So far ssDSSCs employing spiro-OMeTAD have shown good performance, but the PCE of this system is still

lower than liquid electrolyte-based DSSC. Due to low hole mobility of spiro-OMeTAD, high recombination between TiO_2 and HTM and incomplete pore-filling into the pores of nanocrystalline TiO_2 film, IPCE of the devices fabricated by spiro-OMeTAD suffers drastically.

In 2012, Leijtens *et.al.* presented new hole transport materials (HTMs) based on carbazole core substituted by biphenyl amine units at 2 and 7 positions. The compounds were found to be highly suitable for ssDSSCs applications owing to their low glass transition temperatures, low melting points, high solubility and consequently increased pore filling. With 2-μm-thick mesoporous film sensitized by Z907 and AS37, AS44 as hole transporting materials, the power conversion efficiencies up to 2.94% was observed [128]. Two new star-shaped carbazole molecules for ssDSSC applications were reported very recently in 2014 by Michaleviciute *et.al.* The molecules showed to have molecular glasses properties, hole transport properties, high thermal stability and high glass temperature transitions 164-175 °C which is even higher than the classical spiro-OMeTAD. The ssDSSCs with the composition of ITO/ TiO_2/ D102/ T4MPCA/ Au demonstrated a power conversion efficiency of 2.23% under standard AM 1.5 simulated solar irradiation [129].

As a transport material for ssDSSCs organic or inorganic HTM cannot satisfy the practical application owing to their low power conversion efficiencies. The strategy of introducing iodide/triioide redox couple into solid-state electrolytes produced some remarkable results [130]. Iodide/triiodide redox couple can efficiently rejuvenate oxidized dyes and the interfacial contact properties of these solid-state electrolytes are better than that of HTMs. Hence this kind of solid-state electrolyte has a good prospect in practical DSSCs.

2.7.1.5 Counter electrode

Counter electrode in DSSC is needed for sufficiently fast reaction kinetics for the triiodide reduction reaction in order to complete the cycle of electron transportation and dye regeneration. It is made up of a catalyst coating on conducting side of FTO. The most efficient and traditionally used catalyst for this purpose is platinum. The method of deposition on FTO surface has a great influence on the performance of the catalyst. Platinum catalyst can be coated electrochemically, by sputtering, pyrolytically or by spin coating. Due to the drawbacks of instability of electrochemically and vapor deposited Pt, in presence of iodide electrolyte new methods of catalyst deposition have been developed. An alternative Pt catalyst coating method was developed by Papageorgiou *et.al*. in 1997 called "platinum thermal cluster catalyst" which gave the superior kinetic performance with respect to conventional platinum deposition methods. Due to the need of low Pt loading in this method the optical transparency of the counter electrode could be increased and overall cost of fabrication could be reduced to some extent. In 1996 Kay and Grätzel developed a cell design in which a porous carbon counter-electrode was used as a catalyst layer. Main contents of these electrodes are carbon black, graphite powder and nanocrystalline TiO_2 particles where TiO_2 particles are used as a binder. Due to very large surface area of these electrodes, caused by the carbon black, the activity of these electrodes for triiodide reduction is as much as the conventional Pt electrodes.

2.8 SENSITIZERS IN DSSCs

2.8.1 Metal complex dyes: State of the art

Apart from fruit extracts, many different compounds have been explored for sensitization of the semiconductor in a DSSC, such as chlorophyll derivatives, porphyrins,

phthalocyanines, platinum complexes, coumarin, carboxylated derivatives of anthracene [131-142]. However, the best solar to electric power conversion efficiency has been attained by ruthenium (II) polypyridyl complexes with carboxylated ligands. Within two decades, the DSSCs efficiency based on Ru complexes has improved further and recently reported as 12.3% [143]. Ru(II) polypyridyl complexes with the general structure $ML_2(X)_2$ are the most elaborately studied sensitizers, where L stands for 2,2-bipyridyl-4,4'-dicarboxylic acid, M is Ru, and X represents thiocyanate (-NCS). This class presents intense visible metal-to-ligand charge transfer bands where the carboxylic groups enable the necessary electronic coupling between the sensitizer and TiO_2 surface [144]. In fact, the ruthenium complex cis-$RuL_2(NCS)_2$, N3 dye (Figure 2.7) has become a model of heterogeneous charge-transfer sensitizers for mesoporous DSSCs [145].

The ultra-fast electron injection from dye to TiO_2 conduction band and a much slower reverse process is the key to the high-energy conversion efficiency of this dye. It is found to exhibit exceptional properties, such as a broad visible light absorption spectrum, long excited state lifetime (~20 ns) and strong adsorption due to binding with four carboxyl groups which influence the anchoring of dye on TiO_2 film.

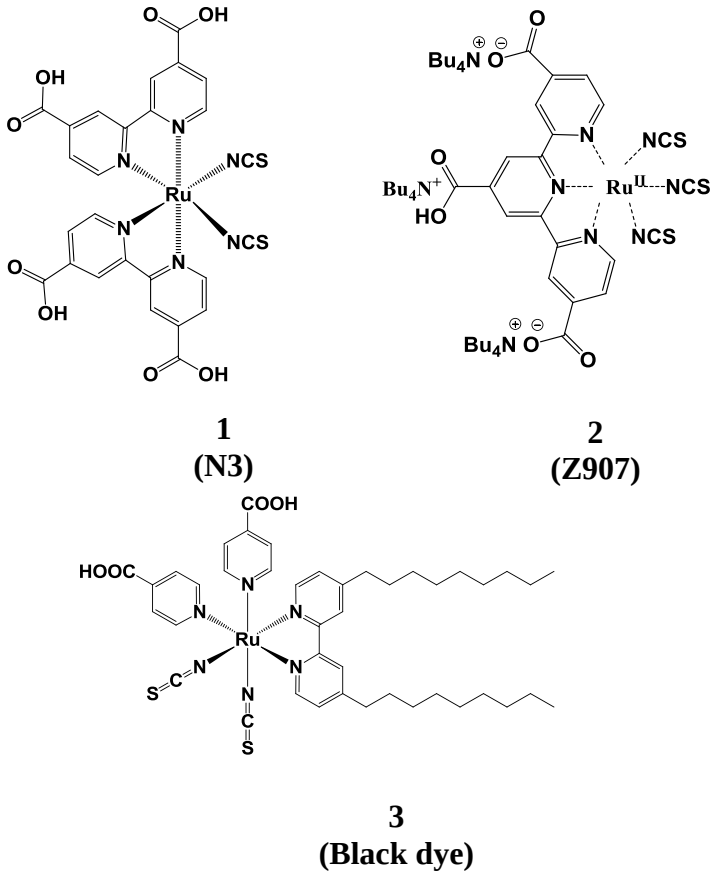

Figure 2.7: Molecular structures of Ru dyes- N3, N749 (Black dye) and Z907.

It had been thought to change the ligands of Ru complexes and thus optimize the efficiency of photosensitizers. In order to extend the spectral response region of the sensitizer to the near-IR region, Grätzel and co-workers designed the N749 dye [146], also called the "black dye" (3). In this dye, one of the thiocyanate ligands of N3 dye was replaced by one terpyridine ligand with three carboxyl groups. This dye gave an efficiency of 10.4 % under AM1.5 [147]. Later an amphiphilic heteroleptic ruthenium sensitizer (Z907) (2) was synthesized by the same group, which demonstrated high thermal stability due to the introduction of two hydrophobic alkyl chains on the bipyridyl ligand [148] (Figure 2.7).

Even though ruthenium (II) complexes are found to be good in terms of power conversion efficiency, their broad utility in the manufacturing of prototype DSSCs panels is prohibited due to some drawbacks. Ruthenium sensitizers are very expensive due to the rarity of the metal and several difficult synthetic protocols. Lack of absorption and lower molar extinction coefficients in the red region of the absorption spectrum limit their use in thin film devices. In order to overcome these problems, a great variety of alternative sensitizers has been considered for the last two decades based on non-ruthenium metal complexes. Many attempts have also been made to construct sensitizers with other metal ions, such as Os, Re, Fe, Pt and Cu [149-153]. Osmium (Os) complexes are found to be promising photosensitizers due to the prominent MLCT absorption band in comparison to the Ru complex (Figure 2.8). Tetrapyrrolic compounds which include porphyrins, phthalocyanines and corroles [154, 155] are also explored.

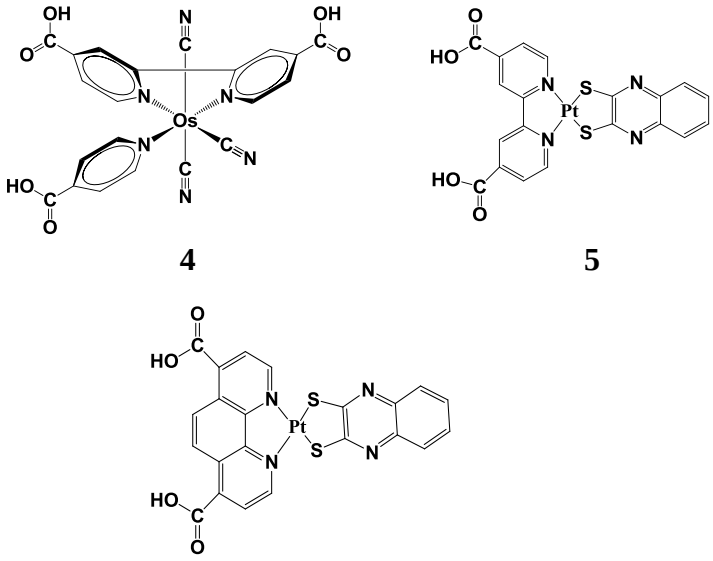

Figure 2.8: Molecular structures of Os and Pt based metal dyes.

Phthalocyanines (Pcs) are tetrapyrrolic cyclic aromatic (18-π electron) organic molecules, demonstrated the thermal and electronic properties, suitable for the sensitization of wide band-gap semiconductor oxides such as TiO_2, SnO_2. The optical, thermal and physical properties of Pcs can be tuned in various ways. Different substituents can be introduced at peripheral, nonperipheral positions as well as at its central cavity. In 1999, for the first time, Nazeeruddin *et.al.* reported zinc(II) (Dye 7 and 9) and aluminium(III) (Dye 8 and 10) symmetrical Pcs bearing carboxylic acid and sulfonic acid anchoring groups to facilitate proper adsorption on to the TiO_2 surface [156] (Figure 2.9).

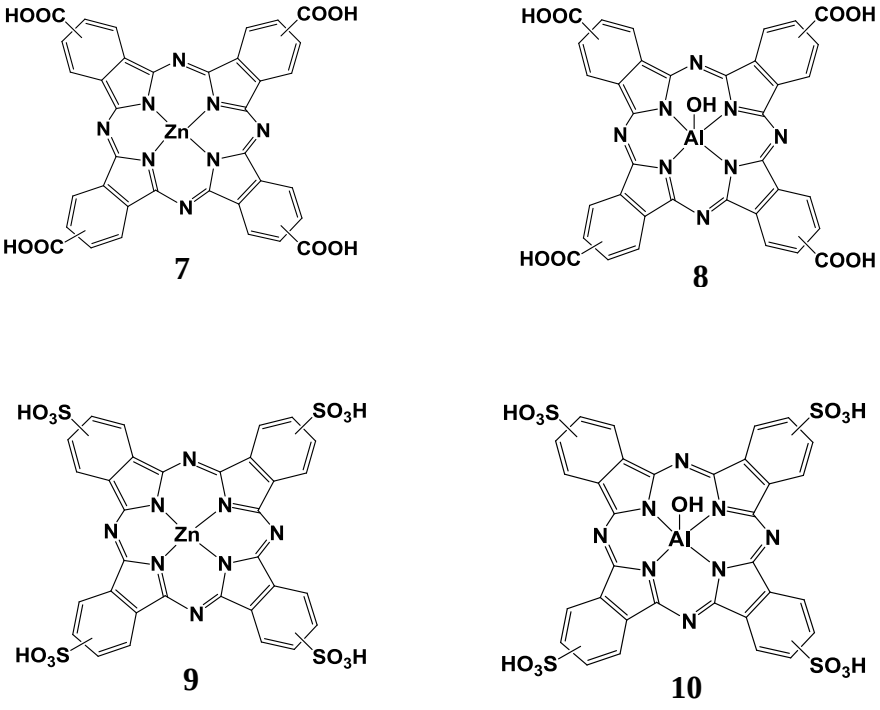

Figure 2.9: Molecular structures of Zn and Al based symmetrical Pcs dyes.

Among these dyes zinc(II) tetracarboxy phthalocyanine showed maximum overall power conversion efficiency of 1% and the IPCE values are between 10% and 45%. The low efficiencies of these Pcs were attributed to deactivation of the excited Pc because of their high aggregation originated from the planar configuration. Since then many efforts appeared in the literature which deal with reducing the aggregation and thereby increasing the efficiency. A few hyper-branched zinc(II) phthalocyanines have also been synthesized and nearly 67% IPCE was observed, but their overall power conversion efficiencies are still restricted to 1% [157]. The main reason for the low performance of these Pc-based DSSC was found to be due to aggregation which promotes nonradiative deactivation of the dye excited states in aggregates. Later He *et.al.* [158] reported a zinc(II) phthalocyanine bearing tyrosine substituents (Dye 11) in order to increase solubility and to reduce aggregation at the semiconductor surface (Figure 2.10).

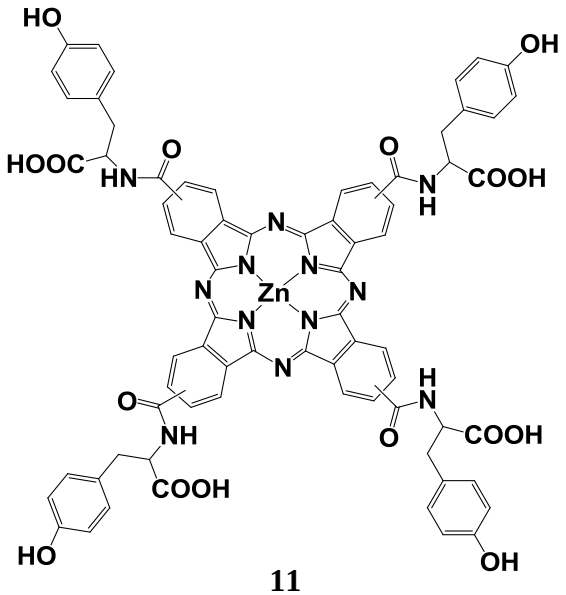

11

Figure 2.10: Molecular structures of Zinc(II) phthalocyanine bearing tyrosine dye.

Torres and Nazeeruddin have developed conjugated panchromatic sensitizers by covalently attaching an organic chromophore at three positions in which triarylamine-terminated bisthiophene units and hexylbisthiophene units are attached. These sensitizers have shown only 40% IPCE and around 3% overall conversion efficiency by using a co-adsorbent. The reduced efficiencies of these dyes have been assigned to the aggregation and poor electron injection efficiencies. Recently, Giribabu, Filippo, Nazeeruddin and co-workers have reported new sterically hindered phthalocyanines based on methoxy substituents having different patterns [159].

The first sensitizer with the phosphonic acid anchoring group was a ruthenium terpyridyl complex coded as Z955 (12) that showed IPCE values up to 70% and the highest efficiency of around 8% [160] (Figure 2.11).

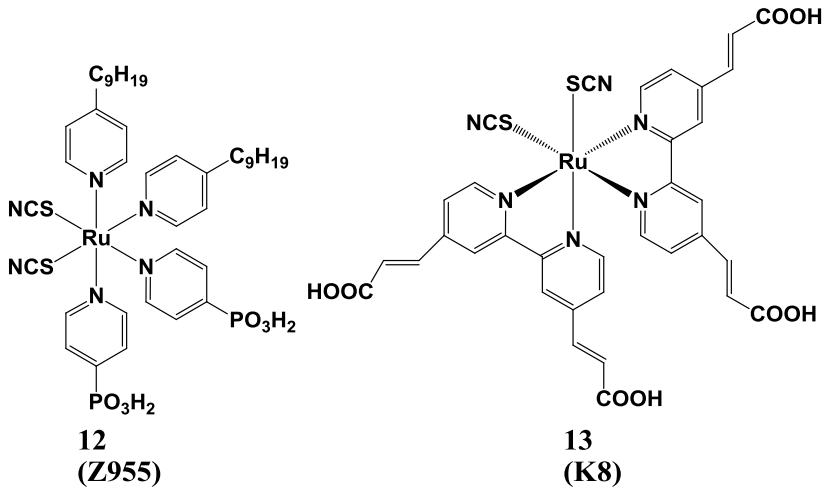

Figure 2.11: Molecular structures of Z955 and K8 dyes.

Recently, Klein *et.al.* have accomplished to fine-tune the spectroscopic properties of ruthenium polypyridyl complexes by incorporating a novel ligand, 4,4'-bis(carboxyvinyl)-2, 2'-bipyridine in ruthenium(II) complex [$RuL_2(NCS)_2$] (K8 (13), Figure 2.11) [161] with higher molar extinction coefficient increased by 30% compared to the star sensitizer N3. A high conversion efficiency of over 9% was recorded for the DSSC based on the K-73 (14) sensitizer (Figure 2.12) with a nonvolatile electrolyte [162]. The K-19 (15) (Figure 2.12) based DSSC in combination with the binary ionic liquid electrolyte exhibited a conversion efficiency of 7.1% but a better thermal stability than the K-73 dye [163]. Reason could be its better adsorption on TiO_2 film which was strengthened in the presence of the long alkyl chains and the presence of nonvolatile electrolyte.

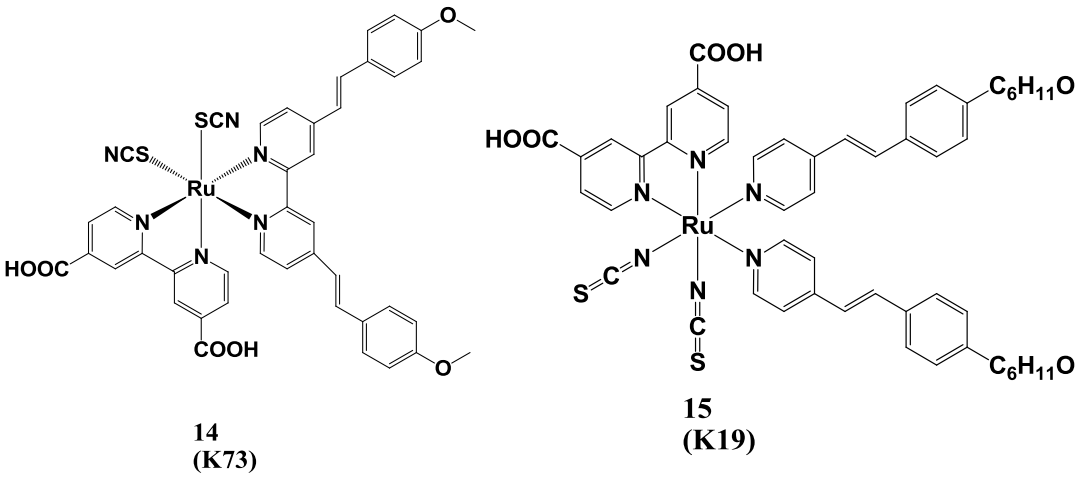

Figure 2.12: Molecular structures of K73 and K19 dyes.

Some hetero-supramolecular systems like binuclear ruthenium and osmium containing polypyridyl complexes [164] (Figure 2.13), TiO_2-Re-Ru [165], TiO_2-Rh-Ru [166] (dye 16, 17) were employed to study the interfacial and intramolecular electron transfer

process. Much work has been done towards the optimization of the performance of the cells for the commercial application in the near future.

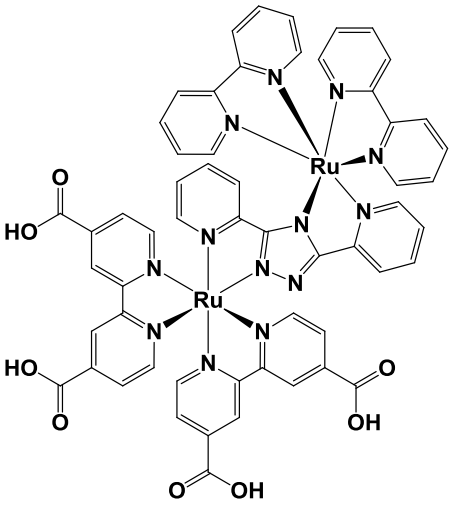

16

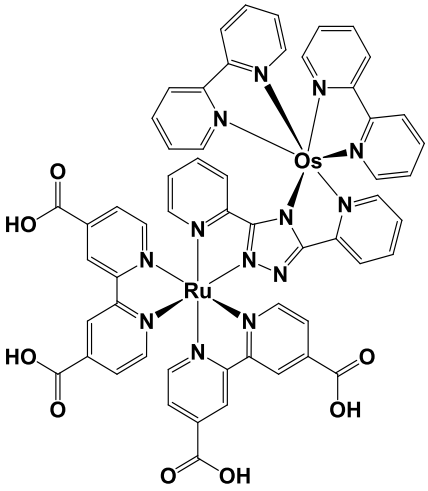

17

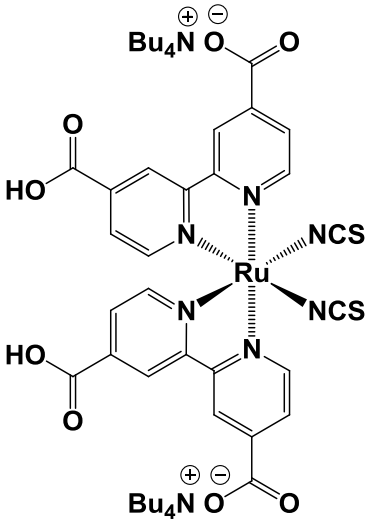

18
(N-719)

Figure 2.13: Molecular structures of Ru-Ru (16), Ru-Os (17) binuclear complexes containing the bridging ligand 3, 5-bis-(pyridin-2-yl)-1,2,4-triazole and N719 (18).

Although the well established Ru complexes N3, N719, "black dye" exhibit high efficiencies in the standard dye-sensitized solar cell with an I^-/I_3^- solution electrolyte, there are still some limits for the massive production.

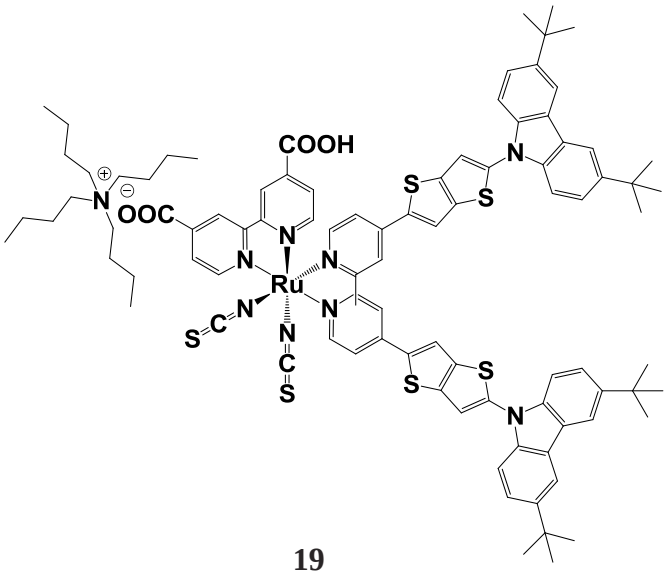

19

Figure 2.14: Molecular structures of heteroleptic ruthenium complex composed of sequential associations of a thienothiophene conjugated bridge and carbazole moiety.

Chen *et.al.* synthesized a new heteroleptic ruthenium complex, 19 (Figure 2.14) [167], which consists of an antenna ligand composed of sequential associations of a thienothiophene conjugated bridge and carbazole hole-transport moiety. A lower energy MLCT band centered at 555 nm as well as a high molar extinction coefficient of 2.24-104 $M^{-1}cm^{-1}$ was exhibited by this new sensitizer. In presence of high volatile electrolyte the DSSC with dye 19 demonstrated a high photovoltaic efficiency of 9.4% under an illumination of standard global AM1.5G sunlight. With a low-volatile electrolyte, the DSSC

did not only show a high efficiency of 8.2% but also an excellent stability for 1000 h in a simulated sunlight under light soaking at 60°C.

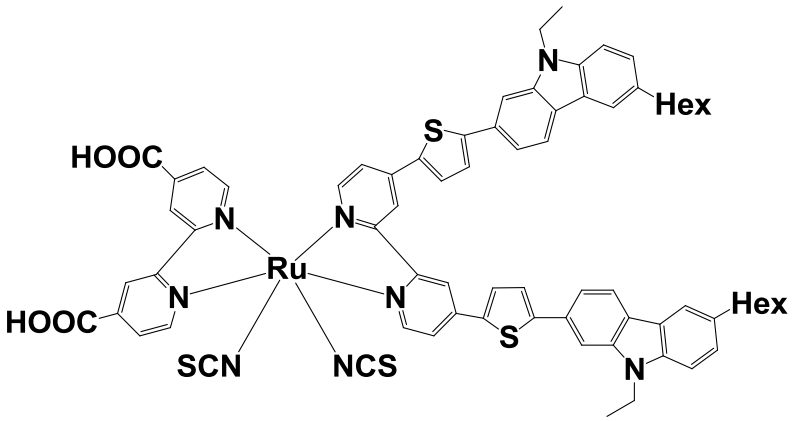

20

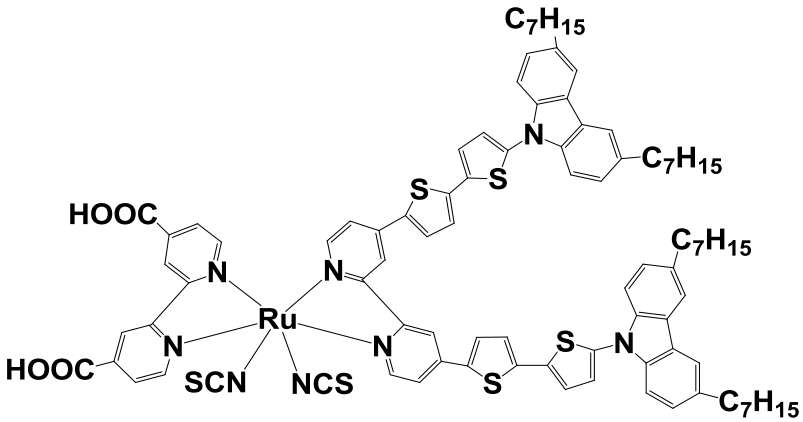

21

Figure 2.15: Ru-based dyes with carbazole donors and thiophene spacer.

Fan *et.al*. has reported a new heteroleptic Ru(II) complex 20 (Figure 2.15) and was compared with its carbazole free parent complexes. It showed a short-circuit photocurrent d. of 19.2 mA cm^{-2}, an open-circuit photovoltage of 630 mV, a fill factor of 57.7% and conversion efficiency of 6.98% which was much higher than its parent complexes that generated efficiency as 2.48% and 6.47%, respectively [168]. Later Fan *et.al*. made

modifications in dye 20 and developed a Ru-complex 21 with an ancillary bipyridyl ligand substituted by a 3-carbazole-2-thiophenyl moiety for DSSC applications. When the dye 21 loaded electrode was co-sensitized by JK-62 dye, a significant improvement in efficiency of up to 10.2% was achieved, which was superior to that (~8.68%) of N719 with the same device configurations [169].

2.8.2 Organic dyes

2.8.2.1 Basic skeleton

An organic dye has a basic skeleton of D-π-A, where "D" stands for donor, which is an electron rich moiety; "A" denotes acceptor which is an electron deficient component and π is a conjugation linker which coordinates between donor and acceptor units in order to facilitate the charge transfer. An add-on to the acceptor is the anchoring group which stabilizes the dye molecule on to the TiO_2 surface. Electrons are directed from donor to acceptor via π linker and injected into the conduction band of TiO_2 followed by the circulation to the external circuit and power generation. Since a dye molecule is the opening spot for the procedure of electron initialization and circulation, it is considered to be the most crucial element in a DSSC.

Figure 2.16: Basic skeleton of organic dye.

The arrangement of all the components in a dye molecule is clear from the schematic diagram of dye in Figure 2.16. Since properties of all elements in a dye separately as well as

collectively contribute to overall performance of a DSSC, molecular engineering plays a crucial role. From chemical synthesis point of view, there are different mechanisms which lead to the synthesis of desired molecule. To name a few, there are coupling reactions i.e. Stille coupling, Suzuki coupling, Heck coupling etc., condensation reaction such as Knoevanegal reaction and other chemical reactions i.e. bromination, formylation etc direct the synthesis of a dye molecule in several steps. By varying the numbers and arrangements of donor which pushes the electrons, acceptor which pulls the electrons and π linker which coordinates the electrons, the structural modifications can be achieved. Depending upon the conjunction of donor and acceptor units, the mechanism of charge transfer in a dye molecule can be of several types such as push-push-pull, push-pull-pull, pull-push-pull, pull-push-push-pull.

Organic dyes based on electron rich donor moieties i.e. triphenylamine, coumarin, merocyanine, indoline, fluorine and carbazole [170-173], has been studied vastly. Thiophene, bi-thiophene, phenyl groups are most commonly used in π-bridge as these groups consist of good conjugation which facilitates electron transfer. Since the π-bridge is the channel through which electrons shift from donor to acceptor, it should have a (quasi) planar geometry for efficient electron transfer. Several standard acceptors, such as carboxylic acid, phosphonic acid, cyano-acrylic acid, rhodanine acetic acid, and benzothiadiazolyl cyanoacrylic acid are used in dye molecules. However, mostly used anchoring unit is cyano acrylic acid due to its relatively good stability as an anchoring unit [174]. The effect of different acceptor units and π-linker is also studied. In some cases donor moieties are used as a π-linker as well.

2.8.2.2 Molecular engineering

Organic dyes have several benefits over the metal complexes, such as lower material costs, elimination of environmental issues, larger molar extinction coefficient, and infinite flexibility in molecular design [175]. However, there are some disadvantages which have to be overcome for practical application of organic sensitizers, such as shorter exciton lifetimes in their excited states, the tendency to aggregate, and a relatively narrow absorption in the visible region [176, 177]. A lot has been done in order to modulate organic dye molecules so that they are efficient enough to be used at the level of commercialization. There are some important aspects of DSSC such as absorption in visible region, electron injection to conduction band, dye regeneration, recombination resistance, open circuit voltage (V_{oc}), long term stability etc which are directly connected to the design of dye molecule and have major impact on the overall performance of the DSSCs. Hence the designing of the dye molecule should be done considering all the aspects.

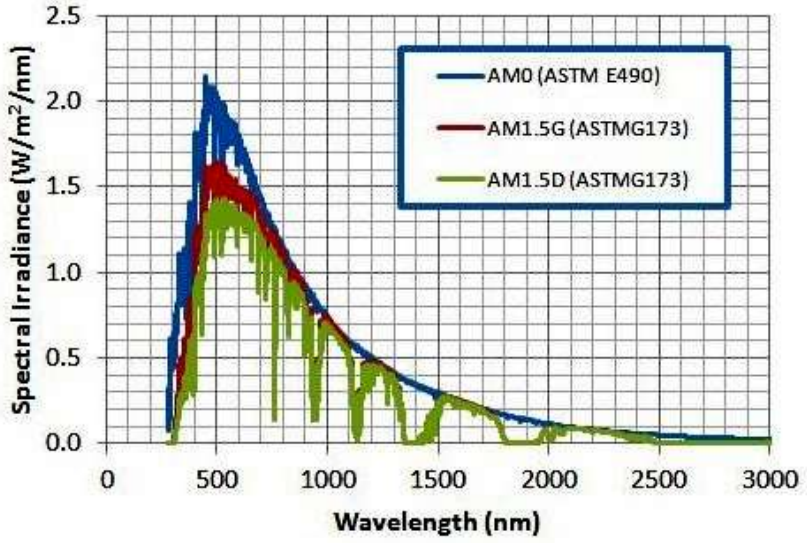

Figure 2.17: Solar irradiance spectra of (a) AM 0 and (b) AM 1.5.

The fundamental condition for photovoltaic energy conversion is directly related to the collection of as much sunlight as possible. The photon flux density indicates the number of photons that can excite ground-state electrons with corresponding energy at the particular wavelength. The highest photon flux region stands around 600 to 800 nm [178] (Figure 2.17).

It is desirable that a dye absorption range to match the high photon flux region of the solar spectrum in order to harvest major part of it which can be done by tailoring the optical band-gap of dyes. Since the absorption band of π-conjugated materials originates from the degree of interaction between π orbital, the extension of the effective conjugation length is one of the common tools to tailor the absorption range of the organic dyes. Tuning of absorption band can also be achieved by D-A structure induced intramolecular charge transfer (ICT), which facilitates π-orbital overlap via the quinoid resonance structure and consequently produces red shift absorption of the dye [179].

In the presence of a strong electron withdrawing group at the proximity of the anchoring moiety, the electron-injection efficiency from the excited dye into TiO_2 suffers drastically due to the charge entrapment effect around the withdrawing group [180]. It has been learned in a recent study that addition if a π-bridge between the electron-withdrawing and anchoring groups prevents the back-electron transfer of the charge-separated state, resulting in slow recombination between TiO_2 and dye [181]. Though the driving force for the electron injection depends upon the energy-level difference between the excited state of dye molecule and conduction band of the semiconducting oxides, yet the molecular orientation and spatial arrangement of dyes cannot be overlooked. It has been observed that the elongation of π-bridge hampers the electron injection owing to the π-stacked aggregation

(*H*-aggregation) through the formation of intermolecular π-π interactions between dye molecules [182]. Design strategy adopted to suppress dye aggregation is to introduce sterically hindered groups, such as a bulky side chain and starburst triarylamines, on the edges of the donor part and on a π-conjugated bridge. Electron injection efficiency is also found to be affected by the shape and geometry of the dye molecule. The asymmetric D-A structure which favors unidirectional flow of electron, is advantageous over symmetric structure. It is seen that asymmetric squaraine dyes exhibit much higher photocurrent than analogous symmetrical squaraine dyes owing to the unidirectional flow of electrons [183].

Exciton binding energy (EBE) is yet another important factor to affect the electron-injection efficiency of organic dyes which is influenced by the geometry of the conjugated molecule. Normally the EBE decreases as the conjugation extends [184] and better energy conversion efficiency is achieved. By tuning conjugation length, chain conformation, and functional groups the energy levels of organic dyes are easily optimized to be best suited for efficient electron generation and dye regeneration.

In DSSC two types of recombination takes place i.e. inner path recombination that occurs between dye cation and the electron in the CB of TiO_2 and outer path recombination between semiconductor oxide and electrolyte. To eliminate the possibility of inner recombination it is very important for the dye cation to be away from oxide layer. Therefore, the vertical arrangement of the dye on TiO_2 surface is preferred which can be achieved by the cyanoacrylic acid as an anchoring group rather than rhodanin acetic acid [185]. To suppress outer path recombination, the strategy of making TiO_2 surface hydrophobic works well. Since electrolytes are hydrophyllic in nature they tend to penetrate into the TiO_2. By introducing hydrophobic alkyle chains into the dye framework can prevent the electrolyte

approaching the TiO_2. While the suppression of charge recombination results in enhanced V_{oc} and elongated electron lifetime [186, 187], introduction of hydrophobic chains also suppress the water induced dye desorption [188].

Long term stability of DSSC is the prime focus of researchers. The presence of certain groups can provide enough chemical stability to the dye. It has been demonstrated that the organic dyes consisting of thiophene and perilene groups exhibit more stability than their counterparts [189, 190]. However, stability is proved to increase with the dye structure D-A-π-A, which has one additional acceptor group [191]. For long term stability of DSSC only chemical strength of the dye is not sufficient enough, it should be firmly attached to TiO_2 surface in order to avoid desorption in presence of electrolyte. Carboxylic acids used as anchoring unit fulfill other criteria for higher efficiency but the bidentate bridge formed by them on the TiO_2 surface can be easily hydrolyzed by water and dye desorption occurs. Recently it has been demonstrated that trialkoxysilane, $Si(OR)_3$ forms firmer link to TiO_2 and the bond between dye and TiO_2 surface remains intact [192].

2.8.2.3 Organic dyes: State of art

For the first time Tian and co-workers have introduced thiophene as π-conjugation between a donor TPA unit and an acceptor anchoring group and reported three new sensitizers (22-24) for DSSC applications [193] (Figure 2.18).

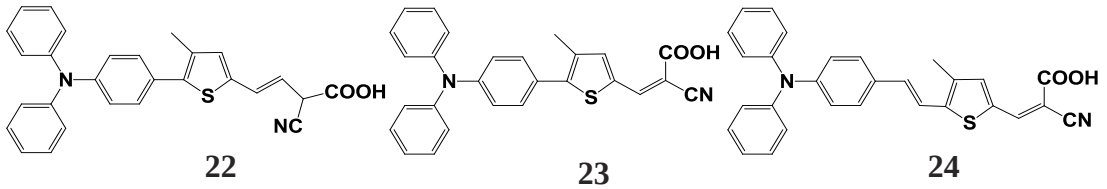

Figure 2.18: Molecular structures of TPA based D-π-A dyes.

Cheng *et.al.* developed a series of dyes (28-34) different from traditional D-π-A sensitizers where traditionally used cyanoacrylic acid anchoring group was replaced by pyridinium [194] (Figure 2.19). The tuning of HOMO and LUMO was achieved by varying the conjugation units and the donating ability of the donor part. The absorption peaks were red shifted in visible spectra on substitution of the methoxyl and n-hexoxyl into 25 to construct dyes 26 and 27.

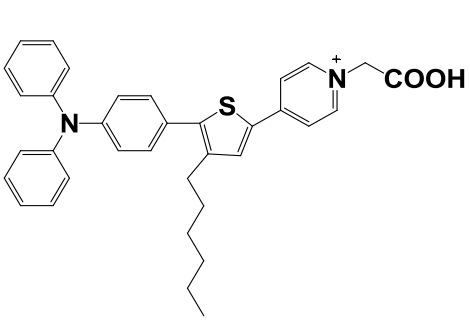

25

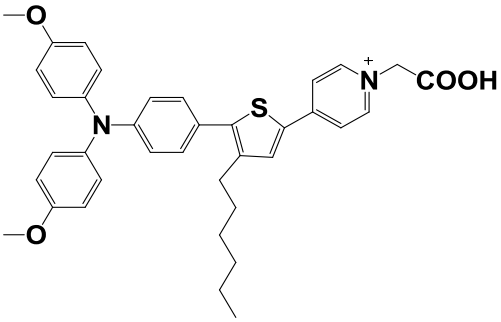

26

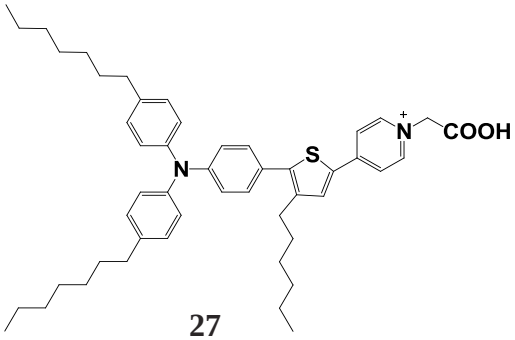

27

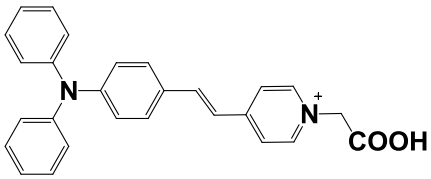

28

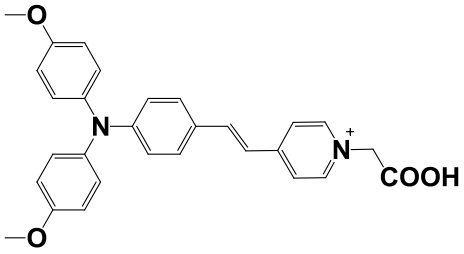

29

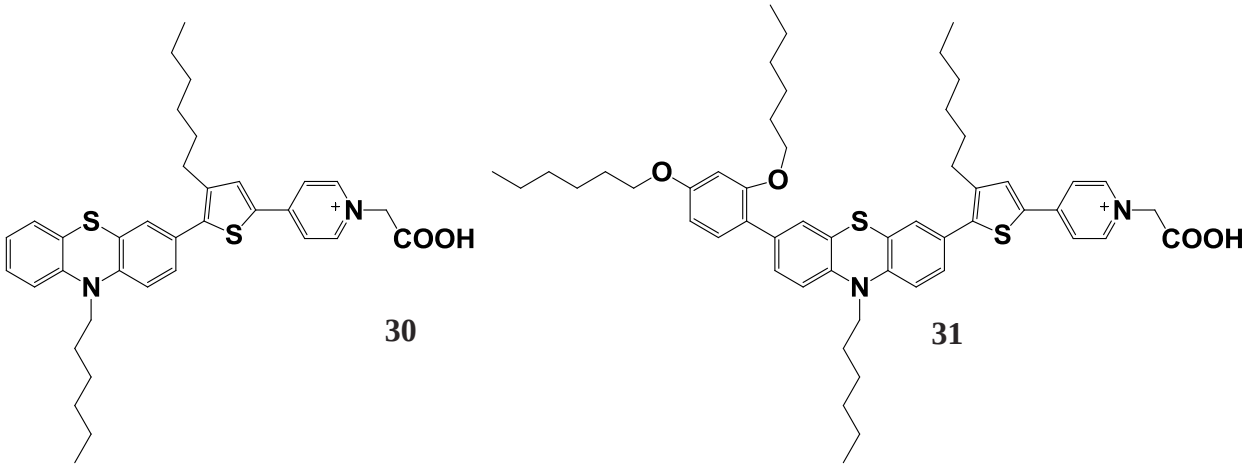

Figure 2.19: Molecular structures of TPA based D- π-A dyes with pyridinium.

J_{sc} and V_{oc} of the devices fabricated with sensitizers 26 and 27 were higher than those of the device sensitized by sensitizer 25, which was mainly attributed to the broader IPCE response and the inhibition of electron recombination between TiO_2 film and electrolyte, respectively. In this series the DSSCs fabricated by phenothiazine (PTZ) electron-donating unit gave a promising efficiency. The effects of different electron donors in DSSCs application are compared, and the results show that sensitizers with a phenothiazine (PTZ) electron-donating unit give a promising efficiency of 7.1% (J_{sc} = 13.6 mA·cm^{-2}, V_{oc} = 710 mV, FF = 73.6%) under AM 1.5G irradiation (100 mW·cm^{-2}) which was more than that of TPA based DSSCs. This study maintained the stronger electron donating ability of phenothiazine than that of TPA.

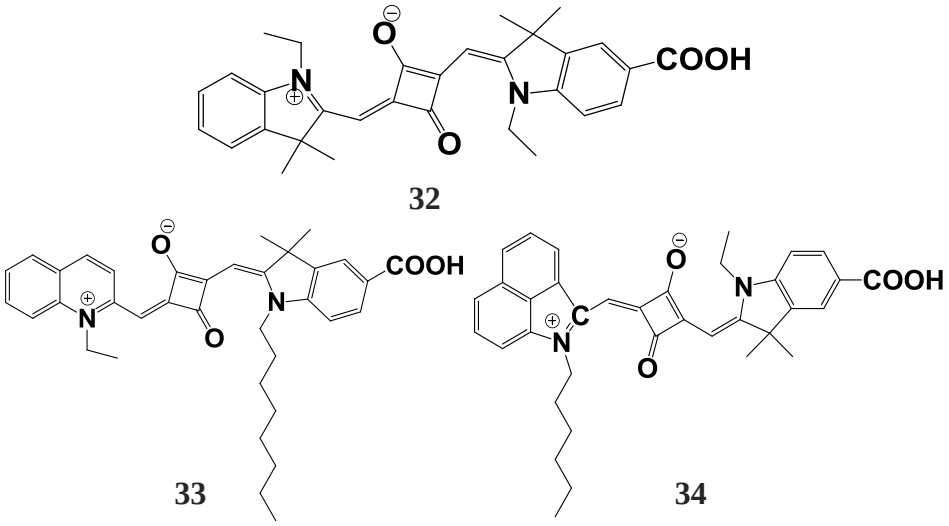

Figure 2.20: Molecular structures of unsymmetrical squaraine dyes.

Aiming towards the far-red to near infra-red (NIR) photon harvesting, a series of three new unsymmetrical squaraine dyes (32-34) were synthesized by Pandey *et.al.* [195] (Figure 2.20). The highest efficiency observed in the DSSCs fabricated by these dyes was 3.3%. The efficiency decreased on elongation of conjugated bridge which was explained on the basis of increased dye aggregation along with its difficulty in facile electron injection as indicated from electronic absorption spectroscopic and DFT calculation results.

Wang and co-workers have further extended this work and introduced more thiophene units in π-bridge [196-198]. Thienothiophene and bisthienothiophene were introduced between an alkoxy TPA moiety and an acceptor anchoring group, this resulted in the novel structures, 35 and 36 [198] (Figure 2.21). An enhanced molar extinction coefficient was observed in both the cases. The overall conversion efficiencies of both 35 and 36 were shown to be 8.02 and 7.5%, respectively.

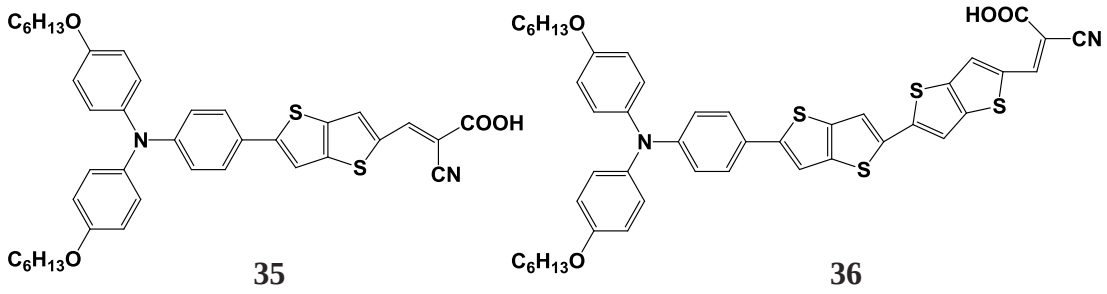

Figure 2.21: Molecular structures of TPA dyes with thienothiophene and bisthienothiophene linkers.

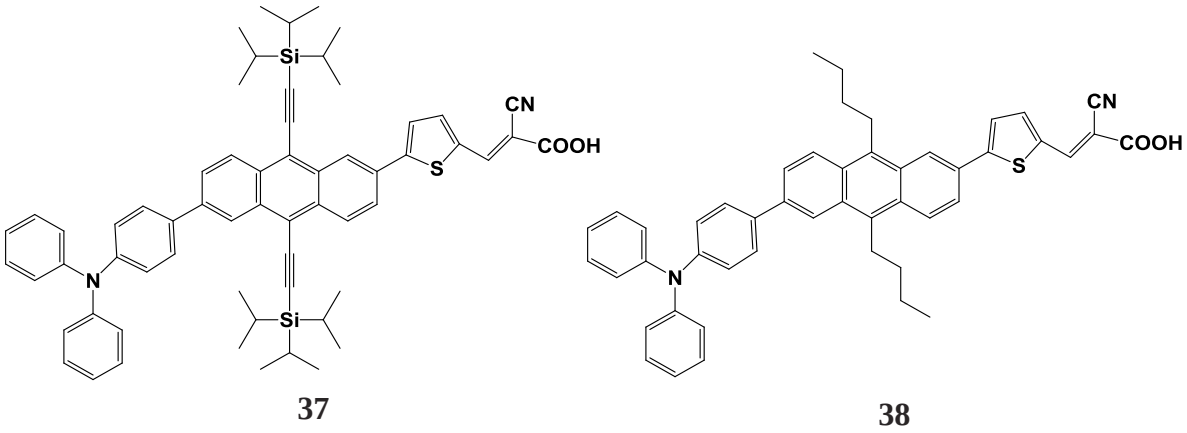

Figure 2.22: Molecular structures of TPA dyes with anthracene moiety in linker.

In a recent study by Lin *et.al.,* organic dyes (37, 38) consisting of an anthracene moiety as a linker between triphenylamine donor group and a cyanoacrylic acid acceptor group showed very promising current conversion efficiency and displayed remarkable solar-to-energy conversion efficiency in dyesensitized solar cells [199] (Figure 2.22). DSSCs made with the dye 38 displayed maximal photon-to-current conversion efficiency (IPCE) 65% in the region of 350-510 nm. Performance resulted in a short-circuit photocurrent density (J_{sc}) 12.78 mA cm^{-2}, an open-circuit photovoltage (V_{oc}) 0.73 V, and a fill factor (*FF*) 0.67,

corresponding to an overall conversion efficiency 6.23%. It was deduced that the planar geometry of anthracene improved the charge transfer and its bulky substituents aided in the dye aggregation on TiO_2 film.

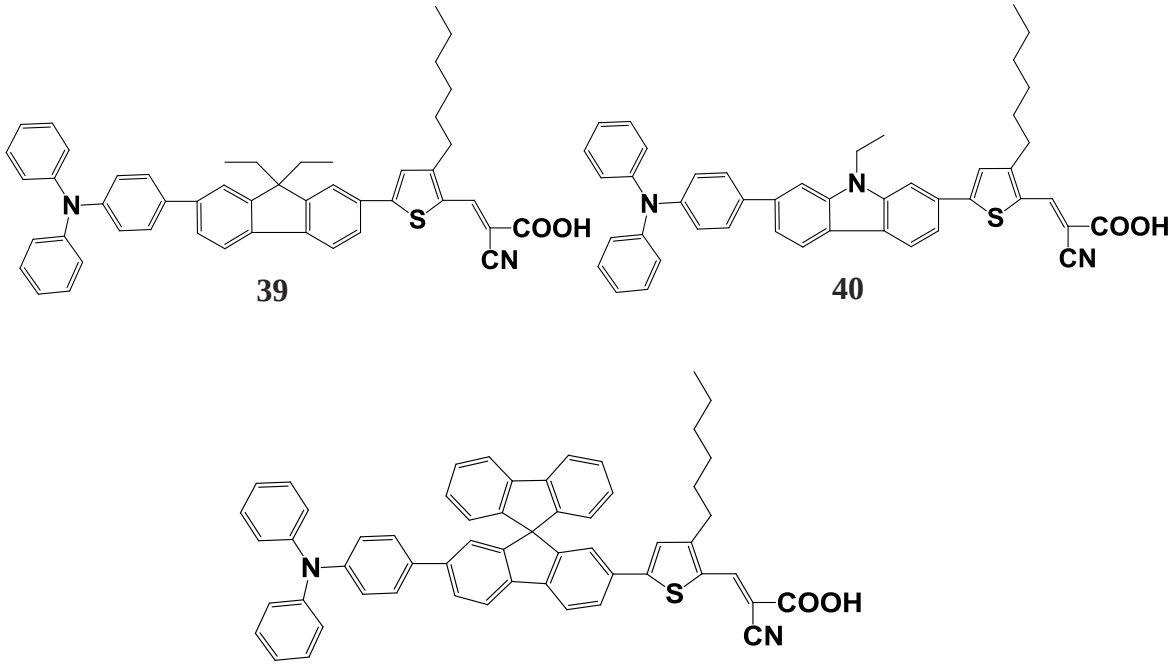

Figure 2.23: Molecular structures of dyes with D-D-π-A skeleton.

Tan and co-workers reported a series of metal free dyes (39-41) with D-D-π-A skeleton featuring carbazole, fluorene and spirobifluorene moieties, apart from the blocks of a triphenylamine as an electron donor [200]. These additional moieties work as secondary donor which enhance the electron density of TPA and results in high IPCE of 73% with an overall conversion efficiency of 7.03% of the devices made by dye 39 (Figure 2.23).

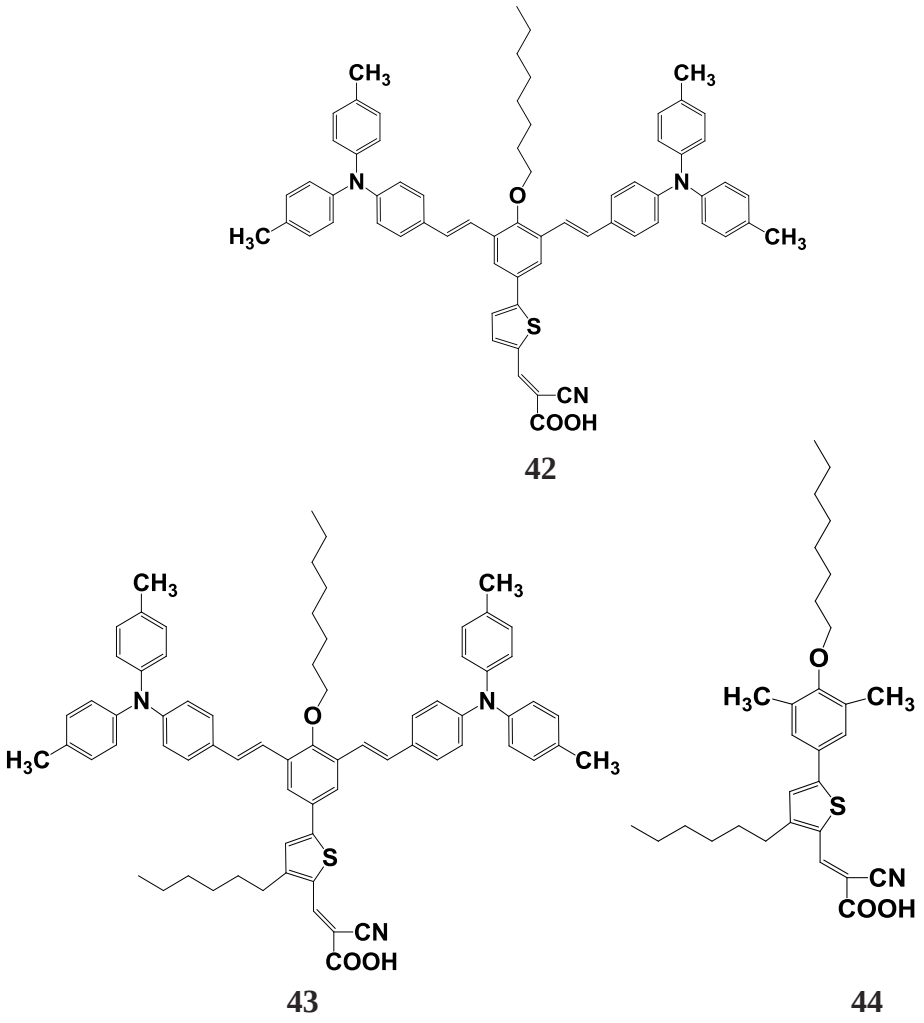

Figure 2.24: Molecular structures of branchlike organic dyes.

In order to explore the effect of incorporation of branching in D-π-A dyes, Chen *et.al.* synthesized two novel branchlike organic dyes (42 and 44) [201] comprising two di(*p*-toyl)phenylamine moieties as the electron donor, cyanoacetic acid moieties as the electron acceptor, thiophene or 3-hexylthiophene moieties as the π-linkers (Figure 2.24). The performance of these dyes was compared with a similar dye 44 with no branching in the structure. It was observed that the charge recombination was effectively retarded between

electrons at TiO_2 and the oxidized dyes in the DSSCs fabricated by dyes 42 and 43 in comparison with 44, due to sufficiently branched structures of dyes 42 and 43. The overall efficiency of 6.41% with high dye J_{sc} of 11.62 mA cm^{-2}, V_{oc} of 0.73 V and *FF* of 0.75 was obtained.

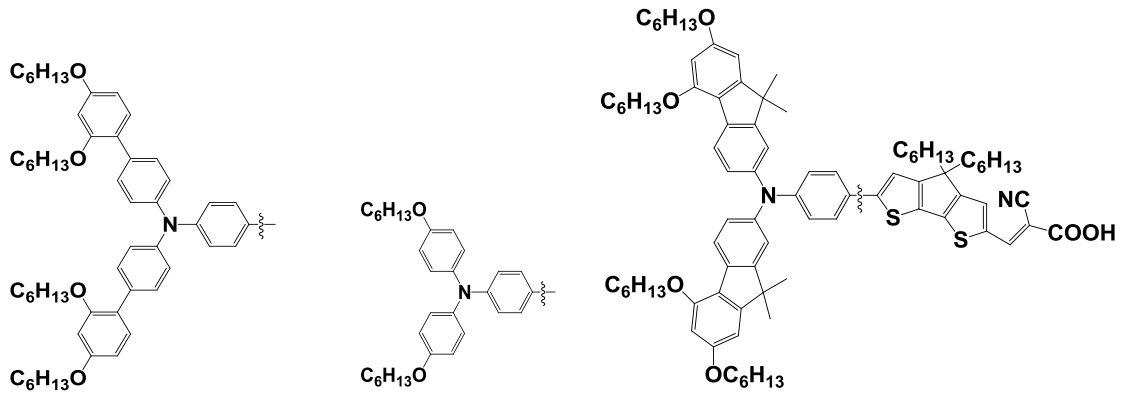

Figure 2.25: Molecular structures of TPA dyes with variation in donor group.

Yella *et.al.* [202] demonstrated a novel designing principle established by incorporating alkoxy substituted flourene donor moieties linked to cyanoacrylic acid acceptor via flourene linker with long alkyl chains (45-47) (Figure 2.25). Furthermore, on comparison with its analogous dyes, 47 showed nearly quantitative regeneration efficiency. It could be highlighted through transient absorption spectroscopy and quantum chemical calculations that the hole delocalization force is much higher in photo-oxidized dye (47). The DSSC based on dye 50 displayed a high efficiency of 10.3% with cobalt-based liquid electrolyte.

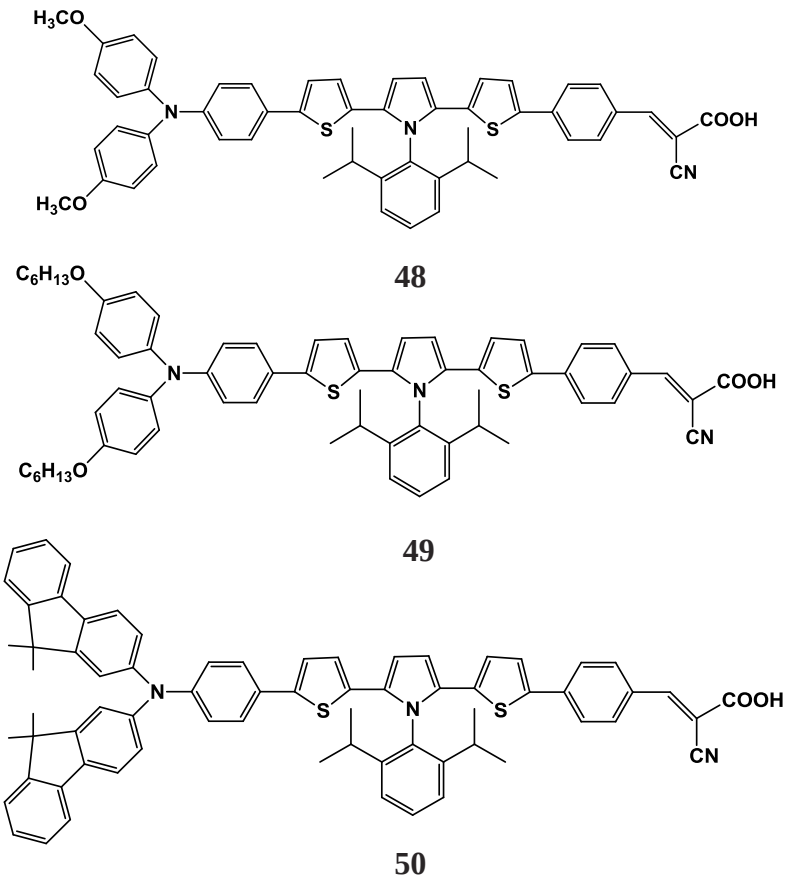

Figure 2.26: Molecular structures of organic dyes based on 1-(2, 6-diisopropylphenyl)-2, 5-di(2-thienyl)pyrrole.

In this study Tamilavan *et.al.* synthesized D-π-A and D-π-A-π-D structured organic dyes (48-50) based on 1-(2, 6-diisopropylphenyl)-2, 5-di(2-thienyl)pyrrole [203] (Figure 2.26). Three different non planar electron donor groups such as methoxy or hexyloxy substituted triphenylamine and difluorenephenylamine were introduced. The aim was to see the effect of electron donor groups on the opto-electrical properties and in dye-sensitized solar cells (DSSC). All three dyes covered a wide range of visible spectrum, i.e. 300 nm-600 nm. The DSSCs fabricated from only sensitizer gave the efficiencies of 5.28% and 5.42% while those with co-adsorbent were observed 5.58% and 5.63%, respectively.

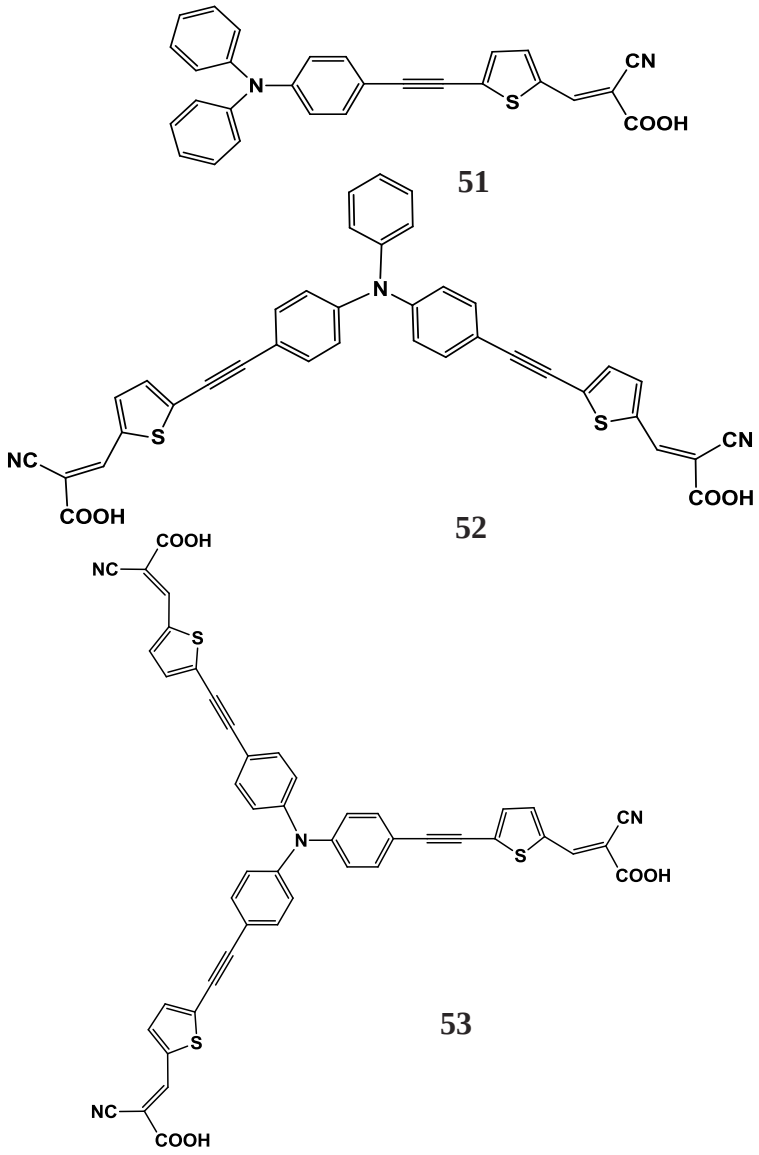

Figure 2.27: Molecular structures of dyes with different number of anchoring groups.

Mba *et.al.* reported a series of triphenyl amine based dyes (51-53) with different numbers of anchoring groups [204] (Figure 2.27). The DSSC analyses were carried out in association with different cobalt based mediators. The study revealed that the adsorption stability of dye onto TiO_2 improved due to the presence of multiple anchoring points on the

dye structure but induced a pseudoplanar adsorption geometry which enhanced the electron recombination due to improper insulation of the surface.

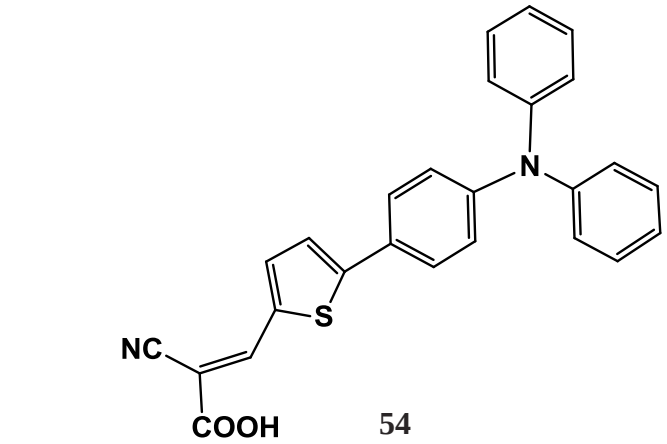

54

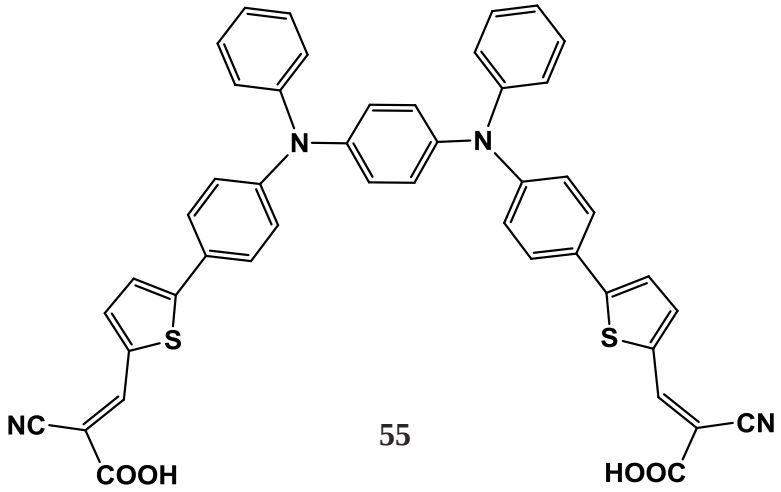

55

Figure 2.28: Molecular structures of monoanchoring dye and its bridged form.

Sirohi *et.al.* studied the effect of bridging of two mono-anchoring dye molecules (54, 55) to give a new di-anchoring bis-merocyanine dye [205] (Figure 2.28). It was observed that the joining of the two molecules efficiently reduce the aggregation on TiO_2 film due to

its non planar configuration. The DSSC based on the bis-merocyanine dye exhibited enhanced power conversion efficiency of 6.1%.

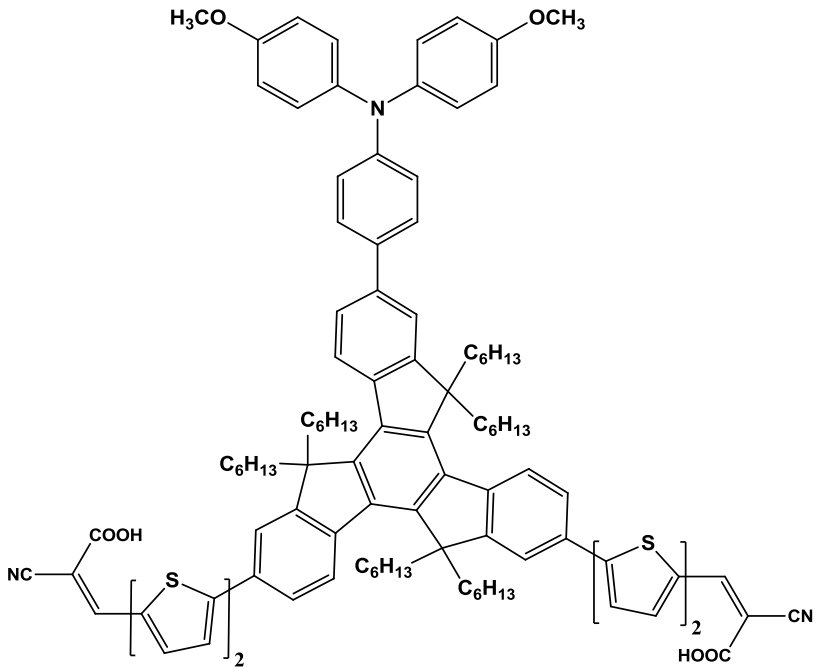

56

Figure 2.29: Molecular structures of D-π-2A organic dye.

Yu *et.al.* synthesized and applied a novel D-π-2A organic dye (56) based on TPA as donor moiety, fused flourene in π-bridge and cyanoacrylic acid as acceptor units [206] (Figure 2.29). Although a lot of work has been reported on D-π-A organic dyes, new trend is developing in order to exploit the presence of more anchoring groups. A maximum monochromatic incident photon-to-current efficiency (IPCE) produced by DSSC based on 56 was 68% at 425 nm with an overall efficiency of 3.62% was achieved.

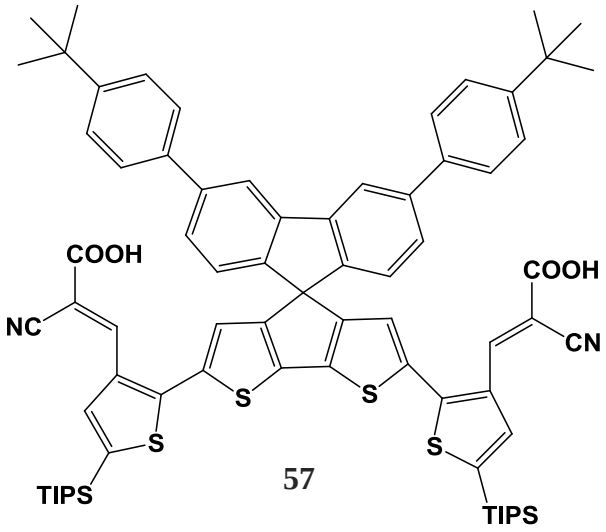

Figure 2.30: Molecular structures of organic dye with cross linking spiro architecture.

Ting *et.al.* presented a smart molecular structure of organic dye (57) for DSSCs with cross linking spiro structure, bulky donor units and dianchoring function [207] (Figure 2.30). The molecular design exhibited favorable influence on reducing the aggregation and achieving a high power conversion efficiency of 6.52% in DSSC.

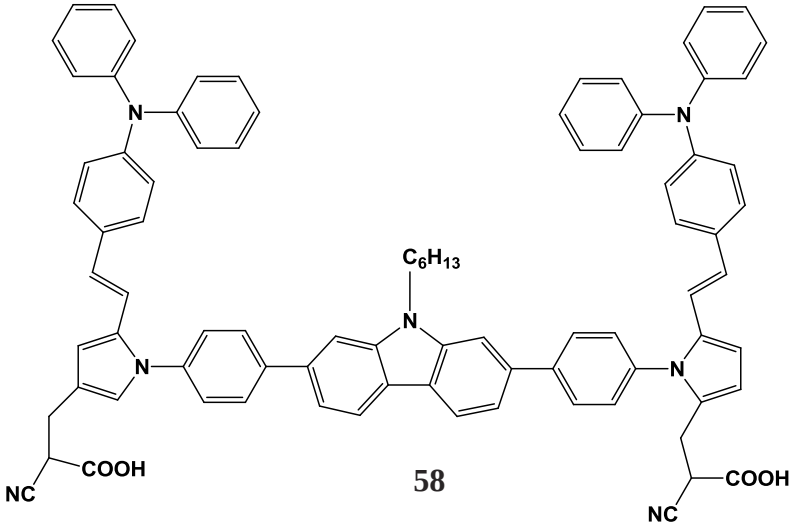

Figure 2.31: Molecular structures of H-type dye.

More recently, H-type dye sensitizers (58) have been reported by Li *et.al.* (Figure 2.31), bearing triphenylamine as donor, *N*-arylpyrrole as conjugated bridge and cyanoacetic acid as acceptor [208] which has a conversion efficiency of 5.22%. It was observed that the photovoltaic performance was not significantly improved with co-adsorbents such as chenodeoxycholic acid, which indicates that these H-type sensitizers did not aggregate on TiO_2 surfaces.

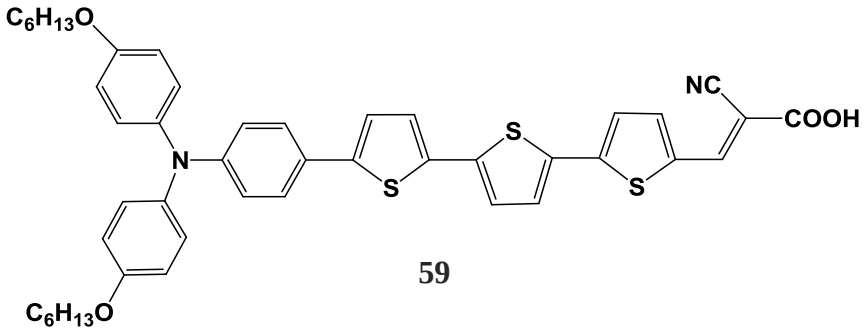

59

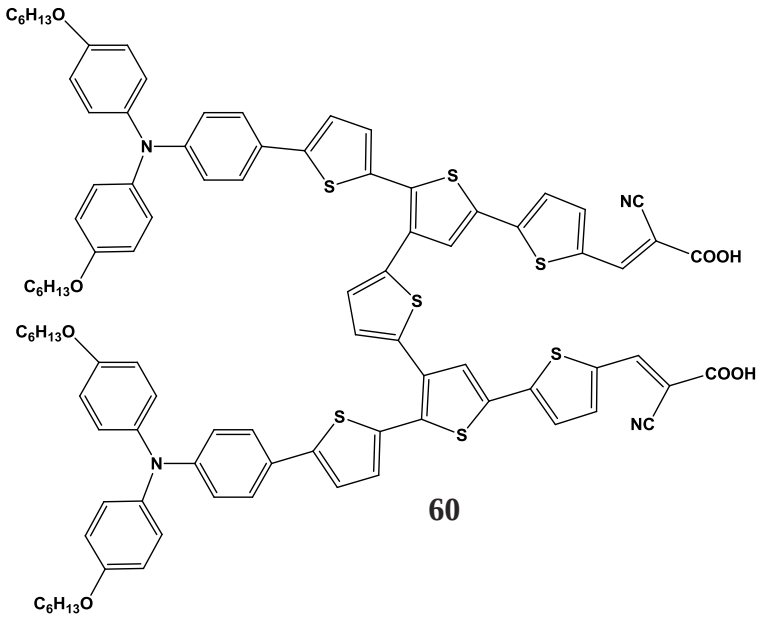

60

Figure 2.32: Molecular structures of dyes with D-π-A architecture and linked D-π-A structure.

In order to study the variation of structure of the traditional D-π-A organic dye different structural approaches have been applied including the branching in one molecule and bridging of two molecules (59, 60). In this study Ren *et.al.* linked two D-π-A branches with a thiophene for efficient dye-sensitized solar cells (DSSCs) [209] (Figure 2.32), which was found to be favorable in reducing the intermolecular interaction and retarding charge recombination. It was revealed by controlled intensity modulated photovoltage spectroscopy that electron lifetime increased 14 times longer for the double D-π-A dye-based DSSC than that for the analogous single D-π-A dye-based DSSC. Consequently power conversion efficiency also enhanced by about 2-fold.

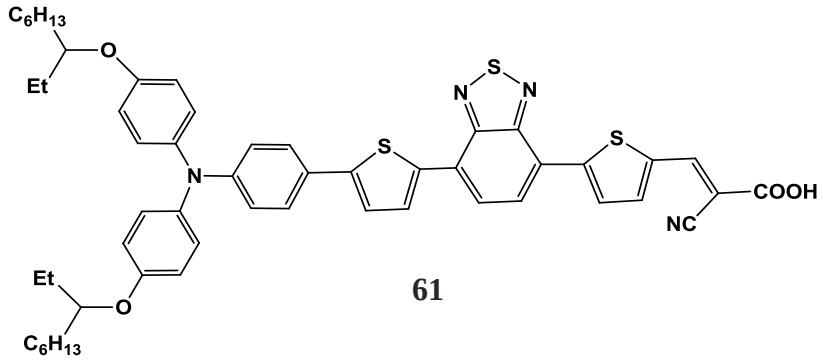

61

Figure 2.33: Molecular structures of organic dye with D-π-A-π-A skeleton.

Nazeeruddin and co-workers introduced benzothiadiazole moiety as an extra electron acceptor group in the π-bridge and achieved D-π-A-π-A skeleton (61) [210]. In order to study the structure-property relationship single, double and triple bonds were introduced between TPA units and benzothiadiazole group. In the sensitizer 61 (Figure 2.33) the electron-donating property of the TPA unit was further increased by positioning electron-releasing

alkoxy groups on the TPA unit resulting in the red shifted absorption maximum. Due to the presence of two bulky alkoxy groups at two phenyl rings of TPA unit and the aggregation of sensitizer on TiO_2 film was reduced and the overall conversion efficiency of 7.30% was achieved.

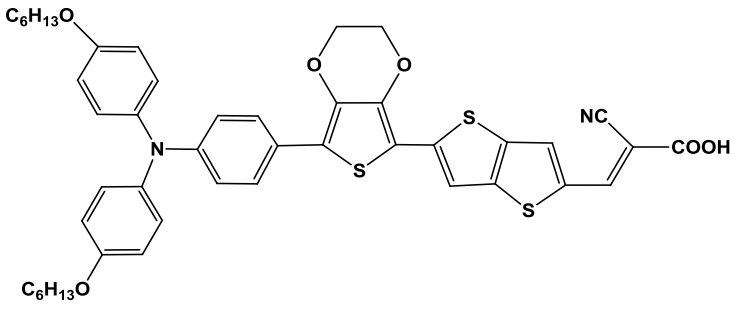

62

Figure 2.34: Molecular structures of organic dye with 3, 4-ethyldioxythiophene as a π-conjugated spacer.

Yanagida and co-workers synthesized dye 62 (Figure 2.34), consisting of 3, 4-ethyldioxythiophene as a π-conjugated spacer between TPA unit and the anchoring group [211]. The red shifted absorption spectrum was observed due to additional acceptor unit in conjugation.

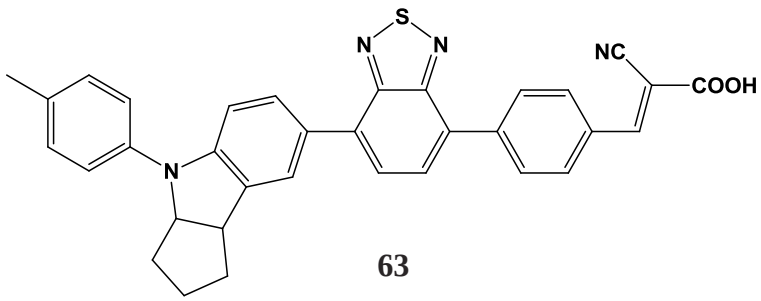

63

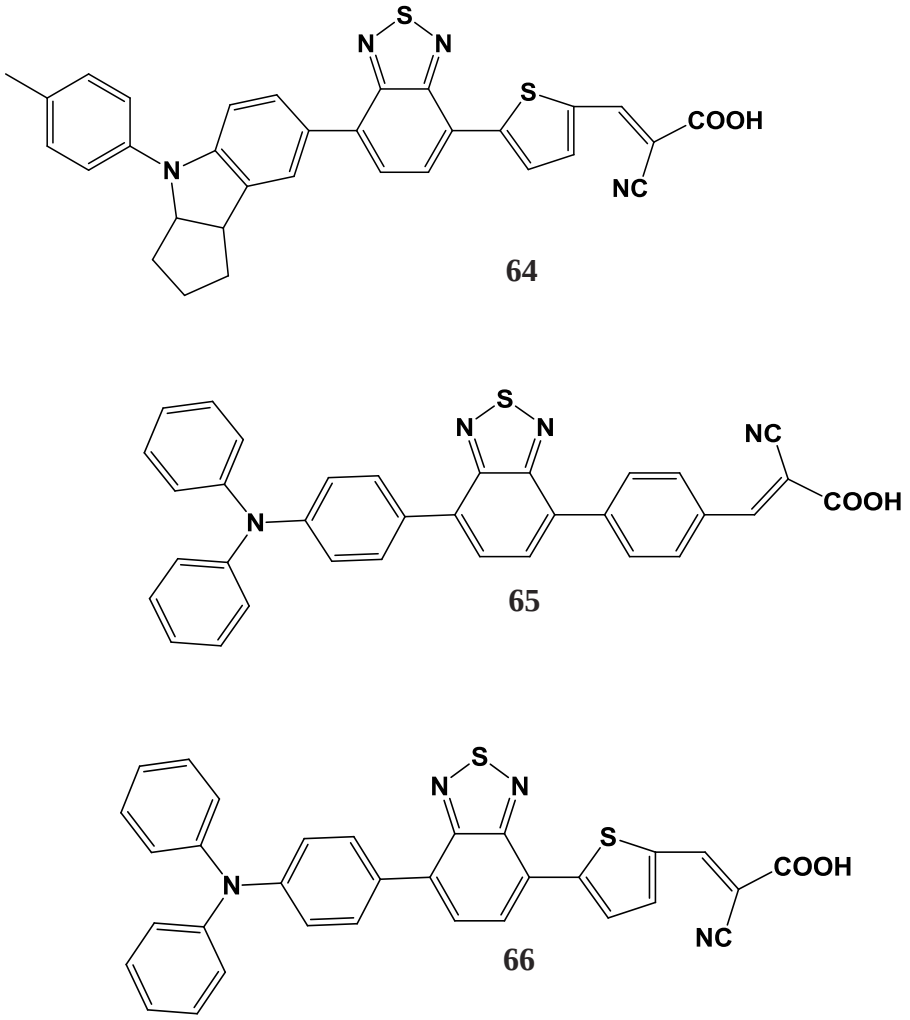

Figure 2.35: Molecular structures of indoline dyes based on D-A-π-A skeleton.

In traditional D-π-A structure a low band gap, strong electron withdrawing unit i.e. benzothiadizole, was incorporated in π-bridge by Zhu *et.al.*, resulted in a series of D-A-π-A dyes (63-66) (Figure 2.35). The integration of benzothiadizole caused improved electron distribution and enhanced photostability of indoline dyes in DSSCs [212]. Among all dyes the highest IPCE nearly at 850 nm was achieved for the DSSCs fabricated by dye 67. The DSSCs with dye 64 showed high power conversion efficiency as high as 8.7% in liquid electrolyte and 6.6% in ionic-liquid electrolyte.

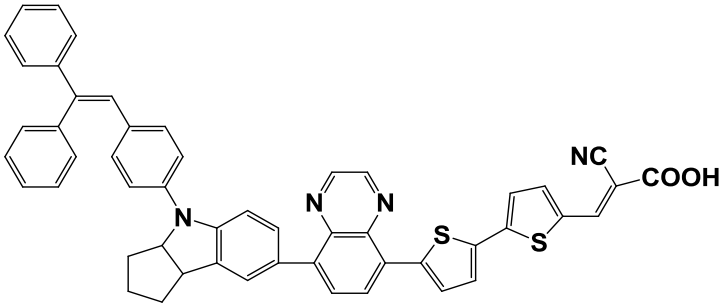

67

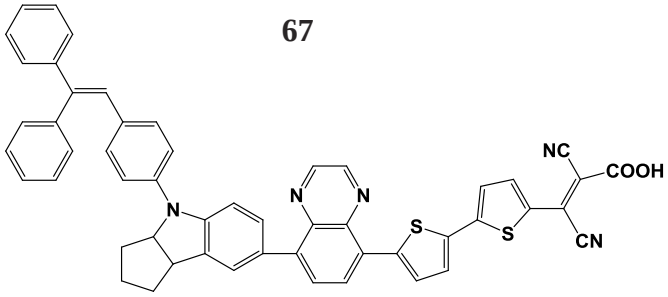

68

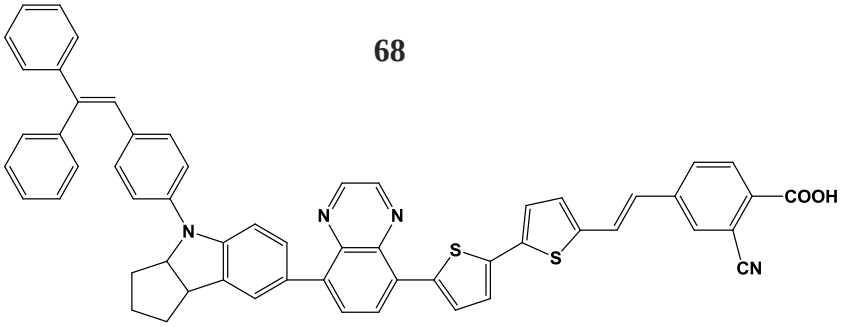

69

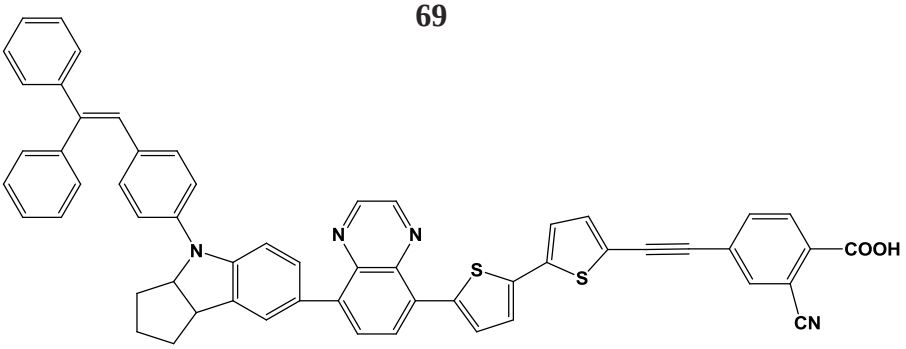

70

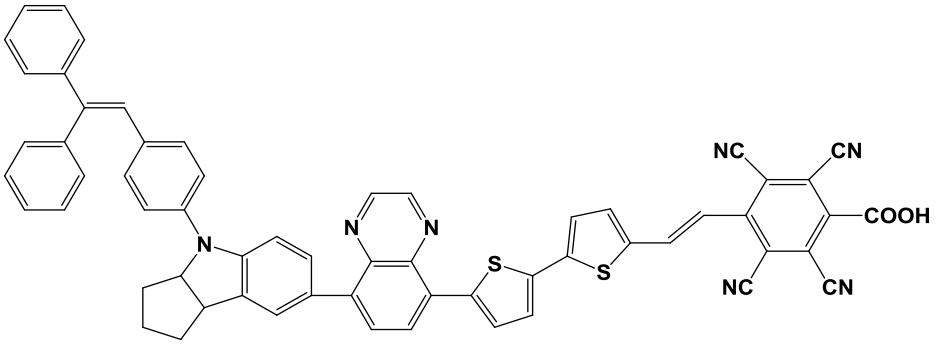

71

Figure 2.36: Molecular structures of indoline dyes with different types of acceptors.

Ding *et.al.* developed a series of new D-A-π-A indoline-based metal-free dyes (67-71) based on the different types of acceptors [213] (Figure 2.36). It was observed that the use of the quinoxaline auxiliary acceptor instead of benzothiadiazole and modification of acceptor from 2-cyanoacrylic acid to 2, 3-dicyanoacrylic acid influenced the DSSC performance positively.

2.8.2.4 Carbazole based organic dyes

2.8.2.4.1 9-Substituted carbazole derivatives

Wan *et.al*. used carbazole as an electron donor moiety, connected to acceptor at 9 position via a phenyl π-spacer (72) and compared with other synthesized organic sensitizer (73) having an electron acceptors with two 9 substituted carbazole units as electron donors connected nia different π-spacer. All sensitizers of the series were tested in dye-sensitized solar cells and showed enhanced conversion efficiencies [214] (Figure 2.37).

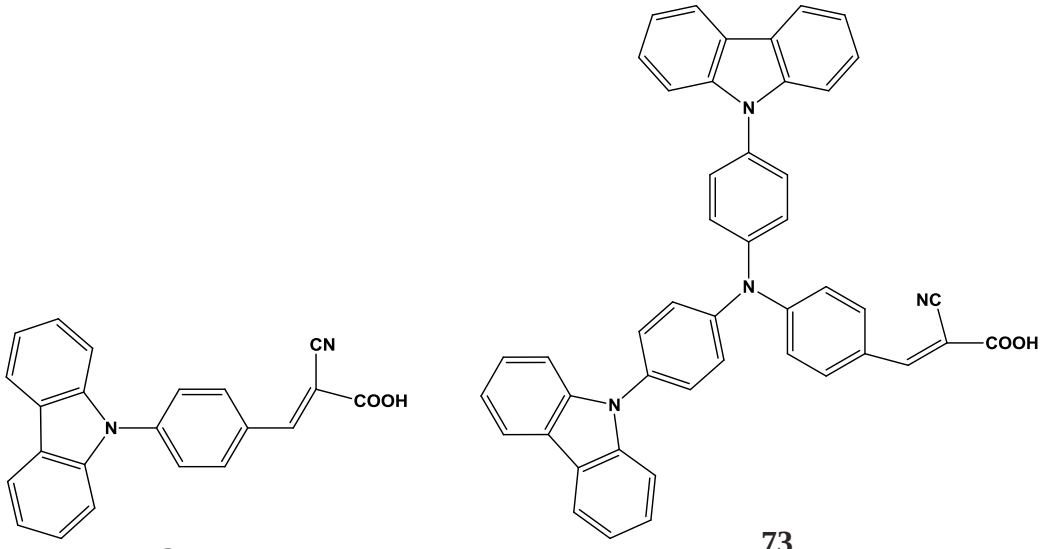

Figure 2.37: Molecular structures dyes with carbazole as donor substituted at position 9.

Recently, A series of new D-D-π-A type organic dyes, 74, 75 and 76, 77 with the 3-(3, 6-di-*tert*-butylcarbazol-*N*-yl)-*N*-dodecylcarbazol-6-yl system as electron donor, were synthesized by Promarak and co-workers [215] (Figure 2.38). The π-linkers were consisted of oligothiophene and oligothiophene-phenylene units and cyanoacrylic acid or cyanoacrylamide were used as anchoring units. The focus of the study was detailed investigation of the relationship between the structures, spectral and electrochemical properties, and performances of the DSSCs. The DSSC devices fabricated by these dyes performed remarkably well, with overall conversion efficiencies in the range of 3.60-5.69%, with IPCEs exceeding 80%. It was observed that DSSCs containing oligothiophene bridging groups performed better than those with oligothiophene-phenylene bridging groups which could be due to the twisting of phenyl group in π-bridge.

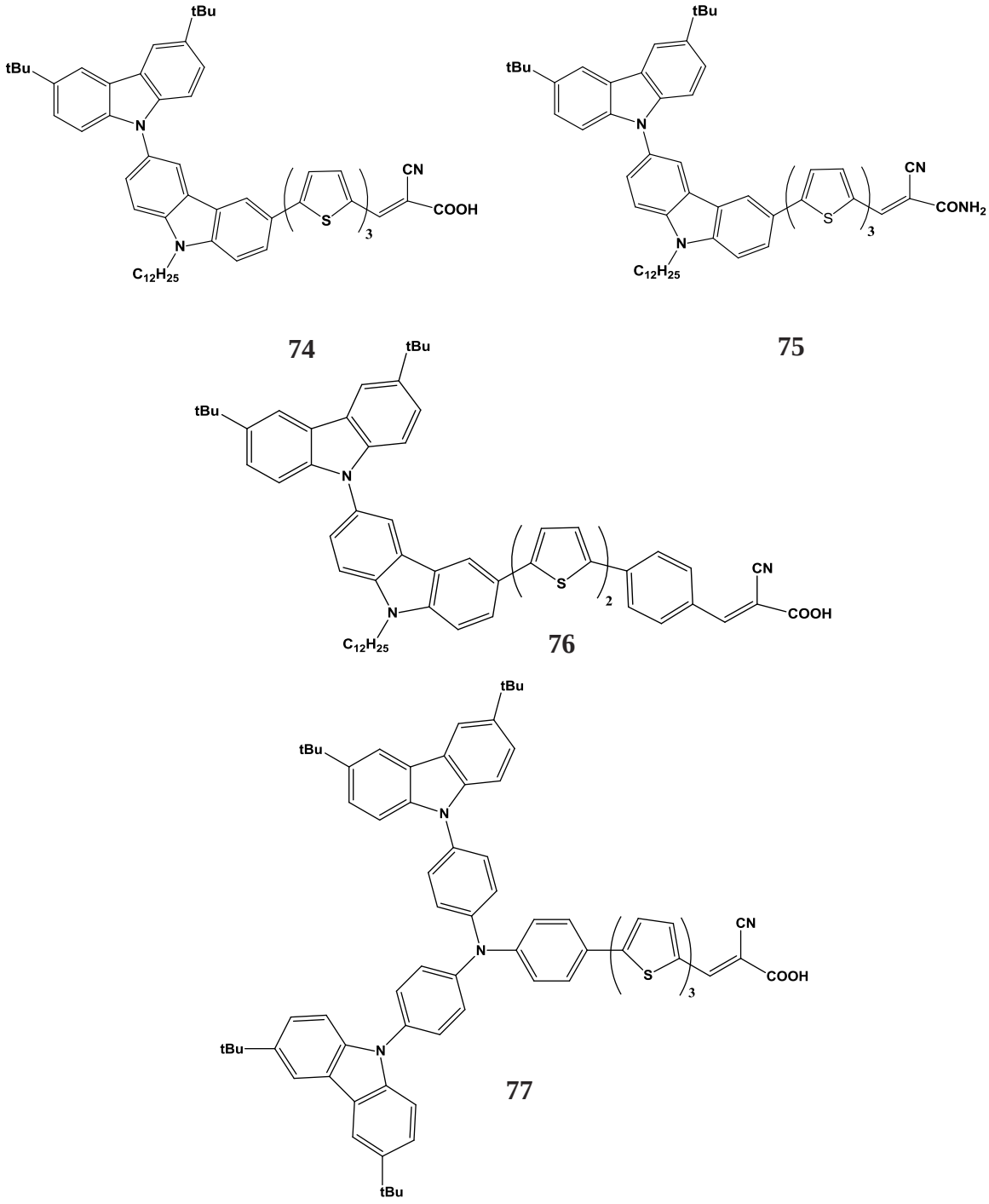

Figure 2.38: Molecular structures of D-D-π-A type organic dyes.

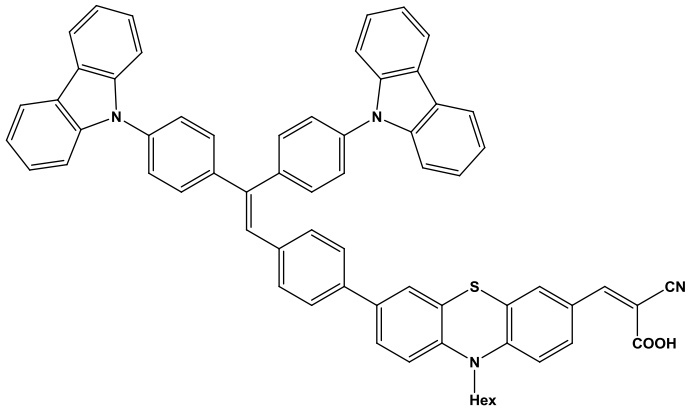

78

Figure 2.39: Starburst triphenylethylene phenothiazine and triphenylethylene carbazole based organic dye.

Chen *et.al.* reported metal free organic dye 78 with triphenylethylene phenothiazine moieties and triphenylethylene carbazole moieties as additional electron donors and reported an overall efficiency of 2.14% [216] (Figure 2.39).

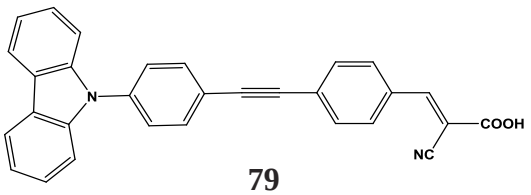

79

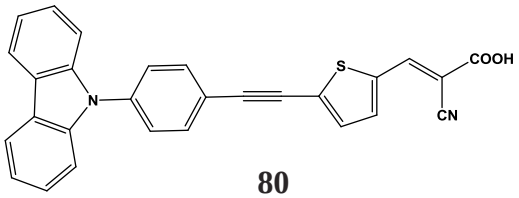

80

Figure 2.40: Dyes with carbazole donor and acetylene spacer.

The D-π-A dyes 79, 80 synthesized by Srinivas *et.al*. with the variations in linkers gave efficiencies of 2.69%, 5.51% in DSSCs [217] (Figure 2.40).

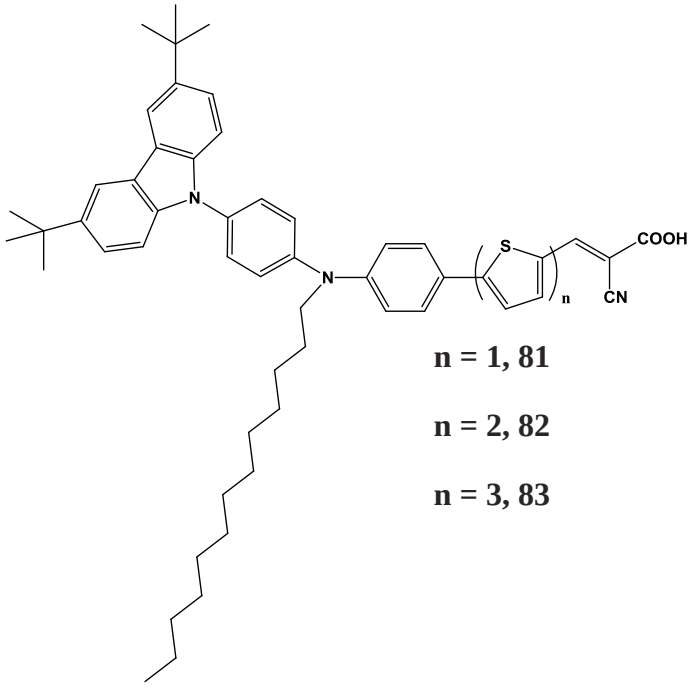

Figure 2.41: Molecular structures of D-D-π-A type carbazole based dyes.

Morada *et.al.* developed a series of organic sensitizers (81-83), exhibiting direct electron injection mechanism and a high molar extinction coefficient consisting of double donors, a π-spacer, and anchoring acceptor groups (D-D-π-A type) [218] (Figure 2.41). The maximam incident photon to electron conversion efficiency of 83% was observed with the highest J_{sc} value of 10.89 mA cm^{-2}, V_{oc} value of 0.70 V, and *FF* of 0.67, corresponded to an overall conversion efficiency of 5.12% under AM 1.5G illumination. It was suggested that the double donor moieties not only enhance the electron-donating capacity, but also restrain aggregation between dye molecules. It also proved to prevent the recombination of injected electrons with iodide/triiodide in electrolyte.

2.8.2.4.2 3-Substituted carbazoe derivatives

Kajiyama *et.al*. has reported the synthesis of D-π-A dyes with the oligohexylthiophene [84-86] linkage having several donor parts, carbazole, indole, and indoline and studied for dye-sensitized solar cells. It was observed that carbazole dyes produced higher values of both the open-circuit voltage and the electron lifetime of dye-sensitized solar cells [219] (Figure 2.42).

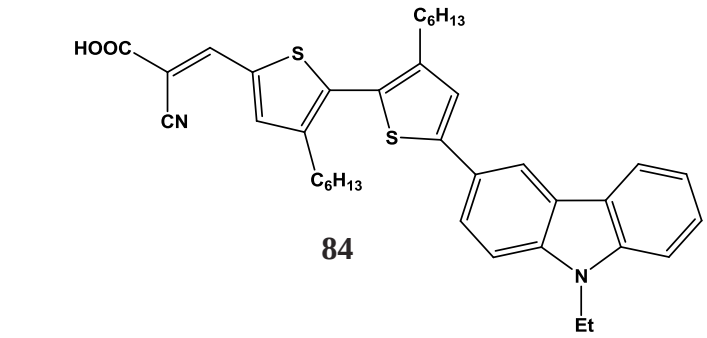

84

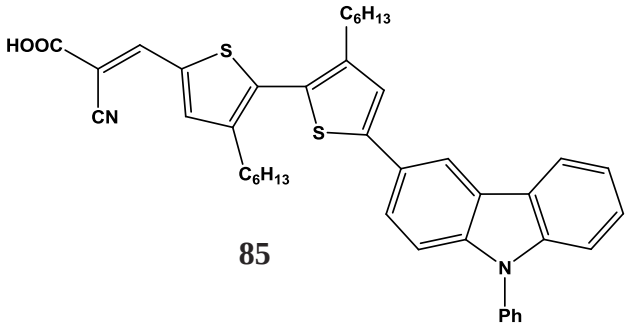

85

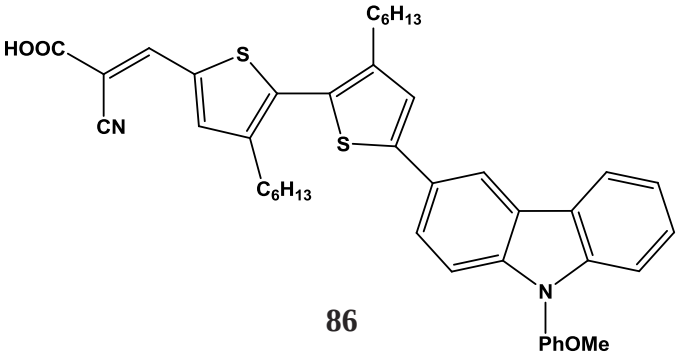

86

Figure 2.42: Dyes with carbazole donors and thiophene spacer attached to position 3.

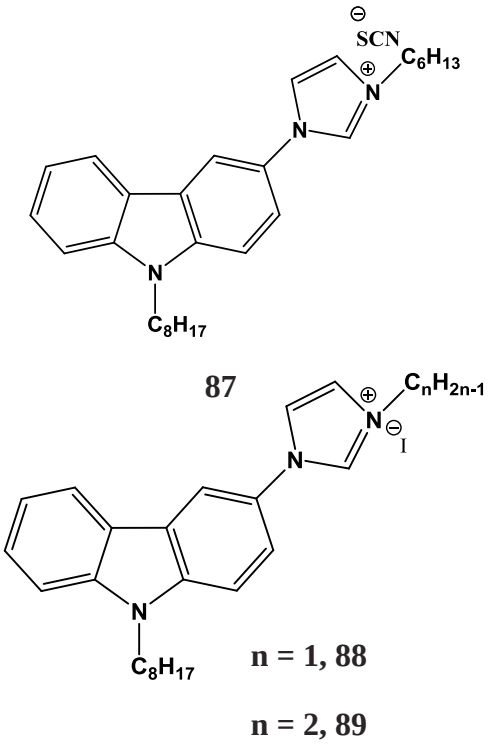

Figure 2.43: Carbazole donors and indolinium ion acceptor.

Midya *et al*. reported solid-state ionic conductors (87-89) based on a carbazole-imidazolium cation structure for application in solid-state dye-sensitized solar cells. These dyes showed good conversion efficiency of 2.85% with solid-state ionic conductors and iodine provide dual channels for hole/triiodide transportation [220] (Figure 2.43).

Koumura *et.al*. has prepared organic dyes (90-95) based on carbazole as an electron donor and a cyanoacrylic acid as an electron acceptor, connected with *n*-hexyl-substituted oligothiophenes as a π-conjugated system for dye-sensitized solar cells (DSSCs). It was observed that open-circuit photovoltage improved on addition of n-hexyl chains to the thiophene groups and hence power conversion efficiency (η) of DSSCs also improved [221] (Figure 2.44).

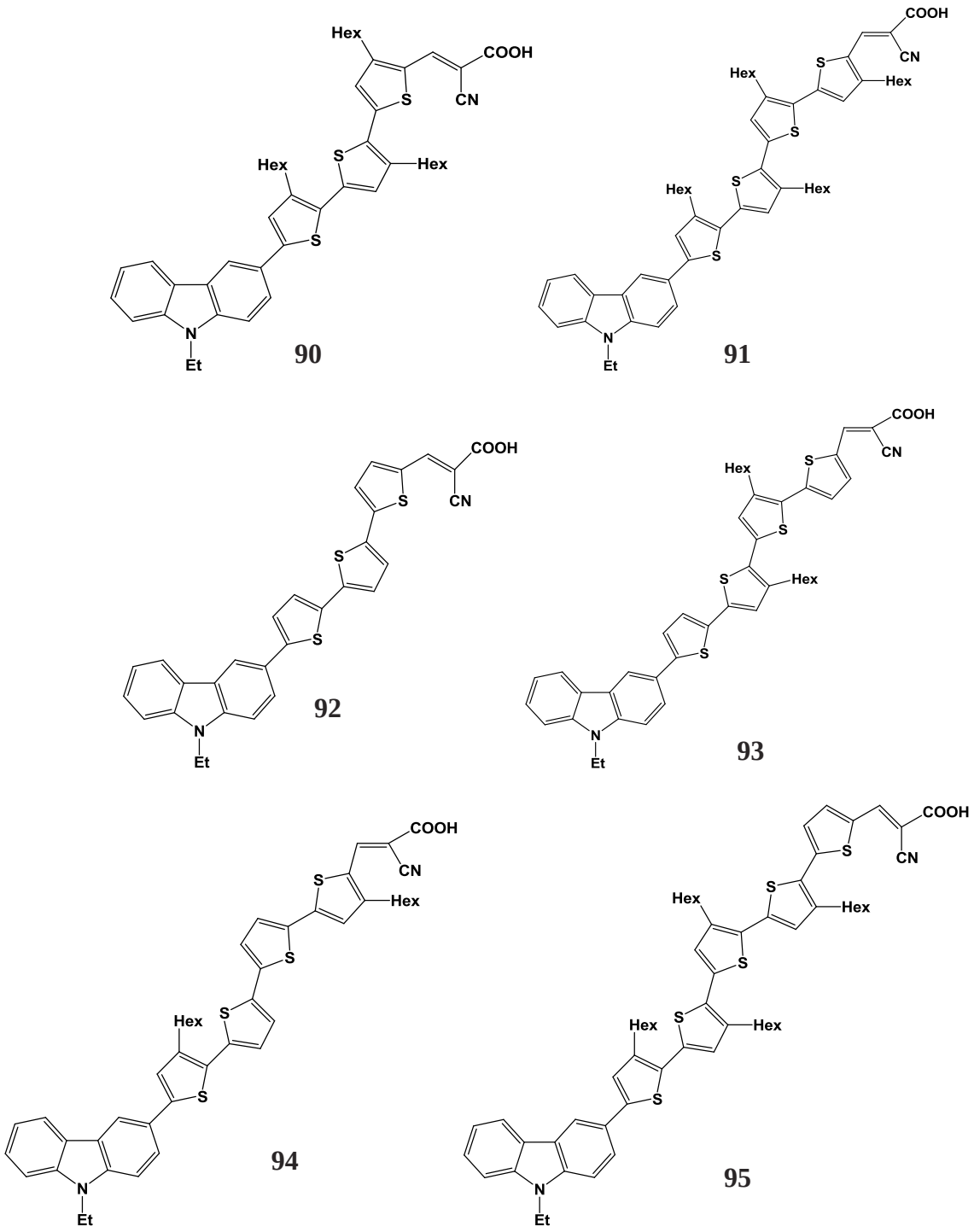

Figure 2.44: Dyes with carbazole donors and thiophene spacer.

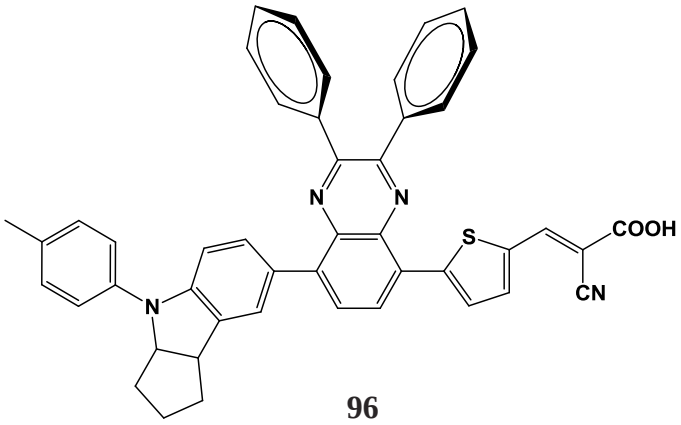

96

Figure 2.45: Carbazole based organic dye with 2, 3-diphenylquinoxaline in D-A-π-A skeleton.

Zhu *et.al.* incorporated a promising building block of 2, 3-diphenylquinoxaline at position 3 of carbazole center, as the additional acceptor and demonstrated a novel D-A-π-A featured dye 96 [222] (Figure 2.45). The inclusion of additional acceptor developed several characteristics, such as decreased molecular HOMO-LUMO energy gap, a moderate electron-withdrawing capability, strong capability of restrained intermolecular aggregation and formation of a compact sensitizer layer due to two twisted phenyl groups placed onto the quinoxaline unit. The coadsorbent-free dye-sensitized solar cell (DSSC) based on dye 96 demonstrated a high conversion efficiency of 9.24 ± 0.05%, with J_{sc} of 17.55 mA cm^{-2}, V_{oc} of 0.74 V, and *FF* of 0.71 under AM 1.5 illumination (100 mW cm^{-2}). It was observed during the stability tests that in the presence of ionic liquid electrolyte, dye 100-based DSSC devices can keep constant performance during a 1000 h aging test under 1 sun at 60°C.

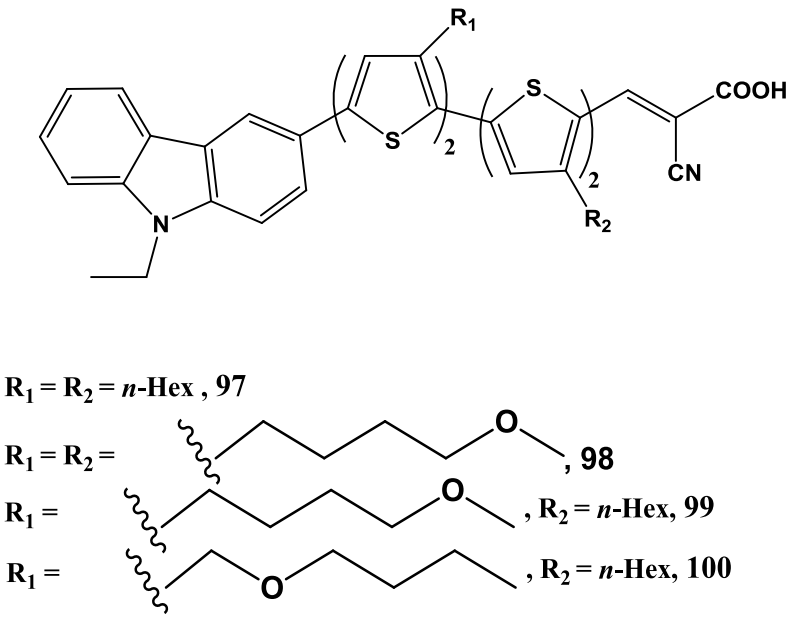

Figure 2.46: Carbazole dye with ether chains in π-conjugation linker.

Hara *et.al.* synthesized carbazole-based MK dyes (97-100) consisting of partial charge distributions by placing ether chains to a π-conjugation linker [223] (Figure 2.46). It was demonstrated that the distance between redox moiety and TiO_2 surface can be controlled by oxygen atoms on ether chains by adjusting the position and number of oxygen atoms. The overall efficiency of 2.9-4.0 % was achieved by this series of sensitizers with increased V_{oc} which was a consequence of reduced charge recombination at the interfaces owing to different positions of oxygen atom in side chains substituted at the π-bridge.

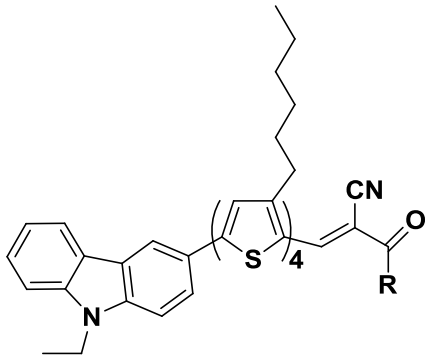

R = OH, **101**

R = NH-CH_2COOH, **102**

R = NH-CH_2CH_2COOH, **103**

Figure 2.47: Carbazole dyes incorporated with nonconjugated methylene unit.

Most metal-free organic dyes for dye-sensitized solar cells are designed by following a donor conjugated-bridge acceptor structure with carboxyl acid as an anchoring unit. In this work, Hara *et.al* extended the work by incorporating nonconjugated methylene unit between the cyano group and carboxyl acid by applying it to a previously reported carbazole dye, MK-2 (101) [224] (Figure 2.47). By inserting glycine and β-alanine two dyes, 102 and 103, were synthesized, respectively. The DSSCs based on dyes 102 and 103 showed lesser values of J_{sc} and higher values of V_{oc} in comparison with the values of dye 101. DFT calculations showed the intermolecular interactions in dye 102. The longer electron lifetime can be explained due to the formation of 3D geometry of enlarged dimers after interaction of molecules. On the other hand, the longer electron lifetime in dye 103 than that with dye 101 was explained due to the longer distance between the TiO_2 surface and conjugated framework of the dye.

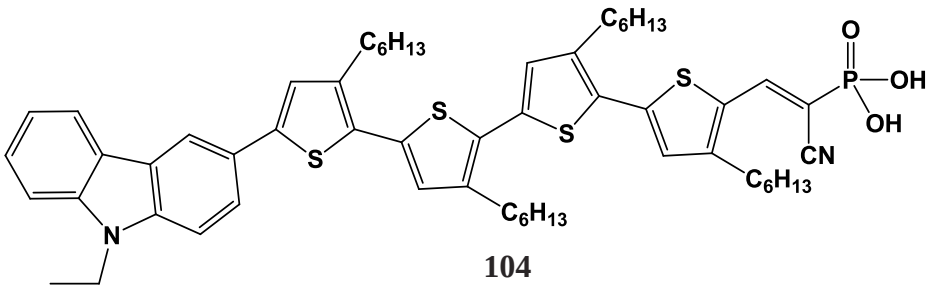

104

Figure 2.48: Phosphonic acid anchored dye molecule.

The binding strength between the dye and TiO_2 and surface arrangements of the dye on TiO_2 affect the heat stability of the DSSCs. Usually carboxylic acids are used as the anchoring groups for the adsorption of dyes on TiO_2 surfaces. However, Koumura *et.al.* synthesized a phosphonic acid anchored dye molecule (104) which was expected to have more stable bonding to a TiO_2 surface due to its tridentate binding capability [225] (Figure 2.48). In this new carbazole dye a phosphonic acid anchor was employed at the end of linker attached to central carbazole at position 3. For studying the effect on heat stability the dye was compared with similar carbazole dye with a carboxylic acid anchoring group, dye 101 (Figure 2.47). It was found during the stability test and photovoltaic performance analysis of DSSCs fabricated by dye 104 and 101 that dye 104 DSSC exhibited longer electron lifetime and larger charge transfer resistance than the other dyes. The IPCE was found to be decreased 27% from the initial value in the DSSC fabricated by MK-2 (101).

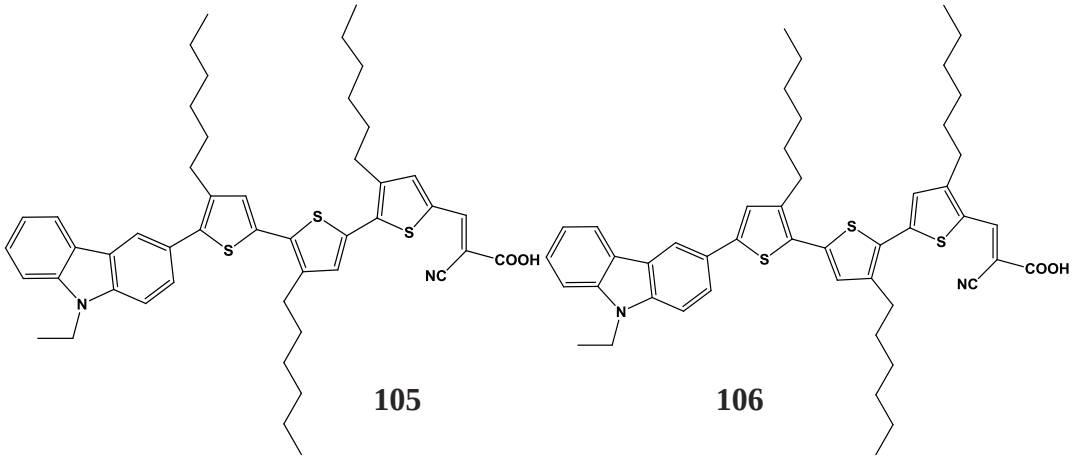

105 **106**

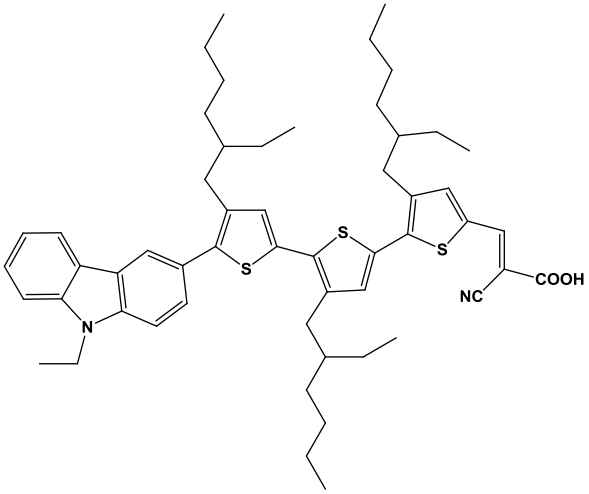

107

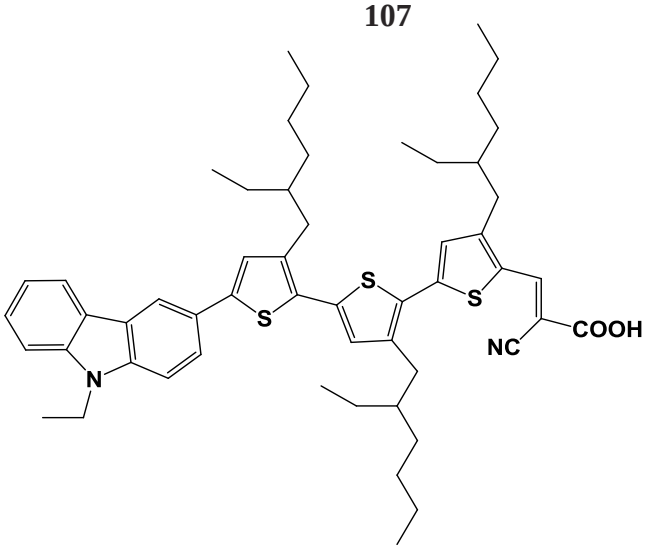

108

Figure 2.49: Carbazole based 3 substituted dyes with different substitution groups in linker.

Wang *et.al.* designed and synthesized two sets of isomeric organic dyes with n-hexyl (105 and 106) and 2-ethylhexyl (107 and 108) groups substituted at the spacer part [226] (Figure 2.49). Only structural difference between the isomers was the incorporation of branched and non branched alkyl chains at the terthiophene spacer close to the donor (D) or anchor (A) side. After the optoelectronic analysis of DSSCs fabricated by this series of dyes it was concluded that the positioning of side chain in π-bridge affects the geometry of the dye molecule which consequently influence the overall performance of the DSSCs. Since, the steric hindrance in (D) series dyes due to closeness of alkyl chain with the donor moity caused remarkable twist in the molecular skeleton, the charge transfer suffered drastically. In contrast, more planar geometry of (A) series dyes caused effective π-conjugation and an overall efficiency of 8.66% has been realized with liquid electrolyte containing Co (II)/(III) redox couple. Isomer 108 based DSSCs displayed the highest η of 7.10% which remained at 98% of the initial value after continuous light soaking for 1000 h with quasi-solid-state electrolyte. This work acclaimed the crucial issue of molecular engineering and demonstrated a novel approach to design organic sensitizers for highly efficient and stable DSSCs.

2.8.2.4.3 3, 6- Disubstituted carbazoe derivatives

Anandan *et.al.* designed and synthesized two bianchored metal free organic dyes for DSSC application by Carbazole (109) and diphenylamine moieties as the donor, cyano vinyl thiophene unit as the π-bridge and cyanoacrylic acid group as the electron acceptor [227] (Figure 2.50). The DSSCs based on carbazole unit as a donor (109) displayed a maximum current conversion efficiency of 4.04% under AM 1.5 illumination (85 mW cm^{-2}) which was higher than that of diphenylamine analogue.

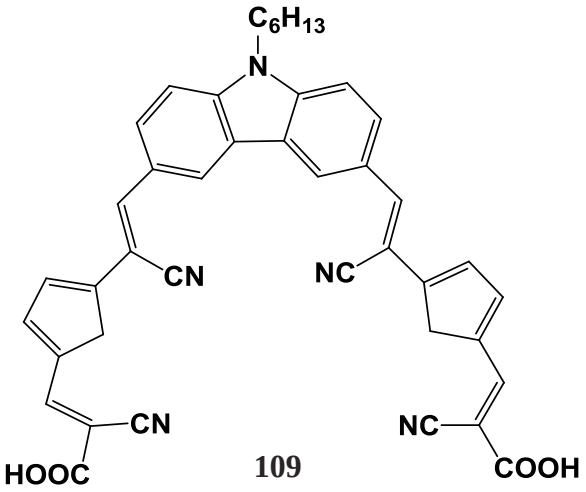

109

Figure 2.50: Bianchored 3, 6 substituted carbazole based dye.

It was concluded that due to the planar nature of carbazole moiety in 109, the adsorbed dye amount increased owing to effective anchoring by both anchoring sides and the overall efficiency increased.

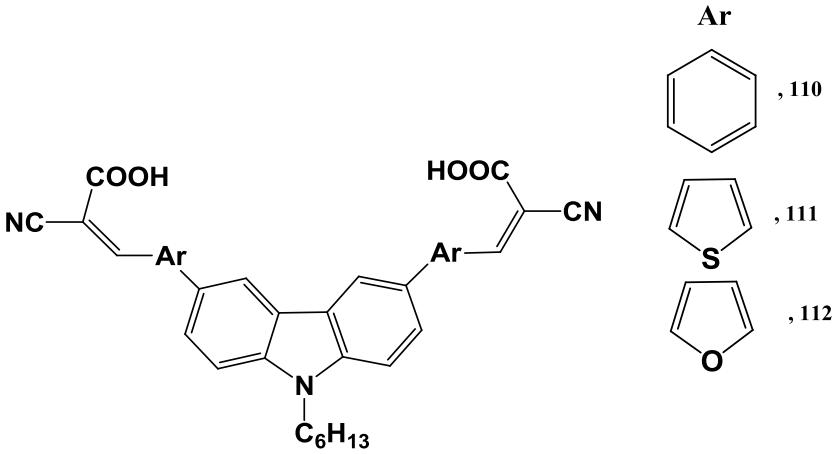

Figure 2.51: Bianchored 3, 6 substituted carbazole based dyes with different conjugations.

Recently, Chandrasekharam *et.al.* reported three novel carbazole-based A-π-D-π-A featured dyes (110-112) for applications in dye-sensitized solar cells [228] (Figure 2.51). The study was based on the effects of different conjugated linkers, such as benzene, furan or thiophene with the share the same donor (*N*-hexylcarbazole) and acceptor/anchoring group (cyanoacrylic acid). It was observed that the power conversion efficiencies were sensitive to the π-bridging linker moiety. Photovoltaic experiments showed that the dye containing a thiophene linker exhibited the maximum overall conversion efficiency of 3.8% (J_{sc} = 8.90 mA cm^{-2}, V_{oc}= 584 mV, *FF* = 0.74) under standard global AM 1.5 G solar condition.

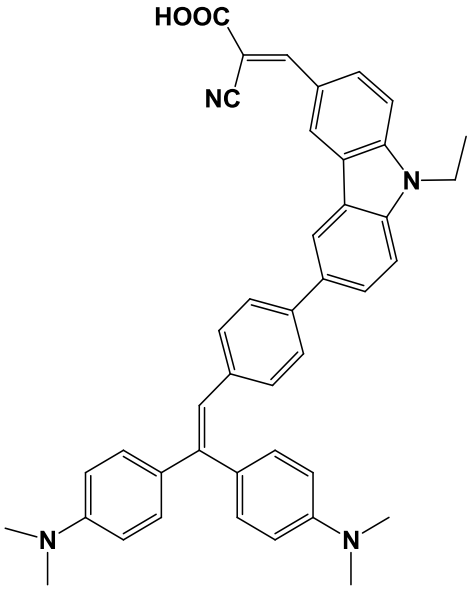

113

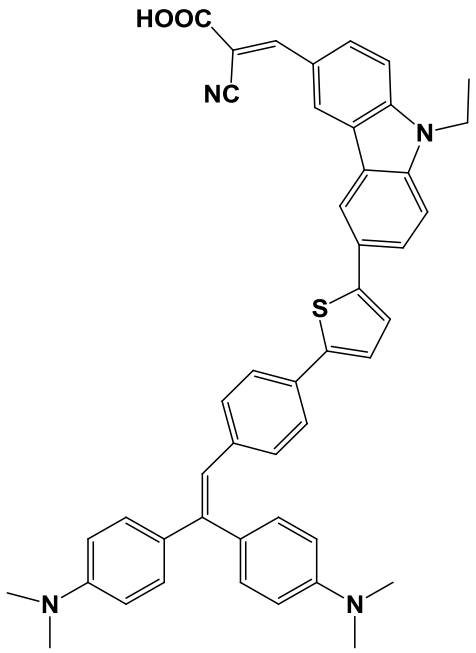

114

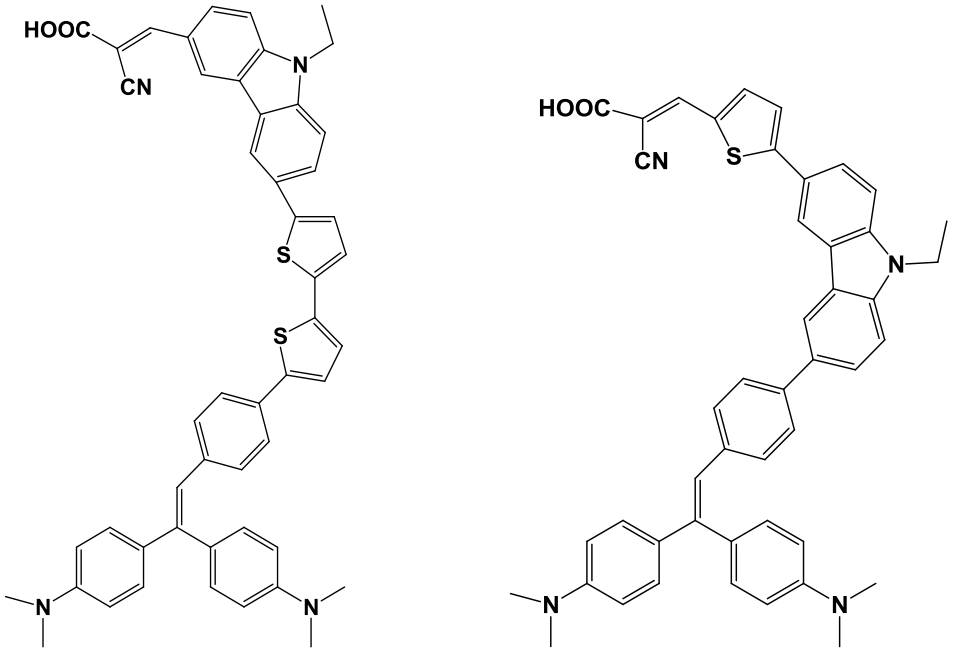

115 **116**

Figure 2.52: D-π-A dyes with carbazole unit in linker.

Liang *et.al.* developed four organic dyes (113-116) [229] employing carbazole unit as electron donor attached to *N*,*N*-dimethylarylamine moiety at position 3 and cyanoacrylic acid as an acceptor at position 6 (Figure 2.52). The presence of electron-donating groups in dimethylarylamine improved the electron density of carbazole moiety and enhanced the molar extinction coefficient of dyes. The DSSCs fabricated with these dyes could reach the maximum IPCE value of 86%, with an overall conversion efficiency of 4.0%.

2.8.2.4.4 2, 7- Disubstituted carbazoe derivatives

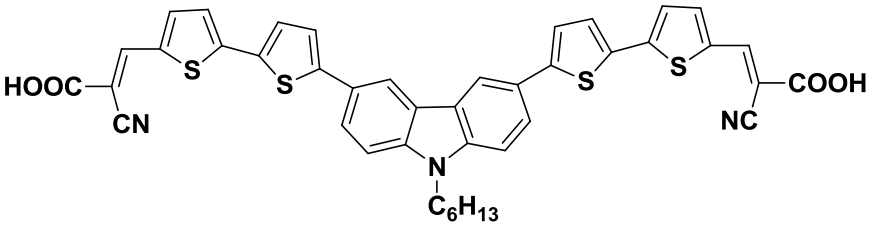

117

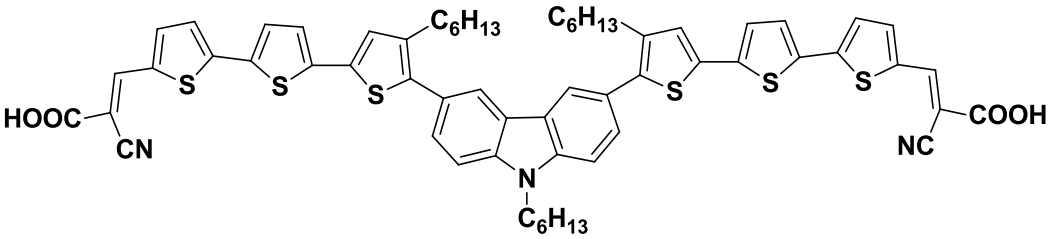

118

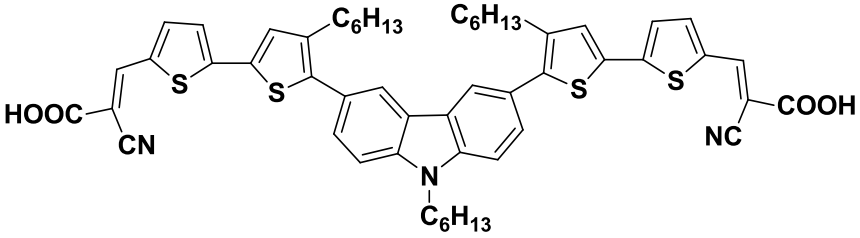

119

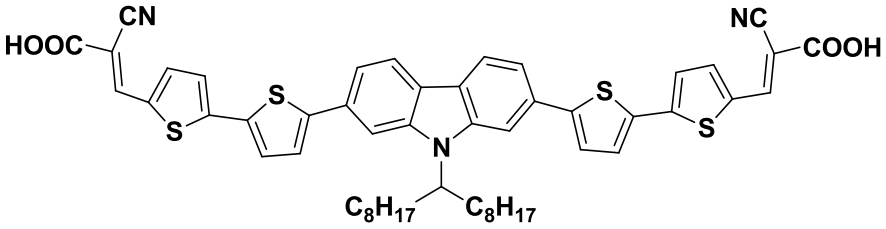

120

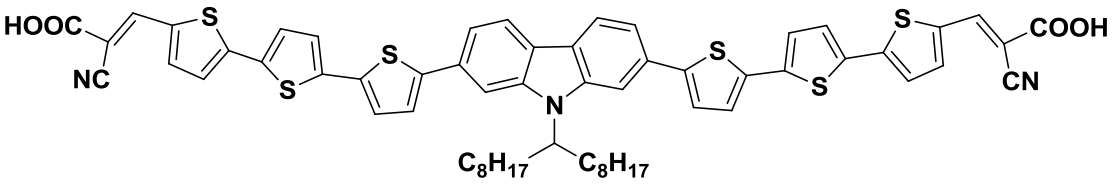

121

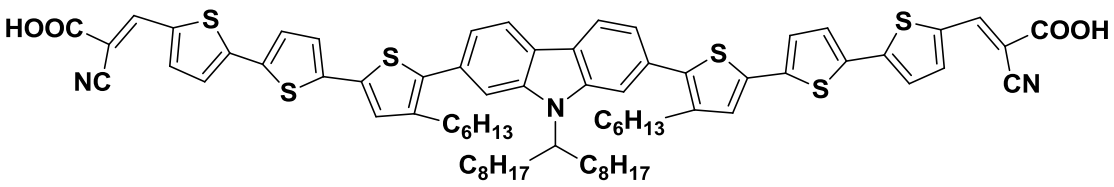

122

Figure 2.53: A- π-D- π-A dyes with 3, 6 and 2, 7 substitutions.

Lin *et.al.* synthesized two series of novel symmetrical acceptor-donor-acceptor organic sensitizers (117-122) containing carbazole cores functionalized at 3, 6- and 2, 7-positions (Figure 2.53) [230]. Thienyl linkers were used for connecting carbazole donor moiety to two anchoring cyanoacrylic acids. In this work the effect of molecular planarity due to 3, 6- and 2, 7-functionalized carbazole cores, on the performance of DSSCs fabricated by this series of dyes was investigated. Among all the dyes, the highest power conversion efficiency obtained in a dye-sensitized solar cell was 4.82%.

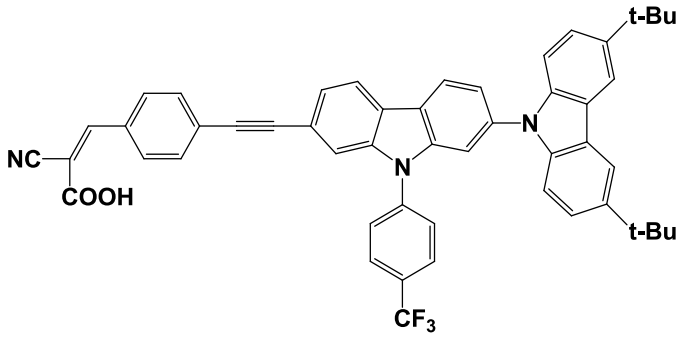

123

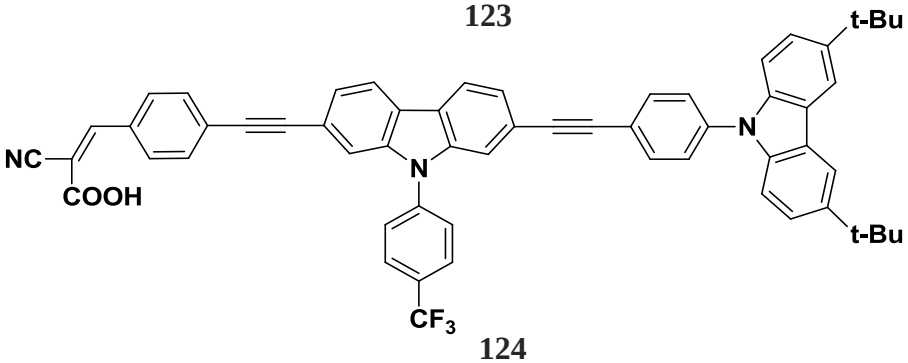

124

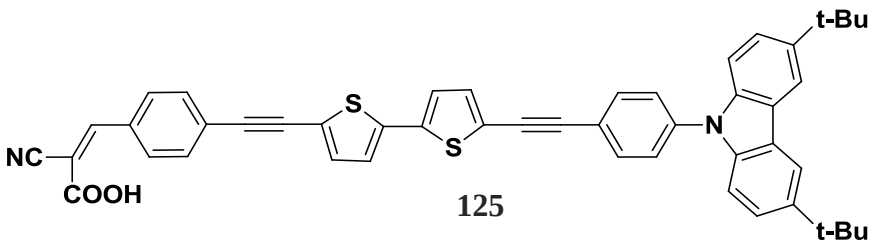

125

Figure 2.54: 2, 7 substituted carbazole based dyes.

Onicha *et.al.* reported three metal-free organic sensitizers (123-125) with carbazole donor, carbazole or bithiophene as the linker and cyanoacrylic acid as the electron acceptor [231] (Figure 2.54). The photovoltaic performance of the sensitizers in operational liquid junction-based DSSCs under AM 1.5 G one-sun excitation (100 mW cm^{-2}) indicated that the sensitizers are promising candidates for use in DSSCs. Sensitizers 123 and 124 produced a power conversion efficiency of 2.70% with a maximum IPCE of 75% at 450 nm, while sensitizer 125 has a power conversion efficiency of 2.23% with a maximum IPCE of 66% at 440 nm. The sensitizers thus exhibited excellent photon-to-current conversion efficiencies in the blue region of the spectrum and served as candidates for further strategic optimization in tandem cells.

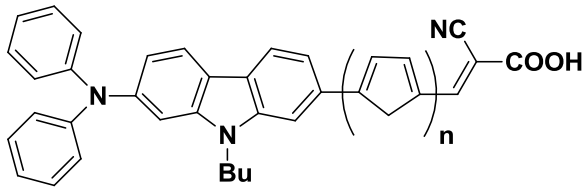

(n = 1, 126)

(n = 2, 127)

Figure 2.55: 2, 7 substituted carbazole based dyes with different conjugation length.

Venkateswararao *et.al.* designed and synthesized two new organic dyes (126, 127) containing diphenylamine donor, 2,7-carbazolyl π-linker, and cyanoacrylic acid as acceptor [232] (Figure 2.55). These dyes displayed to have high molar extinction coefficient. The DSSCs fabricated by these dyes showed overall efficiency up to 6.8%. Since the addition of chenodexoycholic acid (CDCA) assisted in increasing the efficiency to 7.2%, the dyes are suspected to have aggregated on TiO_2 film. The DSSCs fabricated by these dyes showed remarkable stability over 1000 h with ionic liquid electrolytes.

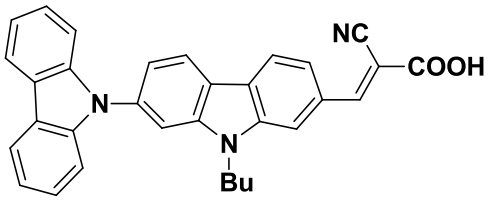

128

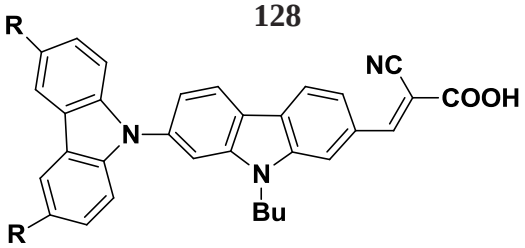

R = H**, 129;** R = *t*-butyl**, 130**

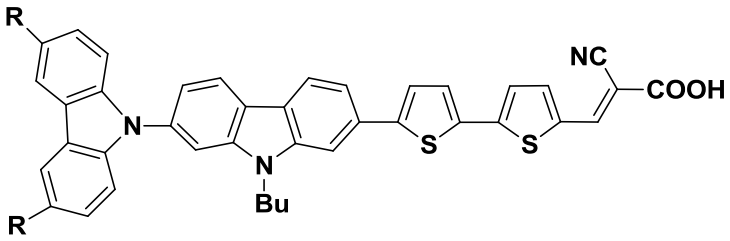

R = H**, 131;** R = *t*-butyl**, 132**

Figure 2.56: 2, 7 substituted carbazole based dyes with different substituting units at donor.

Further extending the work by synthesizing the dyes with carbazole donor as well as linker in the similar structure, Venkateswararao *et.al.* reported a series of five new metal free organic dyes for DSSCs (128-132). In these dyes carbazole functionalized at positions C-2 and C-7 acted as electron-rich bridge [233] (Figure 2.56). The bridge was further extended by insertion of thiophene units near to the acceptor. In order to improve the cell efficiency a bulky tert-butyl group was introduced at 3, 6 positions of donor carbazole, since the bulkiness of donor suppress the electron recombination. All the structural modifications were proved to be beneficial to tune the optical properties of dye molecules and consequently resulted in enhanced cell performance. The efficiency of DSSCs fabricated by this series of dyes ranged from 4.22 to 6.04%.

2.8.2.4.5 Fused carbazoe derivatives

Zafer *et.al.* reported efficient sensitizers composed of two carbazolyle units fused at 3, 4 positions (133) [234] (Figure 2.57). This synthesis was aimed at improving optical and electronic properties such as molar absorption coefficient, spectral coverage and electron injection properties of the sensitizers. The dye exhibited higher molar extinction coefficient than its mono carbazole analogue. The overall conversion efficiency obtained was up to 3.18%.

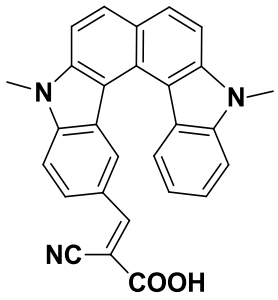

133

Figure 2.57: Organic dye with fuzed carbazolyl units.

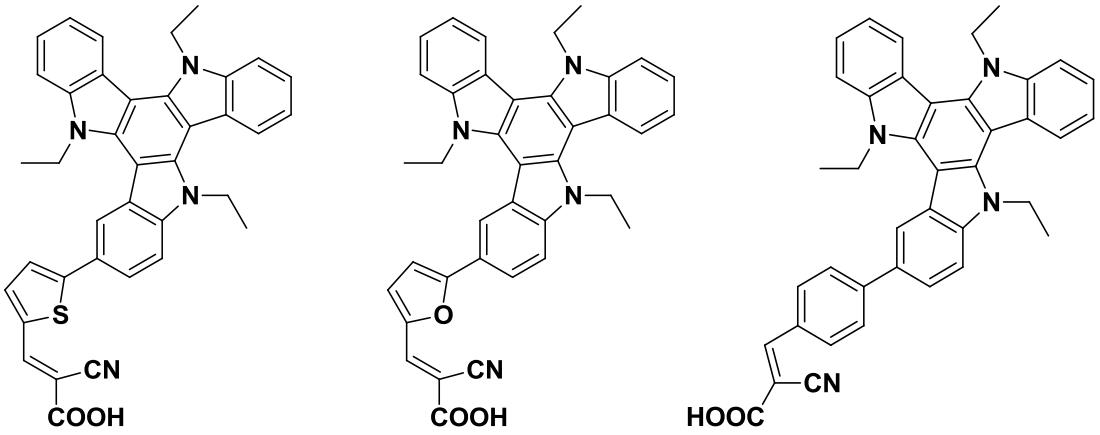

Figure 2.58: Triazatruxene based organic dyes.

Qian *et.al.* reported interesting triazatruxene based organic dye structures (134-136) in which three carbazole moieties were fused in a way to share one phenyl unit coinciding in all carbazole molecules [235] (Figure 2.58). The effect of variation of π-linker was studied by inserting thiophene, furon and phenyl units in π-conjugation with cyanoacrylic acid acceptor. The DSSC based on dye 134 with thiophene as the conjugated linker showed the best performance with an overall efficiency of 6.10%.

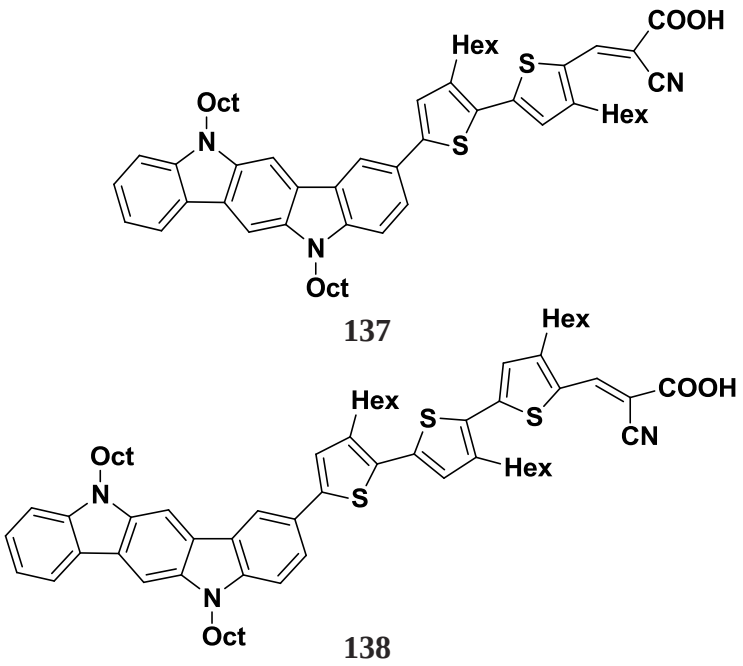

Figure 2.59: Indolo[3,2-b]carbazole based dyes with thiophene spacer.

Zhang has reported metal free organic dyes, 137 and 138, comprising 5, 11-dioctylindolo[3,2-b]carbazole moiety as the electron donor, *n*-hexyl-substituted oligothiophene units as the π-conjugated bridge connected to cyanoacrylic acid anchoring group. It was observed from the photovoltaic analysis of the DSSCs prepared by these dyes that dye 137 showed a better photovoltaic performance with IPCE of 83%, J_{sc} of 15.4 mA cm^{-2}, V_{oc} of 0.71 V, and *FF* of 0.67 which corresponded to an overall conversion efficiency (η) of 7.3% under standard AM 1.5 G irradiation [236] [Figure 2.59].

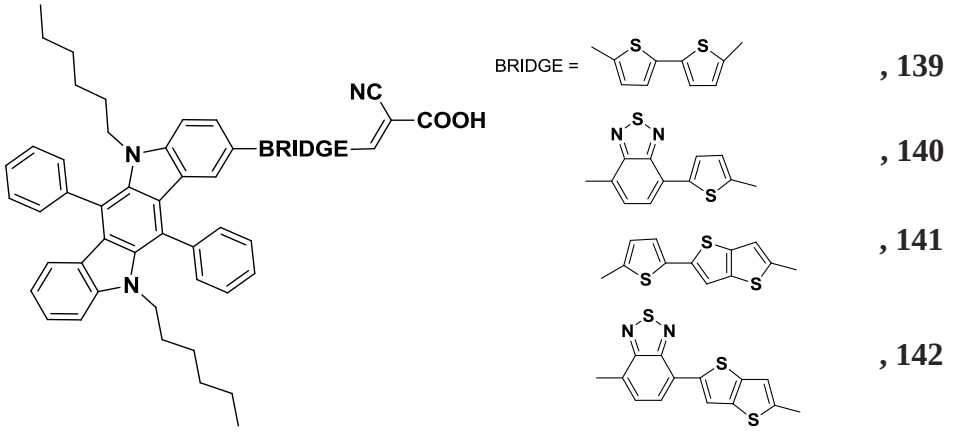

Figure 2.60: Organic dyes based on 5, 7-dihexyl-6, 12-diphenyl-5,7-dihydroindolo[2,3-b]-carbazole (DDC).

Cai *et.al.* reported four novel metal-free organic sensitizers based on 5,7-dihexyl-6,12-diphenyl-5,7-dihydroindolo[2,3-b]-carbazole (DDC) donors with different π-linkers in conjugation attached to cyanoacrylic acid anchoring group (139-142) [237] (Figure 2.60). The stability test was done at continuous illumination for 30 min. The cells showed a good stability and overall efficiency upto 7.03%.

2.8.2.4.6 Push-pull-pull archetectures in carbazole dyes

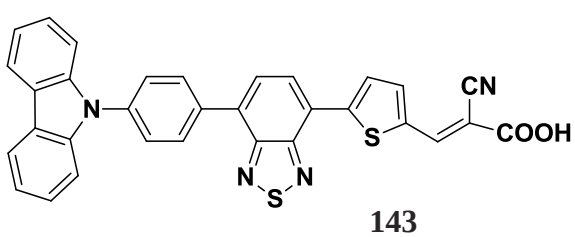

143

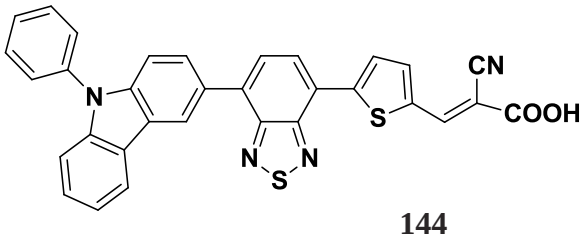

144

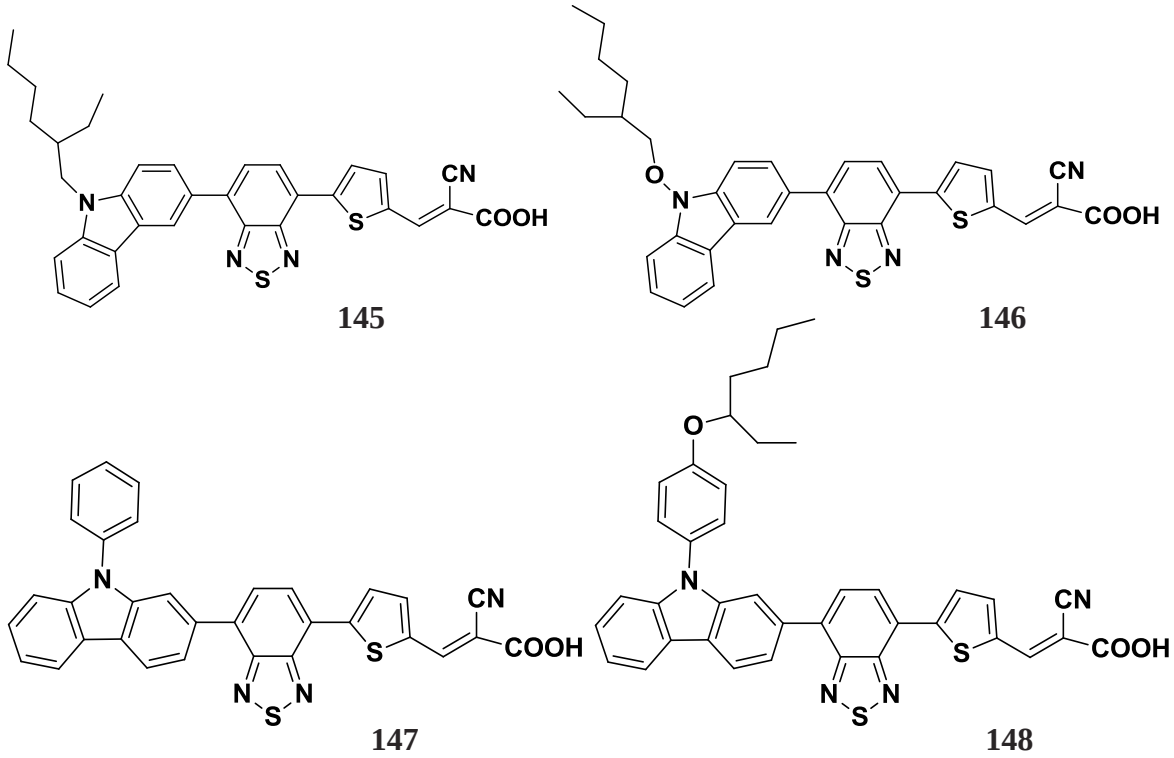

Figure 2.61: A series of Push-pull-pull architectures with carbazole moiety.

Keerthi *et.al.* reported a series of six carbazole based dyes (143-148) in which the effect of the substitution positions i.e. N, 2 and 3 has been studied in a push-pull-pull architecture [238] (Figure 2.61). Carbazole unit is used as donor moiety bridged by benzothiadiazole fragment to the cyanoacrylic acid acceptor. It was observed that the substituent positions on carbazole affected the solubility, packing and molecular orientation on the TiO_2 surface of DSSCs. The best efficiency obtained by the DSSCs of this series of dyes was up to 3.80 %.

2.8.4 Perovskites

2.8.4.1 Perovskite phenomena

The nomenclature given to a substance that adopts the crystal structures same as calcium titanate, namely, ABX_3 is known as perovskite. These materials can be fabricated by solid-state synthesis or from dried solutions of precursor salts [239, 240]. The fundamental properties exhibited by hybrid organic-inorganic perovskites, are largely unknown. It has been observed that the properties such as antiferromagnetic, piezoelectric, thermoelectric, semiconducting, conducting and superconducting, all vary as per the other basic properties of the materials exhibiting perovskite structure [241].

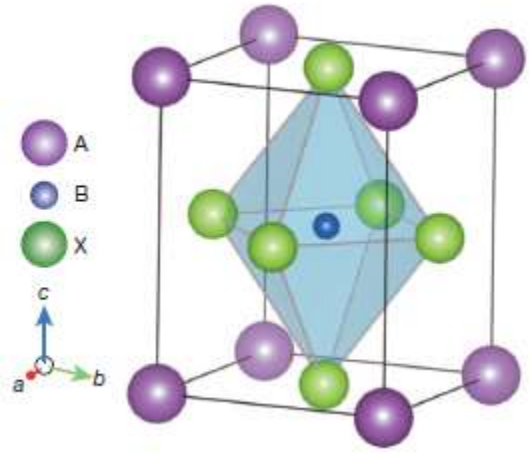

Figure 2.62: Crystal structure of the perovskite absorber adopting the ABX_3 form, where A is methylammonium, B is Pb and X is I or Cl.

The crystal structure of perovskite absorber is demonstrated in figure 2.62 [242]. Due to the tilting and rotation of the BX_6 polyhedra in the lattice [243], perovskites can easily access cubic, tetragonal, orthorhombic, trigonal and monoclinic polymorphs and exhibit

phase complexity of structures. Oxide perovskites (ABO_3) are synthesized from divalent and tetravalent metals and halide perovskites (e.g. ABI_3) are formed from monovalent metals. Due to their self assembling character perovskite-based hybrids can be synthesized using simple and cheap techniques [244]. In the early 1990s, Mitzi, Era, and co-workers extensively investigated the organic-inorganic perovskites in terms of their optoelectronic properties. From their study layered perovskites were revealed to show strong excitonic features and good functioning in transistors and light-emitting diodes [245, 246].

2.8.4.2 State of the art

The electron transport in perovskite based solar cells in conjunction with mesoporous TiO_2 film is shown in Figure 2.63 [247]. In 2009, Kojima *et.al.* [248] introduced organic-inorganic hybrid $CH_3NH_3PbX_3$ (X = Br, I) perovskites as a new class of sensitizers in DSSCs. The study was based on liquid electrolyte and an overall efficiency of 3.8% was observed. Similar composition was used by Im *et.al.* [249] in 2011 and the efficiency of such DSSCs was accelerated to 6.5%.

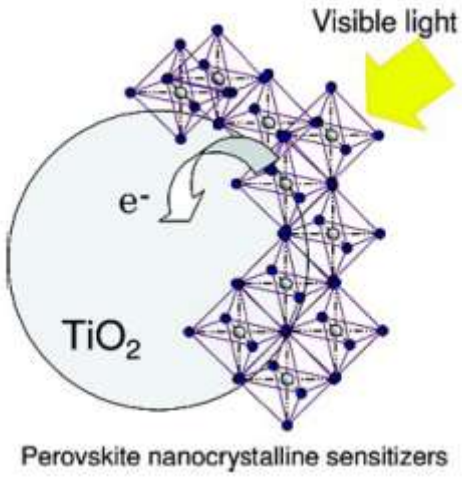

Figure 2.63: The schematic diagram showing electron transport in perovskite solar cells.

Although the conversion efficiency increased well, the stability of the device degraded drastically, due to presence of solvents corrosive to the perovskites. To rectify the corrosion problem the liquid electrolyte was replaced by spiro-MeOTAD. The cells which were based on $CH_3NH_3PbI_3$ perovskite in conjunction with spiro-MeOTAD exhibited as high efficiency as 9.7% by Kim *et.al.* [250]. Being exhibited promising results in DSSCs, $CH_3NH_3PbI_3$ perovskite was used in heterojunction cell by Etgar *et.al.* without the use of hole conductor and the efficiency of 5.5% was obtained [251]. Mixed halide perovskites were also explored in conjunction with HTM and TiO_2 nanoparticles of different shapes. An efficiency of 4.9% has been achieved by applying mixed halide $CH_3NH_3PbI_2Br$ perovskite together with TiO_2 nanowires [252]. Colorful and stable hybrid solar cells with a photovoltaic efficiency of 12.3% were reported by Noh *et.al.* [253], in which chemically tuned $CH_3NH_3Pb\text{-}(I_{1-x}Br_x)_3$ perovskites were used as sensitizers.

Perovskites have been used in solar cells with different types of hole transporting materials and vast variety of semiconductor materials as an electron generator but a recent breakthrough report by Lee *et.al.* [254] changed the perspective about the capabilities of this material. Lee demonstrated that the $CH_3NH_3PbI_2Cl$ perovskite can serve both as light harvester and an electron conductor in meso superstructured solid state solar cells (MSSCs), [254]. These devices employed spiro-MeOTAD as the hole transporter but a mesoporous TiO_2 photoanode was not used as an electron transporter. High efficiency of 10.9% was achieved with the high photocurrent of 17.8 mA/cm^2 and the high photovoltage of 1 V [254]. The extended absorption down to 800 nm and highly crystalline nature of the perovskite electron conductor was found to be the reason behind high J_{sc} and high V_{oc}. The enhanced carrier collection can also be due to the electric dipole and a photoferroic effect of the

methylammonium cation. Further extending the work of the devices based on same architecture, Ball *et.al.* [255] introduced Al_2O_3 based solar cell together with a $CH_3NH_3PbI_{3-x}Cl_x$ perovskite and demonstrated an efficiency of 12.3%. An efficiency of 9% was reported by the same group for flat-junction thin film solar cell, in which the perovskite absorber worked in charge-separation and in ambipolar charge transportation of both carrier species.

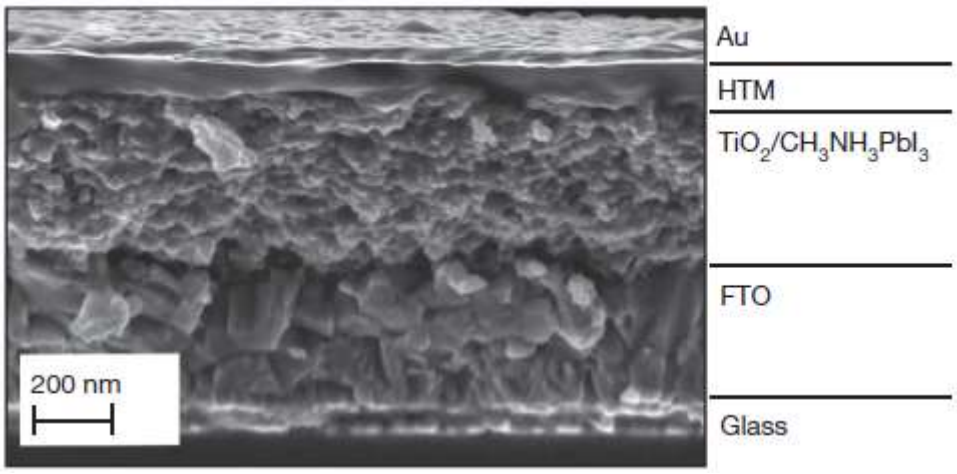

Figure 2.64: FESEM image of cross section of perovskite solar cell based on HTM.

The performance of perovskite solar cells surpassed 15% solar-to-electricity conversion efficiency [256]. The cross section image of perovskite solar cell based on HTM is illustrated in Figure 2.64, where all the layers of every component can be seen. Perovskite based solar cells signify the convergence of inorganic thin film and dye-sensitised solar cells [257] but the conversion efficiencies have grown beyond both the conventional cells very rapidly. Very recently Jacob *et.al.* demonstrated the superior charge collection in nanocomposite of graphene nanoflakes and TiO_2 nanoparticles and reported the efficiency of

perovskite based solar cells as high as 15.6% [258]. By this work perovskite based solar cells have covered one more milestone in a very short span of time.

2.9 METAL-OXIDE SEMICONDUCTOR

2.9.1 State of the art

Since the photocathode in a DSSC participates in the whole process of charge generation and transportation, each of its components is of prime importance for the overall performance of DSSCs. Although, electron generation takes place in the dye molecules, the electrons are collected and guided through the correct path by metal oxide semiconductor. The process of electron generation, collection and transportation should be sufficiently fast enough to suppress the electron recombination. This process depends upon the size, shape and surface area of metal-oxide nano-particles which inturn influence the morphology, porosity and transparency of metal oxide films in DSSC, most important aspects to be considered for the efficient DSSC. The nanoporous structure of the semiconductor allows a high surface concentration of the sensitizing dye to be adsorbed and sufficiently harvest the visible spectrum.

So far many metal oxide systems, such as niobium oxide (Nb_2O_5) [76], zinc oxide (ZnO) [75], tin oxide (SnO_2) [77], have been tested in DSSC, but titanium dioxide (TiO_2) proved to give the highest efficiencies [80] and leads in solar cell applications. The suitability of a semiconductor for optoelectronic purposes can also be improved by incorporating more than one metal oxide by chemical route and mixed oxides can be achieved. Some mixed oxides such as strontium titanate ($SrTiO_3$) [78] and zinc stannate (Zn_2SnO_4) [79] have also been investigated in solar cells, yet the optimum results could be gained by TiO_2 nanoparticles incorporation in photoanodes. The electron density and electron injection is

influenced by band structures of metal oxides which are different for all the metal oxides. It has been observed that TiO_2 and Nb_2O_5 exhibit the same bandgap energies but the conduction band of Nb_2O_5 is approximately 0.2-0.3 eV more negative than that of TiO_2 which makes it unsuitable for DSSC fabrication [76].

The schematic diagram of Ru dye anchored to TiO_2 nanoparticle is shown in Figure 2.65. In 1991 Grätzel *et.al.* demonstrated the superiority of nanoparticle films with a high surface area over a 10 μm flat film and reported an overall conversion efficiency of 7% by using nanometer-sized TiO_2 particles sensitized with a trimeric ruthenium complex [52]. It was also deduced that the anatase TiO_2 with exposed (101) planes provided better connection between the TiO_2 and ruthenium-based dye molecules which fecilitated the formation of a compact dye layer and improved dye concentration in the film.

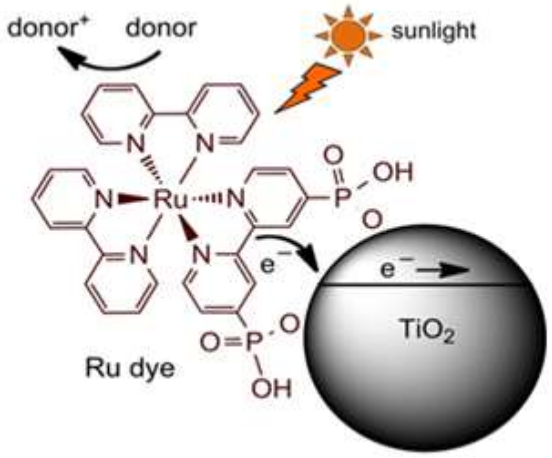

Figure 2.65: Schematic diagram showing the Ru dye anchored to TiO_2 nanoparticle.

The electron lifetime in a DSSC is as short as some milliseconds which makes it very critical to collect the charge efficiently brfore getting recombined with the electrolyte. Since

the nanoparticles give a large internal surface area in TiO_2 film, the probability of charge recombination increases due to close vicinity of semiconductor with electrolyte. A lot of work is being carried out in the direction to surpass this drawback of nanoporous metal oxide film in DSSCs. It has been reported by Hupp *et.al.* that either by accelerating the electrons movement or by reducing the distance between charge generation and charge collection sites, the charge collection efficiency can be improved [259]. In order to extract electrons efficiently a lot of work has been done to create one dimensional morphology which can facilitate the electron transport more proficiently, such as nanowires [260], nanotubes [261, 262] and vertically aligned nanopillers.

Although the synthesis of TiO_2 nanotube arrays on FTO glass substrate has been reported by hydrothermal growth, issues of detachment of the tubes from substrates during the high temperature annealing has restricted their applications. In order to work towards growing more durable nanotube array which can sustain high temperature treatments, Macák *et.al.* for the first time in 2005 reported the possibility of the use of anodic TiO_2 in DSSC [263]. The maximum efficiency achieved by these highly aligned nanotubes was 4.24% for 6 μm long tubes [264].

In order to improve the porosity of the films randomly oriented TiO_2 nanowires have also been studied for DSSC applications. The morphology was further improved by using AC potential instead of DC for anodization to produce bamboo type morphology of the nanotubes [265]. These bamboo-type nanotubes offer a wide range of benefits over rod shaped structures because of higher surface area and superior porosity. The bamboo-type nanotubes grown under AC condition with a sequence of 1 min at 120 V and 5 min at 40 V for 12 h exhibited an efficiency of ~2.96 %. 1D architecture presents the benefit of focused

channeling of electrons for a better charge collection at working electrode but the photoconversion efficiency of nano particles is still much higher in comparison with any 1D structure. This is due to much higher surface area and porosity of films made by nano particles providing better sensitizer adsorbtion in the film and superior electrolyte percolation [266].

For the effective suppression of charge recombination at the interface of nanoparticles and electrolyte an approach of developing energy berrier at the surface of nanoparticles which can retard recombination, was adopted. Such structures are known as core-shell structures in which core would comprise of nanoparticles, nanowires or nanotubes covered by a coating layer i.e. shell. The shell may construct an energy barrier at the interface of semiconductor and electrolyte and impede the reaction between the redox species in the electrolyte and the photogenerated electrons [267].

The porosity of the nanoporous film is a critical aspect and optimization in order to achieve the porosity is very important. Although high porosity is required for good sensitizer loading in the films for DSSC application, it breaks the interconnectivity of the particles and reduces the charge collection efficiency. To rectify this, a fine ordered nanoporous TiO_2 composition with narrow pore size allocation can be used. Due to the easy preparation and low cost, mostly solution based process is used for the deposition of nanoporous films which does not give a uniform structure. Moreover, different procedures are required to construct various nanostructures so it is expected to have different defect density and crystal size for different morphology. Sol-gel method is vastly used in creating sintered nanoparticles and films but it gives completely unoriented films. Self assembly is the promising approach to get a highly uniform morphology because it is based on the replication of self assembled

structures from tamplating systems [268-270]. Connecting the ends of two inequitable polymers covalently produces the self assembling materials which are also termed as diblock polymers [271]. Once the phase separation is achieved one component of a block copolymer can be selectively removed and a mesoporous template will be formed [272] (Figure 2.66).

Du *et.al.* demonstrated the combination of phase selective crosslinking chemistry followed by polymer deterioration [273] which was based on the concept of obtaining spatially controlled nanoporous films by merging lithography and polymer degeneration.

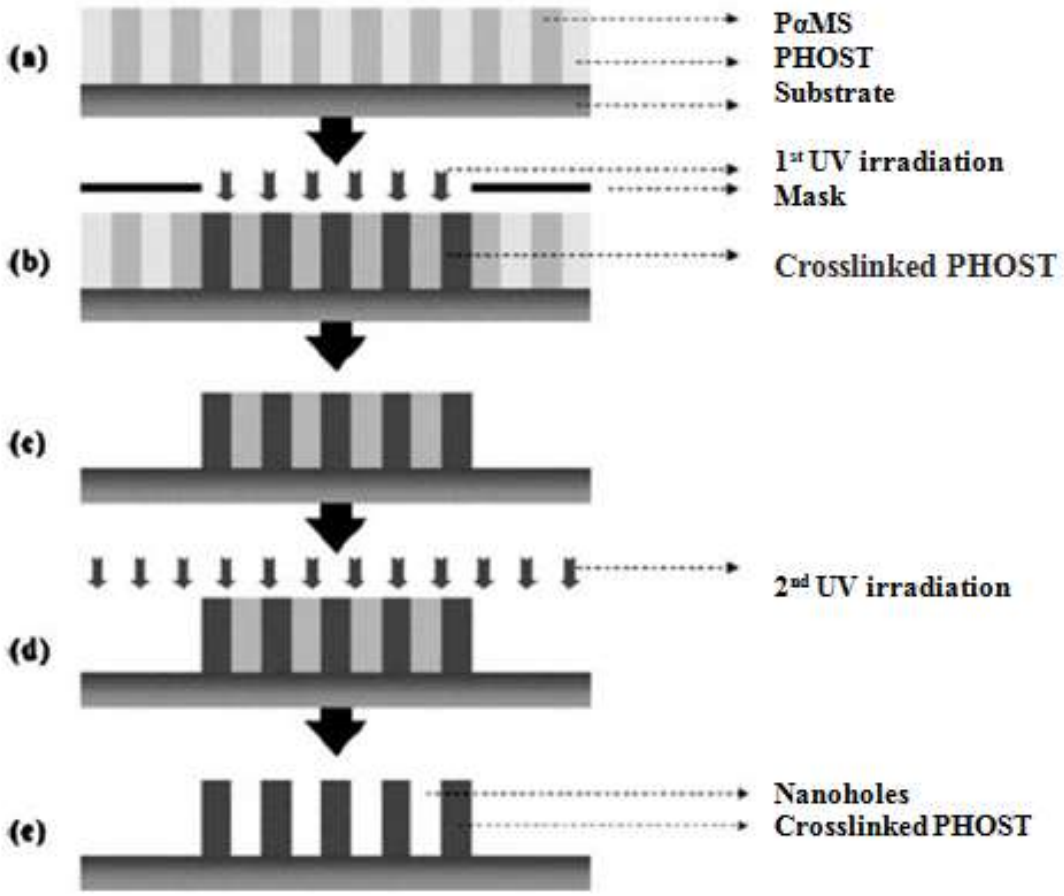

Figure 2.66: Nanofabrication process for obtaining spatially controlled nanopores.

Electrical insulation at the stoichiometric composition and large bandgap (over 3.0 eV) are the two drawbacks of pure TiO_2 to be used practically. It was calculated that quantum yield of rutile TiO_2 and anatase TiO_2 cannot be better than 2.2% and 1.3%, respectively [274]. Owing to the narrower band gap, more visible light absorption and higher electric conductivity, doped TiO_2 is more desirable in photovoltaic applications. There are two ways in which defective TiO_2 can be formed i.e. by controlled addition of metal or non metal impurities and by n-type doping that creates oxygen vacancies and known as Ti_3^+ species in TiO_2 [275, 276]. These species are responsible for the electronic conductivity and lowers the band gap by 0.3 to 0.8 eV below the conduction band of TiO_2 [276].

2.9.2 Synthesis of nanomaterials

Due to enrichment of properties of metal oxides from bulk to nano level, nanomaterials have found wide applications in many fields, which is the main force behind huge attention towards different synthesis procedures of nanomaterials. Top down approach which is a solid phase procedure involves attrition and milling, is not suitable for producing different morphologies. The shape and size can be controlled by chemical methods. It has been studied that use of different acids and alkalies can provide variety of shapes of nanoparticles [277].

2.9.2.1 Sol-gel synthesis

Based on inorganic polymerization reactions, the sol-gel method includes four steps: hydrolysis, polycondensation, drying and thermal decomposition. As shown in equation (2.17) and (2.18) that reaction starts with the hydrolysis of the precursors of the metal or non-metal alkoxides with water or alcohols and after condensation of the solution to a gel, the solvent is removed.

$$Ti(OR)_4+4H_2O \rightarrow Ti(OH)_4+4ROH(\text{hydrolysis}) \quad (2.17)$$

Where R = alkyl group

$$Ti(OH)_4 \rightarrow TiO_2+2H_2O(\text{condensation}) \quad (2.18)$$

It is a versatile process used in making various ceramic materials. Thin films can be produced on a substrate by spin-coating, screen printing or dip-coating. A wet gel will form when the sol is cast into a mold, which will be converted into a dense ceramic with further drying and heat treatment.

In a typical sol-gel process, a colloidal suspension is formed by the hydrolysis and polymerization reactions of the precursors followed by loss of solvent which leads to the transition from the liquid sol into a solid gel phase. A highly porous and extremely low density material called an aerogel can be obtained if the solvent in a wet gel is removed under a supercritical condition. Fibers can also be obtained by adjusting the viscosity of the sol into a proper viscosity range. In sol gel method nanostructured TiO_2 has been synthesized from hydrolysis of a titanium precursor. It proceeds via an acid-catalyzed hydrolysis step of titanium (IV) alkoxide followed by condensation. Low content of water, low hydrolysis rates, and excess titanium alkoxide in the reaction mixture are the important factors for the development of Ti-O-Ti chains. Development of Ti-O-Ti chains with close packing results in three dimensional polymeric skeletons. Highly crystalline anatase TiO_2 nanoparticles with different sizes and shapes could be obtained with the polycondensation of titanium alkoxide in the presence of tetramethylammonium hydroxide.

2.9.2.2 Hydrothermal synthesis

Hydrothermal synthesis is a method of synthesis of single crystals which relies on the solubility of minerals in hot water under high pressure. It is a simple method with minimal requirements of known quantities of precursor materials, autoclaves and ovens. Water is used both as catalyst and the component of solid phases in synthesis under elevated temperatures and pressures [278]. Autoclave is an apparatus consisting of a steel pressure vessel in which a nutrient is supplied along with water. A temperature gradient is maintained between the opposite ends of the growth chamber. The raw materials are placed in the lower part of the autoclave with a specific amount of solvent. In order to create two temperature zones the autoclave is then heated. At the hotter end the nutrient solute dissolves, while at the cooler end it is deposited on a seed crystal, growing into desired crystal. This method has advantages over other types of crystal growth due to its ability to create crystalline phases which are not stable at the melting point. The materials with high vapor pressure near their melting points can also be achieved by hydrothermal method. It maintains a good control over the composition during the growth of large crystals.

2.9.2.3 Solvothermal synthesis

The solvothermal method is almost identical to the hydrothermal method except that the solvent used here is nonaqueous organic solvent. The temperature can be elevated much higher than that in hydrothermal method because of a variety of organic solvents with high boiling points can be used. The solvothermal method normally has better control than hydrothermal methods on the size and shape distributions and the crystallinity of the TiO_2 nanoparticles. The solvothermal method has been found to be a versatile method for the

synthesis of a variety of nanoparticles with narrow size distribution and dispersity. The solvothermal method has been employed to synthesize TiO_2 nanoparticles [279].

2.9.2.4 Microwave synthesis

High-frequency electromagnetic waves can be used to process a dielectric material. The major frequencies of microwave heating are in the range of 900-2450 MHz. Due to the movement of ionic constituents, energy can be transferred from the microwave field to the material at lower microwave frequencies. Microwave radiations have been applied to prepare various TiO_2 nanostructures. TiO_2 synthesis has been realized by strained hydrolysis in hydrothermal condition starting from a 0.5 M solution of $TiOCl_2$ with the employment of both a conventional and a microwave thermal treatment. The microwave assisted syntheses have been conducted by using a microwave digestion system. It was observed that the system used 2.45 GHz microwaves and is controlled by both temperature and pressure. Microwave hydrothermal treatments conducted at 195^{o}C for different times ranging from 5 min to 1 h gave better results than the conventional synthesis which was conducted at the same temperature for the time ranging from 1 to 32 h in an electric oven using bombs with metal bodies and removable PTFE liners.

Owing to several advantages over traditional synthesis such as homogeneous nucleation, rapid synthesis, uniform crystal formation, small crystallites, facile morphology control, energy efficiency, uniform heating and so on, the microwave technique is regarded as a novel synthesis tool. It was observed that crystal morphology, size and orientation and even crystalline phase can be efficiently controlled by microwave technique.

2.9.2.5 Micelle and inverse micelle

When the surfactant concentration exceeds the critical micelle concentration (cmc) in water, it leads to the formation of aggregates of surfactant molecules and these aggregates are called Micelle. Above the cmc, the physical state of the surfactant molecules changes dramatically, and additional surfactant remains as aggregates or micelles. In normal micelles, the hydrophilic groups of the surfactants are in contact with the surrounding aqueous medium and the hydrophobic hydrocarbon chains of the surfactants are oriented toward the interior of the micelle. On the other hand, reverse micelles are formed in non-aqueous medium where the hydrophilic head-groups are directed outwards. The main role in development of some properties i.e. osmotic pressure, turbidity, solubility, surface tension, conductivity, and self-diffusion, is played by the surfactant change around the cmc. The drawbacks of sol-gel methods related to size and shape control can be overcome by synthesis of TiO_2 nanoparticles by micelle and reverse micelle methods.

2.10 CONCLUSION

Chapter contains a historical background of solar cells with basic photovoltaic concept and classification. The structures and working principles of liquid state DSSCs and solid state DSSCs and their components has been discussed in detail. Different type of sensitizers including perovskite has been elaborated with their state of arts. Applications and synthesis of metaloxide semiconductors have also been discussed.

In conclusion, the main points extracted in the chapter are as following:

- The basic processes behind the photovoltaic effect are the absorption of photon, separation of photo-generated charge carriers at the junction and collection of the separated charge carriers at the terminals of the junction.

- A photovoltaic device is an arrangement composed of different components designed to provide electric power using the sun as the power resource.
- Solar cells can be broadly devided as silicon, III-V solar cells, organic solar cells and hybrid solar cells.
- DSSC is a hybrid solar cell and the main events to take place in any solar cell are: light absorption, charge separation and charge transportation.
- Current-voltage (J-V) characteristic and IPCE are the important parameters in ascertaining the solar cell efficiency.
- Sensitizers, metaloxide semiconductors, electrolyte and counter electrode are the vital components of DSSCs.
- Sensitizers are replaced by perovskite materials in perovskite based solar cells.

References:

1. Becquerel, A. E. (1839), “Memoire sur les effets électriques produits sous l’influence des rayons solaires”, C. R. Acad. Sci. Paris, vol. 9, pp. 561-567.

2. Smith, W., (1873), “Effect of light on Selenium during the passage of an electric current”, Nature, Vol.7, pp.303-303.

3. Adams, W. G., Day, R. E., (1877), “The action of light on selenium”, Proc. R. Soc. Lond. A, Vol. 25, pp.113-117.

4. Einstein, A., (1905), “Concerning an Heuristic Point of View Toward the Emission and Transformation of Light”, Ann. Phys., Vol.17, pp. 132-148.

5. Czochralski, Z., (1918), “A new method of measuring the crystallization velocity of metals”, Phys. Chem., Vol.92, pp.219-221.

6. Chapin, D. M., Fuller, C. S. and Pearson, G. L., (1954), “A New Silicon p-n Junction Photocell for Converting Solar Radiation into Electrical Power”, J. Appl. Phys., Vol. 25, pp. 676-677.

7. Kylie, R. Catchpole, Michelle, J. McCann, Klaus J. Weber, Andrew W. Blakers, (2001), “A review of thin film crystalline silicon for solar cell applications”, Part 2: Foreign substrates, Solar Energy Materials & Solar Cells, Vol. 68, pp. 173.

8. Chapin, D. M., Fuller, C. S., and Pearson, G. L., (1954), “A New Silicon p-n Junction Photocell for Converting Solar Radiation into Electrical Power”, J. Appl. Phys., vol. 25, pp. 676-677.

9. Oh, J., Yuan, H. C., and Branz, H. M., (2012), “An 18.2%-efficient black-silicon solar cell achieved through control of carrier recombination in nanostructures, Nature Nanotechnology”, pp.743-748.

10. Yuan, H. C., Yost, V. E., Page, M. R., Stradins, P., Meier, D. L., and Branz, H. M., (2009), "Efficient black silicon solar cell with a density-graded nanoporous surface: optical properties, performance limitations, and design rules", Appl. Phys. Lett., Vol. 95, pp. 123501.

11. Masafumi, Y., Tatsuya, T., Kenji, A., Nicholas Ekins-Daukes, (2005), "Multi-junction III-V solar cells: current status and future potential", Proceedings of Solar Energy, Vol. 79, pp.78-85.

12. Katsuaki, T., (2009), "A Review of Ultrahigh Efficiency III-V Semiconductor Compound Solar Cells: Multijunction Tandem, Lower Dimensional, Photonic Up/Down Conversion and Plasmonic, Nanometallic Structures", Energies, Vol.2, pp.504-530.

13. Tanabe, K., (2009), "A Review of Ultrahigh Efficiency III-V Semiconductor Compound Solar Cells: Multijunction Tandem, Lower Dimensional, Photonic Up/Down Conversion and Plasmonic Nanometallic Structures", Energies, vol. 2, pp. 504-530.

14. Olson, J. M., Kurtz, S. R., Kibbler, A. E., Faine, P., (1990), "A 27.3-percent efficient Ga0.5In0.5P/GaAstandem solar-cell", Appl. Phys. Lett., Vol.56, pp.623-625.

15. King, R. R., Law, D. C., Fetzer, C. M., Sherif, R. A., Edmondson, K. M., Kurtz, S., Kinsey, G. S., Cotal, H. L., Krut, D. D., Ermer, J. H., Karam, N. H., (2005), "Pathway to 40% efficient concentrator photovoltaics, In Proceedings of the 20th European Photovoltaic", Solar Energy Conference, Barcelona, Spain, pp. 118-123.

16. King, R. R., Law, D. C., Edmondson, K. M., Fetzer, C. M., Sherif, R. A., Kinsey, G. S., Krut, D. D., Cotal, H. L., Karam, N. H., (2006), "Metamorphic and lattice-matched solar cells under concentration", In Proceedings of the IEEE 4th World Conference on Photovoltaic Energy Conversion, Waikoloa, HI, USA, pp. 760-763.

17. King, R. R., Law, D. C., Edmondson, K. M., Fetzer, C. M., Kinsey, G. S., Krut, D D., Ermer, J. H., Sherif, R. A., Karam, N. H., (2007), "Metamorphic concentrator solar cells with over 40% conversion efficiency", In Proceedings of the 4th International Conference on Solar Concentrators, El Escorial, Spain, pp. 5-8.

18. King, R. R., Law, D. C., Edmondson, K. M., Fetzer, C. M., Kinsey, G. S., Yoon, H., Sherif, R. A., Karam, N.H., (2007), "40% efficient metamorphic GaInP/GaInAs/Ge multijunction solar cells", Appl. Phys.Lett., Vol. 90, pp.183516-1-183516-3.

19. Guter, W., Schone, J., Philipps, S.P., Steiner, M., Siefer, G., Wekkeli, A., Welser, E., Oliva, E., Bett, A.W., Dimroth, F., (2009), "Current-matched triple-junction solar cell reaching 41.1% conversion efficiency under concentrated sunlight", Appl. Phys. Lett., Vol. 94, pp. 223504-1-223504-3.

20. Takamoto, T., Agui, T., Washio, H., Takahashi, N., Nakamura, K., Anzawa, O., Kaneiwa, M., Kamimura, K., Okamoto, K., Yamaguchi, M., (2005), "Future development of InGaP/(In)GaAs based multijunction solar cells", In Proceedings of the 31st IEEE Photovoltaic Specialists Conference, Lake Buena Vista, FL, USA, pp. 519-524.

21. Law, D.C., Edmondson, K.M., Siddiqi, N., Paredes, A., King, R.R., Glenn, G., Labios, E., Haddad, M.H., Isshiki, T.D., Karam, N.H., (2006), "Lightweight, flexible, high-efficiency III-V multijunction solar cells", In Proceedings of the IEEE 4th World Conference on Photovoltaic Energy Conversion, Waikoloa, HI, USA, pp. 1879-1882.

22. Takamoto, T., Kodama, T., Yamaguchi, H., Agui, T., Takahashi, N., Washio, H., Hisamatsu, Kaneiwa, M., Okamoto, K., Imaizumi, M., Kibe, K., (2006), "Paper-thin InGaP/GaAs solar cells", In Proceedings of the IEEE 4th World Conference on Photovoltaic Energy Conversion, Waikoloa, HI, USA, pp. 1769-1772.

23. Karam, N. H., King, R. R., Haddad, M., Ermer, J. H., Yoon, H., Cotal, H. L., Sudharsanan, R., Eldredge, J. W., Edmondson, K., Joslin, D. E., Krut, D. D., Takahashi, M., Nishikawa, W., Gillanders, M., Granata, J., Hebert, P., Cavicchi, B. T., Lillington, D. R., (2001), "Recent developments in high-efficiency Ga0.5In0.5P/GaAs/Ge dual- and triple-junction solar cells: steps to next- generation PV cells", Sol. Energy Mater. Sol. Cells, Vol. 66, pp. 453-466.

24. King, R. R., Fetzer, C. M., Law, D. C., Edmondson, K. M., Yoon, H., Kinsey, G. S., Krut, D. D., Ermer, J. H., Hebert, P., Cavicchi, B. T., Karam, N. H., (2006), "Advanced III-V multijunction cells for space", In Proceedings of the IEEE 4th World Conference on Photovoltaic Energy Conversion 2006, Waikoloa, HI, USA, pp. 1757-1762.

25. (a) Brabec, C. J., (2004), "Organic photovoltaics: technology and market", Sol. Energy Mater. Sol. Cells, Vol. 83, pp. 273-276; (b) Brabec, C. J., Sariciftci, N. S., and Hummelen, J. C., (2011), "Plastic solar Cells", Adv. Funct. Mater., Vol. 11, pp.15-26.

26. (a) Thompson, B. C., Frechet, J. M. J., (2008), "Polymer-Fullerene Composite Solar Cells", Angew. Chem., Int. Ed., vol 47, pp.58-77; (b) Kroon, R. M., Lenes, J. C., Hummelen, Blom, P. W. M. and Boer, B., (2008), "Small Bandgap Polymers for Organic Solar Cells", de Polym. Rev., vol 48, pp.531-582.

27. Green , M. A., Emery , K. Y., Hishikawa, Warta , W., Dunlop, E. D., (2012), "Solar cell efficiency tables (version 39)", Prog. Photovolt: Res. Appl, Vol. 20, pp.606-614.

28. Dennler, G., Sariciftci, N. S., Brabec, C. J., (2006), "Conjugated Polymer-Based Organic Solar Cells, in Semiconducting Polymers", 2nd edn, Ed. Hadziioannou and Malliaras, Wiley-VCH Verlag GmbH, Weinheim, Vol. 1, pp. 455-519.

29. Chamberlain, G. A., (1983), “Organic solar cells: A Review”, Sol. Cells, Vol.8, pp. 47-83.

30. Tang, C. W., (1986), “Two-layer organic photovoltaic cell”, Appl. Phys. Lett., Vol.48, pp.183-185.

31. Yoo, S., Domercq, B. and Kippelen, B., (2004), “Efficient thin organic solar cells based on pentacene/ C60 heterojunctions”, Appl. Phys. Lett., Vol. 85, pp.5427-5429.

32. Mayer, A. C., Lloyd, M. T., Herman, D. J., Kasen, T. G., Malliaras, G. G., (2004), “Post fabrication annealing of pentacene-based photovoltaic cells”, Appl. Phys. Lett., Vol.85, pp. 6272-6274.

33. Chu, C. W., Shao, Y. V., Shrotriya, Yang, Y., (2005), “Efficient Photovoltaic energy conversion in tetracene -C 60 based heterojunctions”, Appl. Phys. Lett., Vol.86 ,pp. 243506-1-243506-3.

34. Malliaras, G., and Friend, R., (2005), “An organic electronics primer”, Phys. Today, Vol. 58, pp. 53-58.

35. Forrest, S. R., (2003), “The road to high efficiency organic light emitting devices”, Organic Electronics, Vol. 4, pp. 45-48.

36. Gledhill, S. E., Scott, B., Gregg, B. A., (2005), “Organic and nanostructured composite photovoltaics: An overview”, J. Mater. Res., Vol. 20, pp. 3167- 3179.

37. Perzon, E., Wang, X., Zhang, F., Mammo, W., Delgado, J. L., Cruz, P., Inganäs, O., Langa, F., and Andersson, M. R., (2005), “Design, synthesis and properties of low band gap polyfluorenes for photovoltaic devices”, Synthetic Metals, Vol. 154, pp. 53-56.

38. Al-lbrahim, M., Ambacher, O., Sensfuss, S., and Gobsch, G., (2005), “Effects of solvents and annealing on the improved performance of solar cells based on ploy (3 hexylthiophene): fullerene”, Appl. Phys. Lett., Vol. 86, pp. 201120-201123.

39. Saunders, B.R., Turner, M.L., (2008), “Nanoparticle-polymer photovoltaic cells, Advances in Colloid and Interface Science”, Vol. 138, pp.1-23.

40. Greenham, N. C., Peng, X. and Alivisatos, A. P., (1996), “Charge separation and transport in conjugated-polymer/semiconductor-nanocrystal composites studied by photoluminescence quenching and photoconductivity”, Phys. Rev. B:Condens. Matter Mater. Phys., Vol. 54, pp.17628-17637.

41. Huynh, W. U., Dittmer, J. J. and Alivisatos, A. P., (2002), “Hybrid nanorod polymer solar cells”, Science, Vol. 295, pp. 2425-2427.

42. Sun, B., Marx, E. and Greenham, N. C., (2003), “Photovolatic devices using blends of branched CdSe nanoparticles and conjugated polymers”, Nano Lett., Vol. 3, pp. 961-963.

43. Sun, B. and Greenham, N. C., (2006), “Improved efficiency of photovoltaics based on CdSe nanorods and poly (3-hexylthiophene) nanofibers”, Phys. Chem., Vol.8, pp. 3557-3560.

44. Dayal, S., Kopidakis, N., Olson, D. C., Ginley, D. S., Rumbles, G., (2010), “Photovoltaic Devices with a Low Bandgap Polymer and CdSe Nanostructures Exceeding 3% Efficiency”, Nano Lett., Vol. 10, pp. 239-242.

45. Ren, S., Chang, L. Y., Lim, S. K., Zhao, J., Smith, Zhao, M., Bulovi´c, N. V., Bawendi, M., Gradeˇcak, S., (2011), “Inorganic-organic hybrid solar cell: bridging quantum dots to conjugated polymer nanowires”, Nano Lett., Vol. 11, pp. 3998-4002.

46. Gerischer, H., Tributsch, H., (1968), "Elektrochemische Untersuchung der spektralen Sensibilisierung von ZnO-Einkristallen", Ber. Bunsenges. Phys. Chem., vol. 72, pp. 437-445.

47. Tsubomura, H., Matsumura, M., Noyamaura, Y., Amamyiya, T., (1976), "Dye sensitised zinc oxide: aqueous electrolyte: platinum photocell", Nature, Vol. 261, pp. 402-403.

48. Clark, W. D. K., Sutin, N., (1977), "Spectral by polypyridine ruthenium(II) complexes", J. Am. Chem. Soc., 99, 4676-4682.

49. Anderson, S., Constable, E. C., Dare-Edwards, M. P., Goodenough, J. B., Hamnett, A., Seddon, K. R., Wright, R. D., (1979), "Chemical modification of a titanium (IV) oxide electrode to give stable dye sensitisation without a supersensitiser", Nature, Vol. 280, pp. 571-573.

50. Gerischer, H., (1975), "Electrochemical photo and solar cells: Principles and some experiences", J. Electroanal. Chem. Interfac., 58, 263-274.

51. Gerischer, H., (1972), "Electrochemical Techniques for The Study Of Photosensitization", Photochem. Photobiol, Vol. 16, pp. 243-260.

52. Regan, O. and Grätzel, M., (1991), "A low-cost, high-efficiency solar cell based on dye-sensitized colloidal TiO_2 films", Nature, Vol. 353, pp. 737-740.

53. Green, M. A., Emery, K., Hishikawa, Y. and Warta, W., (2009), Prog. Photovolt.: Res. Appl. Vol. 17, pp. 85-94.

54. Grätzel, M., (2003), "Dye-sensitized solar cells", J. Photochem. Photobiol. C, Vol. 4, pp.145-153.

55. Asbury, J. B., Hao, E. and Wang, Y., (2000), "Bridge Length-Dependent Ultrafast Electron Transfer from Re Polypyridyl Complexes to Nanocrystalline TiO_2 Thin Films Studied by Femtosecond Infrared Spectroscopy", J Phys Chem B, Vol. 104, pp.11957-11964.

56. Langdon, B., MacKenzie, V., Asunskis, D., Kelley, D. F., (1999), "Electron Injection Dynamics of Ru^{II}(4,4'-dicarboxy-2,2'-bipyridine)$_2$cis(NCS)$_2$ Adsorbed on MoS_2 Nanoclusters", J Phys Chem B, Vol. 103, pp. 11176-11180.

57. Kalyanasundaram, K. and Grätzel., M., (1998), "Applications of functionalized transition metal complexes in photonic and optoelectronic devices", Coord Chem Rev., Vol. 177, pp. 347-414.

58. Moser, J. E., Noukakis, D. and Bach, U. (1998), "Comments on Measurements of ultrafast photoinduced electron transfer", J Phys Chem B , vol. 102, pp. 3649-3650.

59. Van de Lagemaat, J., Park, N. G., Frank, A. J., (2000), "Influence of Electrical Potential Distribution, Charge Transport, and Recombination on the Photo potential and Photocurrent Conversion Efficiency of Dye-Sensitized Nano crystalline TiO_2 Solar Cells: A Study by Electrical Impedance and Optical Modulation Techniques", J. Phys. Chem. B, Vol. 104, pp. 2044-2052.

60. Forro, L., Chauvet, O., Emin, D., Zuppiroli, L., Berger, H., Levy, F., (1994), "High Mobility N-Type Charge Carriers in Large Single Crystals of Anatase (TiO_2)", J. Appl. Phys., Vol. 75, pp. 633-640.

61. Adachi, M., Murata, Y., Takao, J., Jiu, J., Sakamoto, M., Wang, F., (2004), "Highly efficient dye-sensitized solar cells with a titania thin-film electrode composed of a network structure of single-crystal-like TiO_2 nanowires made by the "oriented attachment" mechanism", J. Am. Chem. Soc., Vol. 126, pp. 14943-14949.

62. Durr, M., Schmid, A., Obermaier, M., Rosselli, S., Yasuda, A. and Nelles, G., (2005), "Low-temperature fabrication of dye-sensitized solar cells by transfer of composite porous layers", Nat. Mater., Vol. 4, pp. 607-611.

63. Jiu, J., Isoda, S., Wang, F. and Adachi, M., (2006), "Dye-sensitized solar cells based on a single-crystalline TiO_2 nanorod film", J. Phys. Chem. B, Vol. 110, pp. 2087-2092.

64. Tan, B. and Wu, Y., (2006), "Dye-sensitized solar cells based on anatase TiO_2 nanoparticle/nanowire composites", J. Phys. Chem. B, Vol. 110, pp. 15932-15938.

65. Argazzi, R., Bignozzi, C. A., Heimer, T. A., Castellano, F. N., Meyer, G. J., (1995), "Long-Lived Photo-Induced Charge Separation Across Nanocrystalline TiO_2 Interfaces", J. Am. Chem. Soc., Vol. 117, pp. 11815-11816.

66. Yum, J. H., Chen, P., Grätzel, M., Nazeeruddin, M. K., (2008), "Recent developments in solid-state dye-sensitized solar cells", Chem Sus Chem, Vol. 1, pp. 699-707.

67. Bach, U., Lupo, D., Comte, P., Moser, J. E., Welssçrtel, F., Salbeck, J., Spreitzer, H., Grätzel, M., (1998), "Solid-state dye-sensitized mesoporous TiO_2 solar cells with high photon-to-electron conversion efficiencies",Nature, Vol. 395, pp. 583-585.

68. Schwarzburg, K., Willig, F., (1991), "Influence of trap filling on photocurrent transients in polycrystalline TiO_2", Appl Phys Lett, Vol. 58, pp. 2520-2523.

69. Li, B., Wang, L., Kang, B., Wang, P. and Qiu, Y., (2006), "Review of recent progress in solid-state dye-sensitized solar cells", Sol. Energy. Mat. Solar Cells, Vol. 90, pp. 549-573.

70. Nogueira, A. F., Longo, C., De Paoli, M.A., (2004), "Polymers in dye sensitizedsolar cells: overview and perspectives", Coord. Chem. Rew., Vol. 248, pp.1455-1468.

71. Grätzel, M., (2009), "Recent Advances in Sensitized Mesoscopic Solar Cells", Acc. Chem. Res., Vol. 42, pp.1788-1798.

72. Gordon R G, "Criteria for choosing transparent conductors", MRS Bull, Vol.25, pp.52-57.

73. Lindstrom, H., Holmberg, A., Magnusson, E., Lindquist, S. E., Malmqvist, L., Hagfeldt, A., (2001), Nano Lett.,Vol. 2, pp.97-100.

74. Wang, Q., Ito, S., Grätzel, M., Fabregat-Santiago, F., Mora-Seró, I., Bisquert, J., Bessho T. and Imai, H., (2006), "Characteristics of High Efficiency Dye-Sensitized Solar Cells", J. Phys. Chem. B, Vol. 110, pp. 25210-25221.

75. Saito, M. and Fujihara, S., (2008), "Large photocurrent generation in dye-sensitized ZnO solar cells", Energy Environ. Sci., Vol. 1, pp. 280-283.

76. Guo, P., Aegerter, M. A., (1999), "RU(II) sensitized Nb_2O_5 solar cell made by the sol-gel process", Thin Solid Films, Vol. 351, pp. 290-294.

77. Onwona-Agyeman, B., Kaneko, Kaneko, S., Kumara, A., Okuya, M., Murakami, K., Konno, A. and Tennakone, K., (2005), "Sensitization of Nanocrystalline SnO_2 Films with Indoline Dyes", Jpn. J. Appl. Phys., Vol. 44, pp. L731-L733.

78. Hore, S., Palomares, E., Smit, H., Bakker, N. J., Comte, P., Thampi, K. R., Kroon, J. M., Hinsch, A., Durrant, J. R., (2005), "Acid versus base peptization of mesoporous nanocrystalline TiO_2 films: functional studies in dye sensitized solar cells", J. Mater. Chem., Vol. 15, pp. 412-418.

79. Benkstein, K. D., Kopidakis, N., van de Lagemaat, J., Frank, A. J., (2003), "Influence of the Percolation Network Geometry on Electron Transport in Dye-Sensitized Titanium Dioxide Solar Cells", J. Phys. Chem. B, Vol. 107, pp. 7759-7767.

80. Grätzel, M., (2006), "Prog. Photovolt: The advent of mesoscopic injection solar cells, Progress in Photovoltaics: Research and Applications", Res. Appl., Vol. 4, pp. 429-442.

81. Bignozzi, C. A., Argazzi, R., Kleverlaan, C., (2000), "Molecular and supramolecular sensitization of nanocrystalline wide band-gap semiconductors with mononuclear and poly nuclear metal complexes", J. Chem. Soc., Vol. 29, pp. 87-96.

82. Qin, P., Yang, X., Chen, R., Sun, L. C., Marinado, T., Edvinsson, T., Boschloo, G., Hagfeldt, A., (2007), "Influence of π-Conjugation Units in Organic Dyes for Dye-Sensitized Solar Cells", J. Phys. Chem. C, 111, 1853-1860.

83. Haque, S. A., Palomares, E., Cho, B. M., Green, A. N. M., (2005), "Charge separation versus recombination in dye-sensitized nanocrystalline solar cells: the minimization of kinetic redundancy", J. Am. Chem. Soc., Vol. 127, pp. 3456 -3462.

84. Li, B., Wang, L. D., Kang, B. N., Wang, P. and Qiu, Y., (2006), "Review of Recent Progress in Solid-State Dye-Sensitized Solar Cells, Solar Energy Materials & Solar Cells", Vol. 90, pp. 549-573.

85. Fukui, A., Komiya, R., Yamanaka, R., Islam, A. and Han, L., (2006), "Effect of a redox electrolyte in mixed solvents on the photovoltaic performance of a dye-sensitized solar cell", Solar Energy Materials & Solar Cells, Vol. 90, pp. 649-658.

86. Hao, S. C., Wu, J. H., Fan, L. Q., Huang, Y. F., Lin, J. M., Wei, Y. L., (2004), "Electrochemical oxidation and the quantitative determination of phosphine on a SPE-based sensor", Sol. Energy, vol. 76, pp. 745-750.

87. Wu, J., Lan, Z., Lin, J., Huang, M. and Li, P., (2000), "Effect of solvents in liquid electrolyte on the photovoltaic performance of dye-sensitized solar cells", Journal of Power Sources, Vol. 173, pp. 585-591.

88. Pichot, F. and Gregg, B. A., (2000), "The Photovoltage-Determining Mechanism in Dye-Sensitized Solar Cells", J. Phys. Chem. B, vol. 104, pp. 6-10.

89. Daeneke, T. , Kwon, T. H., Holmes, A. B., Duffy, N. W., Bach, U., Spiccia, L., (2011), "High-efficiency dye-sensitized solar cells with ferrocene-based electrolytes", Nature Chem. Vol. 3, pp. 211-215.

90. Hara, K., Horiguchi, T., Kinoshita, T., Sayama, K., Arakawa, H., (2001), "Influence of electrolytes on the photovoltaic performance of organic dye-sensitized nanocrystalline TiO_2 solar cells", Solar Energy Materials and Solar Cells, Vol. 70, pp. 151-161.

91. Nusbaumer, H., Moser, J. E., Zakeeruddin, S. M., Nazeeruddin, M. K., Grätzel, M., (2001), "$CoII(dbbip)_2^{2+}$ Complex Rivals Tri-iodide/Iodide Redox Mediator in Dye-Sensitized Photovoltaic Cells", J. Phys. Chem. B, Vol. 105, pp. 10461-10464.

92. Cahen, D., Hodes, G., Grätzel, M., Guillemoles, J. F., Riess, I., (2000), "Nature of Photovoltaic Action in Dye-Sensitized Solar Cells", J Phys Chem B, Vol. 104, pp. 2053-2059 .

93. Nister, D., Keis, K., Lindquist, S. E. and Hagfeldt, A., (2002), "A detailed analysis of ambipolar diffusion in nanostructured metal oxide films", Solar Energy Materials and Solar Cells, Vol. 73, pp. 411-423.

94. Liu, Y., Hagfeldt, A., Xiao, X. R., Lindquist, S. E., (1998), "Investigation of influence of redox species on the interfacial energetics of a dye-sensitized nanoporous TiO< sub> 2</sub> solar cells", Sol. Energy Mater. Sol. Cells, Vol. 55, pp. 267-281.

95. Wang, Z. S., Sayama, K., Sugihara, H., (2005), "Efficient eosin y dye-sensitized solar cell containing Br^-/Br_3^- electrolyte", J. Phys. Chem. B, Vol. 109, pp. 22449-22455.

96. Bergeron, B. V., Marton, A., Oskam, G., (2005), "Dye-sensitized SnO_2 electrodes with iodide and pseudohalide redox mediators", J. Phys. Chem. B, Vol. 109, pp. 937-943.

97. Sapp, S. A., Elliott, C. M., Contado, C., (2002), "Substituted polypyridine complexes of cobalt(II/III) as efficient electron-transfer mediators in dye-sensitized solar cells", J. Am. Chem. Soc., Vol. 124, pp. 11215-22.

98. Kusama, H., Kurashige, M., Arakawa, H., (2005), "Influence of nitrogen-containing heterocyclic additives in I^-/I_3^- redox electrolytic solution on the performance of Ru-dye-sensitized nano crystalline TiO_2 solar cell", J. Photochem. Photobiol., Vol. 169, pp. 169-176.

99. Kusama, H., Arakawa, H., (2005), "Influence of pyrazole derivatives in I^-/I_3^- redox electrolyte solution on Ru(II)-dye-sensitized TiO_2 solar cell performance", Sol. Energy Mater. Sol. Cells, Vol. 85, pp. 333-344.

100. Frank, A. J., Kopidakis, N., Lagemaat, J. V. D., (2004), "Electrons in nanostructured TiO_2 solar cells: transport, recombination and photovoltaic properties", Coord. Chem., Vol. 248, pp. 1165-1179

101. Watson, D. F., Meyer, G. J., (2004), "Cation effects in nanocrystalline solar cells", Coord. Chem., Vol. 248, pp. 1391-1406.

102. Gorlov, M., Kloo, L., (2008), "Ionic liquid electrolytes for dye-sensitized solar cells", Dalton Trans, Vol. 20, pp. 2655-2666.

103. Cao, Y., Zhang, J., Bai, Y., Li, R., Zakeeruddin, S. M., Michael, G., Wang, P., (2008), "Dye-sensitized solar cells with solvent-free ionic liquid electrolytes", Phys. Chem. C, Vol. 112, pp. 13775-13781.

104. Bai, Y., Cao, Y., Zhang, J., Wang, M., Li, R., Wang, P., Zakeeruddin, S. M., Gratzel, M., (2008), "High-performance dye-sensitized solar cells based on solvent-free electrolytes produced from eutectic melts", Nature Materials, Vol. 7, pp. 626-630.

105. Kuang, D., Uchida, S., Humphry-Baker, R., Zakeeruddin, S. M., Gratzel, M., (2008), "Organic Dye-Sensitized Ionic Liquid Based Solar Cells: Remarkable Enhancement in Performance through Molecular Design of Indoline Sensitizers", Angewandte Chemie, International Edition, Vol. 47, pp. 1923-1927.

106. Nogueira, A. F., Longo, C., De Paoli, M. A., (2004), "Polymers in dye sensitized solar cells: overview and perspectives", Coord. Chem, Vol. 248, pp. 1455-1468.

107. Kim, J. H., Kang, M. S., Kim, Y. J., Won, J., and Y. S., (2005), "Poly(butyl acrylate)/NaI/I_2 electrolytes for dye-sensitized nanocrystalline TiO_2 solar cells", Solid State Ionics, Vol. 176 (5-6), pp. 579-584.

108. Kubo, W., Murakoshi, K., Kitamura, T., Yoshida, S., Hakuri, M., Hanabusa, K., Shirai, H., Wada, Y. and Yanagida, S., (2001), "Quasi-solid-state dye-sensitized TiO_2 solar cells: effective charge transport in mesoporous space filled with gel electrolytes containing iodide and iodine", J. Phys. Chem, Vol. 105, pp.12809-12815.

109. Kang, J., Li, W., Wang, X., Lin, Y., Li, X., Xiao, X. and Fang, S., (2004), "Gel polymer electrolytes based on a novel quaternary ammonium salt for dye-sensitized solar cells", Journal of Applied Electrochemistry, Vol. 34, pp. 301-304.

110. Ikeda, N., Teshima, K. and Miyasaka, T., (2006), "Conductive polymer-carbon-imidazolium composite: a simple means for constructing solid-state dye-sensitized solar cells", Chem. Commun, Vol. 16, pp. 1733-1735.

111. O'Regan, Lenzmann, F., Muis, R., (2002), "A solid-state dye-sensitized solar cell fabricated with pressure-treated P25-TiO_2 and CuSCN: Analysis of pore filling and IV characteristics", Chemistry of Materials, Vol. 14, pp. 5023-5029.

112. Wang, P., Zakeeruddin, S. M., Moser, J. E., Baker, R. H., Gratzel, M., (2004), "A solvent-free, $SeCN^-/(SeCN)_3^-$ based ionic liquid electrolyte for high-efficiency dye-sensitized nanocrystalline solar cells", Journal of the American Chemical Society, Vol. 126, pp. 7164-7165.

113. Matsumoto, H., Matsuda, T., Tsuda, T., Hagiwara, R., Ito, Y., Miyazaki, Y., (2001), "The application of room temperature molten salt with low viscosity to the electrolyte for dye-sensitized solar cell", Chem. Lett., Vol. 30, pp. 26-27.

114. Croce, F., Appetecchi, G. B., Persi, L., Scrosati, B., (1998), "Nanocomposite polymer electrolytes for lithium batteries", Nature, Vol. 394, pp. 456-458.

115. Zhang, J., Han, H., Wu, S., Xu, S., Zhou, C., Yang, Y., Zhao, X., (2007), "Ultrasonic irradiation to modify the PEO/P(VDF-HFP)/TiO_2 nanoparticle composite polymer electrolyte for dye sensitized solar cells", Nanotechnology, Vol. 18, pp. 295606-295613.

116. Kang, M. S., Ahnand, K. S., Lee, J. W., (2008), "Quasi-solid-state dye-sensitized solar cells employing ternary component polymer-gel electrolytes", J. Power Sources, vol. 180, pp. 896-901.

117. Bhattacharya, B., Lee, J. Y., Geng, J., Jung, H. T., Park, J. K., (2009), "Effect of cation size on solid polymer electrolyte based dye-sensitized solar cells", Langmuir, Vol. 25, pp. 3276-3281.

118. De Freitas, J. N., Nogueira, V. C., Ito, B. I., Soto-Oviedo, M. A., Longo, C., De Paoli, M. A., Nogueira, A. F., (2006), "Dye-sensitized solar cells and solar module using polymer electrolytes: Stability and performance investigations", Int. J. Photoenergy, Vol. 2006, pp. 1-6.

119. Sirimanne, P. M., Jeranko, T., Bogdanoff, P., Fiechter, S., Tributsch, H., (2003), "On the photo-degradation of dye sensitized solid-state TiO_2/dye/CuI cells", Semiconductor Science and Technology, Vol. 18, pp. 708-712.

120. Kumara, G. R. A., Kaneko, S., Okuya, M., Tennakone, K., (2002), "Fabrication of dye-sensitized solar cells using triethylamine hydrothiocyanate as a CuI crystal growth inhibitor", Langmuir, Vol. 18 , pp. 10493-10495.

121. O'Regan, B., Lenzmann, F., Muis, R. and Wienke, J., (2002), "A solid-state dye-sensitized solar cell fabricated with pressure-treated P25-TiO_2 and CuSCN: Analysis of pore filling and IV characteristics", Chemistry of Materials, Vol. 14, pp. 5023-5029.

122. Itzhaik, Y., Niitsoo, O., Page, M. and Hodes, G., (2009), "Sb_2S_3-sensitized nanoporous TiO_2 solar cells", Journal of Physical Chemistry C, Vol. 113, pp. 4254-4256.

123. Catellani, M., Boselli, B., Luzzati, S., Tripodi, C., (2002), Thin Solid Films, vol. 66, pp. 403.

124. Sirringhaus, H., Brown, P. J., Friend, R. H., Nielsen, M. M., (1999), "Two-dimensional charge transport in self-organized, high-mobility conjugated polymers", Nature, Vol. 401, pp, 685-688.

125. Hung, L. S., Tang, C. W., Mason, M. G., (1997), "Enhanced electron injection in organic electroluminescence devices using an Al/LiF electrode",Appl. Phys. Lett., vol. 70, pp. 152-154.

126. Bach, U., Lupo, D., Comte, P., Moser, J. E., Weissortel, F., Salbeck, J., Spreitzer, H. and Grätzel, M., (1998), "Solid-state dye-sensitized mesoporous TiO_2 solar cells with high photon-to-electron conversion efficiencies", Nature, vol. 395 (6702), pp. 583-585.

127. Kruger, J., Plass, R., Cevey, L., Piccirelli, M., Grätzel, M., Bach, U., (2001), "High efficiency solid-state photovoltaic device due to inhibition of interface charge recombination", Applied Physics Letters, Vol. 79, pp. 2085-2087.

128. Leijtens, T., Ding, I. K., Giovenzana, T., Bloking, J. T., McGehee, M. D. and Sellinger, A., (2012), "Hole Transport Materials with Low Glass Transition Temperatures and High Solubility for Application in Solid-State Dye-Sensitized Solar Cells", ACS Nano, Vol. 6, pp. 1455-1462.

129. Michaleviciute, A., Degbia, M., Tomkeviciene, A., Schmaltz, B., Gurskyte, E., Grazulevicius, J. V., Bouclé, J., Tran-Van, F., (2014), "Star-shaped carbazole derivative based efficient solid-state dye sensitized solar cell", Journal of Power Sources, vol. 253, pp. 230-238.

130. Stergiopoulos, T., Arabatzis, I. M., Katsaros, G., Falaras, P., (2002), "Binary polyethylene oxide/titania solid-state redox electrolyte for highly efficient nanocrystalline TiO_2 photo electrochemical cells", Nano Letters, Vol. 2, pp. 1259-1261.

131. Cherepy, N. J., Smestad, G. P., Grätzel, M., Zhang, J. Z., (1997), "Ultrafast electron injection: implications for a photoelectrochemical cell utilizing an anthocyanin dye-sensitized TiO_2 nanocrystalline electrode", J. Phys. Chem. B, Vol. 101, pp. 9342-9351.

132. Garcia, C. G., Polo, A. S., Murakami Iha, N. Y., (2003), "Fruit extracts and ruthenium polypyridinic dyes for sensitization of TiO_2 in photoelectrochemical solar cells", J. Photochem. Photobiol. A, Vol. 160, pp. 87-91.

133. Kamat, P. V., Chauvet, J. P., Fessenden, R. W., (1986), "Photoelectrochemistry in particulate systems and Photosensitization of a TiO_2 semiconductor with a chlorophyll analogue", Journal of Physical Chemistry, Vol. 90, pp. 1389-1394.

134. Bedja, I., Kamat, P. V., Hotchandani, S., (1996), "Fluorescence and photo electrochemical behavior of chlorophyll a adsorbed on a nanocrystalline SnO_2 film", Journal of Applied Physics, Vol. 80, pp. 4637-4643.

135. Kalyanasundaram, K., Vlachopoulos, N., Krishnan, V., Monnier, A., Grätzel, M., (1987), "Sensitization of titanium dioxide in the visible light region using zinc porphyrins", J. Phys. Chem., Vol., pp. 2342-2347.

136. Mao, H., Deng, H., Li, H., Shen, Y., Lu, Z., Xu, H., (1998), "Photosensitization of TiO_2 semiconductor with prophyrin", J. Photochem. Photobiol. A, Vol. 114, pp. 209-212.

137. He, J. J., Hagfeldt, A., Lindquist, S. E., Grennberg, H., Korodi, F., Sun, L. C., Akermark, B., (2001), "Phthalocyanine-Sensitized Nanostructured TiO_2 Electrodes Prepared by a Novel Anchoring Method", Langmuir, vol. 17, pp. 2743-2747.

138. Aranyos, V., Hjelm, J., Hagfeldt, A., Grennberg, H., (2001), "Free-base tetra-aryl phthalocyanines for dye-sensitised nanostructured solar cell applications", J. Porphyrins Phthalocyanines, Vol. 5, pp. 609-616.

139. Islam, A., Sugihara, H., Hara, K., Singh, L. P., Katoh, R., Yanagida, Takahashi, M., Y., Murata, S., (2001), "Dye sensitization of nano crystalline titanium dioxide with square planar platinum (II) diimine dithiolate complexes", Inorg. Chem., Vol. 40, pp. 5371-53780.

140. Enea, O., Moser, J., Grätzel, M., (1989), "Achievement of incident photon to electric current conversion yields exceeding 80% in the spectral sensitization of titanium dioxide bycoumarin", J. Electroanal. Chem., Vol. 259, pp. 59-65.

141. Kamat, P. V., Ford, W. E., (1987), "Photochemistry on surfaces: triplet-triplet energy transfer on colloidal TiO_2 particles", Chem. Phys. Lett., Vol. 135, pp. 421-426.

142. Kamat, P.V., (1989), "Photoelectrochemistry in Particulate Systems. 9. Photosensitized Reduction in a Colloidal TiO_2, System Using Ant hracene-9-carboxylic Acid as the Sensitizer", J. Phys. Chem., Vol. 93, pp. 859-864.

143. Yella, A., Lee, H., Tsao, H. N., Yi, C., Chandiran, A. K., Nazeeruddin, M. K., Diau, E. W., Yeh, C. Y., Zakeeruddin, S. M. and Grätzel, M., (2011), "Porphyrin-Sensitized Solar Cells with Cobalt (II/III)-Based Redox Electrolyte Exceed 12 Percent Efficiency", Science, vol. 334, pp. 629-634.

144. Meyer, G. J., (1997), "Efficient Light-to-Electrical Energy Conversion: Nanocrystalline TiO_2 Films Modified with Inorganic Sensitizers", J. Chem. Educ., Vol. 74, pp. 652-656.

145. Nazeeruddin, M. K., Kay, A., Rodicio, I., Humphry-Baker, R., Muller, E., Liska, P., Vlachopoulos, N. and Gratzel, M., (1993), "Conversion of light to electricity by cis-X_2bis(2,2'-bipyridyl-4,4'-dicarboxylate)ruthenium(II) charge-transfer sensitizers (X = Cl^-, Br^-, I^-, CN^-, and SCN^-) on nanocrystalline titanium dioxide electrodes", J. Am. Chem. Soc., vol. 115, pp. 6382-6390.

146. Nazeeruddin, M. K., Pechy, P. and Grätzel, M., (1997), "Efficient panchromatic sensitization of nanocrystallineTiO_2 films by a black dye based on atrithiocyanato-ruthenium complex", Chem. Commun., Vol. 18, pp.1705-1706.

147. Nazeeruddin, M. K., Pechy, P., Renouard, T., Zakeeruddin, S. M., Humphry-Baker, R., Comte, P., Liska, P., Cevey, L., Costa, E., Shklover, V., Spiccia, L., Deacon, G. B., Bignozzi, C. A. and Grätzel, M., (2001), "Engineering of Efficient Panchromatic Sensitizers for Nanocrystalline TiO_2-Based Solar Cells", J. Am. Chem. Soc., Vol. 123 pp.1613-1624.

148. Wang, P., Zakeeruddin, S. M., Humphry-baker, R., Moser, J. E. and Grätzel, M., (2003), "Molecular-Scale Interface Engineering of TiO_2 Nanocrystals: Improve the Efficiency and Stability of Dye-Sensitized Solar Cells", Adv. Mater., vol. 15, pp. 2101-2104.

149. Altobello, S., Argazzi, R., Caramori, S., Contado, C., Da Fre, S., Rubino, P., Chone, C., Larramona, G. and Bignozzi, C. A., (2005), "Sensitization of Nanocrystalline TiO_2 with Black Absorbers Based on Os and Ru Polypyridine Complexes", J. Am. Chem. Soc., vol. 127, pp. 15342-15343.

150. Hasselmann, G. M. and Meyer, G. J. Z., (1999), "Diffusion-Limited Interfacial Electron Transfer with Large Apparent Driving Forces", J. Phys. Chem. B, vol. 103, pp. 7671-7675.

151. Ferrere, S., (2002), "New photosensitizers based upon $[Fe^{II}(L)_2(CN)_2]$ and $[Fe^{II}L_3]$, where L is substituted 2, 2′-bipyridine", Inorg. Chim. Acta., vol. 329, pp. 79-92.

152. Geary, E. A. M., McCall, K. L., Turner, A., Murray, P. R., McInnes, E. J. L., Jack, L., Yellowleesa, L. J. and Robertson, N., (2008), "Spectroscopic, electrochemical and computational study of Pt-diimine-dithiolenecomplexes: rationalising the properties of solar cell dyes", Dalton Trans., vol. 28, pp. 3701-3708.

153. Bessho, T., Constable Edwin, C., Grätzel, M., Hernandez Redondo, A., Housecroft Catherine, E., Kylberg, W., Nazeeruddin, M. K., Neuburger, M. and Schaffner, S., (2008), "An element of surprise-efficient copper-functionalized dye-sensitized solar cells", Chem. Commun., vol. 32, pp. 3717-3719.

154. Giribabu, L., Kanaparthi, R. K. and Velkannan, V., (2012), "Molecular engineering of sensitizers for dye-sensitized solar cell applications", Chem. Rec., vol. 12, pp. 306-328.

155. Giribabu, L. and Kanaparthi, R. K., (2013), "Are porphyrins an alternative to ruthenium (II) sensitizers for dye-sensitized solar cells?", Curr. Sci., vol. 104, pp. 847- 855.

156. Nazeeruddin, M. K., Baker, R. H., Gratzel, M., Wohrle, D., Schnurpfeil, G., Schneider, G., Hirth, A. and Trombach, N., (1999), "Efficient near-IR sensitization of nanocrystalline TiO_2 films by zinc and aluminum phthalocyanines", J. Porphyrins Phthalocyanines, vol. 3, pp. 230-237.

157. Yong, L., Peifen, L., Xingzhong, Y., Lu, J. and Zhonghua, P., (2013), "Non-aggregated hyperbranched phthalocyanines: single molecularnanostructures for efficient semi-opaque photovoltaics", RSC Adv., vol. 3, pp. 545-558.

158. He, J., Benko, G., Korodi, F., Polıvka, T., Lomoth, R., Akermark, B., Sun, L., Hagfeldt, A. and Sundstrom, V., (2002), "Modified Phthalocyanines for Efficient Near-IR Sensitization of Nanostructured TiO_2 Electrode", J. Am. Chem. Soc., vol. 124, pp. 4922-4932.

159. Giribabu, L., Singh, V. K., Jella, T., Soujanya, Y., Amat, A., DeAngelis, F., Yella, A., Gao, P. and Nazeeruddin, M. K., (2013), "Sterically demanded unsymmetrical zinc phthalocyanines for dye-sensitized solar cells", Dyes Pigm., vol. 98, pp. 518-529.

160. Wang, P., Klein, C., Moser, J. E., Humphrey-Baker, R., Cevey-Ha, N. L., Charvet, R., Comte, P., Zakeeruddin, S. Grätzel, M., (2004), "Amphiphilic Ruthenium Sensitizer with 4,4'-Diphosphonic Acid-2,2'-bipyridine as Anchoring Ligand for Nanocrystalline Dye Sensitized Solar Cells", M. J.Phys. Chem. B, vol. 108, pp. 17553-17559.

161. Klein, C., Nazeeruddin, Md. K., Liska, P., Di Censo, D., Hirata, N., Palomares, E., Durrant, J. R., Grätzel, M., (2005), "Engineering of a Novel Ruthenium Sensitizer and Its Application in Dye-Sensitized Solar Cells for Conversion of Sunlight into Electricity", M. Inorg. Chem., vol. 44, pp. 178-180.

162. Kuang, D., Ito, S., Wenger, B., Klein, C., Moser, J. E., Humphry-Baker, R., Zakeeruddin, S. M. and Grätzel M., (2006), "High Molar Extinction Coefficient Heteroleptic

Ruthenium Complexes for Thin Film Dye-Sensitized Solar Cells", J. Am. Chem. Soc., vol. 128, pp. 4146-4154.

163. Wang, P., Klein, C., Humphry-Baker, R., Zakeeruddin, S. M., Grätzel, (2005), "A High Molar Extinction Coefficient Sensitizer for Stable Dye-Sensitized Solar Cells", M. J. Am. Chem. Soc., vol.127, pp. 808-809.

164. Lees, A. C., Kleverlaan, C. J., Bignozzi, C. A., Vos, J. G., (2001), "Photophysical properties of TiO_2 surfaces modified with dinuclear RuRu and RuOs polypyridyl complexes", Inorg. Chem., vol. 40, pp. 5343-5349.

165. Argazzi, R., Bignozzi, C.A., Heimer, T.A., Meyer, G. J., (1997), "Structure and Bond Nature of the UF_5 Monomer", Inorg. Chem., vol. 36, pp. 2-3.

166. Kleverlaan, C. J., Indelli, M. T., Bignozzi, C. A., Pavanin, L., Scandola, F., Hasselmann, G. M., Meyer, G. J., (2000), "Stepwise Charge Separation in Heterotriads. Binuclear Ru(II)−Rh(III) Complexes on Nanocrystalline Titanium Dioxide", J. Am. Chem. Soc., vol.122, pp. 2840-2849.

167. Chen, C. Y., Pootrakulchote, N., Hung, T. H., Tan, C. J., Tsai, H. H., Zakeeruddin, S. M., Wu, C. G. and Gratzel, M., (2011), "New Ruthenium Sensitizer with Carbazole Antennas for Efficient and Stable Thin-Film Dye-Sensitized Solar Cells", J. Phys. Chem. C, vol. 115, pp. 20043-20050.

168. Fan, S. H., Zhang, A. G., Ju, C. C., Wang, K. Z., (2011), "A phenylcarbazole functionalized ruthenium dye for efficient dye-sensitized solar cells", Solar Energy, vol. 85, pp. 2497-2506.

169. Fan, S. Q., Kim, C., Fang, B., Liao, K. X., Yang, G. J., Li, C. J. Kim, J. J. Ko, J., (2011), "Improved efficiency of over 10% in dye-sensitized solarcells with a ruthenium

complex and an organic dye heterogeneously positioning on a single TiO_2 electrode", J. Phys. Chem. C, vol. 115, pp. 7747-7754.

170. Zeng, W., Cao, Y., Bai, Y., Wang, Y., Shi, Y., Zhang, M., Wang, F., Pan, C., Wang, P., (2010), "Efficient Dye-Sensitized Solar Cells with an Organic Photosensitizer Featuring Orderly Conjugated Ethylenedioxythiophene and Dithienosilole Blocks", Chem. Mater., vol. 22, pp. 1915-1925.

171. Tian, H., Yang, X., Chen, R., Zhang, R., Hagfeldt, A., Sun, L., (2008), "Effect of Different Dye Baths and Dye-Structures on the Performance of Dye-Sensitized Solar Cells Based on Triphenylamine Dyes", J. Phys. Chem. C, vol. 112, pp. 11023-11033.

172. Chen, C. H., Hsu, Y. C., Chou, H. H., Thomas, K. R. J., Lin, J. T., Hsu, C. P., (2010), "Dipolar Compounds Containing Fluorene and a Heteroaromatic Ring as the Conjugating Bridge for High-Performance Dye-Sensitized Solar Cells", Chem. Eur. J., vol. 16, pp. 3184-3193.

173. Wang, Z. S., Koumura, N., Cui, Y., Takahashi, M., Sekiguchi, H., Mori, A., Kubo, T., Furube, A., Hara, K., (2008), "Hexylthiophene-Functionalized Carbazole Dyes for Efficient Molecular Photovoltaics: Tuning of Solar-Cell Performance by Structural Modification", Chem. Mater., vol. 20, pp. 3993-4003.

174. Nazeeruddin, M. K., Humphry-Baker, R., Liska, P., Gratzel, M., (2003), "Investigation of Sensitizer Adsorption and the Influence of Protons on Current and Voltage of a Dye-Sensitized Nanocrystalline TiO_2 Solar Cell", J. Phys. Chem. B, vol. 107, pp. 8981-8987.

175. Xu, M., Wenger, S., Bala, H., Shi, D., Li, R., Zhou, Y., Zakeeruddin, S. M., Grätzel, M., Wang, P., (2009), "Tuning the Energy Level of Organic Sensitizers for High-Performance Dye-Sensitized Solar Cells", J. Phys. Chem. C, vol. 113, pp. 2966-2973.

176. Hara, K., Sato, T., Katoh, R., Furube, A., Ohga, Y., Shinpo, A., Suga, S., Sayama, K., Sugihara, H., Arakawa, H., (2003), "Molecular Design of Coumarin Dyes for Efficient Dye-Sensitized Solar Cells", J. Phys. Chem. B, vol. 107, pp. 597-606.

177. Kohle, O., Grätzel, M., Meyer, A. F., Meyer, T. B., (1997), "The photovoltaic stability of, bis(isothiocyanato)rlutheniurn(II)-bis-2, 2′bipyridine-4, 4′-dicarboxylic acid and related sensitizers", Adv. Mater., vol. 9, pp. 904-906.

178. Reference Solar Spectral Irradiance: Air Mass 1.5 [online:http://rredc.nrel.gov/solar/spectra/am1.5/] (2012)

179. Yang, K. L., Zhou, H., Price, S. C., You, W., (2011), "Low-Band-Gap Polymers That Utilize Quinoid Resonance Structure Stabilization by Thienothiophene: Fine-Tuning of HOMO Level", Macromolecules, vol. 44, pp. 872-877.

180. Kim, B. G., Zhen, C. G., Jeong, E. J., Kieffer, J., Kim, J., (2012), "Organic Dye Design Tools for Efficient Photocurrent Generation in Dye-Sensitized Solar Cells: Exciton Binding Energy and Electron Acceptors", Adv. Funct. Mater., vol. 22, pp. 1606-1612.

181. Wu, Y., Zhu, W., (2013), "Organic sensitizers from D-π-A to D-A-π-A: effect of the internal electron-withdrawing units on molecular absorption, energy levels and photovoltaic performances", Chem. Soc. Rev., vol. 42, pp. 2039-2058.

182. An, B. K., Kwon, S. K., Jung, S. D., Park, S. Y., (2002), "Enhanced Emission and Its Switching in Fluorescent Organic Nanoparticles", J. Am. Chem. Soc., vol. 124, pp. 14410-14415.

183. Chen, Y., Zeng, Z., Li, C., Wang, W., Wang, X., Zhang, B., (2005), "Highly efficient co-sensitization of nanocrystalline TiO_2 electrodes with plural organic dyes", New J. Chem., vol. 29, pp. 773-776.

184. Knupfer, M., (2003), “Exciton binding energies in organic semiconductors”, Appl. Phys. A, vol. 77, pp. 623-626.

185. Wiberg, J., Marinado, T., Hagberg, D. P., Sun, L., Hagfeldt, A., Albinsson, B., (2009), “Effect of Anchoring Group on Electron Injection and Recombination Dynamics in Organic Dye-Sensitized Solar Cells”, J. Phys. Chem. C, vol. 113, pp. 3881.

186. Ning, Z., Tian, H., (2009), “Triarylamine: a promising core unit for efficient photovoltaic materials”, Chem. Commun., pp. 5483-5495.

187. Lin, H., Hsu, Y. C, Lin, J. T., Lin, C. K., Yang, J. S., (2010), “Isotruxene-derived cone-shaped organic dyes for dye-sensitized solar cells”, J. Org. Chem., vol. 75, pp. 7877-7886.

188. Zhang, X. H., Wang, Z. S., Cui, Y., Koumura, N., Furube, A., Hara, K., (2009), “Organic Sensitizers Based on Hexylthiophene-Functionalized Indolo[3, 2-b]carbazole for Efficient Dye-Sensitized Solar Cells”, J. Phys. Chem. C, vol. 113, pp. 13409-13415.

189. Edvinsson, T., Li, C., Pschirer, N., Schçneboom, J., Eickemeyer, F., Sens, R., Boschloo, G., Herrmann, A., Mullen, K., Hagfeldt, A., (2007), “Intramolecular Charge-Transfer Tuning of Perylenes: Spectroscopic Features and Performance in Dye-Sensitized Solar Cells”, J. Phys. Chem. C, vol. 111, pp. 15137-15140.

190. Kim, J. J., Choi, H., Lee, J. W., Kang, M. S., Song, K., Kang, S. O., Ko, J., (2008), “A polymer gel electrolyte to achieve ≥6% power conversion efficiency with a novel organic dye incorporating a low-band-gap chromophore”, J. Mater. Chem., vol. 18, pp. 5223-5229.

191. Pei, K., Wu, Y., Wu, W., Zhang, Q., Chen, B., Tian, H., Zhu, W., (2012), “Constructing Organic D-A-π-A-Featured Sensitizers with a Quinoxaline Unit for High-Efficiency Solar

Cells: The Effect of an Auxiliary Acceptor on the Absorption and the Energy Level Alignment", Chem. Eur. J., vol. 18, pp. 8190-8200.

192. Baik, C., Kim, D., Kang, M. S., Kang, S. O., Ko, J., Nazeeruddin, M. K., Grätzel, M., (2009), "Novel asymmetric Cy5 dyes: Synthesis, photostabilities and high sensitivity in protein fluorescence labeling", J. Photochem. Photobiol. A, vol. 201, pp. 168-172.

193. Tian, Z., Huang, M., Zhao, B., Huang, H., Feng, X., Nie, Y., Shen, P., Tan, S., (2010), "Low-cost dyes based on methylthiophene for high-performance dye-sensitized solar cells", Dyes Pigments, vol. 87, pp. 181-187.

194. Cheng, M., Yang, X., Zhang, F., Zhao, J.and Sun, L., (2013), "Tuning the HOMO and LUMO Energy Levels of Organic Dyes with N-Carboxomethylpyridinium as Acceptor To Optimize the Efficiency of Dye-Sensitized Solar Cells", J. Phys. Chem. C., vol. 117, pp. 9076-9083.

195. Pandey, S. S., Watanabe, R., Fujikawa, N., Shivashimpi, G. M., Ogomi, Y., Yamaguchi, Y., Hayase, S., (2013), Tetrahedron, vol. 69, pp. 2633-2639.

196. Bai, Y., Zhang, J., Zhou, D., Wang, Y., Zhang, M., Wang, P., (2011), "Engineering organic sensitizers for iodine-free dye-sensitized solar cells: red-shifted current response concomitant with attenuated charge recombination", J. Am. Chem. Soc., vol. 133, pp. 11442-11445.

197. Lim, K., Kim, C., Song, J., Yu, T., Lim, W., Song, K., Wang, P., Zu, N., Ko, J., (2011), "Enhancing the Performance of Organic Dye-Sensitized Solar Cells via a Slight Structure Modification", J. Phys. Chem. C, vol. 115, pp. 22640-22646.

198. Zhang, G., Bai, Y., Li, R., Shi, D., Wenger, S., Zakeeruddin, S. M., Gratzel, M., Wang, P., (2009), "Employ a bisthienothiophene linker to construct an organic chromophorefor efficient and stable dye-sensitized solar cells", Energy Environ. Sci., vol. 2, pp. 92-95.

199. Lin, Y., Z., Huang, C. H., Chang, Y. J., Yeh, C. W., Chin, T. M., Chi, K. M., Chou, P. T., Watanabe, M., Chow, T. J., Lin, Y. Z., (2014), Tetrahedron vol. 70, pp. 262-269.

200. Shen, P., Tang, Y., Jiang, S., Chen, H., Zheng, X., Wang, X., Zhao, B., Tan, S., (2011), "The Role of the Conjugate Bridge in Electronic Structures and Related Properties of Tetrahydroquinoline for Dye Sensitized Solar Cells", Org. Electron., vol. 12, pp. 125-135.

201. Chen, H., Huang, H., Huang, X., Clifford, J. N., Forneli, A., Palomares, E., Zheng, X., Zheng, L., Wang, X., Shen, P., Zhao, B. and Tan, S., (2010), "High Molar Extinction Coefficient Branchlike Organic Dyes Containing Di(p-tolyl)phenylamine Donor for Dye-Sensitized Solar Cells Applications", J. Phys. Chem. C, vol. 114, pp. 3280-3286

202. Yella, A., Baker, R. H., Curchod, B. F. E., Astani, N. A., Teuscher, J., Polander, L. E., Mathew, S., Moser, J. E., Tavernelli, I., Rothlisberger, U., Grätzel, M., Nazeeruddin, Md. K. and Frey, J., (2013), "Molecular Engineering of a Fluorene Donor for Dye-Sensitized Solar Cells", Chem. Mater., vol. 25, pp. 2733-2739.

203. Tamilavana, V., Chob, N., Kimb, C., Kob, J., Hyuna, M. H., Tamilavan, V., (2012), "Influences of the electron donor groups on the properties of thiophene-(N-aryl)pyrrole-thiophene-based organic sensitizers", Synthetic Metals vol. 162, pp. 2155-2162

204. Mba, M., D'Acunzo, M., Salice, P., Carofiglio, T., Maggini, M., Caramori, S., Campana, A., Aliprandi, A., Argazzi, R., Carli, S. and Bignozzi, C. A., (2013), "Sensitization of Nanocrystalline TiO_2 with Multibranched Organic Dyes and Co(III)/(II) Mediators:

Strategies to Improve Charge Collection Efficiency", J. Phys. Chem. C, vol. 117, pp. 19885-19896.

205. Sirohi, R., Kim, D. H., Yu, S. C., Lee, S. H., Sirohi, R., (2012), "Novel di-anchoring dye for DSSC by bridging of two mono anchoring dye molecules: A conformational approach to reduce aggregation", Dyes and Pigments, vol. 92, pp. 1132-1137.

206. Yu, L., Xi, J., Chan, H. T., Su, T., Antrobus, L. J., Tong, B., Dong, Y., Chan, W. K. and Phillips, D. L., (2013), "Novel Organic D-π-2A Sensitizer for Dye Sensitized Solar Cells and Its Electron Transfer Kinetics on TiO_2 Surface", J. Phys. Chem. C, vol. 117, pp. 2041-2052.

207. Ting, H. C., Tsai, C. H., Chen, J. H., Lin, L. Y., Chou, S. H., Wong, K. T., Huang, T. W. and Wu, C. C., (2012), "A novel amine-free dianchoring organic dye for efficient dye-sensitized solar cells", Org. letters, Vol. 14(24), pp. 6338-6341.

208. Li, Q., Shi, J., Li, H., Li, S., Zhong, C., Guo, F., Peng, M., Hua, J., Qina, J., Li, Z., (2012), "Novel pyrrole-based dyes for dye-sensitized solar cells: From rod-shape to "H" type", J. Mater. Chem., vol. 22, pp. 6689-6696.

209. Ren, X., Jiang, S., Cha, M., Zhou, G. and Wang, Z. S., (2012), "Thiophene-Bridged Double D-π-A Dye for Efficient Dye-Sensitized Solar Cell", Chem. Mater., vol. 24, pp. 3493-3499.

210. Lee, D. H., Lee, M. J., Song, H. M., Song, B. J., Seo, K. D., Pastore, M., Anselmi, C., Fantacci, S., De Angelis, F., Nazeeruddin, M. K., Grätzel, M., Kim, H. K., (2011), "Organic dyes incorporating low-band-gap chromophores based on π-extended benzothiadiazole for dye-sensitized solar cells", Dyes Pigments, vol. 91, pp. 192-198.

211. Zhang, G., Bala, H., Cheng, Y., Shi, D., Lv, X., Yu, Q., Wang, P., (2009), "High efficiency and stable dye-sensitized solar cells with an organicchromophore featuring a binary π-conjugated spacer", Chem. Commun., pp. 2198-2200.

212. Zhu, W., Wu, Y., Wang, S., Li, W., Li, X., Chen, J., Wang, Z. S. and Tian, H., (2011), "Organic D-A-π-A Solar Cell Sensitizers with Improved Stability and Spectral Response", Adv. Funct. Mater., vol. 21, pp. 756-763.

213. Ding, W. L., Wang, D. M., Geng, Z. Y., Zhao, X. L. and Yan, Y. F., (2013), "Molecular Engineering of Indoline-Based D-A-π-A Organic Sensitizers toward High Efficiency Performance from First-Principles Calculations", J. Phys. Chem. C., vol. 117, pp. 17382−17398.

214. Wan, Z., Jia, C., Zhou, L., Huo, W., Yao, X., Shi, Y., (2012), "Influence of different arylamine electron donors in organic sensitizers for dye-sensitized solar cells", Dyes Pigments, vol. 95, pp. 41-46.

215. Sudyoadsuk, T., Pansay, S., Morada, S., Rattanawan, R., Namuangruk, S., Kaewin, T., Jungsuttiwong, S. and Promarak, V., (2013), "Synthesis and Characterization of D-D-π-A-Type Organic Dyes Bearing Carbazole-Carbazole as a Donor Moiety (D-D) for Efficient Dye-Sensitized Solar Cells", Eur. J. Org. Chem., pp. 5051-5063.

216. Chen, C., Liao, J. Y., Chi, Z., Xu, B., Zhang, X., Kuang, D. B., Zhang, Y., Liu, S., Xu, J., (2012), "Metal-free organic dyes derived from triphenylethylene for dye-sensitized solar cells: tuning of the performance by phenothiazine and carbazole", J. Mater. Chem., vol. 22, pp. 8994-9005.

217. Srinivas, K., Kumar, C. R., Reddy, M. A., Bhanuprakash, K., Rao, V. J., Giribabu, L., (2011), "D-π-A organic dyes with carbazole as donor for dye-sensitized solar cells", Synth. Metals, vol. 161, pp. 96-105.

218. Morada, S., Kaewin, T., Jungsuttiwong, S., Sudyoadsuk, T. and Promarak, V., (2012), "D-D-π-A-Type Organic Dyes for Dye-Sensitized Solar Cells with a Potential for Direct Electron Injection and a High Extinction Coefficient: Synthesis, Characterization, and Theoretical Investigation", J. Phys. Chem. C, vol. 116, pp. 25653-25663.

219. Kajiyama, S., Uemura, Y., Miura, H., Hara, K., Koumura, N., (2012), "Organic dyes with oligo-n-hexylthiophene for dye-sensitized solar cells: Relation between chemical structure of donor and photovoltaic performance", Dyes Pigments, vol. 92, pp. 1250-1256.

220. Midya, A., Xie, Z., Yang, J. X., Chen, Z. K., Blackwood, D. J., Wang, J., Adams, S., Kian P., (2010), "A new class of solid state ionic conductors for application in all solid state dye sensitized solar cells", Chem. Commun., vol. 46, pp. 2091-2093.

221. Wang, Z. S., Koumura, N., Cui, Y., Takahashi, M., Sekiguchi, H., Mori, A., Kubo, T., Furube, A., Hara, K., (2008), "Hexylthiophene-functionalized carbazole dyes for efficient molecular photovoltaics: tuning of solar-cell performance by structural modification", Chem. Mater., vol. 20, pp. 3993-4003.

222. Pei, K., Wu, Y., Islam, A., Zhang, Q., Han, L., Tian, H. and Zhu, W., (2013), "Constructing High-Efficiency D-A-π-A-Featured Solar Cell Sensitizers: a Promising Building Block of 2,3-Diphenylquinoxaline for Antiaggregation and Photostability", ACS Appl. Mater. Interfaces, vol. 5, pp. 4986-4995.

223. Uemura, Y., Mori, S., Hara, K. and Koumura, N., (2012), "Carbazole Dyes with Ether Groups for Dye-Sensitized Solar Cells: Effect of Negative Charges in Dye Molecules on Electron Lifetime", Jpn. J. Appl. Phys., vol. 51, pp. 10-14.

224. Zhang, X. H., Ogawa, J., Sunahara, K., Cui, Y., Uemura, Y., Miyasaka, T., Furube, A., Koumura, N., Hara, K. and Mori, S., (2013), "Alternation of Charge Injection and Recombination in Dye-Sensitized Solar Cells by the Addition of Nonconjugated Bridge to Organic Dyes", J. Phys. Chem. C., vol. 117, pp. 2024-2031.

225. Murakami, T. N., Yoshida, E., Koumura, N., (2014), "Carbazole dye with phosphonic acid anchoring groups for long-term heat stability of dye-sensitized solar cells", Electrochimica Acta, vol. 131, pp. 174-183.

226. Feng, Q., Zhang, Q., Lu, X., Wang, H., Zhou, G. and Wang, Z. S., (2013), "Facile and Selective Synthesis of Oligothiophene-Based Sensitizer Isomers: An Approach toward Efficient Dye-Sensitized Solar Cells", ACS Appl. Mater. Interfaces, vol. 5, pp. 8982-8990.

227. Ramkumar, S., Anandan, S., (2013), "Synthesis of bianchored metal free organic dyes for dye sensitized solar cells", Dyes and Pigments vol. 97, pp. 397-404.

228. Gupta, K. S. V., Suresh, T., Singh, S. P., Islam, A., Han, L., Chandrasekharam, M., (2014), "Carbazole based A-π-D-π-A dyes with double electron acceptor for dye-sensitized solar cell", Organic Electronics vol. 15, pp. 266-275.

229. Liang, M., Wang, Z. Y., Zhang, L., Han, H. Y., Sun, Z., Xue, S., Liang, M., (2011), "New organic photosensitizers incorporating carbazole and dimethylarylamine moieties for dye-sensitized solar cells", Renewable Energy, vol. 36, pp. 2711-2716.

230. Chu, H. C., Sahu, D., Hsu, Y. C., Padhy, H., Patra, D., Lin, J. S., Bhattacharya, D., Lu, K. L., Wei, K. H., Lin, H. C., (2012), "Structural planarity and conjugation effects of novel

symmetrical acceptor-donor-acceptor organic sensitizers on dye-sensitized solar cells", Dyes and Pigments, vol. 93, pp. 1488-1497.

231. Onicha, A. C., Panthi, K., Kinstle, T. H., Castellano, F. N., Onicha, A. C., (2011), "Nanostructured ZnO electrodes for dye-sensitized solar cell applications", Journal of Photochemistry and Photobiology A: Chemistry, vol. 223, pp. 57- 64.

232. Venkateswararao, A., Thomas, K. R. J., Lee, C. P., Ho, K. C., (2013), "Synthesis and characterization of organic dyes containing 2,7-disubstituted carbazole π-linker", Tetrahedron Letters, vol. 54, pp. 3985-3989.

233. Venkateswararao, A., Thomas, K. R. J., Lee, C. P., Li, C. T.and Ho, K. C., (2014), "Organic Dyes Containing Carbazole as Donor and π-Linker: Optical, Electrochemical and Photovoltaic Properties", ACS Appl. Mater. Interfaces, vol. 6(4), pp. 2528-2539

234. Zafer, C., Gultekin, B., Ozsoy, C., Tozlu, C., Aydin, B., Icli, S., Zafer, C., (2010), "Carbazole-based organic dye sensitizers for efficient molecular photovoltaics", Solar Energy Materials & Solar Cells, vol. 94, pp. 655-661.

235. Qian, X., Zhu, Y. Z., Song, J., Gao, X. P. and Zheng, J. Y., "New Electrode-Friendly Triindole Columnar phases with High Hole Mobility", Org. Lett., Vol. 15, No. vol. 23, 2013, pp. 6034-6037.

236. Zhang, X. H., Wang, Z. S., Cui, Y., Koumura, N., Furube, A., Hara, K., (2009), "Organic sensitizers based on hexylthiophene-functionalized indolo[3,2-b]carbazole for efficient dye-sensitized solar cells", J. Phys. Chem. C., vol. 113, pp. 13409-13415.

237. Cai, S., Tian, G., Li, X., Su, J. and Tian, H., (2013), "Efficient and stable DSSC sensitizers based on substituted dihydroindolo[2,3-b]carbazole donors with high molar extinction coefficients", J. Mater. Chem. A, vol. 1, pp. 11295-11305.

238. Keerthi, A., Sriramulua, D., Liub, Y., Yuan, C. T., Wang, T. Q., Valiyaveettil, S., Keerthi, A., (2013), "Architectural influence of carbazole push-pull-pull dyes on dye sensitized solar cells", Dyes and Pigments, vol. 99, pp. 787-797.

239. Cheng, Z., Lin, J., (2010), "Layered Organic-Inorganic Hybrid Perovskites: Structure, Optical Properties, Film Preparation, Patterning and Templating Engineering", Cryst EngComm, vol. 12, pp. 2646-2662.

240. Mitzi, D. B., Wang, S., Feild, C. A., Chess, C. A., Guloy, A. M., (1995), "Conducting Layered Organic-Inorganic Halides Containing ⟨110⟩- Oriented Perovskite Sheets", Science, vol. 267, pp. 1473-1476.

241. Bednorz, J. G., Muller, K. A., (1986), "Possible High-Tc Superconductivity in the Ba-La-Cu-O System", Z. Phys. B: Condens. Matter, vol. 64, pp. 189-193.

242. Liu, M., Johnston, M. B. & Snaith, H. J., (2013), "Efficient planar heterojunction perovskite solar cells by vapour deposition", Nature, vol. 501, pp. 395-398.

243. Glazer, A. M., (1972), "The classification of tilted octahedra in perovskites", Acta Cryst. B., vol. 28, pp. 3384.

244. Cheng, Z., Lin, (2010), "Layered organic-inorganic hybrid perovskites: structure, optical properties, film preparation, patterning and templating engineering", J. Cryst Eng Comm., vol. 12, pp. 2646-2662.

245. Mitzi, D. B., Karlin, K. D., (1999), "In Progress in Inorganic Chemistry", Ed., Wiley-Interscience: New York, Vol. 48, pp. 1-121.

246. Tanaka, K., Takahashi, T., Kondo, T., Umeda, K., Ema, K., Umebayashi, T., Asai, K., Uchida, K., Miura, N., (2005), "Electronic and Excitonic Structures of Inorganic-Organic

Perovskite-Type Quantum-Well Crystal ($C_4H_9NH_3)_2PbBr_4$", Jpn. J. Appl. Phys., vol. 44(1), pp. 5923-5932.

247. Kojima, A., Teshima, K., Shirai, Y., Miyasaka, T., (2009), "Organometal Halide Perovskites as Visible-Light Sensitizers for Photovoltaic Cells", J. Am. Chem. Soc., vol. 131, pp. 6050-6051.

248. Im, J. H., Lee, C. R., Lee, J. W., Park, S. W., Park, N. G., (2011), "6.5% Efficient Perovskite Quantum-Dot-Sensitized Solar Cell", Nanoscale, vol. 3, pp. 4088-4093.

249. Snaith, H. J., (2013), "Perovskites: The Emergence of a New Era for Low-Cost, High-Efficiency Solar Cells", J. Phys. Chem. Lett., vol. 4, pp. 3623-3630.

250. Chung, I., Lee, B., He, J., Chang, R. P. H., Kanatzidis, M. G., (2012), "All- Solid-State Dye-Sensitized Solar Cells with High Efficiency", Nature, vol. 485, pp. 486-489.

251. Kim, H. S., Lee, C. R., Im, J. H., Lee, K. B., Moehl, T., Marchioro, A., Moon, S. J., Humphry-Baker, R., Yum, J. H., Moser, J. E., (2012), "Lead Iodide Perovskite Sensitized All-Solid-State Submicron Thin Film Mesoscopic Solar Cell with Efficiency Exceeding 9%", Sci. Rep., vol. 2, pp. 591.

252. Etgar, L., Gao, P., Xue, Z., Peng, Q., Chandiran, A. K., Liu, B., Nazeeruddin, M. K., Grätzel, M., (2012), "Mesoscopic $CH_3NH_3PbI_3/TiO_2$ Heterojunction Solar Cells", J. Am. Chem. Soc., vol. 134, pp. 17396-17399.

253. Qiu, J., Qiu, Y., Yan, K., Zhong, M., Mu, C., Yan, H., Yang, S., (2013), "All-Solid-State Hybrid Solar Cells Based on a New Organometal Halide Perovskite Sensitizer and One-Dimensional TiO_2 Nanowire Arrays", Nanoscale, vol. 5, pp. 3245-3248.

254. Noh, J. H., Im, S. H., Heo, J. H., Mandal, T. N., Seok, S. I., (2013), "Chemical Management for Colorful, Efficient, and Stable Inorganic−Organic Hybrid Nanostructured Solar Cells", Nano Lett., vol. 13, pp. 1764-1769.

255. Lee, M. M., Teuscher, J., Miyasaka, T., Murakami, T. N., Snaith, H. J., (2012), "Efficient Hybrid Solar Cells Based on Meso-Superstructured Organometal Halide Perovskites", Science, vol. 338, pp. 643-647.

256. Ball, J. M., Lee, M. M., Hey, A., Snaith, H. J., (2013), "Low-Temperature Processed Meso-Superstructured to Thin-Film Perovskite Solar Cells", Energy Environ. Sci., vol. 6, pp. 1739-1743.

257. Burschka, J., Pellet, N., Moon, S. J., Baker, R. H., Gao, P., Nazeeruddin, M. K. & Grätzel, M., (2013), "Sequential deposition as a route to high-performance perovskite-sensitized solar cells", Nature, vol. 499, pp. 316-319.

258. Wang, J. T. W., Ball, J. M., Barea, E. M., Abate, A., Alexander-Webber, J. A., Huang, J., Saliba, M., Mora-Sero, I., Bisquert, J., Snaith, H. J. and Nicholas, R. J., (2014), "Low-Temperature Processed Electron Collection Layers of Graphene/TiO_2 Nanocomposites in Thin Film Perovskite Solar Cells", Nano Lett., vol. 14, pp. 724−730.

259. Martinson, A. B. F., Elam, J. W., Liu, J., Pellin, M. J., Marks, T. J. and Hupp, J. T., (2008), "Radial Electron Collection in Dye-Sensitized Solar Cells", Nano Lett., vol. 8(9), pp. 2862-2866.

260. Baxter, J. B. and Aydil, E. S., (2005), "Nanowire-based dye-sensitized solar cells", Appl. Phys. Lett., vol. 86(5), pp. 1-3.

261. Martinson, A. B. F., Elam, J. W., Hupp, J. T. and Pellin, M. J., (2007), "ZnO Nanotube Based Dye-Sensitized Solar Cells", Nano Lett., vol. 7(8), pp. 2183-2187.

262. Varghese, O. K., Paulose, M. and Grimes, C. A., (2009), "Long vertically aligned titania nanotubes on transparent conducting oxide for highly efficient solar cells", Nat. Nanotechnol., vol. 4(9), pp. 592-597.

263. Macak, J. M., Tsuchiya, H., Ghicov, A. and Schmuki, P., (2005), "Facile synthesis of flower like copper oxide and their application to hydrogen peroxide and nitrite sensing", Electrochem Commun. vol. 7, pp. 133-1137.

264. Paulose, M., Shankar, K., Varghese, O. K., Mor, G. K., Hardin, B. and Grimes, C. A., (2006), "Backside illuminated dye-sensitized solar cells based on titania nanotube array electrodes", Nanotechnology vol. 17, pp. 1446-1448.

265. Kim, D., Ghicov, A., Albu, S. P. and Schmuki, P., (2008), "Bamboo-Type TiO_2 Nanotubes: Improved Conversion Efficiency in Dye-Sensitized Solar Cells", J. Am. Chem. Soc., vol. 130, pp. 16454-16455.

266. Melas-Kyriazi, J., Marchioro, I. K., Punzi, A., Hardin, B. E., Burkhard, G. F., Tetreault, N., Grätzel, M., Moser, J. E. and McGehee, M. D., (2011), "The Effect of Hole Transport Material Pore Filling on Photovoltaic Performance in Solid-State Dye-Sensitized Solar Cells", Adv. Energy Mater., vol. 1(3), pp. 407-414.

267. Diamant, Y., Chappel, S., Chen, S. G., Melamed, O., Zaban, A., (2004), "Core-shell nanoporous electrode for dye sensitized solar cells: the effect of shell characteristics on the electronic properties of the electrode", Chem. Rev., vol. 248, pp. 1271-1276.

268. Groenewolt, M., Brezesinski, T., Schlaad, H., Antonietti, M., Groh P. W. and Ivan, B., (2005), "poly isobutylene-block-Poly(ethylene oxide)", Adv. Mater., vol. 17, pp. 1158-1162.

269. Steunou, N., Forster, S., Florian, P., Sanchez, C. and Antonietti, M., (2002), "Synthesis of nanostructured polymer-titanium oxide composites through the assembly of titanium-

oxo clusters and amphiphilic block copolymers micelles", Mater. Chem. vol. 12, pp. 3426-3430.

270. Wang, H., Oey, C. C., Djurisic, A. B., Xie, M. H., Leung, Y. H., Man, K. K. Y., Chan, W. K., Pandey, A., Nunzi, J. M. and Chui, P. C., (2005), "Titania bicontinuous network structures for solar cell applications", Appl. Phys. Lett., vol. 87, pp. 023507.

271. Lodge, T. P., (2003), "Block Copolymers: Past Successes and Future Challenge", Macromol Chem Phys., vol. 204, pp. 265-273.

272. Li, M., Douki, K., Goto, K., Li, Z., Coenjarts, C., Smilgies, D. M., Ober, C. K., (2004), "Fabrication of Hierarchically Ordered Hybrid Structures over Multiple Length Scales via Direct Etching of Self-Organized Polyhedral Oligomeric Silsesquioxane (POSS) Functionalized Block Copolymer Films", Chem Mater vol. 16, pp. 3800-3808.

273. Li, L., Yokoyama, H., Nemoto, T., Sugiyama, K., (2004), "Facile Fabrication of Nanocellular Block Copolymer Thin Films Using Supercritical Carbon Dioxide", Adv Mater., vol. 16, pp.1226-1229.

274. Li, Z., Luo, W., Zhang, M., Feng, J. and Zou, Z., (2013), "Photoelectrochemical cells for solar hydrogen production: current state of promising photoelectrodes, methods to improve their properties, and outlook", Energy Environ. Sci., vol. 6, pp. 347-370.

275. Zuo, F., Wang, L., Wu, T., Zhang, Z., Borchardt, D. and Feng, P., (2010), "Self-doped Ti^{3+} enhanced photocatalyst for hydrogen production under visible light", J. Am.Chem. Soc., vol. 132, pp. 11856-11857.

276. Wang, G., Wang, H., Ling, Y., Tang, Y., Yang, X., Fitzmorris, R. C., Wang, C., Zhang, J. Z. and Li, Y., (2011), "Hydrogen-Treated TiO_2 Nanowire Arrays for Photoelectrochemical Water Splitting", Nano Lett., vol. 11, pp. 3026-3033.

277. Zhou, J., Song, B., Zhao, G. and Han, G., Zhou, (2012), "Effects of acid on the microstructures and properties of three-dimensional TiO_2 hierarchical structures by solvothermal method", Nanoscale Research Letters, vol. 7, pp. 217-228.

278. Xia, T., Li, Q., Liu, X., Meng, J. and Cao, X., (2006), "Morphology-Controllable Synthesis and Characterization of Single-Crystal Molybdenum Trioxide", J. Phys. Chem. B, vol. 110, pp. 2006-2012.

279. Byranvanda, M. M., Kharata, A. N., Fatholahi, L., Beiranvand, Z. M., (2013), "A Review on Synthesis of Nano-TiO_2 via Different Methods", Journal of Nanostructure, vol. 3, pp. 1-9.

Chapter 3: FORMULATION OF PROBLEM BASED ON RESEARCH GAP IDENTIFIED

3.1 CHAPTER OVERVIEW

This chapter starts with mentioning the challenges in DSSCs followed by the extraction of research gap and objective of the research work. It also presents a snapshot of the whole research work including the synthesis of photovoltaic materials i.e. organic dyes and TiO_2 nanoparticles with their expected photophysical and photovoltaic properties.

3.2 CHALLENGES IN DYE SENSITIZED SOLAR CELLS (DSSCs)

Till today the output current density of dye-sensitized solar cells has reached to ~18 mA/cm^2 [1], which is basically much lower than that of the inorganic solar cells, especially silicon based solar cells. When DSSCs came into consideration due to expensive silicon used in Si solar cells, the nanoporous working electrode was said to be a key component in DSSC. It was established that it facilitated interpenetration of liquid electrolyte and dye loading with consecutively enhancedlight absorption in a DSSC. But practically most of the times electrons are quenched due to a lot of trapping spots caused by non-uniform interface in nanoporous structures and consequently a decrease of the output current takes place, irrespective of the amount of dye loaded or other enhanced property.

Photon absorption coefficient is the capability of a chemical species to absorb light at a specific wavelength [2]. In order to further improve the light absorption, dye structures are being modified to exhibit higher photon absorption coefficient; yet it is awaited to find an appropriate organic dye that fits the requirements, balancing the photo voltage and photo current at the same time.

Iodide/triiodide (I^-/I_3^-) is the most accepted electrolyte in the photovoltaic system. However, its relatively low redox potential limits the open-circuit voltage and results in reduced output energy. For being a good candidate an electrolyte should be able to fulfill three conditions i.e. a driving force for more dye regeneration, efficient electron transport at the solid/liquid interface and less electron recombination rate. Although a lot of work has been done with cobalt polypyridine redox mediator [3], copper complexes [4], ferrocenium/ferrocene (Fc^+/Fc) [5], it still remains a challenge to find an alternative electrolyte with such advantages.

Since the dye-sensitized solar cells (DSSCs) with liquid electrolyte lack long term stability, attempts have been made to replace the liquid electrolyte by other materials, such as nonvolatile gel-like polymer electrolyte or solid hole-transporting materials. Generally, the gel-like polymer electrolyte is a system which is made of a polymer network inflated with liquid electrolytes [6]. Wang *et.al*. fabricated a DSSC with polymer gel electrolyte having an efficiency of ~6 % in 2003. The device passed the stability test under extreme conditions, e.g., light soaking at 60°C for 1000 hours and thermal stress at 80°C for 1000 hours [7] but the problem of partial leakage could not be resolved. In order to completely avoid the leakage problem of the liquid electrolyte, the solid-state hole conductors have been introduced into DSSC system in the late 1990s. In 1998, Grätzel's group utilized amorphous organic hole conductor 2, 2', 7, 7'-tetrakis(N,N-di-pmethoxyphenyl-amine) 9, 9'-spirobifluorene (MeOTAD) in solid-state DSSC. Though high photon-to-electron conversion efficiencies were observed yet the overall power conversion efficiency was only 0.74%, due to the incomplete pore filling [8]. Though the efficiency has been improved to around 5% [9] it's still at the lower side in comparison with DSSCs based on liquid electrolyte. The reason

behind this was established as the large size of the polymerized molecules which causes the poor pore filling [10]. Besides this, they were found to be unstable when exposed to air or high temperature [11]. Several solid hole conductors are thus under investigation in solid-state DSSCs. In short, the problems of low current density, low open circuit voltage, limited power conversion efficiency, high processing temperature and liquid leakage are the main concern of recent research in this field.

3.3 AIM OF THE WORK

Present work aims at the synthesis and application of photovoltaic materials for solar devices. It comprises of both types of solar devices i.e. liquid state DSSCs based on organic sensitizers and ssDSSCs based on perovskite sensitizer. Being the key components of the solar devices TiO_2 nanoparticles and organic sensitizers are the focal point of the study. Perovskite based DSSCs are the result of rigorous research that has been undertaken in order to overcome the drawbacks of traditional design of DSSCs. In this study, for perovskite solar cells, TiO_2 nanoparticles are used as semiconductor and the sensitizer is replaced by halide perovskites.

Since, dyes performing the best till date in this research field are the Ru-complexes, which also suffer from low extinction coefficient and low stability. It is high time to look at other dyes with better optical and photovoltaic properties with high stability. In this conclusion, a series of carbazole based organic dyes with multiple anchoring sites is synthesized and employed in DSSC. The current work is of purely experimental nature and sustained by structural, optical, electrochemical and photovoltaic analysis.

In a precise way, the focus of the proposed work is to synthesize suitable organic dyes and TiO_2 nanoparticles and to study their structure-property co-relationships on the performance of the solar cells.

3.4 SCOPE FOR THE DESIGN OF WORK

Considering the significance of dye and semiconductor in overall performance of dye sensitized solar cells, the work is carried out on modulation of dye molecules with the skeleton being different than conventional D-π-A skeleton and synthesis of various sizes of TiO_2 nano particles with enhanced surface area which are suitable for more dye adsorption and more charge transportation.

Systematic review of literature established the availability of enormous number of 9-; 3-; 3, 6-; 2, 7- substituted and fused monoanchoring carbazole derivatives for DSSCs applications [12-27]. The latest developments also reveal the existence of bi-anchoring carbazole derivatives functional at different positions [19, 21, 28]. Although, the tetra-substituted carbazole derivatives are documented for organic light emitting diodes (OLED) [29-32], it is so far never reported for DSSCs applications.

Present work also explores the scope for synthesis and applicability of tetrasubstituted at different positioning carbazole based organic dyes for DSSCs, with four anchoring sites having different conjugation lengths. It has been tried to fulfill the gap existing between well defined mono and di substituted and not yet reported tetrasubstituted carbazole derivatives consisting of four anchoring units for DSSCs. It has been observed from literature so far that tetra anchoring organic dye does not exist even with any other donor moiety. The developed structures are harmonized with structural, photo physical, electrochemical and photovoltaic parameters.The work carried out is illustrated in Figure 3.1.

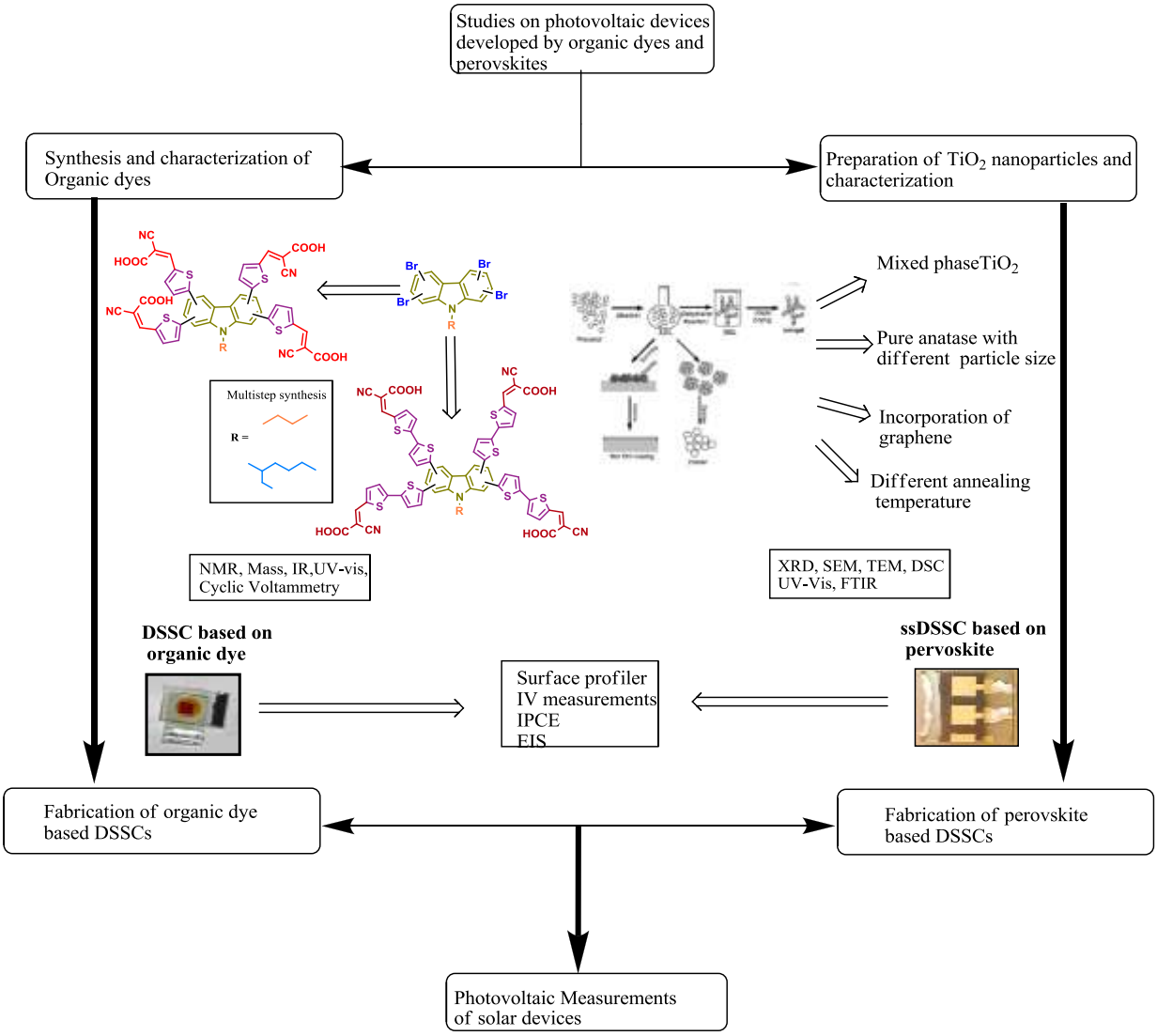

Figure 3.1: Schematic diagram for design of the work.

A series of isomeric carbazole derivatives possessing nuclear substitutions at 1, 3, 6, 8- and 2, 3, 6, 7- have been synthesized. Butyl and ethylhexyl chains are substituted on nitrogen at position 9. Two types of π-bridges, mono- and bithiophene, are introduced at four positions of carbazole core. The diversity in photophysical and photovoltaic properties offered by mono- and bithiophene linkages at different substituted positions are critically

analyzed. Based on the results of previous studies related to anchoring groups [33] cyanoacrylic acid is introduced as electron withdrawing group in all the derivatives synthesized in this study.

Since photoanode is the leading player among all the components of DSSCs and composed of both sensitizer and semiconductor, the work has been extended from synthesis of organic dyes towards developing the semiconductor nanoparticles of different size and surface areas. Synthesized nanoparticles have been applied in photoanode of DSSCs with commercialized sensitizers and for ssDSSCs with perovskite material. It has been observed from literature that incorporation of graphene is not well explored in perovskite based DSSCs. Therefore, the effect of graphene component in different percentage and at different sintering temperatures is studied in photoanodes of perovskite based DSSCs. The influence of annealing temperatures on the composition of mixed phase TiO_2 nanoparticles has also been explored on photovoltaic performance.

3.5 CONCLUSION

The whole process, planning and methodology adopted for the research work has been illustrated in a graphical representation. It briefly discribes challenges in DSSCs, aim of the work and scope of the design of the work. The whole research work including the synthesis of photovoltaic materials and their expected photophysical and photovoltaic properties has been concisely put together for a better perceptive.

References

1. Ito, S., Murakami, T. N., Comte, P., (2008), "Fabrication of thin film dye sensitized solar cells with solar toelectric power conversion efficiency over 10%", Thin Solid Film, vol. 516, pp. 4613-4619.

2. Wang, P., Klein, C., and Shaik, H., (2005), "A High Molar Extinction Coefficient Sensitizer for Stable Dye-Sensitized Solar Cells", J. Am. Chem. Soc., vol. 127, pp. 808-809

3. Feldt, S., Gibson, E. A., Gabrielsson E., (2010), "Design of Organic Dyes and Cobalt Polypyridine Redox Mediators for High-Efficiency Dye-Sensitized Solar Cells", J. Am. Chem. Soc., vol. 132, pp. 16714-16724.

4. Hattori, S., Wada, Y., Yanagida, S., (2005), "Blue Copper Model Complexes with Distorted Tetragonal Geometry Acting as Effective Electron-Transfer Mediators in Dye-Sensitized Solar Cells", J. Am. Chem. Soc., vol. 127, pp. 9648-9654.

5. Bessho, T., Yoneda, E., Yum, J., Guglielmi, M., (2009), "New Paradigm in Molecular Engineering of Sensitizers for Solar Cell Applications", J. Am. Chem. Soc., vol. 131, pp. 5930-5934.

6. Hagfeldt, A., Boschoo, G., Sun, L., (2010), "Dye-Sensitized Solar Cells", Chem. Rev., vol. 110, pp. 6595-6663.

7. Wang, P., Zakeeruddin, S. M., Moser, Jacques. E., (2003), "A stable quasi-solid-state dye-sensitized solar cell with an amphiphilic ruthenium sensitizer and polymer gel electrolyte", Nat. Mater. vol. 2, pp. 402-407.

8. Bach, U., Lupo, D., Comte, P., (1998), "Solid-state dye-sensitized mesoporous TiO_2 solar cells with high photon-to-electron conversion efficiencies", Nature, vol. 395, pp. 583-585.

9. Snaith, H. J., Moule, A. J., Klein, C., (2007), "Efficiency Enhancements in Solid-State Hybrid Solar Cells via Reduced Charge Recombination and Increased Light Capture", Nano Lett., Vol. 7, pp. 3372-3376.

10. Koh, J. K., Kim, J., Kim, B., (2011), "Highly Efficient, Iodine-Free Dye-Sensitized Solar Cells with Solid-State Synthesis of Conducting Polymers", Adv. Mater., Vol. 23, pp. 1641.

11. Hoppe, H., Sariciftci, N. S., (2004), "Organic solar cells: An overview", J. Master. Res. 19, pp. 1924-1945.

12. Sudyoadsuk, T., Pansay, S., Morada, S., Rattanawan, R., Namuangruk, S., Kaewin, T., Jungsuttiwong, S., Promarak, V., (2013), "Synthesis and Characterization of D-D-π-A-Type Organic Dyes Bearing Carbazole-Carbazole as a Donor Moiety (D-D) for Efficient Dye-Sensitized Solar Cells", Eur. J. Org. Chem., pp. 5051-5063.

13. Srinivas, K., Kumar, C. R., Reddy, M. A., Bhanuprakash, K., Rao, V. J., Giribabu, L., (2011), "D-π-A organic dyes with carbazole as donor for dye-sensitized solar cells", Vol. 161, pp. 96-105.

14. Morada, S., Kaewin, T., Jungsuttiwong, S., Sudyoadsuk, T., Promarak, V., (2012), "D-D-π-A-Type Organic Dyes for Dye-Sensitized Solar Cells with a Potential for Direct Electron Injection and a High Extinction Coefficient: Synthesis, Characterization, and Theoretical Investigation", J. Phys. Chem. C., Vol. 116, pp. 25653-25663.

15. Kajiyama, S., Uemura, Y., Miura, H., Hara, K., Koumura, N., (2012), "Organic dyes with oligo-n-hexylthiophene for dye-sensitized solar cells: Relation between chemical structure of donor and photovoltaic performance", Dyes Pigments, vol. 92, pp. 1250-1256.

16. Midya, A., Xie, Z., Yang, J. X., Chen, Z. K., Blackwood, D. J., Wang, J., Adams, S., Loh, K. P., (2010), "A new class of solid state ionic conductors for application in all solid state dye sensitized solar cells", Chem. Commun., Vol. 46, pp. 2091-2093.

17. Wang, Z. S., Koumura, N., Cui, Y., Takahashi, M., Sekiguchi, H., Mori, A., Kubo, T., Furube, A., Hara, K., (2008), "Hexylthiophene-functionalized carbazole dyes for efficient molecular photovoltaics: tuning of solar-cell performance by structural modification", Chem. Mater., Vol. 20, pp. 3993-4003.

18. Sekar, R., Sambandam, A., (2013), "Synthesis of bianchored metal free organic dyes for dye sensitized solar cells", Dyes and Pigments, Vol. 97, pp. 397-404.

19. Gupta, K. S. V., Thogiti, S. A., Singh, S. P., Islam, A. B., Liyuan, H. B., Malapaka, C., (2014), "Carbazole based A-π-D-π-A dyes with double electron acceptor for dye-sensitized solar cell", Organic Electronics, Vol. 15, pp. 266-275.

20. Liang, M., Wang, Z. Y., Zhang, L., Han, H. Y., Sun,Z., Xue, S., (2011), "New organic photosensitizers incorporating carbazole and dimethylarylamine moieties for dye-sensitized solar cells", Renewable Energy, Vol. 36, pp. 2711-2716.

21. Chu, H. C., Sahu, D., Hsu, Y. C., Padhy, H., Patra, D., Lin, J. T. S., Bhattacharya, D., Lu, K. L., Wei, K. H., Lin, H. C., (2012), "Structural planarity and conjugation effects of novel symmetrical acceptor-donor-acceptor organic sensitizers on dye-sensitized solar cells", Dyes and Pigments, Vol. 93, pp. 1488-1497.

22. Onicha, A. C., Panthi, K., Kinstle,T. H., Felix, N., Castellano, A., (2011), "Carbazole donor and carbazole or bithiophene bridged sensitizers for dye-sensitized solar cells", Journal of Photochemistry and Photobiology A: Chemistry, Vol. 223, pp. 57-64.

23. Venkateswararao, A., Justin Thomas, K. R., Lee, C. P., Ho, K.C., (2013), "Synthesis and characterization of organic dyes containing 2, 7-disubstituted carbazole π-linker", Tetrahedron Letters, Vol. 54, pp. 3985-3989.

24. Venkateswararao, A., Justin Thomas, K. R., Lee, C. P., Li, C. T., Ho, K. C., (2014), "Organic Dyes Containing Carbazole as Donor and π-Linker: Optical, Electrochemical, and Photovoltaic Properties", ACS Appl. Mater. Interfaces, vol. 6 (4), pp. 2528-2539.

25. Zafer, C., Gultekin, B., Ozsoy, C., Tozlu, C., Aydin, B., Icli, S., (2010), "Carbazole-based organic dye sensitizers for efficient molecular photovoltaics", Solar Energy Materials & Solar Cells, Vol. 94, pp. 655-661.

26. Qian, X., Zhu, Y. Z., Song, J., Gao, X. P. and Zheng, J. Y., (2013), "New Donor-π-Acceptor Type Triazatruxene Derivatives for Highly Efficient Dye-Sensitized Solar Cells", Org. Lett., Vol. 15, No. 23, pp. 6034-6037.

27. Zhang, X. H., Wang, Z. S., Cui, Y., Koumura, N., Furube, A., Hara, K., (2009), "Organic sensitizers based on hexylthiophene-functionalized indolo[3,2-b]carbazole for efficient dye-sensitized solar cells", J. Phys. Chem. C, Vol. 113, pp. 13409-15.

28. Li, Q., Shi, J., Li, H., Li, S., Zhong, C., Guo, F., Peng, M., Hua, J., Qina, J., Li, Z. J., (2012), "Novel pyrrole-based dyes for dye-sensitized solar cells: From rod-shape to "H" type", Mater. Chem., Vol. 22, pp. 6689-6696.

29. Wang, H. Y., Liu, F., Xie, L. H., Tang, C., Peng, B., Huang, W. and Wei, W., (2011), "Topological Arrangement of Fluorenyl-Substituted Carbazole Triads and Starbursts: Synthesis and Optoelectronic Properties", J. Phys. Chem. C, Vol. 115, pp. 6961-6967.

30. Huang, H., Fu, Q., Pan, B., Zhuang, S., Wang, L., Chen, J., Dongge Ma., Yang, C., (2012), "Butterfly-Shaped Tetrasubstituted Carbazole Derivatives as a New Class of Hosts

for Highly Efficient Solution-Processable Green Phosphorescent Organic Light-Emitting Diodes," Org. Lett., Vol. 14(18), pp. 4786-89.

31. Gong, W. L., Zhong, F., Matthew. P. Aldred, Fu, Q., Chen, T., Huang, D. K., Shen, Y., Qiao, X. F., Ma, D. and Zhu M. Q., (2012). "Carbazole oligomers revisited: new additions at the carbazole 1- and 8-positions", RSC Adv., Vol. 2, pp. 10821-10828.

32. Kochapradist, P., Prachumrak, N., Tarsang, R., Keawin, T., Jungsuttiwong, S., Sudyoadsuk, T., Promarak, V., (2013), "Multi-triphenylamine-substituted carbazoles: synthesis, characterization, properties, and applications as hole-transporting materials", Tetrahedron Letters, Vol. 54, pp. 3683-3687.

33. Kim, B. G., Chung, K., Kim, J., (2013), "Molecular Design Principle of All-organic Dyes for Dye-Sensitized Solar Cells", Chem. Eur. J., Vol. 19, pp. 5220-5230.

Chapter 4: EXPERIMENTAL

4.1 CHAPTER OVERVIEW

This chapter embraces a short explanation of different characterization techniques used in this work alongwith their main principle of operation. The materials used are discussed briefly. The general procedures of organic dye synthesis and TiO_2 nanoparticles preparation are illustrated in schematic diagrams. All steps involved in fabrication of DSSC and perovskite based ssDSSC are explained in the form of schematic diagrams with short description. Structural characterizations are carried out by NMR and Mass Spectroscopic techniques. For optical characterization UV-vis, Fluorescence Spectrophotometer was used. Morphology of the films and particles are analyzed by Scanning Electron Microscope (SEM), Tunneling Electron Microscope (TEM) and Atomic Force Microscope (AFM). The phase composition, crystallinity and surface area of synthesized materials is obtained by X-ray Diffraction (XRD), Fourier Transform Infrared Spectroscopy (FTIR) and Brunauer-Emmett-Teller (BET) Measurements. Photovoltaic evaluation of all solar cells fabricated in this work is done by *I-V*, incident photon-to-collected-electron conversion (IPCE) efficiency and Electrochemical Impedance Spectroscopy (EIS).

4.2 MATERIALS

Precursors used in all the chemical synthesis are commercially available and used without further purification. Reactions were carried out under standard inert atmosphere as per the requirement. All solvents used in the reactions were dried by standard procedures. Compounds were purified by column chromatography with silica gel (230-400 mesh) as a stationary phase. Glass substrates which are conducting on one side by FTO coating (Nippon Sheet with sheet resistivity 10 ohm per square) were used for the DSSC fabrication.

Readymade colloidal TiO_2 paste (Dyesol) was used without any further processing for making TiO_2 films for dye study.

4.3 STEPS IN SYNTHESIS OF ORGANIC DYES

The dye molecule consists of moieties like pyrene, carbazole, TPA, phenothiazine due to their electron donor ability and highly conjugated systems. Novel dye molecules were synthesized by incorporating C-N coupling, cross coupling reactions i.e. Stille coupling and condensation reaction such as Knoevanegal reaction. These reactions were conducted among the donor, accepter and anchoring groups to attain organic dye molecules. In general, the synthetic scheme of any dye molecule could be demonstrated as in Figure 4.1.

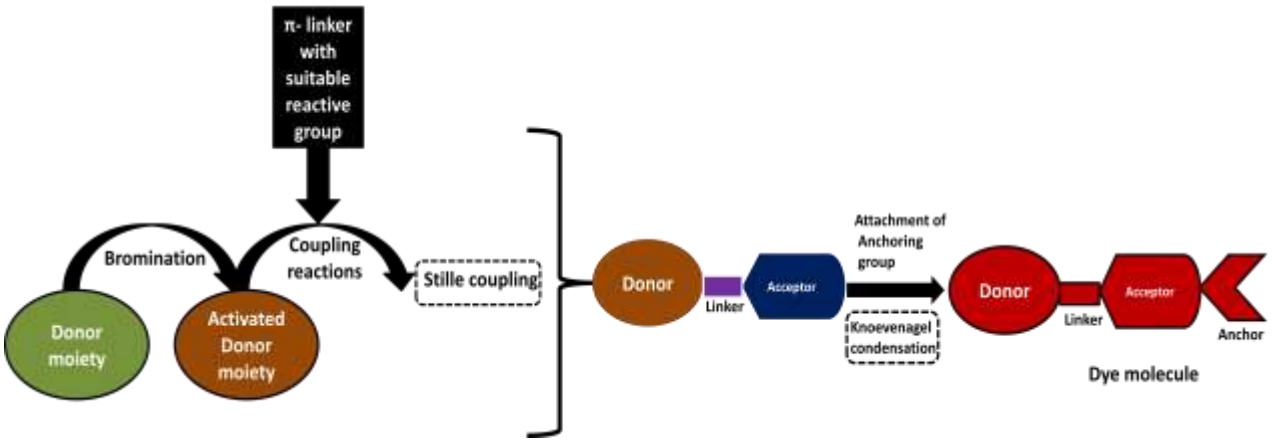

Figure 4.1: Steps in synthesis of organic dyes.

As synthesized organic compounds were purified by column chromatography and characterized by NMR, Mass and IR spectroscopic techniques for structural determination. Photophysical and electrochemical measurements were carried out by UV-vis spectroscopy and cyclic voltammetry, respectively.

4.3.1 Structural characterization

The structures of all the organic dyes and intermediate compounds as a consequence of multistep organic reactions were harmonized by ^{1}H NMR, ^{13}C NMR and mass spectroscopic techniques.

Nuclear magnetic resonance (NMR) permits the examination of particular quantum mechanical magnetic properties of the atomic nucleus. It is a physical phenomenon in which magnetic fieldis absorbed and electromagnetic radiations are emitted at a specific resonance frequency which depends on the strength of the magnetic field and the magnetic properties of the isotope of the atoms. The frequency of a signal is known as its chemical shift,

$$Chemical\ shift, \delta = \frac{Frequency\ of\ signal - frequency\ of\ reference}{spectrometer\ frequency} * 10^{6} \quad (4.1)$$

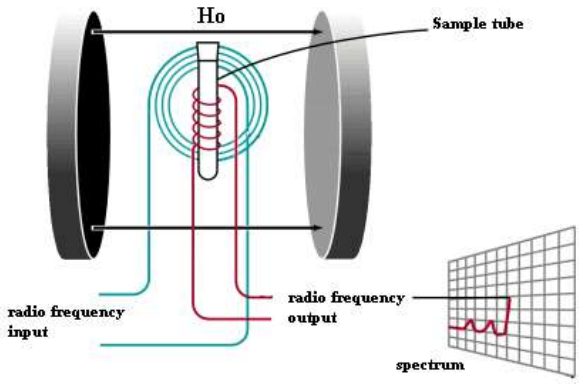

Figure 4.2: Basic arrangement of NMR spectrometer.

Figure 4.2 displays the vital structure of an NMR spectrometer. The sample is placed in the magnetic field and the excitation takes place by pulsation of the radio frequencies. An output signal is then generated by realigned magnetic fields and the actual spectrum is

produced by fourier analysis of complex output. In order to identify the signal, the pulse is repeated as many times as required [1, 2]. ^{1}H and ^{13}C NMR spectra were measured on a Bruker AV 500 O FT -NMR spectrometer in this work. Deuterated chloroform ($CDCl_3$), deuterated tetrafluoro acetic acid (TFA) and dimethyl sulfoxide (DMSO-d6) were used as solvents and tetramethylsilane (TMS) as internal standard.

Mass spectrometry (MS) is an analytical tool to reveal the chemical structure of molecules by ionizing chemical compounds to generate charged molecules or molecule fragments and measuring their mass-to-charge ratio. It generates spectra of the masses of the atoms or molecules in a sample which are used to determine the elemental or isotopic compostition of the sample and the masses of molecules.

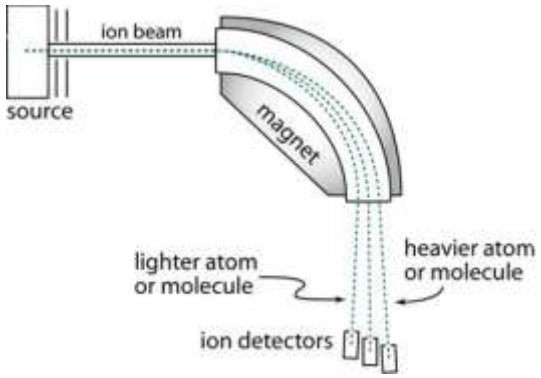

Figure 4.3: Basic arrangement of Mass spectrometer.

In this procedure, a sample, which may be solid, liquid, or gas, is ionized by bombarding it with electrons, resulting in breaking of some of the sample's molecules into charged fragments. These charged fragments are then separated according to their mass-to-charge ratio, by subjecting them to an electric or magnetic field. In this way, ions of the same mass-to-charge ratio undergo the same amount of deflection and are detected by an electron

multiplier (Figure 4.3). Results are displayed as spectra of the atoms or molecules in the sample and are identified by correlating to known masses to the identified masses [1, 3, 4]. In this work, mass Spectra were recorded in positive-ion mode on an ESI TOF high resolution mass spectrometer (Bruker Daltonics).

Fourier transform infrared (FTIR) spectroscopy is a measurement technique that allows one to record infrared spectra which is based on absorption measurement of IR radiation (wave numbers from 13,000 to 10 cm^{-1}, wavelengths from 0.78 to 1,000 nm) due to vibrational excitation. Molecules absorb specific frequencies which match the transition energy of the bond or group that vibrates. Infrared light is channelized through an interferometer to the sample. The distribution of infrared light that passes through the interferometer is altered by a moving mirror inside the apparatus. Directly recorded signal is called an "interferogram" which represents light output as a function of mirror position. This raw data is turned into the desired form of result by a data-processing technique called Fourier transform [1, 5]. In the present work infrared spectra were obtained by FTIR Thermo-Nicolet. KBr pellets were used to develop thin films of organic compounds and TiO_2 films were made by spin coating or screen printing on FTOs for IR spectra.

4.3.2 Optical characterization

The optical properties of synthesized materials were measured by UV-visible and fluorescence spectroscopic tools in suitable solvents. TiO_2 powder was spin coated on FTO and sintered at 450°C prior to recording absorbance. Absorbance of all organic dyes on films were recorded by adsorbing dye on transparent TiO_2 film screen printed on FTO and sintered at 450°C.

UV-visible spectroscopy measures the light absorption at different wavelengths in ultraviolet (wavelengths 190-400 nm) and visible (wavelengths 400-780 nm) part of the spectrum due to electronic excitations. In general, the total potential energy of a molecule can be represented as the sum of its electronic, vibrational and rotational energies. Since light is a form of energy, absorption of light by substance causes an increase in the energy of the molecules or atoms. The energy required to move an electron from lower energy level to higher energy level is equivalent to the wavelength of light absorbed. These transitions between different electronic energy levels are caused when absorbed photons posses enough energy. The amount of light absorbed is the difference between the incident radiation (I_o) and the transmitted radiation (I) and can be expressed as either transmittance or absorbance [1, 6], equations (4.2) and (4.3):

$$\text{Transmittance, } T = \frac{I}{I_0} \tag{4.2}$$

$$\text{Absorbance, } A = -logT \tag{4.3}$$

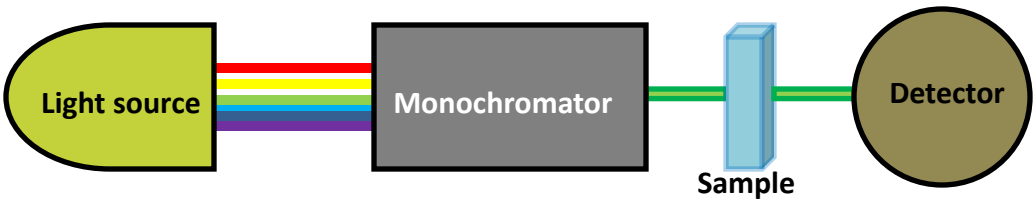

Figure 4.4: Key components of UV-Vis spectrophotometer.

The key components of UV-Vis spectrophotometer include a tungsten-halogen or deuterium lamp to generate the radiation, a monochromator and a detector, which converts visible light into electrical signal and are schematically illustrated in Figure 4.4. Experiments

were done on UV-1800 Shimadzu spectrophotometer for this work in suitable solvents and on films loaded with dyes.

Fluorescence spectroscopy is a type of electromagnetic spectroscopy which analyzes emission from a sample. A beam of light is used to excite the electrons in molecules of compounds and causes them to emit light i.e. fluorescence. Devices that measure fluorescence are called fluorimeter. Generally, ground state is the preferred state of electrons in a molecule and excited state is the higher energy state. There are various vibrational levels within each excited state in which the excited species jumps after absorbing photon. Since it is a high energy state, collisions with other molecules are bound to take place which cause excited species to lose vibrational energy until it reaches to lowest vibrational state of excited state. Molecule then continues to drop down through various vibrational levels of ground state until it reaches the lowest vibrational level of ground state. During this process the absorbed photons would be emitted but with different energies and thus different frequencies.

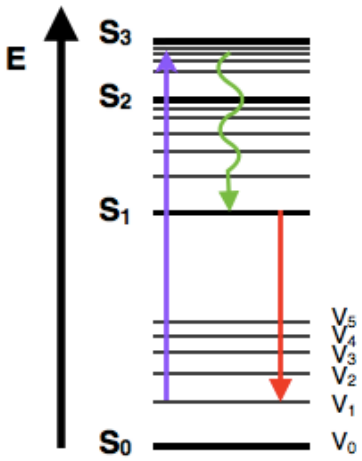

Figure 4.5: Jablonski diagram.

Jablonski diagram is the best way to illustrate the electronic states of a molecule and the transitions between them (Figure 4.5). By analyzing the emitted light frequencies and intensities, the structure of different vibrational levels can be found out. The instrument consists of a monochromator or filter, through which the light strikes the sample. Some fraction of light is absorbed by the sample and emitted in all directions. The part of emitted light which falls on secondary filter, reaches the detector and spectra is generated. Fluorescence spectra of all organic dyes in this work were obtained from Shimadzu RF-5301-PC spectrofluoro photometer in dimethylsulfoxide (DMSO).

4.3.3 Electrochemical characterization

Differential pulse voltammeter (DPV) was used for the electrochemical characterization of the organic dyes synthesized in this work. DPV has the same system as it is used in cyclic voltammetry which consists of an electrolytic cell, a current-to-voltage converter, a potentiostat that controls a three electrode cell and a data acquisition system. Three electrodes work simultaneously in cell, namely, working electrode, counter electrode and reference electrode in electrolytic solution. The electricity is conducted from the signal source to the working electrode via counter electrode. The electrolytic solution provides ions to the electrodes during oxidation and reduction of the species to be analyzed. The organic dyes were dissolved in *N, N*-dimethylformamide (DMF) and DPV was recorded at room temperature with a three-electrode cell consisting of a platinum wire as auxiliary electrode, a non-aqueous $Ag/AgNO_3$ reference electrode and a glassy carbon working electrode. All potentials were internally referenced to the ferrocene/ ferrocenium (Fc/Fc^+) couple during this work.

4.4 PREPERATION OF TiO_2 NANOPARTICLES AND CHARACTERIZATION

TiO_2 nanoparticles can be synthesized in many ways namely hydrothermal synthesis, solvothermal synthesis, vapor phase synthesis and microwave synthesis etc. In this study the synthesis of TiO_2 nanoparticles was based on sol-gel process which is a wet-chemical technique, used widely in the field of materials to produce nano particles, due to simplicity of the procedure. The process starts with a chemical solution which acts as the precursor for an integrated network, i.e. gel. Generally, precursors used are metal alkoxides and metal chlorides, which undergo hydrolysis and then polycondensation reactions and result in either an elastic solid or a colloidal suspension. Later, enhanced mechanical properties are achieved by thermal treatment and structural stability is gained by final sintering, densification and grain growth. A general procedure of nanoparticle synthesis is demonstrated in schemetic diagram in Figure 4.6.

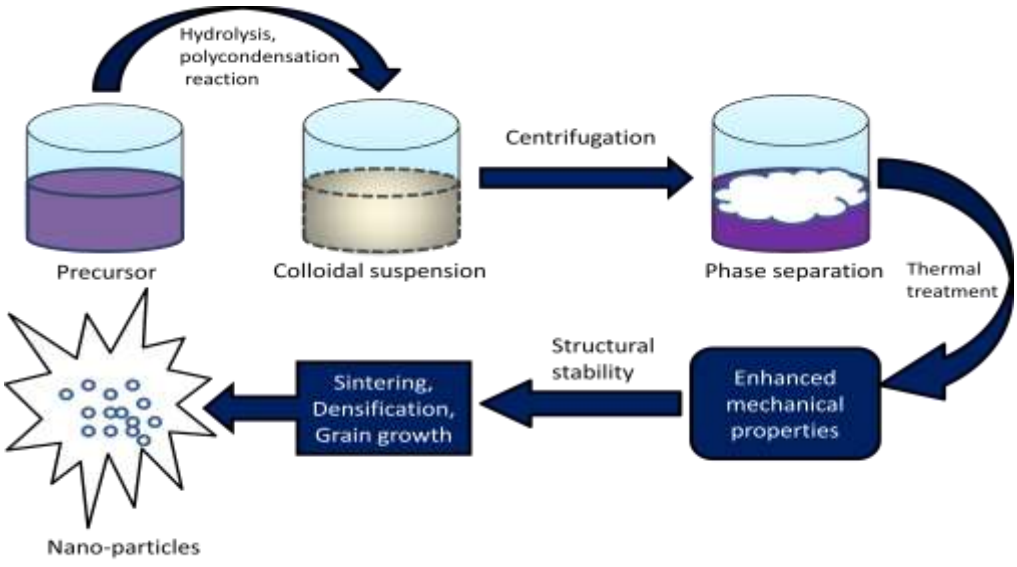

Figure 4.6: Steps in preparation of TiO_2 nanoparticles by sol-gel method.

As synthesized TiO_2 nanoparticles were characterized by electron microscopy (TEM, SEM) for finding out the shape and structure, power X-ray diffrection (XRD) for ascertaining the grain size and phase, Fourier Transform Infrared Spectroscopy (FTIR), UV-vis for optical properties.

4.4.1 Material composition

Information about the phase composition, crystallinity and surface area of synthesized materials was obtained by x-ray diffraction, Fourier Transform Infrared Spectroscopy (FTIR) and Brunauer-Emmett-Teller (BET) measurements.

X-ray diffraction (XRD) is a technique which helps in determining the chemical composition and crystallographic structure of solids. More specific crystal information such as lattice constant, orientation of single crystal, defects and stresses are also achieved by this technique. The sample is bombarded with a beam of x-rays with wavelengths within a range of 0.7 and 2 Å. The rays are then diffracted at certain angles by the crystalline phases present in the sample (Figure 4.7). These angles are depicted by Bragg's law as in equation (4.2),

$$n\lambda = 2dsin\theta \tag{4.2}$$

Where, the spacing between atomic planes in the crystalline phase is denoted by d, λ is the wavelength of the x-ray and θ is the angle between the incident ray and scattering planes. In a crystal lattice the atoms are arranged as a 3D array, in a series of parallel planes separated by a distance of d [7]. This distance varies in all materials due to different orientation of planes. If the distance travelled by the rays reflected from successive planes, differ by a whole number n of wavelengths, diffraction takes place. By plotting the angular

positions and intensities of the resultant diffracted peaks, the XRD pattern is obtained. An XRD (Bruker) diffractometer with Cu Kα radiation was used in this work.

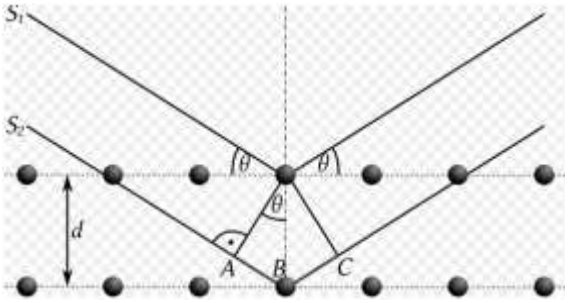

Figure 4.7: Schematic diagram depicting the technique of x-ray diffraction.

Brunauer-Emmett-Teller (BET) measurements are used to find out the total surface area of a material. An article about the BET theory was first published in 1938 by Stephen Brunaur, Paul Hugh Emmett and Edward Teller [8]. The basic concept of BET lies in the physical adsorption of inert gas molecules on a solid surface by which the specific surface area of the material can be calculated. It is based on Langmuir theory, which is a theory for monolayer molecular adsorption and multilayer adsorption on a solid. It is hypothesized that there is no interaction between these layers. Nitrogen adsorption/desorption isotherms are used to measure surface area and pore size distribution, at liquid nitrogen temperature and relative pressures (*P/Po*) ranging from 0.05-1.0. BET measurements of samples were conducted using Micro meritics, ASAP 2020, V3.05 with N_2 as the adsorbate at liquid nitrogen temperature.

4.4.2 Material morphology

The structure and morphology of the synthesized materials were studied by Scanning Electron Microscope (SEM), Tunneling Electron Microscope (TEM) and Atomic Force Microscopy (AFM).

Scanning electron microscope (SEM) is the most widely used equipment for in the morphological characterization of nanostructures. Electrons are used to generate the images in this technique. The schematic diagram of a typical SEM instrument is shown in Figure 4.8. The main source of electrons is tungsten filament, which works as a cathode. Electron gun works as anode which is situated near to tungsten filament and exerts attractive force on electrons to initiate their flow towards sample. A condenser lens is used to condense this electron beam to a very fine area on the sample. The scan coil generates a magnetic field by varying the voltage produced by the scan generator which controls the movement of electron beam. On hitting and penetrating surface of the sample electrons from the electron beam gets emitted and are collected by a detector, where they are converted to voltage and amplified. The amplified voltage is then applied to the grid of the cathode-ray tube (CRT). Final image is made up of thousands of spots of varying intensity which corresponds to the topography of the sample [9]. In this study the morphology and thickness of different nanoparticles and films were directly observed under field emission scanning electron microscope, FESEM-EDAX (QUANTA 200 F, FEI Netherlands). It has a cold cathode field emission gun, ultra-high vacuum, and sophisticated digital technologies for high-resolution high quality imaging of microstructures.

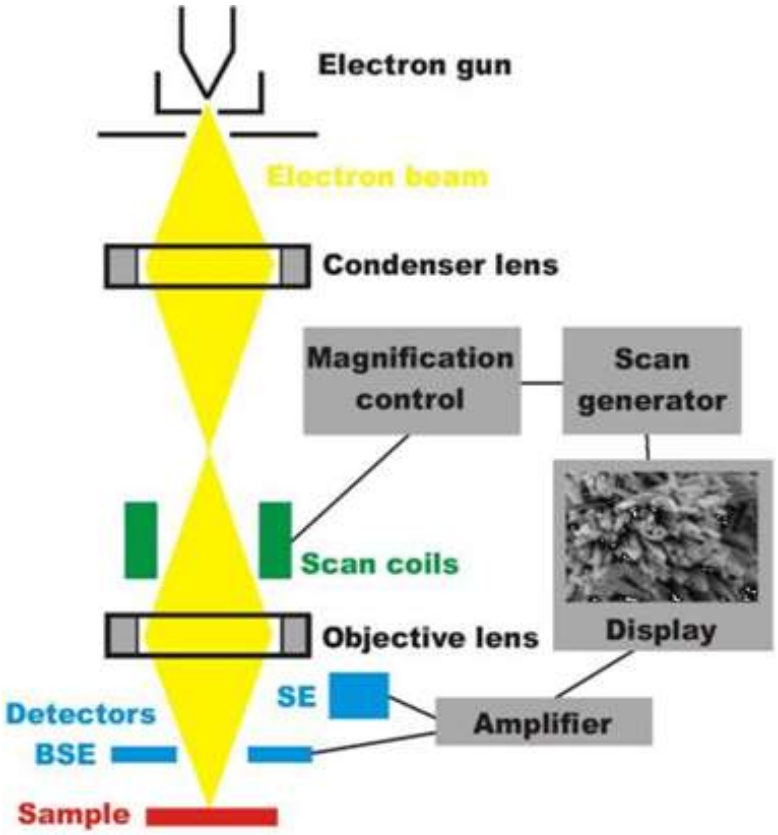

Figure 4.8: Schematic diagram of SEM instrument showing the layout of components inside SEM.

Energy dispersive X-ray (EDX) is used in combination with SEM. When an atom is struck by x-ray or γ-ray, an electron from an inner electron shell is emitted and leaves a "hole" or vacancy site in the shell. This hole is then filled by a more energetic outer shell electron which causes loss of energy, which is released in the form of x-ray emission. The energy of x-ray emission depends upon the type of elements found in the specimen which results in an x-ray spectrum. This spectrum is analyzed for information on the composition of the specimen [10].

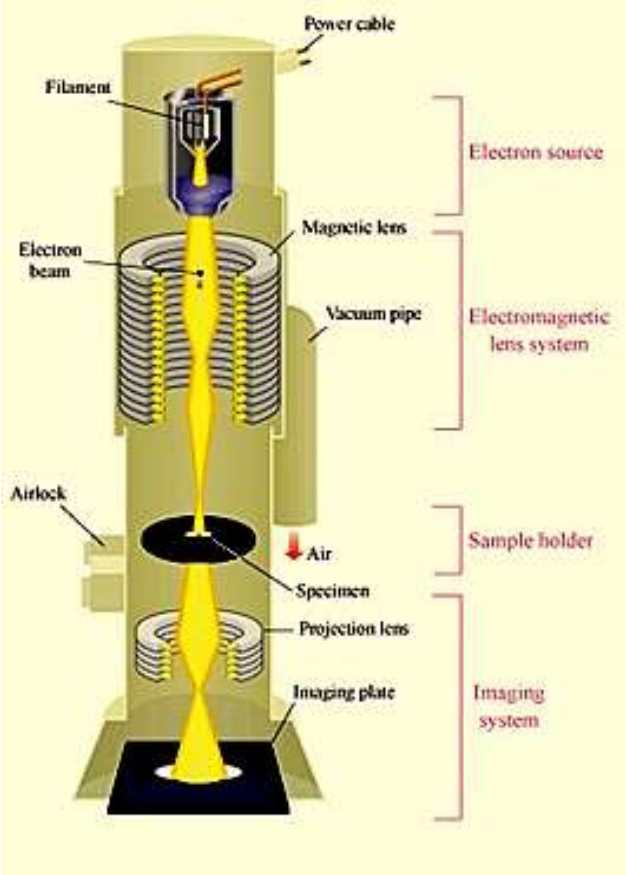

Figure 4.9: Schematic diagram showing the layout of components inside TEM.

Tunneling Electron Microscope (TEM) is a very useful tool in material characterization which works on the similar microscopy technique as used in a scanning electron microscope. It is highly used for getting information on both surface topography and crystallography of a specimen. A consistent beam of electrons is directed at the specimen, which interacts and transmits electrons as it penetrates through the specimen. The objective lens focuses the transmitted electrons into an image, which is then magnified and focused onto a phosphor image screen by intermediate and projector lenses [11, 12]. Due to different amount of electrons transmitting through the specimen an image of dark and light contrast is formed. Since electrons penetrate through the sample in this technique, the sample

preparation is very critical for accurate information generated by TEM. For the present work, all the samples were dispersed in ethanol and dropped onto the copper grid. The measurements were performed on a Phillips CM12 model at 120 kV.

Atomic Force Microscopy (AFM) is a very high-resolution scanning probe microscopy, which is in order of fractions of a nanometer. It is one of the leading tools for imaging and measuring substances at nanoscale. In this technique the substrate is sensed by a mechanical probe which is built with piezoelectric materials, in order to gather the information. These materials facilitate tiny but accurate movements on electronic commands enabling very precise scanning of the surface. It consists of a cantilever with a sharp tip i.e. probe at its end that is used to scan the specimen surface. The cantilever is made of silicon or silicon nitride with a tip having radius of curvature in the order of nanometers. When it is in proximity of sample surface, forces between the tip and the sample lead to a deflection of the cantilever according to Hooke's law [13]. Then the deflection is measured using a laser spot reflected from the top surface of the cantilever into an array of photodiodes in order to confine the images. Atomic force microscope (AFMNTEGRA, TS 150) has been used for the current work. All the films were made on FTOs by the aid of screen printing and spin coating. For dye aggregation studies dyes were adsorbed on to the TiO_2 films and for perovskite study the pervoskite was sequentially developed on TiO_2 films.

4.5 DYE SENSITIZED SOLAR CELLS (DSSCs)

4.5.1 Fabrication of DSSCs based on organic dyes with liquid electrolyte

The steps of DSSC device fabrication are shown in Figure 4.10. A compact TiO_2 blocking layer is created on pre-cleaned FTO (Nippon Sheet with sheet resistivity of 10 Ohm/sq) by chemical deposition method in which the FTO was immersed in dilute stock of

$TiCl_4$ (2M) into 0.04 M solution in DI water and heat treated at 70°C for 30 min. The cell consists of a mesoporous TiO_2 film composed of transparent layers of 25 nm sized TiO_2 anatase nanoparticles and a scattering layer of 150-250 nm sized TiO_2 nanoparticles, subsequently (Figure 4.10 (a)).

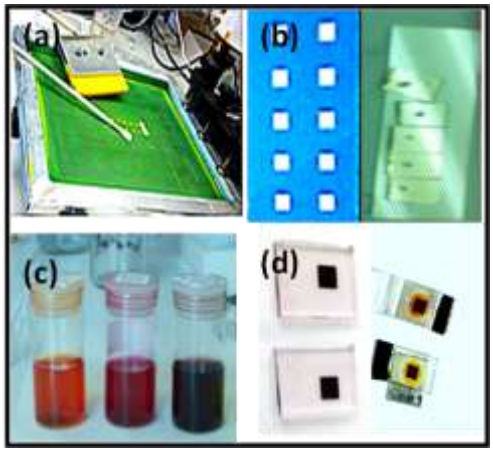

Figure 4.10: Steps in DSSC fabrication (a) Screen printing on bl-FTOs, (b) TiO_2 films and counter electrode, (c) TiO_2 films dipped in dye solutions for dye loading and (d) Dye sensitized TiO_2 films and complete devices.

The thickness of the film can be controlled by the number of consecutive film deposition on FTO. Then films were sintered from 125ºC to 500ºC for the duration of 1.5 h and set to cool down to 80°C. A blocking layer was produced over TiO_2 film by post $TiCl_4$ treatment and then the films were annealed at 450ºC for 30 min. After cooling down to 80ºC it was immersed into the dye solution (Figure 4.10 (c)). To prepare counter electrode, FTO substrates were drilled by sandblasting in order to make conical holes and washed with 0.1M HCl aq. solution, later ultrasonicated in acetone. 4.8 mM chloroplatinic acid solution in ethanol was chemically deposited by drop casting method and annealed at 450°C for 15 min

(Figure 4.10 (b)). Both the electrodes were joined together by a 25 µm thick surlyn spacer. The cells were then filled with electrolyte solution through a predrilled hole in the counter electrode and sealed with surlyn polymer and cover slip. Finally, the cells were soldered to connect to the external circuit (Figure 4.10 (d)). The cells made in such a way have an active area of 0.16 cm^2. The schematic diagram of DSSCs fabricated in this study is shown in Figure 4.11.

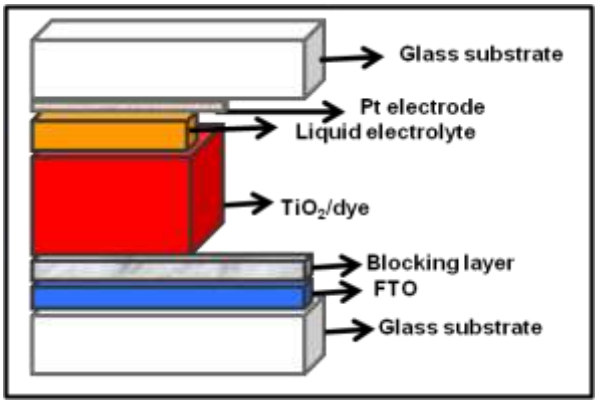

Figure 4.11: Schematic diagram of DSSC with liquid electrolyte.

To optimize the dye loading time for enhancing the device efficiency, TiO_2 films has been soaked in 0.3 mmol solution of dyesin DMSO for 5 h, 12 h and 24 h at room temperature. Two methods of indirect ex-situ surface coverage studies were used for determining the dye concentration in films during this study [14]. Firstly, sensitized TiO_2 films were dipped into 4.00 mL of 20 mmol aq. NaOH solution until complete desorption of the dye took place. Secondly, a solution of 0.1M $(CH_3)NOH$ in ACN and DI water in 1:1 ratio was used instead of NaOH solution [15] for some of the dye concentration studies. The resulting dye solutions were analyzed spectrophotometrically in a 1.00 cm^2 quartz optical

cell. The concentrations were determined by using fresh standard solutions, prepared by dissolving a known amount of dyes in aq. NaOH and $(CH_3)NOH$ solutions, separately.

Two types of electrolytes coded Z008 and Z960 were used to analyze the effect of binary additive in some of the studies under this work. The Z008 electrolyte consists of 3-propyl-1-methyl imidazoliumiodide, bis (Trifluoromethane) sulfonimide lithium salt and 1-methylbenzimidazole in 1: 0.1: 0.1 in acetonitrile. The composition of Z960 electrolyte is 1.0 M 1, 3-dimethylimidazolium iodide, 0.03 M I_2, 0.05 M lithium iodide, 0.1 M guanidinium thiocyanate and 0.5 M *tert*-butylpyridine in acetonitrile and valeronitrile solvent mixture (85:15, v/v) [16].

4.5.2 Fabrication of perovskite devices with hole transport material (HTM)

Figure 4.12 shows the schematic diagram of a typical perovskite solar cell. A 60 nm thick dense blocking layer (bl) of TiO_2 was deposited onto a F-doped SnO_2 substrate by spray pyrolysis, for which a 20 mM titanium diisopropoxide bis(acetylacetonate) solution was deposited on FTO at 450°C. Later the bl-FTOs were immersed in a 40 mM $TiCl_4$ aqueous solution at 70°C for 30 min for making the blocking layer more compact. Blocking layer was created in order to prevent direct contact between FTO and the hole-conducting layer to restrict recombination. Dysol TiO_2 paste was diluted by ethanol in 1:3.5 ratio and stirred overnight. 300-500 nm thick mesoporous TiO_2 films were spin coated onto the bl-TiO_2/FTO substrate (Figure 4.13 (a)).

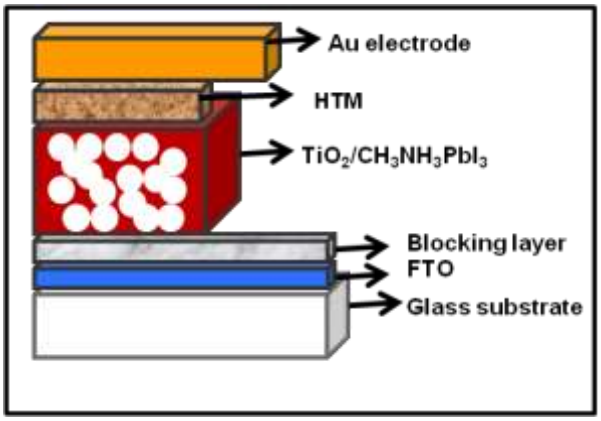

Figure 4.12: Schematic diagram of perovskite devices with hole transporting material.

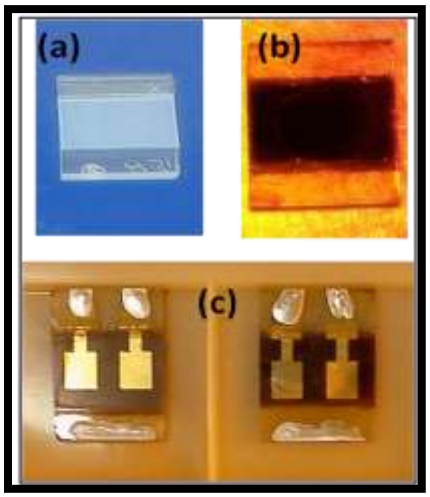

Figure 4.13: Steps in Perovskite based DSSC fabrication. (a) Spincoated TiO_2 film on blocking layer, (b) Sequential deposition of perovskite and (c) Complete cell with metal electrode.

Films were then calcined at 500°C for 1 h to remove the organic component and heat-treated at 500°C for 30 min to improve interfacial contact with nanocrystalline TiO_2. CH_3NH_3I was synthesized as per the reported method [17]. The mesoporous TiO_2 films were infiltrated with PbI_2 by spin coating at 6,500 rpm for 5 sec and dried at 70°C for 30 min. For the solution preparation, 462 mg ml^{-1} (1 M) of PbI_2 dissolved in *N*,*N*-dimethylformamide

(DMF) and was kept on stirring at 70°C. The use of such a high PbI_2 concentration is critical for obtaining the high loading of the mesoporous TiO_2 films to enhance the performance of the device. After cooling down to room temperature, the films were pre-wetted in 2-propanol and dipped in a solution of CH_3NH_3I in 2-propanol (10 mg ml^{-1}) for 15-20 min, rinsed with 2-propanol and dried at 70°C for 30 min. The HTM was then deposited by spin coating at 4,000 r.p.m. for 30 sec (Figure 4.13 (b)). The spin coating solution of HTM was prepared as per the reported method [18]. Finally, 80 nm of gold was thermally evaporated on top of the device to form the back contact (Figure 4.13 (c)). The device fabrication was carried out under controlled atmospheric conditions. The active area of the cells was 0.20 cm^2.

4.5.3 Photovoltaic device characterization

All solar cells fabricated in this work were evaluated by measuring *I-V* characteristics and incident photon-to-collected-electron conversion (IPCE) efficiency. The electron transportation, recombination resistance and electron lifetime in solar cells were studied by electrochemical impedance spectroscopy (EIS). The stability tests were performed for various duration of time with specific intervals. The cells were stored in desiccators after every test, during the stability evaluation.

A surface profiler is an instrument to measure a surface's profile such as its roughness and thickness. A diamond stylus is moved down vertically to rest on the surface and then moved horizontally across the sample. The distance to be travelled by stylus on the sample is predefined which is fixed by considering the surface to be covered on FTO also. In order to calculate the thickness of the film, the distance travelled by stylus while shifting from FTO to film, is considered. The height position of the diamond stylus generates an analog signal which is converted into a digital signal stored, analyzed and displayed. The

radius of diamond stylus ranges from 20 nm to 50 μm, and the horizontal resolution is controlled by the scan speed and data signal sampling rate. In the current work the thickness of TiO_2 layers were measured by Alpha-step IQ surface profiler.

A Solar simulator is used to reproduce full spectrum light equal to natural sunlight for evaluation of solar cells in laboratory. Sun's radiations travel through the atmosphere before reaching the earth. Due to the changing angle of sun during the whole day, the distance that sunlight has to travel keeps changing. The radiations travel the shortest distance through atmosphere when the sun is directly overhead. The spectrum of this radiation is termed as "Air Mass 1 Direct" (AM1D). Since, sea level is used as a standard reference site, the global radiation with the sun overhead is referred to as "Air Mass 1 Global" (AM1G). The solar simulator is composed of a light source and a power supply. The light source is surrounded by an ellipsoidal reflector that collects most of the lamp output. A uniform diverging beam is focused onto an optical integrator which is diverted 90° by a mirror onto a collimating lens. Special filters are situated in between the mirror and the collimating lens to shape the radiation spectra so that it matches with various air masses. Finally, a uniform beam is produced which is closely identical to the sun's radiation spectra for a given air mass. The stable light intensity is assured by a standard closed loop light intensity controller in solar simulators.For this work, the current-voltage (*I*-*V*) measurements were carried out with an active area of 0.16 cm^2 by Solar Simulator(Keithley 2612 A) at 25 °C with a source measure unit under AM 1.5 global simulated sunlight (100 mW/cm^2). The incident light intensity was calibrated to 1.0 sun by a photovoltaic reference cell system.

Incident photon-to-current conversion efficiency (IPCE) value of a solar cell indicates the amount of current that the cell will produce when irradiated by photons of a

particular wavelength. It denotes the ratio of number of electrons produced by the solar cell to the number of photons of a given energy absorbed by a solar cell. IPCE ideally has a square shape, where the efficiency value is fairly constant across the entire spectrum of wavelengths measured. The reduced value of efficiency at any wavelength illustrates recombination effects in the solar cell. IPCE is also sometimes referred to as quantum efficiency. In present work the photovoltaic performances of the DSSCs were determined by considering the incident photon to current conversion efficiency (IPCE) using Bentham-605.

Electrochemical Impedance Spectroscopy (EIS) is a recent technique in laboratories with an exclusive ability to distinguish the individual contribution of components under investigation in a solar cell. It is also known as AC Impedance Spectroscopy and gives time dependent information about the ongoing processes. The values of resistance and capacitance for the coating can be determined through modeling of the electrochemical data. Small sinusoidal potential perturbations are applied to an electrochemical system over a wide frequency in order to measure the magnitude and phase of the resulting current. Electrical circuits built from components such as resistors and capacitors, represent behaviors of the material under investigation [19]. The behavior and performance of individual components in a solar cell are evaluated on the basis of changes in their values. During the EIS measurement a small sinusoidal voltage is placed on the sample over a wide frequency range of 10^{5}-10^{-3} Hz. The controlling computer system measures the magnitude of the current induced by the potential and in addition the phase angle between the potential and current maxima. The photoelectrochemical impedance spectroscopic measurements for DSSCs were carried out with an Autolab potentiostat (PGSTAT 302) using together with a white LED (LUXEON) for this work.

Figure 4.14 shows the transmission line model used to model a DSSC. The complex impedance measurements derived the conductivity of the electrolyte system. The model applies to porous electrodes. Here R_s describes the resistance of the liquid electrolyte, *R1* and *CPE1* describe the recombination resistance and the chemical capacitance of the DSSC and D_{x1} relates to the interface of the photoelectrode and the electrolyte.

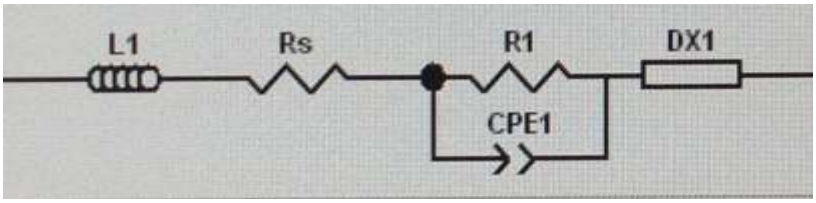

Figure 4.14: Model used for EIS measurements for DSSC.

4.6 CONCLUSION

In conclusion chapter explains all the experimental aspects involved in this research work. The materials which are used in this work are listed briefly. Basic steps followed for organic dye synthesis are outlined along with their structural, electrochemical and optical characterization techniques. Preparation of TiO_2 nanoparticles is summarized and techniques used for their compositional, morphological and optical characterizations are pointed out with their equipment details and working principle. The steps involved in DSSC and perovskite based solar cell fabrication are described with the characterization tools for material's property and performance correlation.

References:

1. Silverstein, R. M., Bassler, G. C., Morill, T. C., (1974), "Spectrometric identification of organic compounds", Wiley, New York.

2. Hornak, J. P., (2002), "The basics of NMR." http://www.cis.rit.edu/htbooks/nmr. Accessed 29 April 2010.

3. McLafferty, F. W., Turecck, F., (1993), "Interpretation of mass spectra", University Science Books, Sausalito CA.

4. Pramanik, B. N., Ganguly, A. K., Gross, M. L., (2002), "Applied electrospray mass spectrometry", Marcel Dekker, New York.

5. Coates, J., (2000), "Interpretation of infrared spectra, a practical approach. In: Meyers RA (ed) Encyclopedia of analytical chemistry", Wiley, Chichester.

6. Huber, L., (1989), "Application of diode-array detection in high performance liquid chromatography", Hewlett-Packard Co. Publication number 12-5953-2330,

7. Warren, B. E., (1990), "X-ray Diffraction", Addison-Wesley Pub. Co.

8. Brunauer, S., Emmett, P. H., Teller, E., (1938), "Adsorption of gases in multimolar layers", J. Am. Chem. Soc., Vol. 60, pp. 309-319.

9. Cao, G. Z., (2004), "Nanostructures & Nanomaterials: Synthesis, Properties & Applications", Imperial College Press London.

10. Lin, C. C., Chen, H. P., Chen, S. Y., (2005), "Synthesis and optoelectronic properties of arrayed p-type ZnO nanorods grown on ZnO film/Si wafer in aqueous solutions", Chemical Physics Lett., Vol. 404, pp. 30-34.

11. Bendersky, L. A., Gayle, F. W. J., (2001),"Electron DiffractionUsing Transmission Electron Microscopy", Res. Natl. Stand. Technol, Vol. 106, pp. 997-1012.

12. Stadtländer, C. T. K. H., (2003), “Microscopy and Microanalysis”, vol. 9, pp. 269-271.

13. Cappella, B., Dietler, G., (1999), "Force-distance curves by atomic force microscopy", Surface Science Reports, Vol. 34(1-3), pp. 1-104.

14. Dembele, A. Rahman, M., MacElroy, J. M., Dowling, D. P., (2012), “Evaluation of Microwave Plasma Sintering for the Fabrication of Dye Sensitized Solar Cell (DSSC) Electrodes”, J Nanosci Nanotechnol, vol. 12(6), pp. 4769-4774.

15. Burnside, S. D., Shklover, V., Barbe, C., Comte, P., Arendse, F., Brooks, K., Grätzel, M., (1998), “Self-Organization of TiO_2 Nanoparticles in Thin Films”, Chem. Mater., vol.10, pp. 2419-2425.

16. Alibabaei, L. K., Wang, M., Pootrakulchote, N., Teuscher, J., Di Censo, D., Humphry-Baker, R., Moser, J. E., . Yu, Y. J., Kay, K. Y., Zakeeruddin, S. M., (2010), “Molecular design of metal-free D-π-A substituted sensitizers for dye-sensitized solar cells”, M. Energy Environ. Sci, Vol. 3, pp. 1757-1764.

17. Noh, J. H., Jeon, N. J., Choi, Y. C., Nazeeruddin, M. K.,Grätzel, M., Seok, S. J., (2013), “Nanostructured $TiO_2/CH_3NH_3PbI_3$ heterojunction solar cells employing spiro-OMeTAD/Co-complex as hole-transporting material”, J. Mater. Chem. A, Vol. 1, pp. 11842-11847.

18. Burschka, J., Pellet, N., Moon, S. J., Baker, R. H., Gao, P., Nazeeruddin, M. K., Grätzel, M., (2013), “Sequential deposition as a route to high-performance perovskite-sensitized solar cells”, Nature, Vol. 499, pp. 316-319.

19. Conway, B. E., Bockris, J., White, R. E., (1999), “Electrochemical Impedance Spectroscopy and its Applications”, Modern Aspects of Electrochemistry, Kluwer Academic/Plenum Pub., New York, Vol. 32, pp. 143-248.

Chapter 5: FABRICATION AND CHARACTERIZATION OF DYE SENSITIZED SOLAR CELLS (DSSCs)

5.1 CHAPTER OVERVIEW

Current chapter concentrates on one of the vital components of DSSCs i.e., photoanode. In a DSSC photoanode is the platform where photons generate electrons. It is composed of two elements, i.e., dye molecules and semiconductor. Since both of these elements contribute to the performance of DSSCs, an elaborate depiction is conceived in this chapter revolving around both the components. For the purpose to keep it simple, this chapter has been divided into two sections:

Section 5.2: Study of Carbazole based tetra anchoring organic dyes for DSSC.

Section 5.3: Study of low band gap semiconductor for DSSC.

Section 5.2 elaborates the synthesis and application of a series of carbazole based tetra-anchoring cruciform organic dyes (P1-P5) and the effect of cosensitization by indoline dye D-205 on the photovoltaic performance of the DSSCs. The carbazole cruciform functionalized at 1, 3, 6, 8 and 2, 3, 6, 7 positions and attached to thiophene and bithiophene units capped by cyanoacrylic acids were synthesized by organic synthetic route incorporating C-C coupling and Knoevenagal reaction. All the dyes have been characterized for structural verification by NMR, FTIR and Mass spectroscopic methods. The optical and electrochemical measurements are done by UV-vis and Cyclic Voltammetry (CV) and studied by DFT/TDDFT computational method. The Photovoltaic characterizations are completed by using solar simulator, IPCE and Electron Impedance Spectroscopy (EIS). The first part of this section reveals a systematic study of the DSSC device modulation by varying the parameters such as photoanode thickness, dye adsorption time and additives. The second

part confers the effect of different substitution positions and different π-bridge lengths of organic dye molecule on the photovoltaic performance of DSSCs. The third part thoroughly discusses the cosensitization effect on optical, morphological and photovoltaic characteristics caused by post adsorption of organic dye D-205 with all the synthesized organic dyes in this study (P1-P5). In addition to rest of the characterization techniques as mentioned in chapter, Atomic Force Microscopy (AFM) has been used to analyze all the morphological changes of sensitized TiO_2 film post coadsorption of D-205. The maximum efficiency obtained in the study of organic dyes in DSSCs is 2.6 % which is enhanced upto 4.1 % which is achieved after cosensitization.

Section 5.3 of the chapter focuses on the photovoltaic properties of low band gap TiO_2 nano-composites consisting of different proportions of anatase and rutile phases. The variation in phase contents is caused by heat treatment at different temperatures given to TiO_2 nanoparticles synthesized by aqueous sol-gel route. The influence of different heat treatment temperatures on the phase composition of TiO_2 nanoparticles and its effect on optical band gap and the photovoltaic performance are analyzed. It corroborates the thermal analysis, phase analysis, morphology and energy band gap analysis of as synthesized TiO_2 nanoparticles which have been characterized by DTA/TG, X-Ray Diffraction (XRD), Field Emission Scanning Electron Microscope (FESEM), Transmission Electron Microscope (TEM) and Ultraviolet-Visible-Near Infrared (UV-Vis-NIR), respectively. The results are shown to be evaluated on the basis of photovoltaic performance of synthesized mixed phase TiO_2 NPs on DSSC devices. The DSSC devices are fabricated in conjunction with ruthenium based dye N-719 and the best efficiency obtained in this study is 6.08 %.

5.2 STUDY OF CARBAZOLE BASED TETRA ANCHORING ORGANIC DYES FOR DSSCs

5.2.1 OPTIMIZATION OF DSSC DEVICE PARAMETERS WITH DYE P1

5.2.1.1 Introduction

Solar Cells are optoelectronic devices that alter solar energy with electrical energy directly by photovoltaic effect. In this system an electric current is produced in an illuminated junction [1]. There are mainly three types of solar cells as per the materials used: inorganic, organic and hybrid. The manufacturing processes of inorganic such as silicon-based solar cells often involve costly steps, resulting in a high production cost and high energy consumption, still such cells are dominating the solar cell market due to their high power conversion efficiency. Organic solar cells have relatively low power conversion efficiency and have not yet entered into the commercial use [2]. The third type of solar cell is hybrid solar cell commonly known as Dye-Sensitized Solar Cell (DSSC), in which organic dye molecules anchored onto TiO_2 plays an important role. The typical DSSC is composed of a photoanode and a counter electrode (cathode) sandwiching a redox mediator. It consists of five components: (1) a fluorine-doped SnO_2 (FTO) glass substrate, (2) a nanocrystalline TiO_2 thin film as a semiconductor, (3) a dye sensitizer, (4) an electrolyte (redox mediator), and (5) a platinum-coated glass substrate [3].

One of the key roles in DSSCs is credited to the sensitizers, which are responsible for light absorption and the generation of electric charge. Although ruthenium sensitizers exhibit record solar to electricity power conversion efficiencies (PCEs) of 11-12% under AM 1.5 G irradiation [4], high extinction coefficients of organic dyes and the ease of tuning their spectral properties by standard synthetic methods turned out to be of superior advantage.

Thereby, more research activities are now focused on modulation of new metal-free organic sensitizers. An organic dye for DSSCs consists of electron donor-acceptor (DA) system linked through conjugated spacer. The anchoring group is integrated onto the acceptor moieties which anchor dye molecule onto TiO_2 surface. The photo generated electrons must flow into the TiO_2 film without much interfacial recombination in order to get high conversion efficiency [5]. Studies show that cell performance is influenced by parameters such as morphology of TiO_2 nano particles, optical properties of nano-crystalline TiO_2 films, electrochemical characteristics of redox electrolytes and photochemical properties of molecular sensitizers [6]. Designing of dye molecule is the key task which takes much of the optimization for preferential orientation of dye on TiO_2 surface. The improvement in charge injection and reduction of back electron transfer processes are controlled by maintaining the distance of photo-oxidized donor from photo-injected electrons [7]. The open-circuit voltage (V_{oc}) for DSSCs based on novel organic dyes is found to be on the lower side as compared to that of ruthenium dye based DSSCs. The dye structure seems to have an impact on V_{oc} and is attributed to different electron lifetime [6, 8]. Variation of π-conjugated linker seriously affects the efficiency of the intra-molecular charge transfer, and partially determines the DSSC performance of corresponding cell [9].

Carbazole is a well-known electron-donating material and is observed to act as a good light harvester due to its planar nature. In addition, its low HOMO level allows efficient regeneration of the oxidized dye and minimizes charge recombination [10]. It contributes in providing a vast variety of modes for connecting to other units due to its facile functionalization at C1, C2, C3, C6, C7, C8 and N9 positions [11]. Different connecting sites of carbazole play a significant role towards its optical properties. Thiophene conjugated

carbazole dyes cover a broad range of spectrum and show absorbance up to 800 nm that matches with the photocurrents of ruthenium-based dyes [12]. Multi-carbazole derivatives have also been investigated for their photovoltaic properties [13]. The effect of number of acceptors on single carbazole moiety has been compared on A-π-D and A-π-D-π-A structures, consisting of an electron-donating *N*-alkyl carbazolyl unit and electron-withdrawing cyano or carboethoxy group. It is evident from previous studies [14] that the introduction of electron accepting groups at C3 position of carbazole with elongated π-bridge induces intra-molecular charge transfer and depending upon the electron affinity of acceptor groups, the charge transfer band is red shifted [15]. In a recent study conducted by K.S.V. Gupta *et.al.,* the π-bridging linker moieties were observed to be dominant in the power conversion efficiencies [16]. Other crucial factor is the binding strength of dye on to the TiO_2 surface, which affects the conversion efficiency and stability of DSSC device [16]. The dye should be adsorbed to make a compact monolayer on TiO_2 film yet should not get aggregated. Formation of aggregates on the TiO_2 surface is an obstinate drawback of organic dyes in DSSC. A unique approach for suppression of dye aggregation is bridging of two chromophores into a spiro configuration similar to Ru-dyes [17].

Based on the requirement of red shifted absorption, reduced tendency towards aggregation and strong binding to TiO_2, a novel dye P1 was synthesized by bridging four anchoring groups at one *N*-butyl carbazole via four π-linkers. This cruciform molecule is composed of multi-conjugated arms, which are stretched in different orientations. A unique feature of P1 is its cross-shaped conformation which is expected to minimize the aggregation as well as increase the binding strength of dye on TiO_2. Due to their thermal stability, good film-forming properties and high luminescence [18], the cruciform molecules have attracted

much attention to the application in OLEDs, photovoltaics and field effect transistors [19]. Organic dye based on carbazole/ thiophene/ cyanoacrylic acid, arranged as four acceptors on one donor moiety is explored in this study. However, the use of the molecular engineering alone does not eliminate both charge recombination and the aggregation of the dyes and can be reduced to some extent by improvising DSSC fabrication methods [20]. Hence, device engineering has also been exploited in this study by diverging the parameters i.e., thickness of TiO_2 film, dye adsorption time and additives. Dye P1 is successfully synthesized and applied for DSSC applications and the results of photophysical, electrochemical and photovoltaic characteristics of a newly synthesized dye are thoroughly investigated.

5.2.1.2 Results and discussions

5.2.1.2.1 Synthesis of P1

The synthetic scheme of P1 is shown in scheme 5.1. The carbazole-based organic dye containing four thiophene units as π-conjugation pathways is synthesized in three steps. Firstly, 1, 3, 6, 8-tetrabromo-9-butyl-9*H*-carbazole (1a) was synthesized via alkylation of carbazole followed by poly bromination as per reported methods [21]. Secondly, Stille coupling between compound (1a) with (5-(1, 3-dioxolan-2-yl)thiophen-2-yl)tributylstannane produced desired carbazole consisting of thiophene aldehyde (1b). In the final step dye P1 was prepared by condensation reaction of compound (1b) with cyanoacetic acid using glacial acetic acid as the solvent and ammonium acetate in a catalytic amount [11].

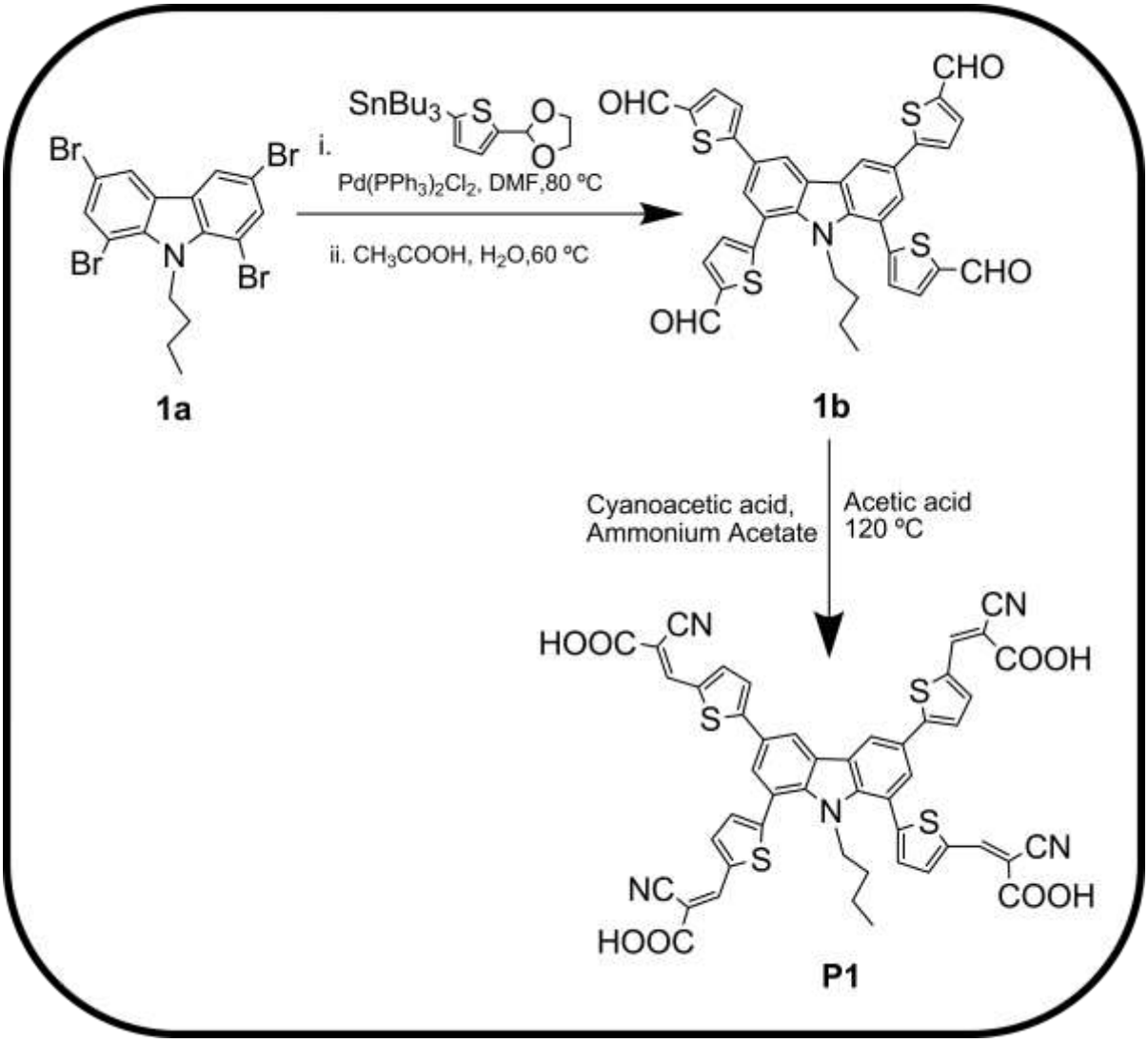

Scheme 5.1: Synthetic scheme of dye molecule P1.

5.2.1.2.2 Optical properties of P1

The absorption and emission spectra of dye P1 were recorded in DMSO, displayed in Figure 5.1 (a). Absorption covering the range of 300-530 nm with single prominent peak is observed. It has been deduced in the previous studies that the effective conjugation length affects the peak position of a π- π^* transition band while the charge-transfer band will be influenced by the nature of electron donor, acceptor and the connecting bridge [22]. Peak at

381 nm in near visible region suggests a transition originating from the whole molecule with a strong intramolecular charge transfer character from carbazole donor moity to the cyanoacrylic acid anchoring unit [23], creating an efficient charge separated state.

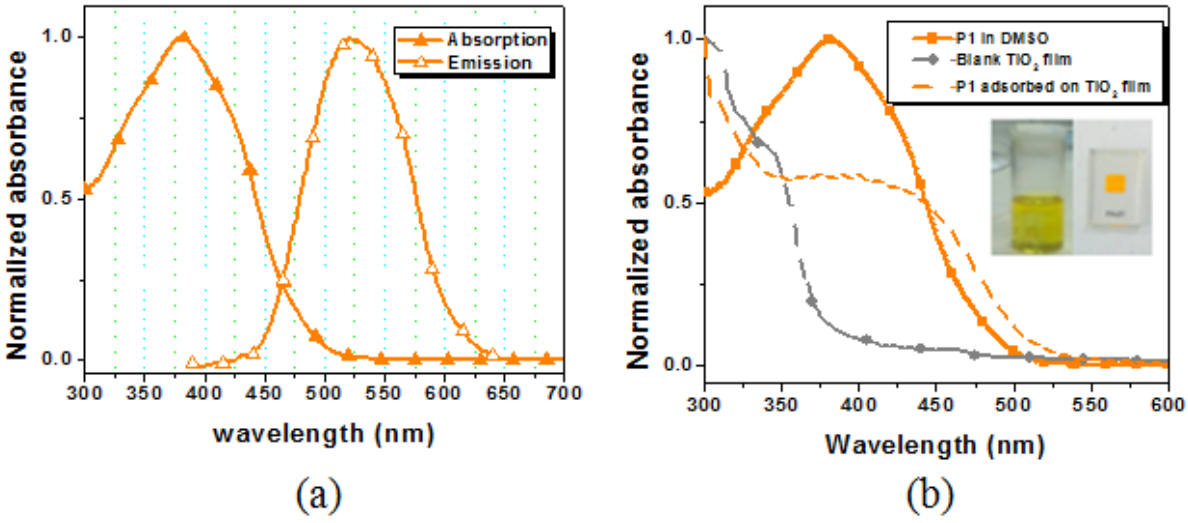

Figure 5.1: Absorption and emission spectra of P1 (a) in DMSO, (b) on TiO_2 film (Inset - P1 solution in DMSO and P1 adsorbed on TiO_2 film).

Absorption and emission spectra of P1 is shown in Figure 5.1 (a). A small humph is seen in the range of 324-352 nm representing a low energy shoulder which shows the possibility of π- π^* transition. The excitation wavelength for emission was observed as 390 nm. The maximum absorption and emission in DMSO were at 381 and 522 nm, respectively. Absorption spectrum of P1on transparent TiO_2 film was recorded, shown in Figure 5.1 (b). The wavelength of the absorption peak of P1 has significantly red shifted by 50 nm compared to that in DMSO, covering a broad range of 300-575 nm which could be more precisely observed by inset pictures of dye solution and dye adsorbed film in Figure 5.1 (b). The similar phenomenon had also been observed for other organic dyes which may be

ascribed to *J*-type aggregation of the dyes on the TiO_2 surface [24]. The red-shifting and broadening favor the light harvesting of the solar cells and thus increase the photocurrent response region, resulting in the increase of $J_{sc.}$

5.2.1.2.3 Electrochemical Properties of P1

The electrochemical characteristics of P1 are investigated by differential pulse voltammetry (DPV) in DMF with 0.1 M tetrabutylammonium hexafluorophosphate as the electrolyte. It is significant to ascertain the probability of electron transition from the excited dye molecule to the conduction band of TiO_2 and regeneration of dye molecule, to determine the photovoltaic performance of the device. It is evident from the DPV graph in Figure 5.2 (a) that P1 exhibits two irreversible oxidation peaks. Figure 5.2 (b) shows the HOMO-LUMO level of P1 in respect with TiO_2 conduction band and redox couple.

The ground state oxidation potential corresponding to the HOMO levels is 1.34 V (vs. NHE). The band gap energy ($E_{0\text{-}0}$) is calculated as 2.67 eV by taking an intersection point of absorption and emission spectra of P1 in Figure 5.1 (a). The calculated excited state potential corresponding to the LUMO level is -1.33 eV, which is an estimation of E_{HOMO}-$E_{0\text{-}0}$. Table 5.1 summarizes the electrochemical properties of as-synthesized dye. It is extracted from the data that the HOMO level of P1 to be sufficiently more positive than the iodine/iodide redox potential value (0.4 V), indicating the thermodyanamic feasibility of the oxidized dye to get regenerated by accepting electrons from I^- ions. The LUMO level is also found to be sufficiently more negative than the conduction-band-edge energy level (E_{cb}) of the TiO_2 electrode (0.5 V vs. NHE), shown in Figure 5.4. As the driving forces are sufficient for efficient charge injection, it is concluded that the electron insertion from the excited dye

molecule to the TiO_2 conduction band and the subsequent dye regeneration are energetically permitted [12].

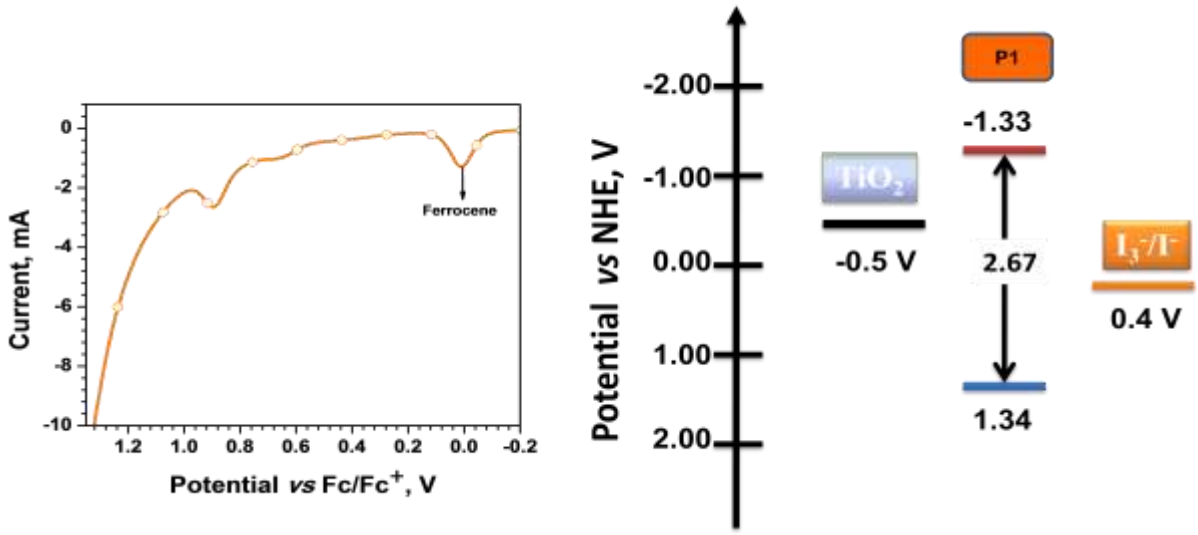

Figure 5.2: Electrochemical properties of P1 (a) DPV recorded in DMF, (b) Energy band diagram.

Table 5.1: Electro-optical data of the dye P1.

Dye	λ_{abs}[a], nm	λ_{em}, nm	λ_{abs}[b], nm	E_{ox}	HOMO,eV w.r.t Ferrocene	LUMO,eV	$E_{o\text{-}o}$,eV	E_{ox}^{*},eV
P1	387	522	425	0.62	5.42	2.75	2.67	-1.33
a- Recorded in DMSO, b- Recorded on TiO_2 film								

5.2.1.2.4 Frontier Molecular Orbital (FMO) study of P1

Molecular Orbital calculations are carried by TD-DFT technique which has been currently usefor the modulation of novel sensitizers for the DSSCs. DFT/TDDFT computational investigationshave also been done using B3LYP exchange functional and 6-

31G (d, p) basis set as implemented in the Gaussian (G09) program package [25] for getting an insight about the character of the excited states of the dye P1. Electronic distributions observed in the frontier molecular orbital of the dye are illustrated in Figure 5.3.

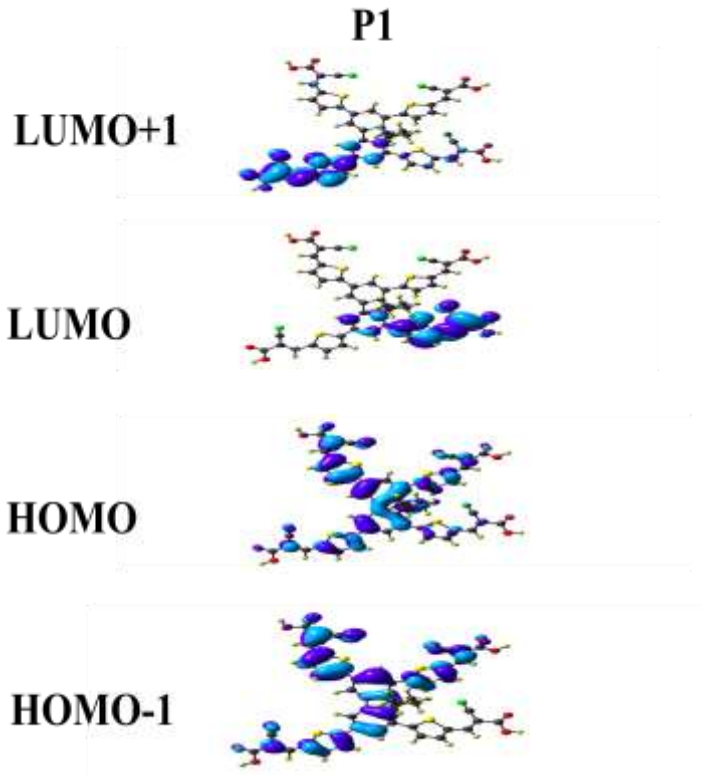

Figure 5.3: Electron density distribution in molecular orbital of dye P1 after structural optimization at B3LYP exchange function and 6-31G (d, p) basis set.

It is observed that HOMO of the dye is mainly centralized on the carbazole donor unit and spread up to the thiophene units at 3, 6 and 8 positions. The LUMO associated with π^* molecular orbital (MO) of the dye is completely located on thiophene unit and cyanoacrylic acid at position 1. It is anticipated to have a charge migration on electronic excitation from the HOMO to the LUMO [13] where such a well separated frontier molecular orbitals are

present at donor and acceptor units in the molecule. It is observed that in second excited state (LUMO+1), the excited electrons density is centralized at the thiophene unit and cyanoacrylic acid at position 3. The presence of electron density at different positions in both excited states triggers the probability of two directional flows of electrons. As per the B3LYP [22] computations, HOMO to LUMO electronic excitations are originated from the longer wavelength vertical transitions in the dye molecule. Excited state TD-DFT calculation on this dye reveals an intense absorption at 476 nm with oscillation strength of 0.4076 due to excitations from HOMO to LUMO+1(+93%). Another intense absorption was observed at 407.4 nm (f = 0.4968) owing to excitations from HOMO-1 to LUMO+1(+84%) and minor absorption at 542.4 nm (f = 0.0863) due to excitations from HOMO to LUMO (+98%). The examination of molecular orbital corroborates that the lack of adequate unidirectional electron flow could be accountable for impeding the electron injection after the photo-excitation of the dye [26], due to which J_{sc} suffered drastically in the cells fabricated by dye P1.

5.2.1.2.5 Photovoltaic performance

5.2.1.2.5.1 Optimization of TiO_2 film thickness

The thickness of TiO_2 film is an important parameter which affects the performance of the DSSC [27]. Therefore, it is necessary to analyze the electron transport on different thicknesses of TiO_2 film to improve the efficiency of the DSSC. Considering the influence of electron transport distance of the film on electron penetration through TiO_2 film and consecutively on charge collection, thickness of TiO_2 mesoporous film was taken as 9, 12, 15 and 18 μm. The photovoltaic performance of the DSSCs and variation in parameters are shown in Figure 5.4 (a) and IPCE is shown in Figure 5.4 (b) *I-V* parameters of this study are

summarized in Table 5.2. Figure 5.4 (c) elaborates the effect of thickness of TiO_2 film on all *I-V* parameters.

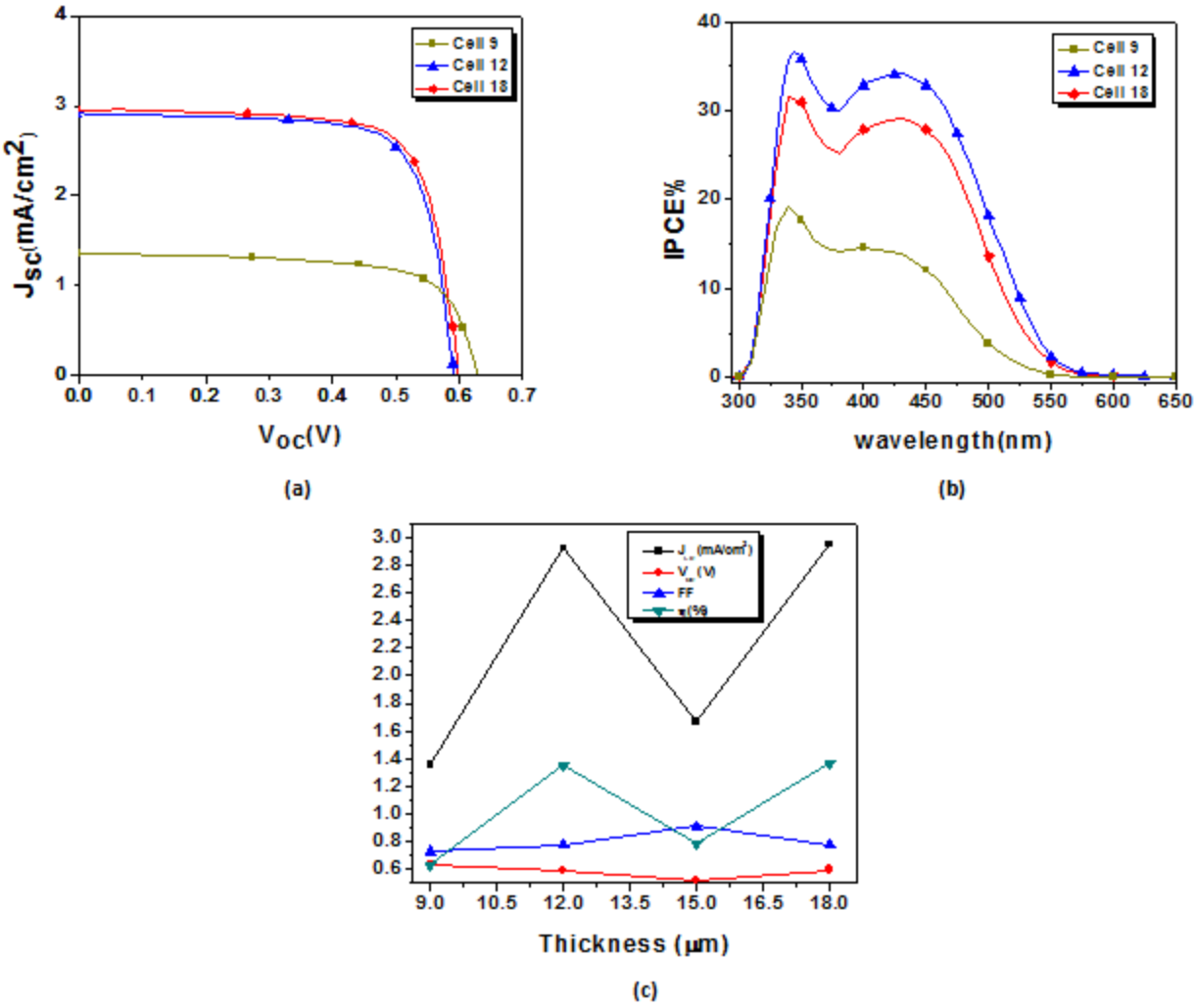

Figure 5.4: Photovoltaic performance of cell 9, cell 12 and cell 18 (a) *I-V* parameters, (b) IPCE and (c) Effect of thickness on all the DSSC parameters.

Table 5.2: *I-V* specific parameters of cell 9, cell 12 and cell 18.

Thickness	J_{sc} (mA/cm^2)	V_{oc} (V)	*FF* (%)	η (%)
Cell 9	1.36	0.629	0.73	0.63
Cell 12	2.92	0.591	0.78	1.35
Cell 18	2.95	0.598	0.78	1.37

The most commonly utilized TiO_2 thickness in the various studies has been found to be around 11 µm, although it can be thicker than that because the diffusion distance of injected electrons in DSSC is expected to be longer than 20 µm [28]. It is noted that J_{sc} increases from 1.36 mA/cm^2 to 2.95 mA/cm^2, with increasing film thickness from 9 to 18 µm. Over the same thickness range, V_{oc} decreased from 0.629 V to 0.598 V. The variations of the J_{sc} and η are similar in all the cases, indicating that the increase in η is largely due to the increase in J_{sc}. On the other hand, at 425 nm it is found that the IPCE values are maximum at 12 µm which is even higher than the IPCE value of 18 µm thick cell. Although *I-V* measurements observed at 18 µm thickness, showed the best results. This could be explained by the relationship between the aggregation and the sensitization efficiency. A disorder in the packing of dye chromophores in the *H*-like aggregate causes the decrease of IPCE [29]. It is suggested that the formation of *H*-aggregate in case of 18 µm thick cell, caused a decrease of the quantum yield and the fluorescence lifetime due to the self-quenching of excited state in the aggregate [30]. Figure 5.6 (c) depicts the overall effect of thickness of TiO_2 film on all the photovoltaic parameters of DSSCs.

5.2.1.2.5.2 Optimization of the soaking time for TiO_2 films in P1 dye

Dye loading involves three steps [31] namely, 1) diffusion of the dye into TiO_2 layer, 2) adsorption of the dye onto the surface of TiO_2 film and 3) agglomeration of the dye molecules. An optimum loading time allows the dye to diffuse into the mesoporous structure of TiO_2 film to develop a monolayer of dye. Too long loading time, however, reduces the efficiency due to shielding effects from the extra dye, which blocks the underlying dye adsorbed on the TiO_2 surface from solar irradiance [32].

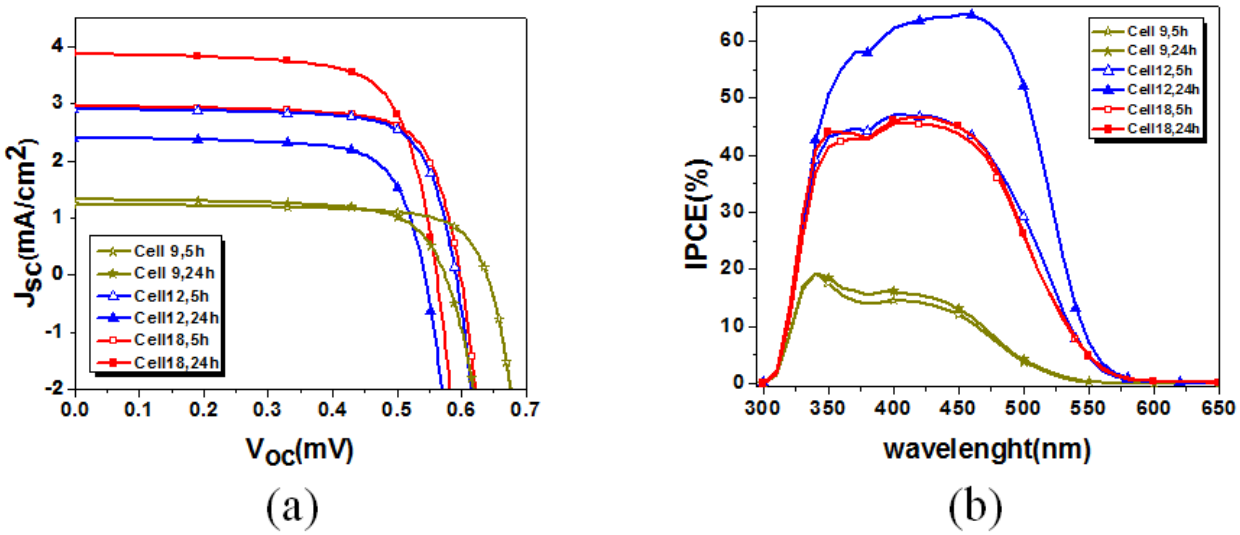

Figure 5.5: Photovoltaic performance of cell 9, cell 12 and cell 18 at dye loading time of 5 hours and 24 hours (a) *I-V* and (b) IPCE measurements.

As the amount of the dye adsorbed on the TiO_2 film is influenced by dye loading time as well as thickness of the film, the study was performed on all the thicknesses taken earlier i.e., 9, 12 and 18 μm. Current-voltage (*I-V*) measurements and IPCE of DSSC with different dye loading times are shown in Figures 5.5 (a) and (b), respectively and *I-V* specific

parameters are depicted in Table 5.3. In case of TiO_2 film thickness of 9 and 12 μm, the J_{sc} and η of the sample decreased with the dye-loading time and reached a minimum at loading duration of 24 hours. The initial rise in the efficiency at 5 hours is suggested because of more amount of dye diffused into TiO_2 layer to cover a larger area for solar excitation. After TiO_2 surface was completely covered, further dye loading did not improve the efficiency as only the dye adsorbed directly onto the TiO_2 surface could inject electrons and contribute to the photocurrent.

Table 5.3: *I-V* specific parameters of cell 9, cell 12 and cell 18 at dye loading time of 5 hours and 24 hours.

	5 h				24 h			
	J_{sc} (mA/cm^2)	V_{oc} (V)	*FF* (%)	η (%)	J_{sc} (mA/cm^2)	V_{oc} (V)	*FF* (%)	η (%)
Cell 9	1.36	0.629	0.73	0.63	1.24	0.640	0.73	0.58
Cell 12	2.92	0.591	0.78	1.35	2.40	0.543	0.78	1.01
Cell 18	2.95	0.598	0.78	1.37	3.87	0.561	0.74	1.62

As the dye-loading time was extended, the efficiency has been observed to drop rapidly. This could be due to undesirable shielding effects from the extra amount of dye [31, 32]. No trend is seen in V_{oc} and *FF*, in both the cases. The efficiency increased when the dye was adsorbed on to the TiO_2 surface with thickness of 18 μm as the dye loading time increased from 5 to 24 hours. A significant improvement in J_{sc} and η has been observed when dye was loaded for longer time on 18 μm thick TiO_2 film which is further evident by the calculated amount of dye adsorbed onto it. Indirect ex-situ surface coverage studies based on dye adsorption-desorption process represents the most common tool in which the amount of

adsorbed dye is determined by desorbing the dye from the TiO_2 surface by treating the sample with a hydroalcoholic solution of NaOH and then measuring the desorbed dye concentration by spectroscopy in the ultraviolet-visible (UV-Vis) spectral range [33]. The amount of adsorbed P1 dye is determined following the same procedure. Thus, it is easy to quantify the amount of desorbed dye, i.e., the original amount of the dye loaded into TiO_2 layer, by comparing the spectra corresponding to 12 and 18 µm thick sensitized surfaces to those of freshly made solutions at known concentrations with dye loading time of 24 hours. It can be deduced from the absorption spectra in Figures 5.6 (a) and (b), that the dye concentration is much higher in the TiO_2 film with 18 µm thickness than in 12 µm thick films.

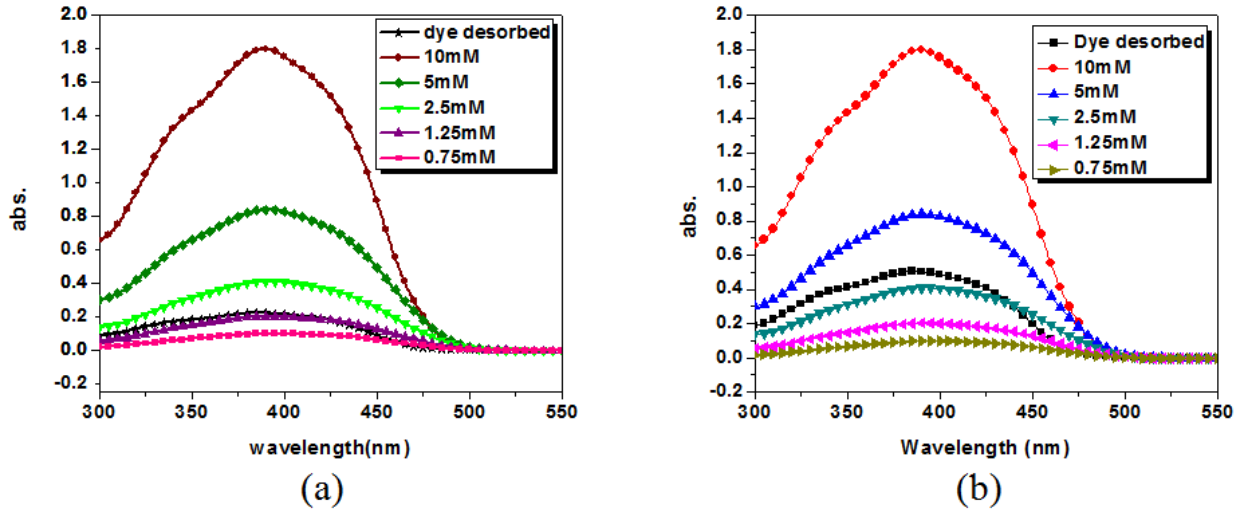

Figure 5.6: Dye desorption trends (a) Absorption spectra of dye desorbed form 12 µm thick TiO_2 film with dye loading time 24 h and standard solutions of P-1 of known concentrations. (b) Absorption spectra of dye desorbed form 18 µm thick TiO_2 film with dye loading time 24 h and standardsolutions of P1 of known concentrations.

The increased dye adsorption contributes to the light harvesting efficiency (LHE) of DSSC [34]. It is concluded that enhanced efficiency of sample with thickness of 18 μm than 12 μm, when dye loading time of 24 hours, is due to higher concentration of dye in TiO_2 film. A considerable decrease in IPCE of 18 μm thick cell with dye loading time 24 hours is observed which can again be explained on the basis of the disorder in packing of dye chromophores in the *H*-like aggregate [35].

5.2.1.2.5.3 Optimization of additives in the electrolyte

It is established that the photovoltaic performance of DSSCs can be enhanced significantly by adding a small amount of electric additive. The effect on the photovoltaic parameters observed by changing the chemical nature of the additives is related to the electron donating ability and the hydrogen bonding of the additives. The influence of nitrogen-containing heterocyclic additives on the photovoltaic performance of DSSCs was investigated [36], and it was found that some efficient electric additives such as 4-*tert*-butylpyridine could enhance V_{oc} due to a positive band edge movement but decrease J_{sc}. Upon adsorption on TiO_2 surface pyridine ring induces electron density into TiO_2 creating a surface dipole causing decease in J_{sc}. TBP is a strong electron donor, thus, not only increases the photoconversion efficiency but decreases the dark current and blocks the back electron reaction [37, 38].

The effect of GuSCN as additive on the photovoltaic performance of the DSSC was first reported by Grätzel [39]. It was concluded that GuSCN improved the V_{oc} of the DSSC as it not only shifts the band edge to negative potential but also shields the surface against recombination [40]. The onset potential for the reduction of triiodide shows negative shift which indicates that the addition of GuSCN reduces the electron recombination between

TiO_2 surface and I_3^- [39, 41]. The change in J_{sc} observed by using different additives is related to the interface interactions between the TiO_2 and the electrolyte. The additives generally increase the desirable electron transfer reaction and decrease the efficiency loss steps like the back electron transfer reaction [42]. The effect of single additive has been explored in most of the earlier studies but very less work exploits the effect of the binary additives. H. S Lee *et.al.* [42] concluded that the combination of different types of additives in different concentrations imparts positive effect on J_{sc} and consecutively on efficiency. Keeping this in consideration, experiments are performed by applying two types of liquid electrolyte systems with volatile solvents for the purpose of device fabrication, coded as Z008 and Z960. The compositions of both the liquid electrolyte systems are given in earlier section.

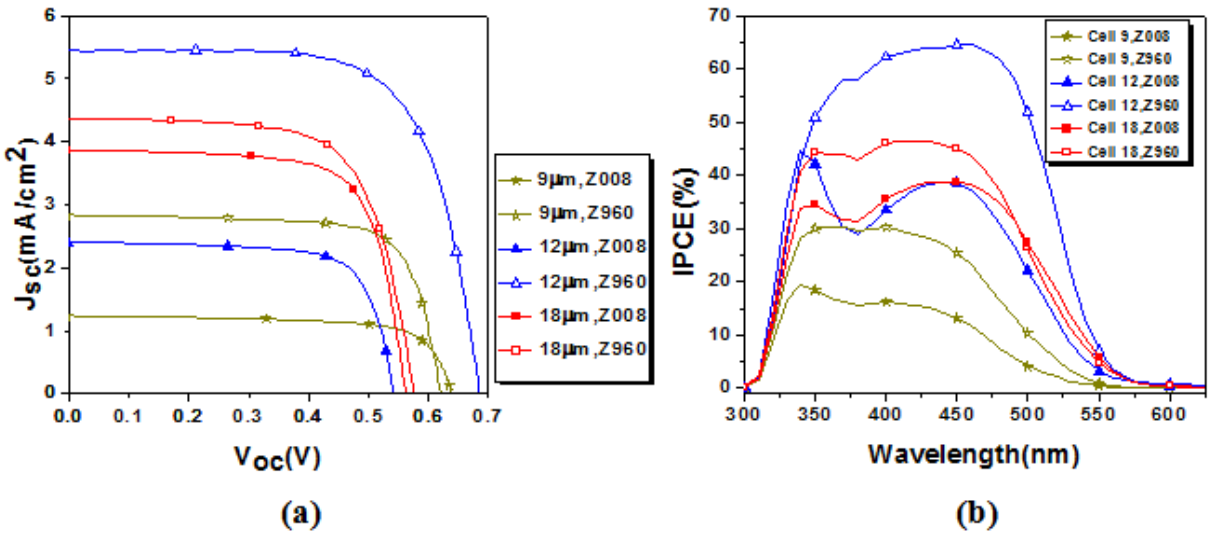

Figure 5.7: Photovoltaic performance of cell 9, cell 12 and cell 18 in presence of binary additives for dye loading time of 24 hours (a) *I-V* and (b) IPCE measurements.

Although the best performance was achieved only at the thickness of 18 μm, during the thickness optimization , the additive effect is studied at all the thicknesses i.e. 9, 12, 15 and 18 μm for dye loading time of 5 and 24 h to see whether the presence of additive can be effective in suppressing the other detrimental factors. The main difference in both the electrolytes is the presence of binary additives, guanidinium thiocyanate and *tert*-butylpyridine, in Z960. The Z008 is free from additives.

Table 5.4: *I-V* specific parameters of cell 9, cell 12 and cell 18 in presence of binary additives for dye loading time of 24 hours.

	Z008				Z960			
	J_{sc} (mA/cm^2)	V_{oc} (V)	*FF* (%)	η (%)	J_{sc} (mA/cm^2)	V_{oc} (V)	*FF* (%)	η (%)
Cell 9	1.24	0.640	0.73	0.58	2.84	0.620	0.76	1.34
Cell 12	2.40	0.543	0.78	1.01	5.45	0.685	0.70	2.61
Cell 18	3.87	0.561	0.74	1.62	4.37	0.576	0.70	1.77

For comparison, the *I-V* and IPCE were recorded with both the electrolytes in Figures 5.7 (a) and (b), for 5 and 24 h, respectively. Table 5.4 summarizes the *I-V* data which clearly indicates the remarkable increase in J_{sc} as well as in η in all the cases in presence of Z960. In 5 h study the improvement in J_{sc} at 18 μm thickness is around 42 % with highest efficiency of 2.1%. The increase of 56% in J_{sc} at 12 μm is observed when the study is conducted for 24 h. The overall performance of the device is improved remarkably in the presence of binary additives and highest efficiency of 2.61% is observed with highest J_{sc} and V_{oc} of 5.447 mA cm^{-2} and 0.685 V, respectively.

The results were further justified by Electron Impedence Spectroscopy (EIS). There are four internal impedances in the DSSC represented in a typical Nyquist diagram [43], each of which has a significant effect on the electron transport. Among them the impedance related to the electron transport in the TiO_2/dye/electrolyte interface is placed in the middle-frequency peak (in the 1-100 Hz). The sum of the resistance components (R1, R2, R3, and Rh) represents the total internal impedance of the DSSC which is inversely proportional to the phovoltaic performance of a DSSC. Figure 5.8 shows the Niquest plot of cell 12 and cell 18 with binary additives. As the second semi-circle found to be reduced at the thickness of 18 μm, it is concluded that the resistance related to the electron transport is decreased when the thickness of TiO_2 is more, results in improved electron lifetime [43]. Elongated electron lifetime affects the diffusion length favorably which finally facilitates the electron transfer.

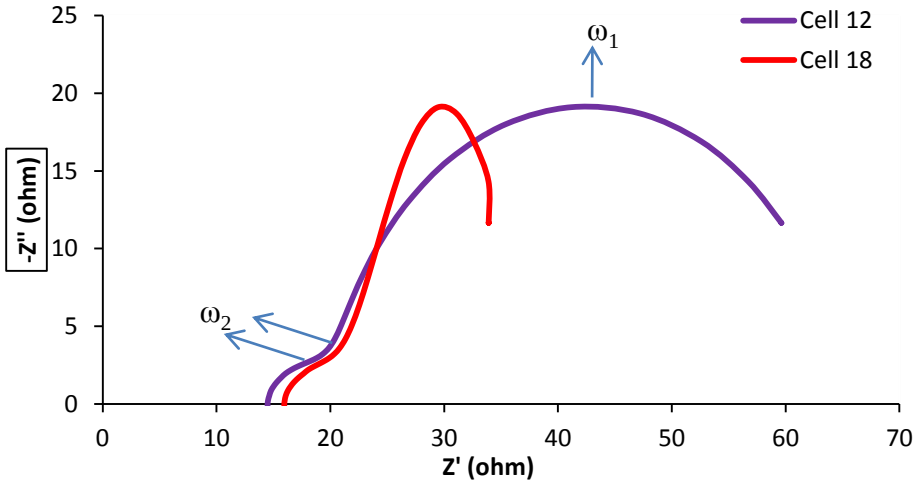

Figure 5.8: Niquest plots of cell 12 and cell 18 at dye loading time 24 h with binary additive.

It can be realized that the electron diffusion and transport become easy with the increment of the TiO_2 thickness due to the increased number of adsorbed dye molecules. The Bode phase plots observed for the devices as fabricated are shown in Figure 5.9.

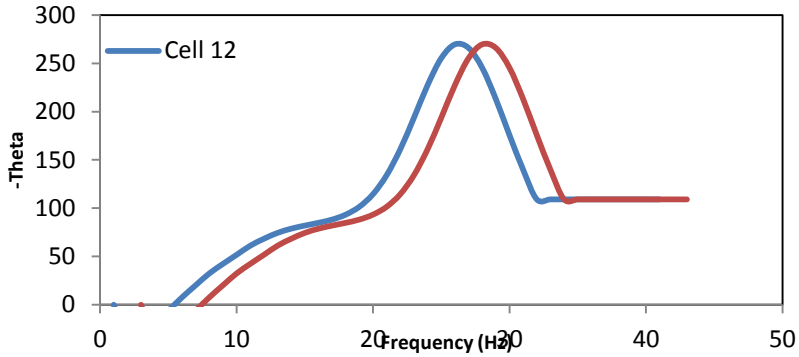

Figure 5.9: Bode plot of cell 12 and cell 18 at dye loading time 24 h with binary additive.

Table 5.5: Recombination resistance and electron life time of cell 12 and cell 18 at dye loading time 24 h with binary additive.

Cell Name	TiO_2 thickness	Dye conc. (mol.L^{-1})	J_{sc} (mA/cm^2)	V_{oc} (V)	*FF* (%)	η (%)	R_{rc} (ohm)	Electron lifetime (ms)
Cell 12	12 µm	0.015	5.48	0.685	0.70	2.61	93.27	4.9
Cell 18	18 µm	0.02	4.37	0.576	0.70	1.77	17.14	7

The electron lifetime can be extracted from the angular frequency (ω_{min}) [11] at the mid-frequency peak in the Bode phase plot using $\tau_e = 1/\omega_{min}$ and falls in the range of 4.9 to 7 ms for the DSSC with the thicknesses of 12 and 18 µm, respectively. It is shown in Table 5.5 that the resistance of the electron recombination is higher in case of cell 12 at 12 µm thickness of TiO_2 film which contributes in more electrons to reach to FTO and consequently enhances the J_{sc}. It is deduced that at less thickness of TiO_2 film the electrolyte penetration is

superior than that in thick layer due to which the effect of the binary additives is more prominent in cell 12. This finding concludes that the electron recombination resistance surpasses the resistance to charge transfer in terms of contributing to the enhancement of the cell performance.

5.2.1.2.5.4 Stability of DSSC

The device with highest efficiency with the composition of 12 μm thickness, 24 h dye loading time and binary additives, was further tested for the endurance at room temperature. The *I-V* parameters (Figure 5.10, Table 5.6) are recorded at 7 days gap for 15 days. The performance of the cell increased with time, which is ascribed to a large increase in J_{sc}. The cell achieved J_{sc}, V_{oc} and *FF* in the range of 6.043 mA cm^{-2}, 0.675 V and 70.928%, respectively and consequently an excellent photovoltaic conversion efficiency of 2.89% by 7^{th} day of test. According to the improvement in cell efficiency following the long-term test, the electrolyte is suspected to have penetrated into the TiO_2 film.

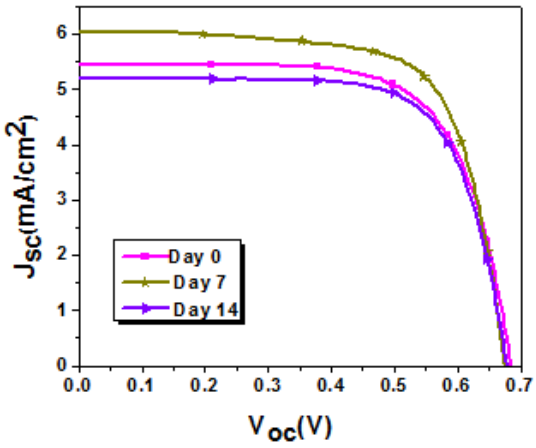

Figure 5.10: The current-voltage (*I-V*) measurements of device with 12 μm thickness exhibited η = 2.61%.

Further aging of the cell resulted in decrease of efficiency to 2.543 % with increase in V_{oc} and decrease in J_{sc}. It is reasonable to suggest that the increase in V_{oc} upon aging is partly due to a negative or upward shift of TiO_2 conduction band edge relative to redox potential, which is fixed by the electrolyte composition [44].

Table 5.6: *I-V* parameters of device with 12 µm thickness (stability test).

Day	J_{sc} (mA/cm^2)	V_{oc} (mV)	*FF* (%)	η (%)
0	5.447	0.685	70.033	2.614
7	6.043	0.675	70.928	2.895
14	5.210	0.678	71.982	2.543

5.2.1.3 Experimental

5.2.1.3.1 Synthetic details of dye

All reactions and optimizations were carried out using standard inert atmosphere as per the requirement. Solvents were dried by standard procedures. All column chromatography were performed by using silica gel of 100-200 mesh size as stationary phase in the column. The compounds were characterized by IR, NMR (^{1}H and ^{13}C) and mass spectral methods and it was observed that the spectroscopic data are consistent with the proposed structures. P1 was found to be soluble in DMSO and partially soluble in DMF.

Synthesis of 5,5',5",5"'-(9-butyl-9H-carbazole-1,3,6,8-tetrayl)tetrakis(thiophene-2-carbeldehyde)(1b): A round bottom flask was charged with 1, 3, 6, 8-tetrabromo-9-butyl-9*H*-carbazole (0.54 g, 1 mmol), (5-(1,3-dioxolan-2-yl)thiophen-2-yl)tributylstannane (2.50 g, 5

eq.) and 7 mL DMF. Nitrogen was purged followed by the addition of $Pd(PPh_3)_2Cl_2$ (28.0 mg). This was kept on heating at 80 ºC for 36 h under nitrogen atmosphere. After completion of reaction time, the mixture was poured into cold water and extracted with dichloromethane followed by washing with brine solution and dried over anhydrous sodium sulfate. Then the solvent was evaporated by applying vacuum. The resultant liquid was dissolved in 5 mL acetic acid and heated to 60ºC for 30 min. 10 mL of water was added and heating was continued for 6 h. The resulting solution was extracted with dichloromethane and washed with brine solution and dried over anhydrous sodium sulfate. Further purification was performed by silica gel column chromatography using hexane and chloroform as eluent giving yellow colored solid compound in 38% yield. Mp 160ºC. HRMS (ESI): *m/z* calcd for $C_{36}H_{25}NO_4S_4$: 686.0564 $[M+Na]^+$, found:686.0569. ^{1}H NMR (500 MHz, $CDCl_3$): δ = 9.97 (s, 2H), 9.92 (s, 2H), 8.49 (d, *J* = 1.5 Hz, 2H), 7.81 (d, *J* = 10 Hz, 2H), 7.79 (d, *J* = 5 Hz , 2H),7.75 (s, 2H), 7.52 (d, *J* = 4Hz, 2H), 7.35 (d, *J* = 3.5Hz, 2H), 3.69 (t, *J* = 7.5Hz, 2H), 1.01 (td, *J* = 29.5 Hz, 7.5 Hz, 2H), 0.89-0.79 (m, 2H), 0.48-0.44 (m, 3H) . ^{13}C NMR (125 MHz, $CDCl_3$): δ = 182.8, 182.6, 153.5, 149.6, 144.4, 142.3, 141.0, 137.6, 136.4, 129.2, 128.9, 126.3, 126.2, 124.0, 119.3, 119.1, 99.9, 46.5, 31.4, 19.4, 13.2 ppm; FTIR (KBr, cm^{-1}): 1664 (C=O).

Synthesis of (2Z, 2'E, 2''E, 2'''E)-3,3',3'',3'''-(5,5',5'',5'''-(9-butyl-9H-carbazole-1,3,6,8-tetrayl)tetrakis(thiophene-5,2-diyl)) tetrakis(2-cyanoacrylic acid) (P1) **:** Dye P1 was synthesized by compound 2 (100 mg, 0.15 mmol), cyanoacetic acid (63 mg, 0.75 mmol), acetic acid (5 mL) and ammonium acetate (5 mg), mixed together and kept for refluxing at 120ºC for 22 h. The resulting orange solution was poured into ice-cold water in order to produce an orange precipitate. This was filtered and washed thoroughly with water and dried.

The solid was further recrystallized with chloroform giving an orange colored solid in 89% yield. Mp >300 ºC; ^{1}H NMR (500 MHz, $CDCl_3$+THF): δ = 8.69 (s, 2H), 8.55 (d, *J*= 23.5 Hz, 4H), 7.99 (s, 2H), 7.90 (s, 4H), 7.71 (s, 2H), 7.54 (d, *J* = 2.5, 2H), 3.80-3.79 (m, 2H), 1.07-1.06 (m, 2H), 0.546-0.518 (m, 2H), -0.006 (d, *J* = 3, 3H). ^{13}C NMR (125 MHz, $CDCl_3$+ THF): δ = 157.4, 152.4, 150.2, 142.8, 142.0, 140.3, 136.1, 134.3, 130.1, 128.9, 126.9, 126.1, 125.2, 120.4, 118.9, 93.5, 47.5, 31.3, 19.3, 12.7 ppm. FTIR (KBr, cm^{-1}): 2208 (C≡N), 1608 (C=O).

5.2.1.3.2 Fabrication of DSSC

FTO was cleaned by soap solution followed by rinsing with de-ionized water and ethanol. A compact TiO_2 blocking layer was chemically deposited onto the conducting surface of FTO (Nippon Sheet Glass10 Ohm/sq) by immersing it in a 0.04 M $TiCl_4$ aq. solution at 70ºC for 30 minutes. Nanoporous TiO_2 films were developed on the blocking layer by screen printing colloidal TiO_2 paste. The particle sizes for transparent and scattering layers were 25 nm and 150 nm, respectively. For better interfacial contacts the films were sintered up to 500ºC. The films were rinsed with de-ionized water and annealed at 450ºC for 30 minutes, prior to dye loading. For making counter electrodes, conical holes were drilled on FTOs. Drilled FTOs were washed with 0.1 M HCl aq. solution and ultrasonicated in acetone. Further 4.8 mM chloroplatinic acid solution in ethanol was used as platinum precursor and deposited on FTO by drop casting method. Annealing was carried out at 450°C for 15 minutes to have better adhesion. Both the electrodes were clubbed together by a 25 µm thick surlyn spacer. The cells were filled with electrolyte solution through a predrilled hole in the counter electrode and the whole assembly was sealed with surlyn polymer and cover slip by hot pressing. Finally, the cells were soldered to connect to the external circuit.

The cells made in such a way have an active area of 0.16 cm^2. While fabricating, cells were subjected to various fabrication parameters for studying the structure-property correlation in DSSC containing dye, TiO_2 mesoporous film and electrolyte. Therefore, three types of photoanodes were prepared with different thicknesses of 9, 12 and 18 μm. To optimize the dye loading time for enhancing the device efficiency, TiO_2 film has been soaked in 0.3 mmol solution of dye P1 in DMSO for 5 h and 24 h at room temperature. The amount of adsorbed dye P1 was determined following the indirect ex situ surface coverage studies[45] for which sensitized TiO_2 film was dipped into 4.00 mL of 20 mmol aq. NaOH solution until complete desorption of the dye. For this purpose instead of hydroalcoholic solution, aqueous solution of NaOH was made in de-ionized water. The resulting dye solution was analyzed spectrophotometrically in a 1.00 cm^2 quartz optical cell. The concentration was determined by using fresh standard solutions, prepared by dissolving a known amount of dye in aq. NaOH solution.

Two types of electrolytes coded Z008 and Z960 were used to analyze the effect of binary additive. The Z008 electrolyte consists of 3-propyl-1-methyl imidazoliumiodide, bis (Trifluoromethane) Sulfonimide Lithium Salt and 1-methylbenzimidazole in 1: 0.1: 0.1 in Acetonitrile. The composition of Z960 electrolyte is 1.0 M 1,3-dimethylimidazolium iodide, 0.03 M I_2, 0.05 M lithium iodide, 0.1 M guanidinium thiocyanate and 0.5 M *tert*-butylpyridine in acetonitrile and valeronitrile solvent mixture (85 : 15, v/v) [46].

5.2.2 DESIGNING OF D-(π-A)$_4$ ORGANIC MOLECULES (P2, P3, P4, P5) WITH A NOVEL APPROACH TO REDUCE AGGREGATION AND TUNE THE OPTICAL PROPERTIES IN DYE SENSITIZED SOLAR CELLS

5.2.2.1 Introduction

Currently, Dye sensitized solar cells (DSSCs) are one of the major driving force behind the research in the novel organic semiconductors. It is crucial to synthesize materials with optimal band gap values and well defined chemical structures possessing relatively low highest occupied molecular orbital (HOMO) and high charge mobility. Well matched absorption spectra of dye with the solar irradiance spectrum are primary requirements for a photovoltaic application. Since efficient charge transport from dye to the conduction band of TiO_2 and dye regeneration are the most significant steps in the procedure of current generation [47], dye molecule is the focus of research in the field of photovoltaics for decades. Due to the high cost and rarity of silicon used in traditional silicon solar cells, metal complexes have been widely in use as photosensitizers in cost effective DSSCs. Ru dyes i.e. N3 and N719 have achieved high conversion efficiencies of around 11% under AM 1.5 irradiation [48]. Recently a record break efficiency of 12.3% has been reported by using a Zn based metal dye (YD2-o-C8) and an organic dye (Y123) together in combination with a tris(2,20-bipyridine) cobalt(II/III) redox couple [49].

The performance of metal based dyes has been at the verge of saturation due to less structural versatility of metal complexes for getting tuned to the optical and electrochemical properties, therefore, more attention is being focused towards synthetically more flexible organic dyes. Apart from structural dexterity, organic dyes show many exceptional properties which are desirable in advancement of photovoltaics such as high molar extinction

coefficient, simple synthesis procedure, and environmental affability. Since organic dyes are yet to reach the threshold set by metal complex dyes, major research is being done for structural amendments.From the perspective of molecular engineering several structural factors i.e. rigidity of conjugated system, enhancement of quinoid character, incorporation of suitable electron donor and acceptor groups and intermolecular effects, are inevitably crucial [50].

Inspite of taking all these factors under consideration the DSSC device fabricated by D-π-A organic dyes would not performance expectedly sometimes due to dye aggregation on semiconductor film which causes self quenching leading to insufficient electron injection [51]. To surpass this drawback in the traditional D-π-A frame of the organic dyes, the bulky group has been attached to the donor moiety [52]. Bi-anchoring dyes with the structure A-π-D-π-A have also been reported [53] which proved to improve photocurrent and stability due to the extended π-conjugated framework and higher molar extinction coefficient in comparison to their monoanchoring counterparts. The effects of π-bridge have also been studied in D-π-A dyes in which the elongation or bulkiness in spacer is found to be effective in suppressing the dark current caused by dye aggregation on film [54].

Though dual channel system dye (A-π-D-π-A) exhibits interesting optical and electrochemical properties, it suffers serious aggregation and charge recombination owing to large intermolecular π-π stacking between sites adsorbed on the TiO_2 surface [51]. Recently the work has been done on the series of number of anchoring group at triphenylamine (TPA) donor, where mono, bi and tri anchoring organic dyes have been studied [55]. It was observed by spectroscopic and computational methods that light harvesting improved due to branching of D-π-A sensitizer. Earlier it has already been concluded that noncoplanar

geometry can also lead to decreased contact between molecules, therefore, enhance their thermal stability [56]. Among several donors used in organic dyes, carbazole is one of the best known moieties and its use in organic [57] as well as ruthenium [58] based dyes is well exploited. Due to the presence of unpaired electrons on nitrogen atom at position 9, carbazole behaves as full aromatic compound and leads to highly chemically and environmentally stable oligomers and polymers.

We have earlier reported a carbazole based cruciform dye (P1) with the D-$(\pi$-A$)_4$ structural frame, which was the first reported tetra anchoring dye. Current work is the structural amendment of P1 in which we have designed a series of novel D-$(\pi$-A$)_4$ dyes with branched side chain substituted on nitrogen and elongated π-bridges at different active sites of carbazole. The anchoring unit is cyanoacrylic acid in all the dyes attached to the carbazole core at 1, 3, 6, 8 positions via mono and bithoiphene π-bridges (P2 and P4, respectively) and at 2, 3, 6, 7 positions in the same manner resulting in dyes P3 and P5 (Figure 5.11). Introduction of ethylhexyle side chain increased hydrophobicity of all chain. Elongation of π-bridge explicitly shifted the absorption maxima from 384 nm to 465 nm and widened the coverage from 300 to 570 nm in visible spectrum. AFM images of sensitized TiO_2 thin films clearly indicated the reduction of aggregation caused by π-π stacking on film. The synthesized dyes have been well characterized for molecular structure, photophysical, electrochemical and photovoltaic aspects, theoretically as well as experimentally. The structures of dyes synthesized and used for DSSCs in this work, are given in Figure 5.13.

5.2.2.2 Results and discussion

5.2.2.2.1 Synthesis and characterization of dyes

The approach used for the preparation of new carbazole-based dyes is outlined in Scheme 5.2 and scheme 5.3. Conversion of 9-(2-ethylhexyl)-9*H* carbazole (2) to 1, 3, 6, 8-tetrabromo-9-(2-ethylhexyl)-9*H*-carbazole (2a) and 2, 7-dibromo-9-(2-ethylhexyl)-9*H* carbazole (3) to 2, 3, 6, 7- tetrabromo-9-(2-ethylhexyl)-9*H*-carbazole (3a) was carried out using *N*-bromosuccinimide (NBS) and bromine, respectively [59, 60].

The aldehyde derivatives (2b-5b) were prepared in moderate yield by Stille coupling reaction between the bromo derivatives (2a and 3a) and the tin reagents of the suitably protected aryl aldehydes and followed by acidic hydrolysis [61]. Finally, dyes P2, P3, P4 and P5 were prepared by Knoevenagel condensation reaction of compounds 2b, 3b, 4b and 5b with cyanoacetic acid using glacial acetic acid as the solvent and ammonium acetate in a catalytic amount [62]. The dyes exhibited different colors in solution such as P2 was orange colored, P3 was yellow colored, P4 was dark brown in color and P5 was red. All the dyes are found to be soluble in DMSO and moderately soluble in DMF. The dyes were thoroughly characterized by IR, NMR (^{1}H and ^{13}C) and mass spectral methods and observed parameters were consistent with the proposed structures.

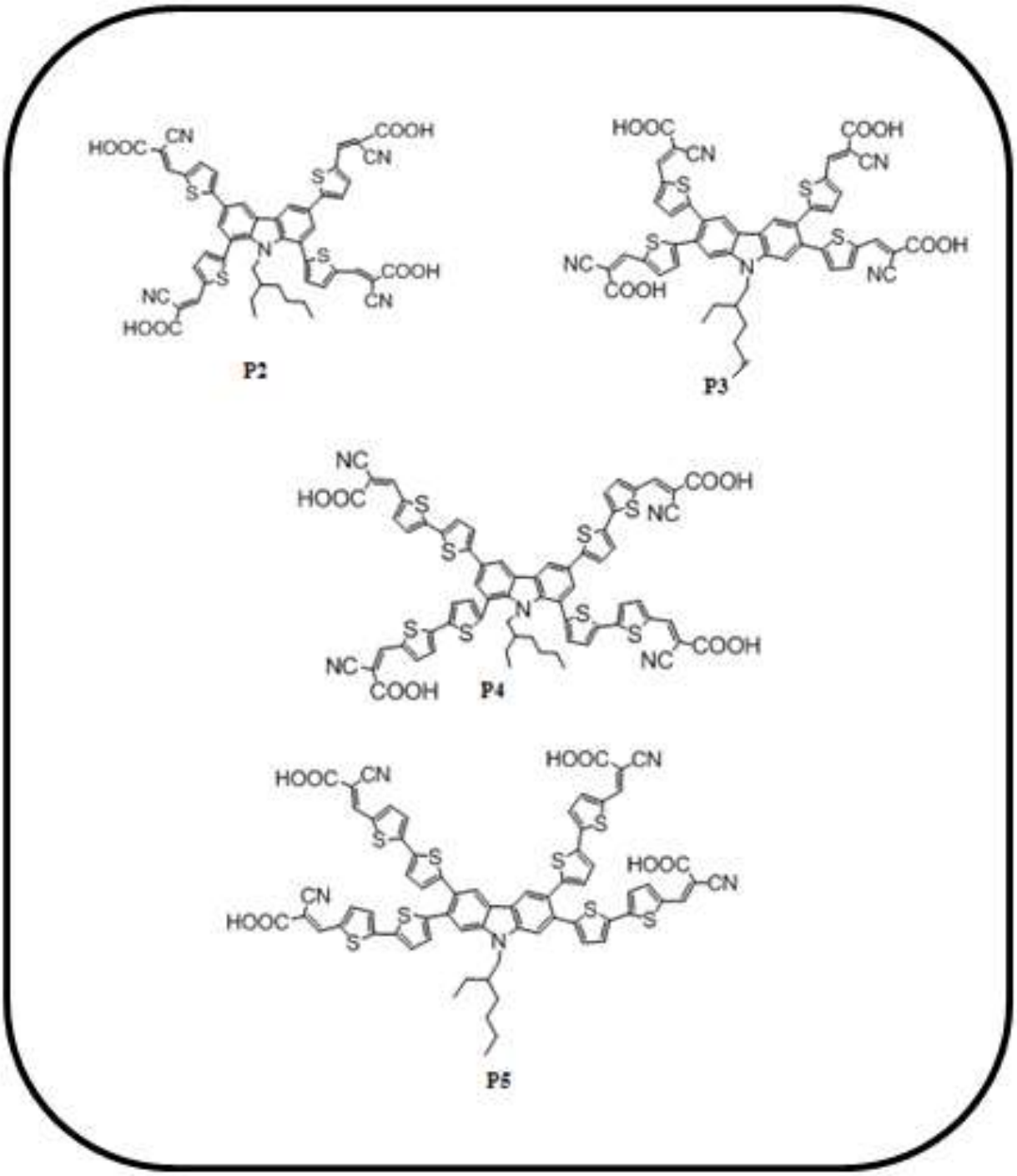

Figure 5.11: Molecular structures of dyes P2, P3, P4 and P5.

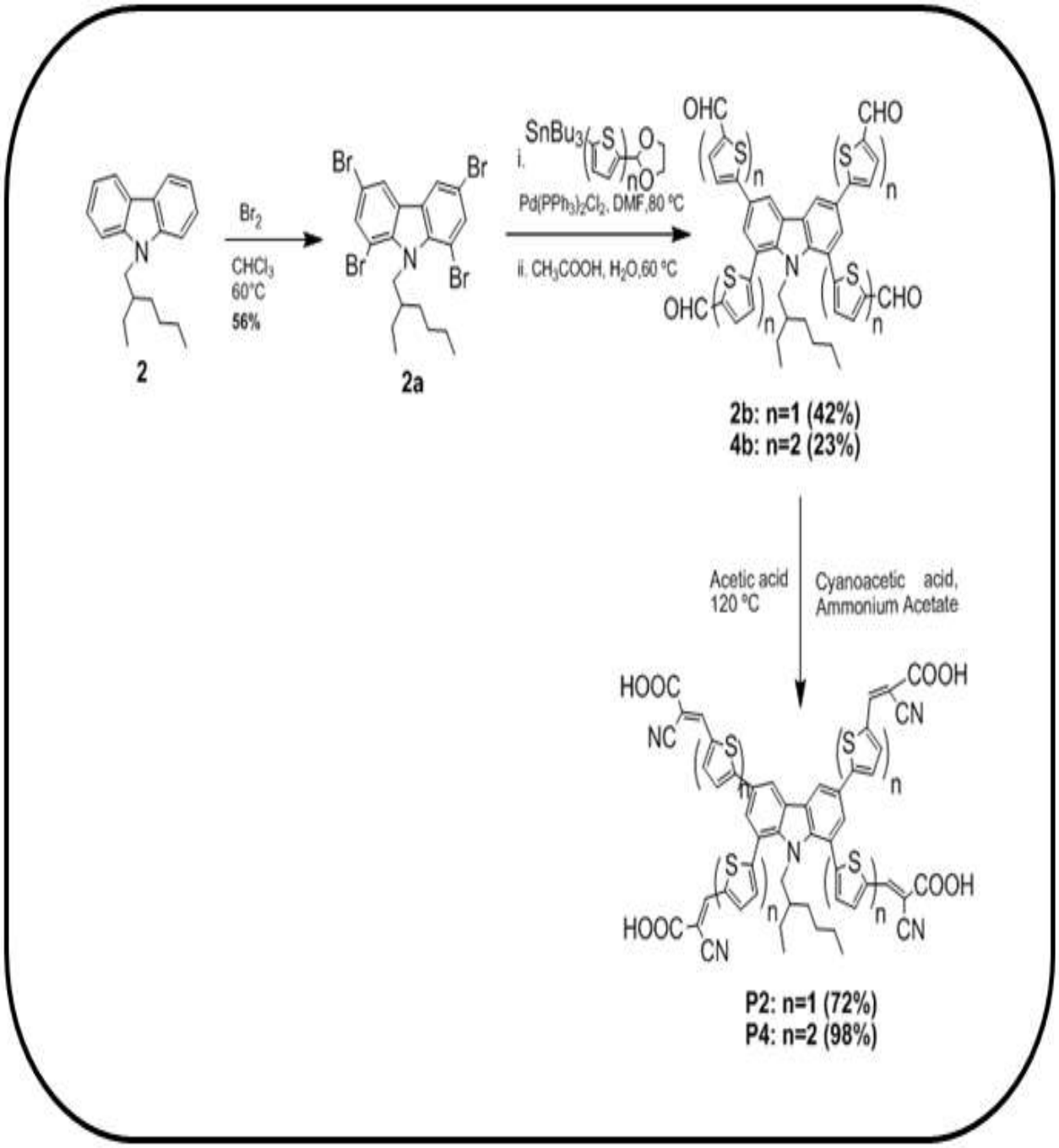

Scheme 5.2: Synthetic scheme of dye molecules P2 and P4.

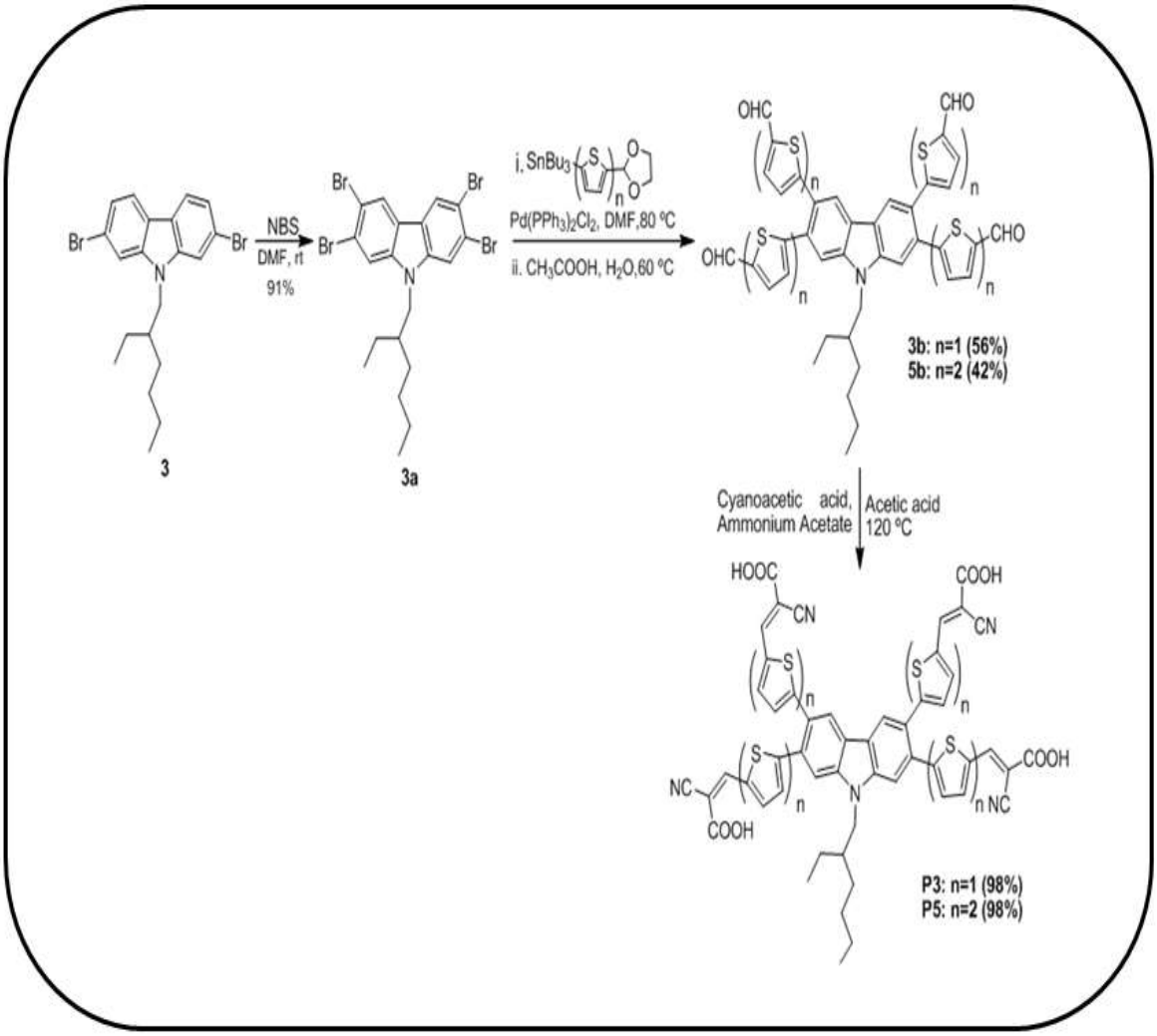

Scheme 5.3: Synthetic scheme of dye molecule P3 and P5.

5.2.2.2.2 Optical Properties of dyes

The optical behavior of organic dyes (P2, P3, P4 and P5) was evaluated on the basis of absorption and fluorescence spectra of all the dyes recorded in DMSO (Figure 5.12 (a)). The origin of the absorption in all the dyes was examined and evidenced by analyzing the absorption spectra of all aldehyde derivatives (Figure 5.12 (b) and Figure 5.13 (a)). For further correlation of optical properties of the dyes with the photovoltaic performance of

DSSCs, the absorption spectra of all dyes were also recorded on TiO_2 film which is displayed in Figure 5.13 (b).

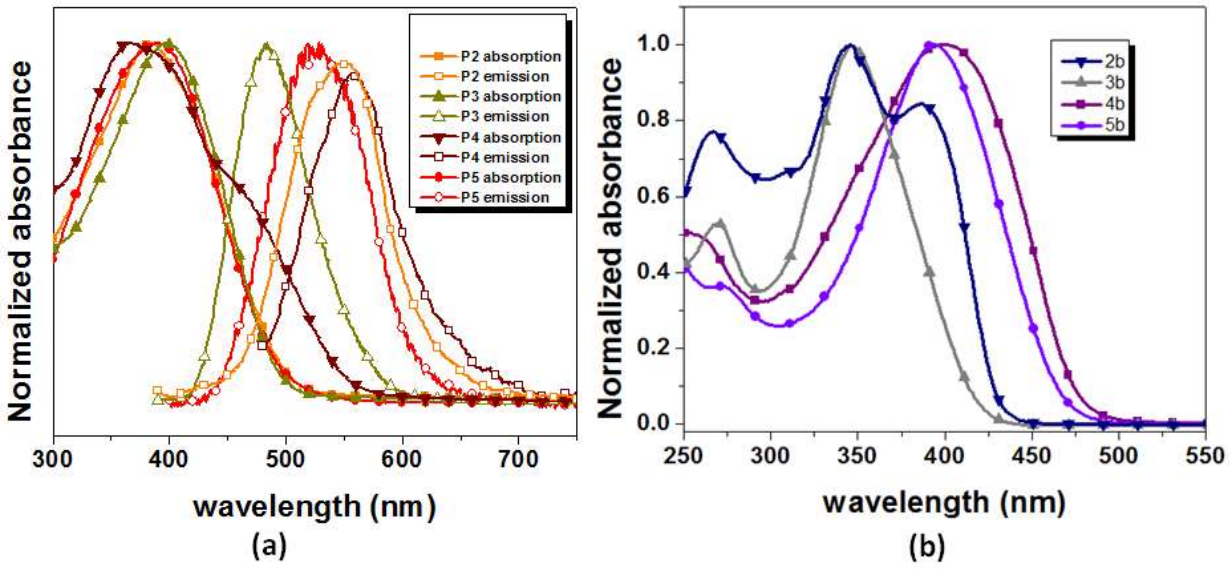

Figure 5.12: (a) Absorption and emission spectra of dyes P2, P3, P4 and P5 in DMSO, (b) Absorption spectra of aldehydes 2b, 3b, 4b and 5b in DCM.

Dyes P2, P3 and P5 showed one prominent absorption peak in the range from 380 to 400 nm (Figure 5.13 (a)). These lower energy transitions showing absorption maximum above 380 nm correspond to the charge transfer from the carbazole donor to the cyanoacrylic acid acceptor units. This was again evidenced by longer wavelength absorption of all dyes in comparison with the corresponding aldehyde derivatives which proves the efficient charge transfer within the chromophores. Although no clear peak was observed in the higher energy transition region, a small shoulder could be noticed in case of P2 and P3 suggesting the possibility of either localized π-π* transitions or n-π* transitions. It was seen that charge transfer band progressively shifted to the longer wavelength region on introduction of

additional thiophene units in the conjugation pathway. Since carbazole is a moderate electron releasing donor, incorporation of more thiophene units boosts electron richness of donor moity owing to the delocalization of contributing molecular orbital. The absorption range was visibily broadened for bithiophene dyes (P4 and P5) as compared to monothiophene containing dyes (P2 and P3) which can be explained on the basis of induced planarity of π-bridge caused by the elongation of conjugation by oligothiophene units which leads to facile donor-acceptor interactions in dipolar compounds [63]. There is an obviously large bathochromic shift in case of P4 and π-π* band seems merged with CT band. The small energy difference leads to the overlap of the two peaks, which explains the broad peak observed for P4 in the visible spectrum.

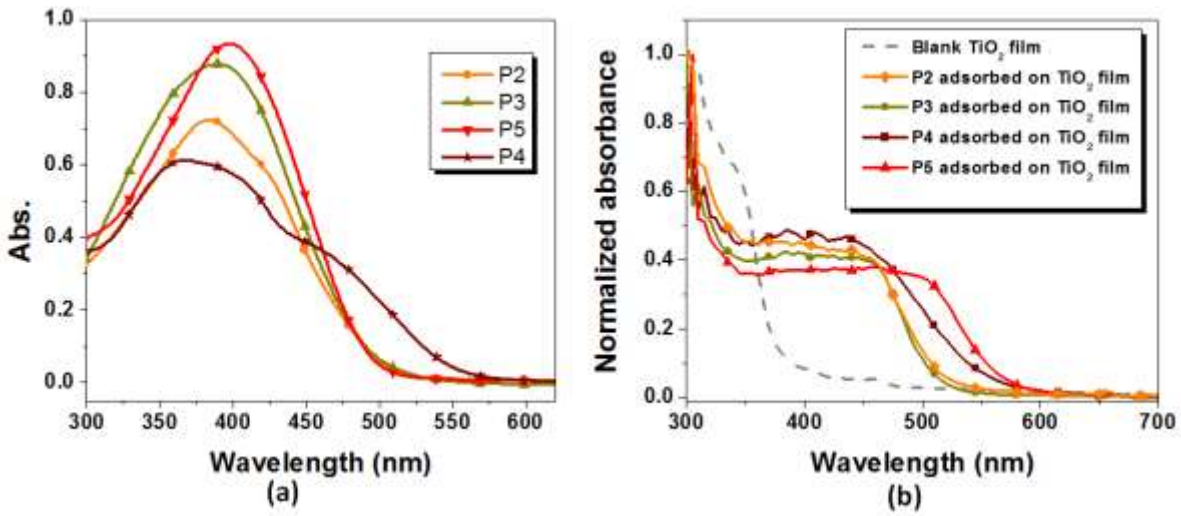

Figure 5.13: Absorption spectra of dyes P2, P3, P4 and P5 in (a) DMSO, (b) on TiO_2 film.

It is well explained in literature [64] by theoretical and experimental studies that the absorption energy decreases from *p*-, *o*- and *m*- results in shifting of absorption maxima in the same order. Absorption maxima of 2, 3, 6, 7 substituted monothiophene dye (P3) as

compared to 1, 3, 6, 8 substituted monothiophene dye (P2) was distinguished with bathochromic shift due to longer conjugation modes resulted by 2, 3, 6, 7 substitutions of anchoring units on carbazole core. Due to the same reason the similar optical behavior was expected from oligothiophene derivatives, 1, 3, 6, 8 substituted bithiophene dye (P4) and 2, 3, 6, 7 substituted bithiophene dye (P5) but apparently opposite conduct was observed. P4 displayed a huge bathochromic shift than P5, which could be explained due to less crowding of bulky π-linkers in P4 because of the positioning of anchoring groups with bithiophene units at alternate position i.e. 1, 3, 6 and 8, keeping the structure sufficiently planar and maintaining the charge transport more efficient. The planarity of conjugated arms was completely shattered in P5 due to adjacent positions (2, 3 and 6, 7) of longer π-arms resulting in twisted conjugation between donor and acceptor units, which proved to be detrimental for charge transfer. Further, on analysis of emission spectra a blue shifted emission maxima was observed for P3 and P5 than P2 and P4 which could be explained by less planar excited state of P3 and P5.

Absorption range of dyes (P2-P4) further broadened by 5-20 nm, in visible region after getting anchored on TiO_2 films. A strong red shift in the absorption of P5 suspects to the formation of *J* aggregates at the surface of TiO_2. This can be attributed to the extended conjugation in the π-bridge due to the presence of the bithiophene linker. This finding is incoherent with the absorption spectra of P4 and P5 in solution where P4 with 1, 3, 6, 8 tetra substituted bithiophene linker covered much wider range in visible region than P5 with 2, 3, 6, 7 tetra substituted bithiophene linker due to high planarity of its conjugation segments. Depending upon the nature of the aggregate formation at the surface of TiO_2, either blue-shifted or red-shifted absorption can be observed. In general, the *J* aggregation causes red

shift and *H* aggregation causes blue shift of the absorption maxima. Highly planar structures induce *H* aggregates on TiO_2 film causing nonradiative decays and non planar structures originate *J* aggregation which minimizes the nonradiative pathway for the aggregated species and lead to efficient light harvesting. Therefore, the twisted structure of π-linkers in P5 highly benefitted the charge transfer in TiO_2 films because of *J* aggregation, resulting in huge red shifted absorption and highly planar structure of π-linkers in P4 caused *H* aggregates on TiO_2 film, resulted in quenching of charge transport in films.

5.2.2.2.3 Electrochemical properties

For conjugated molecules used in photovoltaic devices, band gap and molecular energy levels bear central value for device performance [65]. Electrochemical properties analysis of these compounds depicts molecular energy levels and energy band gap between HOMO and LUMO, as presented in Figure 5.14 (a) and (b). The redox properties of organic dyes were investigated by measuring oxidation potentials using differential pulse voltammetry (DPV) in DMF with 0.1 M tetrabutylammonium hexafluorophosphate as electrolyte. It is evident from the DPV graph in fig. 6 that all dyes exhibited two irreversible oxidation peaks. The electrochemical properties of dyes are summarized in Table 5.7. The first oxidation signal was originated due to the removal of electrons from the donor moiety to give a radical cation, and the second corresponded to the oxidation of thiophene units. In all the dyes of this series first oxidation potentials remained same irrespective to the conjugation length. The ground state oxidation potential corresponding to the HOMO levels were 1.34 V (vs. NHE) for all the dyes, which were sufficiently more positive than the iodine/iodide redox potential value (0.4 V). This ensured the thermodynamic feasibility for the regeneration of the oxidized dye by accepting electrons from I^- ions. By taking a junction of absorption and

emission spectra of dyes, the band gap energies ($E_{0\text{-}0}$) were calculated which fell in the range of 2.47-2.75 eV. It was observed that the band gap energies for bithiophene dyes (P4, P5) were lower than their corresponding monothiophene dyes (P2, P3), which could be attributed to the enhanced quinoid character of the ground state on increasing the number of thiophene ring in π-bridge [66]. Band gap energy was observed the least for P4 and can be harmonized by more elongated as well as more planar connecting channels between donor and acceptor units of the dye.

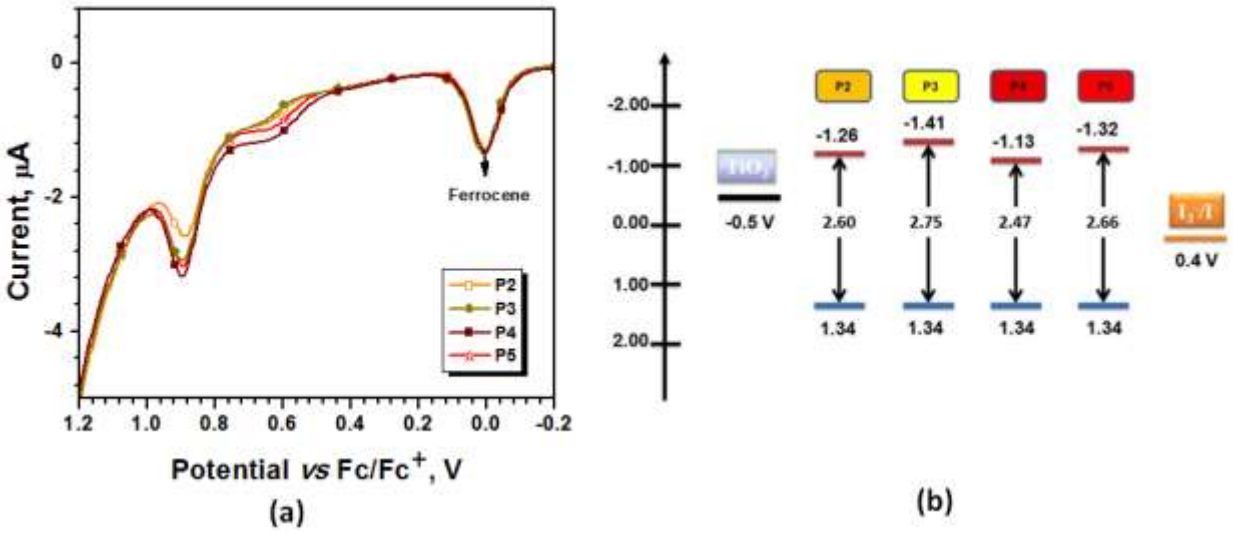

Figure 5.14: Electrochemical properties of dyes P2, P3, P4 and P5 in DMF (a) DPVs, (b) Ground and excited state oxidation potentials.

The calculated excited state potential (LUMO level) which is an estimation of E_{HOMO}-$E_{0\text{-}0}$, were calculated from -1.32 to -1.13 eV and found desirably more negative than the conduction-band-edge energy level (E_{cb}) of the TiO_2 electrode (0.5 V vs. NHE). With the electrochemical analysis of the dyes it was substantiated that all dyes possess adequate

driving forces for electron injection from the excited dyes to the conduction band of TiO_2 and consequently have enough driving force to be used as efficient sensitizers in DSSCs with TiO_2 in presence of I^-/I_3^- redox couple.

Table 5.7: Electro-optical data of the dyes P2, P3, P4 and P5.

Dye	λ_{abs}[a], nm	λ_{em}[b], nm	E_{ox}[c]	HOMO[d], eV w.r.t Ferrocene	LUMO[e], eV	E_{o-o}[f], eV	E_{ox}^*[g], eV
P2	384	519	0.62	5.42	2.82	2.60	-1.26
P3	399	519	0.62	5.42	2.67	2.75	-1.41
P4	465, 367	493	0.62	5.42	2.95	2.47	-1.13
P5	388	497	0.62	5.42	2.76	2.66	-1.32

[a] Recorded in DMSO. [b] Recorded on TiO_2 film. [c] Potentials quoted with reference to internal ferrocene standard. [d] HOMO = 4.8 + E_{ox}. [e] LUMO = HOMO- E_{0-0}. [f] Obtained from optical edge. [g] Excited state oxidation potential.

5.2.2.2.4 Photovoltaic performance:

The photovoltaic properties of DSSCs fabricated by photoanodes sensitized by organic dyes (P2-P5), measured under simulated AM 1.5 irradiation (100 mW/cm^2) are presented in the form of *J-V* curves in Figure 5.15 (a) and Table 5.8 depicts their corresponding data. The PCE (η) of all DSSCs fell in between 1.8 to 2.4 %. The highest efficiency was observed in device P5 though dye uptake by TiO_2 film was not as much as of dyes P2 and P3.

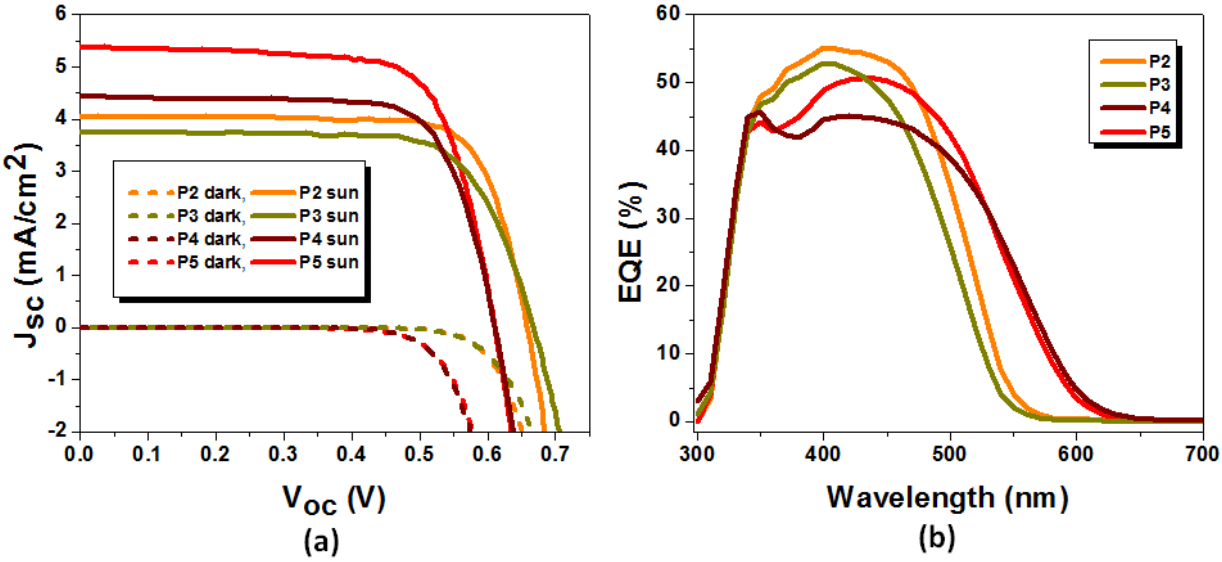

Figure 5.15: Photovoltaic characteristics of DSSC devices P2, P3, P4 and P5, (a) *I-V* curves, (b) IPCE plots.

Table 5.8: *I-V* specific parameters of DSSCs fabricated by dyes P2, P3, P4 and P5.

DSSCs	Dye concentration in film (mol L^{-1})	J_{sc} (mA/cm^2)	V_{oc} (V)	*FF*	η (%)
P2	0.015	4.05	0.66	77	2.1
P3	0.0125	3.78	0.67	72	1.8
P4	0.0075	4.44	0.61	74	2.0
P5	0.0075	5.37	0.61	72	2.4

The second highest J_{sc} was exhibited by DSSC fabricated by P4. The J_{sc} can be directly associated with the dark current induced due to aggregation caused quenching in the molecules adsorbed on TiO_2 film which was visualized in AFM images of dye sensitized thin TiO_2 films in Figure 5.16 (a, b, c). It was deduced by AFM images that π-π stacking substantially diminished on the films, sensitized by bithiophene anchored dyes (P4, P5) and

yet is quite visible in the films adsorbed with their monothiophene analogues (P2, P3). The reason behind no aggregation on TiO_2 films sensitized by P4 and P5 could be the crowded periphery of dye molecule which resulted in twisted arms and inhibited the intermolecular stacking. Further it was deduced that the cruciform structures of P4 and P5, consisting twisted arms in all directions induced hydrophobic character on the film and assisted in suppressing charge recombination at TiO_2 film with redox couple which subsequently resulted in longer electron lifetimes. J_{sc} of DSSCs fabricated by P2 and P3 suffered drastically due to severe aggregation on TiO_2 films which was well demonstrated in 3D images and cross sectional analysis of the sensitized films (Figure 5.16 (a, b, c)) [67].

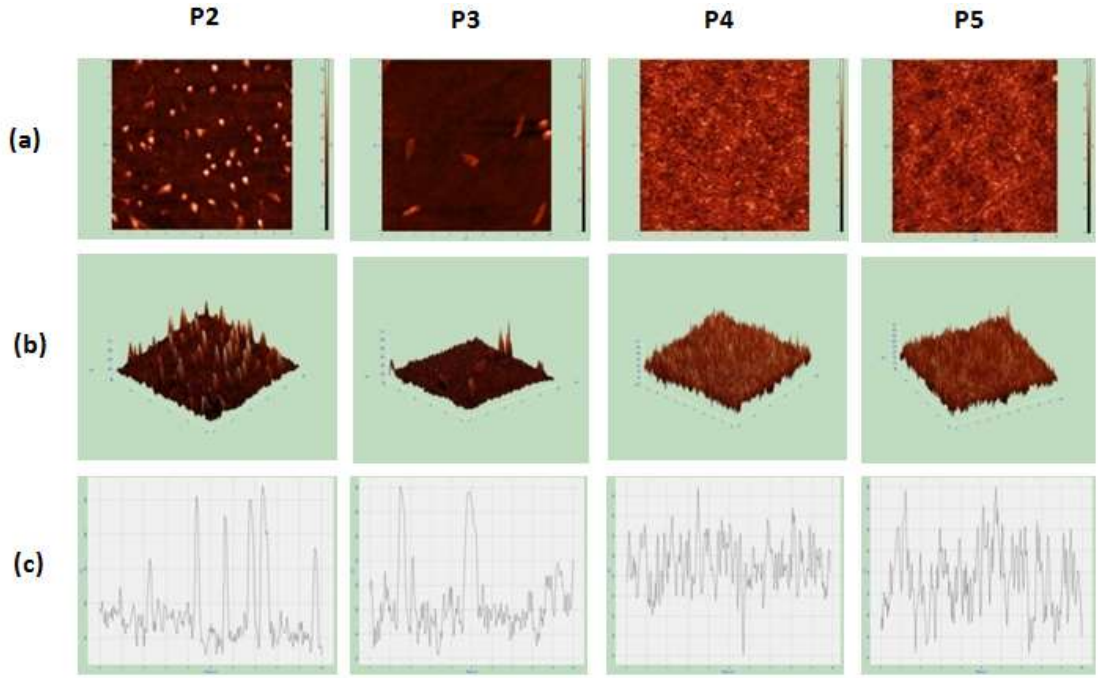

Figure 5.16: AFM images of TiO_2 films sensitized with dyes P2, P3, P4 and P5. (a) Surface morphology, (b) 3D images, (c) cross section.

The V_{oc} of DSSCs fabricated by P4 and P5 were found to be lower than that of DSSCs with P2 and P3, which did not support the optical properties exhibited by this series of dyes. It was established with the amount of the dye uploaded in TiO_2 films which was less in case of both bithiophene dyes (P4, P5) than monothiophene dyes (P2, P3) (Table 5.8) and affected V_{oc} adversely. *FF* of all the DSSCs was in the range of 72-77% which explains the least internal resistance in all the DSSCs fabricated by this series of dyes. Although much more proficiency was expected from the DSSCs fabricated by P4 and P5 due to red shifted absorption maxima and broader coverage of the visible spectra of them in solution as well as on TiO_2 films, the poor dye loading of TiO_2 films retarded the overall conversion efficiencies.

Incident photon-to-current conversion efficiency (IPCE) for the DSSCs is displayed in Figure 5.15 (b). The highest IPCE of 55% was achieved by P2. IPCE dropped for bithiophene dyes due to dubious dye anchoring. The broad coverage of visible spectrum was demonstrated by DSSCs fabricated with P4 and P5 which was consistent with the absorption spectra of dyes (Figure 5.13 (a)). Figure 5.17 (a) shows the recombination resistance and Figure 5.17 (b) shows chemical capacitance of all the DSSC devices fabricated by dyes P2, P3, P4 and P5. At low voltage recombination resistance is observed to be decreasing slowly which decreases rather faster beyond the voltage of 0.4 V. The least resistance is seen in the P2 device where as device P3 seems to be most stable in terms of recombination resistance achieving the highest V_{oc}.

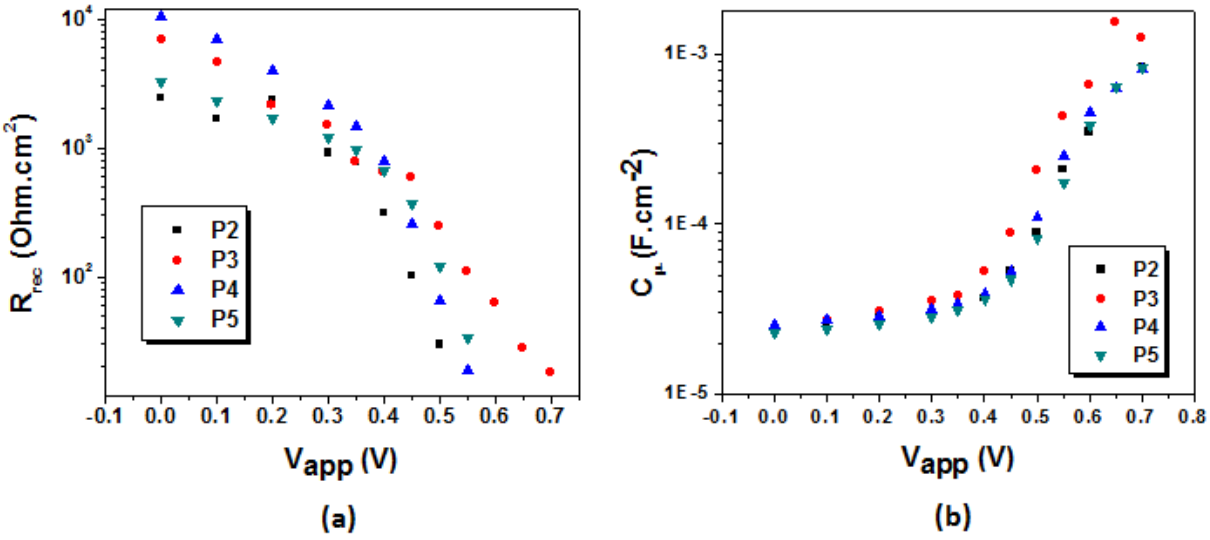

Figure 5.17:(a) Recombination resistance and (b) Chemical capacitance of DSSCs devices P2, P3, P4 and P5 at applied voltage.

5.2.2.2.5 Experimental

5.2.2.2.5.1 Synthetic details of dyes

***Synthesis of 1, 3, 6, 8-tetrabromo-9-(2-ethylhexyl)-9H-carbazole* (2a):** 9-(2-ethylhexyl)-9*H*-carbazole (2) (10.8 mmol) was dissolved in chloroform (20 ml). Bromine (45 mmol) was dissolved in chloroform (10 ml) and added to carbazole solution dropwise for half an hour at 60ºC with continuous stirring. Reaction was constantly analyzed by TLC. Excess of bromine was removed and further purification was performed by silica gel column chromatography. White powder was obtained. Yield: 56%. ^{1}H NMR (500 MHz, $CDCl_3$): δ =8.05 (d, *J* = 2, 2H), 7.77 (d, *J* = 1.5, 2H), 5.12 (d, *J*=8, 2H), 1.81-1.85 (m, 1H), 1.04-1.25 (m, 6H), 0.72 (m, 8H).

***Synthesis of 5, 5', 5", 5'"-(9-(heptan-3-yl)-9H-carbazole-1, 3, 6, 8- tetrayl) tetrathiophene-2-carbaldehyde* (2b):** A round bottom flask was charged with a mixture of 2a

(297.5 mg, 0.5 mmol), (5-(1, 3-dioxolan-2-yl)thiophen-2-yl)tributylstannane (1.2 g, 5 eq.) and 3 mL dry DMF followed by the addition of $Pd(PPh_3)_2Cl_2$ (14 mg) under inert atmosphere and heated at 80ºC for 36 h under nitrogen atmosphere. The mixture was poured into cold water, extracted with dichloromethane followed by washing with brine solution and dried over anhydrous sodium sulfate. The volatile solvent was evaporated by applying vacuum. The resultant liquid was dissolved in 5 mL acetic acid and heated to 60ºC for 30 min. 10 mL of water was added and heating was continued for 6 h. The resulting solution was extracted with dichloromethane, washed with brine solution and dried over anhydrous sodium sulfate. Further purification was performed by silica gel column chromatography using hexane and chloroform as eluent giving yellow colored solid compound. Yield: 42%. mp 200-210ºC.^{1}H NMR (500 MHz, $CDCl_3$): δ = 9.99 (s, 2H), 9.92 (s, 2H), 8.49 (d, *J* = 2 hz, 2H), 7.87 (d, *J* = 3.5 hz, 2H), 7.79-7.81 (m, 4H), 7.53 (d, *J* = 4 hz, 2H), 7.36 (d, *J* = 4 hz, 2H), 3.71 (d, *J* = 8 hz, 2H), 1.26 (dd, *J* = 12 hz, 6 hz, 1H), 0.68-0.87 (m, 2H), 0.55 (t, *J*= 15 hz, 7.5, 5H), 0.307-0.436 (m, 3H), 0.242-0.271 (m, 4H). ^{13}C NMR (125 MHz, $CDCl_3$): δ =182.8, 182.6, 153.5, 150.0, 144.2, 142.4, 141.8, 137.5, 136.5, 129.0, 128.7, 126.5, 126.3, 124.0, 119.8, 119.2, 51.1, 39.0, 28.9, 27.2, 22.6, 22.4, 13.7, 9.6 ppm. FTIR (KBr, cm^{-1}): 1642.22 (C=O).

Synthesis of (2'Z, 2"E, 2'"E)-3, 3', 3", 3"'-(5, 5', 5", 5"'-(9-(heptan-3-yl)-9H-carbazole- 1, 3, 6, 8- tetrayl) tetrakis (thiophene-5,2-diyl)) tetrakis (2-cyanoacrylic acid) (P2): Dye P2 was synthesized by compound 2b (100 mg, 0.14 mmol), cyanoacetic acid (60 mg, 0.70 mmol), acetic acid (5 mL) and ammonium acetate (5 mg), mixed together and refluxed at 120ºC for 22 h. The resulting orange solution was poured into ice-cold water and an orange precipitate was obtained which was filtered and washed thoroughly with water and then dried. The solid was further recrystallized with chloroform giving an orange colored

solid. Yield: 72%. mp >300 ºC. ^{1}H NMR (500 MHz, $CDCl_3$+TFA): δ = 8.68 (s, 2H), 8.57 (s, 2H), 8.53 (s, 2H), 8.01 (d, *J* = 3.5 hz, 2H),7.94 (s, 2H),7.29 (d, *J* = 4 hz, 2H), 7.56 (d, *J* = 3.5 hz, 2H), 3.77 (d, *J* = 7.5 hz, 2H), 1.59-1.68 (m, 1H),0.54-0.61 (m, 6H), 0.41-0.43 (m, 4H), 0.30-0.32 (m, 4H). ^{13}C NMR (125 MHz, $CDCl_3$ + THF): δ = 168.7, 168.1, 157.4, 152.8, 150.7, 150.2, 142.8, 142.7, 140.6, 135.9, 134.3,129.9, 128.6, 127.0, 126.5, 125.32, 120.4, 119.6, 52.2, 39.1, 28.9, 27.2, 22.3, 13.14, 13.0, 9.0 ppm. FTIR (KBr, cm^{-1}): 2210.22 (C≡N), 1621.79 (C=O).

Synthesis of 5, 5', 5", 5'"-(9-(heptan-3-yl)-9H-carbazole-1, 3, 6, 8- tetrayl) tetra-2, 2'-bithiophene-5-carbaldehyde (4b): Compound 4b was prepared by taking 1, 3, 6, 8-tetrabromo-9-(2-ethylhexyl)-9*H*-carbazole (2a) (595 mg, 1 mmol), (5'-(1, 3-dioxolan-2-yl)-2,2'-bithiophen-5-yl)tributylstannane (3.25 g, 5 eq.) and 3 mL DMF in a round bottom flask under nitrogen atmosphere. The same procedure as in 2b was followed, giving brown colored solid compound. Yield: 23%. mp 210-220ºC. ^{1}H NMR (500 MHz, $CDCl_3$): δ = 9.89 (d, *J* = 7.5 hz, 4H), 8.38 (d, *J* = 1 hz, 2H), 7.72(dd, *J* = 9 hz, 4 hz, 6H), 7.47 (d, *J* = 3.5 hz, 2H), 7.41 (s, 4H), 7.32 (dd, *J* = 14.5 hz, 4, 4H), 7.22 (d, *J* = 3.5 hz, 2H), 3.87(d, *J* = 7.5 hz, 2H), 1.86-1.87 (m, 1H), 0.79-0.93 (m, 4H), 0.62 (s, 2H), 0.50-0.53 (m, 4H), 0.29-0.34 (m, 4H). ^{13}C NMR (125 MHz, $CDCl_3$): δ = 182.4, 147.2, 146.9, 145.2, 145.0, 141.7, 141.6, 141.4, 137.4, 137.3, 136.6, 136.1, 131.8, 128.8, 128.5, 126.4, 126.3, 124.6, 124.1, 123.9, 123.4, 122.4, 111.5, 47.7, 39.4, 30.8, 28.6, 24.3, 23.1, 14.1, 10.9 ppm. FTIR (KBr, cm^{-1}): 1658.70 (C=O).

Synthesis of (2E)-3, 3',3",3"'-(5',5,",5"',5""-(9-(heptan-3-yl)-9H-carbazole-1,3,6,8-tetrayl) tetrakis (2,2'-bithiophene-5',5-diyl)) tetrakis (2-cyanoacrylic acid) (P4): Dye P4 was synthesized by compound 4b (100 mg, 0.1 mmol), cyanoacetic acid (51 mg, 0.60 mmol), acetic acid (5 mL) and ammonium acetate (5 mg), mixed together and same

procedure was followed as described for P2. A maroon precipitate was obtained which was filtered and washed thoroughly with water and then dried. The solid was further recrystallized with chloroform giving a dark brown colored solid. Yield: 98%. mp >300ºC. ^{1}H NMR (500 MHz, $CDCl_3$ +TFA): δ = 8.47 (d, *J* = 10.5 hz, 5H), 8.42 (s, 3H), 7.88 (d, *J* = 8 hz, 1H), 7.83 (d, *J* = 3.5 hz, 2H), 7.79 (d, *J*= 4 hz, 2H), 7.68 (s, 3H), 7.40 (d, *J* = 8 hz, 1H), 7.16 (d, *J* = 4 hz, 3H), 7.11 (d, *J* = 3.5 hz, 3H), 7.04 (s, 1H), 4.34 (d, *J*= 6.5 hz, 2H), 1.67-1.74 (m, 1H), 0.97 (dd, *J* = 15 hz, 6H), 0.85 (t, *J* = 7 hz, 7 hz, 8H). FTIR (KBr, cm^{-1}): 2209.08 (C≡N), 1594.61 (C=O).

Synthesis of 2, 3, 6, 7-tetrabromo-9-(2-ethylhexyl)-9H-carbazole (3a): 2, 7-dibromo-9-(2-ethylhexyl)-9*H*-carbazole (3) (5.7 mmol) was dissolved in DMF (20 ml) and stirred. *N*-bromo succinimide (NBS) (13.7 mmol) was dissolved in DMF (5 ml) and drop wise added in 2, 7-dibromo-9-butyl-9*H*-carbazole solution at room temperature. Mixture was stirred at room temperature for 16 hours and poured into water and extracted by chloroform. Solvent was removed by vacuum and product was recrystallized by ethanol as white crystalline solid, Yield: 91%. ^{1}H NMR (500 MHz, $CDCl_3$): δ = 8.21 (s, 2H), 7.62 (s, 2H), 3.97-4.06 (m, 2H), 1.97 (t, *J*= 12 Hz, 6 Hz, 1H), 1.22-1.39 (m, 8H), 0.82 (m, 6H). ^{13}C NMR (125 MHz, $CDCl_3$): δ = 140.7, 124.7, 122.2, 122.0, 114.65, 114.0, 47.8, 39.0, 30.7, 28.5, 24.3, 22.9, 14.0, 10.8 ppm.

Synthesis of 5, 5', 5'', 5'''- (9-(2-ethylhexyl)-9H-carbazole-2, 3, 6, 7-tetrayl) tetrathiophene-2-carbaldehyde (3b): A round bottom flask was charged with 2, 3, 6, 7-tetrabromo-9-(2-ethylhexyl)-9*H*-carbazole (3a) (400 mg, 0.67 mmol), (5-(1,3-dioxolan-2-yl)thiophen-2-yl)tributylstannane (1.2 g, 5 eq.) and 3 mL DMF. Further the same procedure described in 2b was followed, giving yellow colored solid compound. Yield 56%. mp 180-

190ºC. ^{1}H NMR (500 MHz, $CDCl_3$): δ =9.89 (s, 2H), 9.87 (s, 2H), 8.26 (s, 2H), 7.65-7.66 (m, 4H), 7.56 (s, 2H), 6.99 (dd, *J* = 3.5 hz, 3 hz, 4H), 4.23-4.26 (m, 2H), 2.09-2.12 (m, 1H), 1.25-1.34 (m, 5H), 0.95 (m, 4H), 0.86-0.88 (m, 5H). ^{13}C NMR (125 MHz, $CDCl_3$): δ = 182.9, 182.8, 153.1, 152.7, 144.0, 143.7, 141.8, 136.6, 136.5, 131.3, 128.9, 128.5, 124.6, 123.7, 122.8, 112.0, 47.9, 39.4, 29.7, 28.5, 24.3, 23.0, 14.0, 10.9 ppm. FTIR (KBr, cm^{-1}): 1663.90 (C=O).

Synthesis of (2E, 2′E, 2′′E, 2′′′Z)-3, 3′, 3′′, 3′′′-(5, 5′, 5′′, 5′′′-(9-(2-ethylhexyl)-9H-carbazole-2, 3, 6, 7-tetrayl) tetrakis (thiophene-5,2-diyl)) tetrakis (2-cyanoacrylic acid) (P3): Dye P3 was synthesized by compound 3b (100 mg, 0.14 mmol), cyanoacetic acid (60 mg, 0.70 mmol), acetic acid (5 mL) and ammonium acetate (5 mg), mixed together and processed in the same way as in P2, producing an orange precipitate. This was filtered and washed thoroughly with water and dried. The solid was further recrystallized with chloroform giving an orange colored solid. Yield: 98%. mp >300ºC. ^{1}H NMR (500 MHz, $CDCl_3$ + TFA): δ = 8.70(s, 2H), 8.59 (s, 2H), 8.54 (s, 2H), 8.03 (d, *J* = 4 hz, 2H), 7.96 (s, 2H), 7.92 (d, *J* = 3.5 hz, 2H), 7.74 (d, *J* = 4 hz, 2H), 7.58 (d, *J* = 3.5 hz, 2H), 3.80 (d, *J* = 7 hz, 2H), 1.92-2.13 (m, 1H), 0.82-0.89 (m, 2H), 0.36-0.59 (m, 8H), 0.30-0.31 (m, 4H), ^{13}C NMR (125 MHz, $CDCl_3$ + THF): δ = 168.5, 156.8, 156.0, 150.5, 150.4, 142.3, 140.8, 140.4, 136.1, 135.6, 130.6, 130.2, 129.7, 124.2, 124.0, 123.3, 47.8, 39.5, 29.6, 28.4, 24.1, 22.8, 13.4, 10.4 ppm. FTIR (KBr, cm^{-1}): 2215.13 (C≡N), 1584.07 (C=O).

Synthesis of 5′, 5′′, 5′′′, 5′′′′-(9-(2-ethylhexyl)-9H-carbazole-2, 3, 6, 7-tetrayl) tetra-2,2′-bithiophene-5-carbaldehyde (5b): A round bottom flask was charged with 2, 3, 6, 7-tetrabromo-9-(2-ethylhexyl)-9*H*-carbazole (3a) (179 mg, 0.3 mmol), (5'-(1,3-dioxolan-2-yl)-2,2'-bithiophen-5-yl)tributylstannane (760 mg, 5 eq.) and 3 mL DMF. Nitrogen was purged

followed by the addition of $Pd(PPh_3)_2Cl_2$ (8.4 mg). Same procedure was used as explained earlier for 2b, giving brown colored solid compound Yield: 42%. mp 200-220ºC. ^{1}H NMR (500 MHz, $CDCl_3$): δ = 9.86 (d, *J* = 5 hz,4H), 8.23 (s, 2H), 7.66 (dd, *J* = 5.5 hz, 4 hz, 4H), 7.545 (s, 2H), 7.27-7.29 (m,4H), 7.24 (d, *J* = 3.5 hz, 2H), 7.22 (d, *J* = 4 hz, 2H), 6.95 (d, *J* = 3.5 hz, 2H), 6.92 (d, *J* = 4 hz, 2H), 4.21-4.27 (m, 2H), 2.12-2.14 (m, 1H), 1.30-1.34 (m, 4H), 0.97-1.00 (m, 4H), 0.88-0.91 (m, 6H). ^{13}C NMR (125 MHz, $CDCl_3$): δ = 182.4, 147.3, 146.9, 145.2, 145.0, 141.6, 141.6, 141.4, 137.4, 137.3, 136.6, 131.3, 128.8, 128.5, 126.4, 126.3, 124.6, 124.1, 123.9, 123.4, 122.4, 111.5, 47.9, 39.4, 30.8, 28.6, 24.3, 23.1, 14.1, 10.9 ppm. FTIR (KBr, cm^{-1}): 1657.24 (C=O).

Synthesis of (2E, 2'E, 2''Z, 2'''Z)-3, 3', 3'', 3'''-(5', 5'', 5''', 5''''-(9-(2-ethylhexyl)-9H-carbazole-2,3,6,7-tetrayl) tetrakis(2,2'-bithiophene-5',5-diyl)) tetrakis(2-cyanoacrylic acid) (P5): Dye P5 was synthesized by compound 3b (100 mg, 0.1 mmol), cyanoacetic acid (51 mg, 0.60 mmol), acetic acid (5 mL) and ammonium acetate (5 mg), mixed together and the same procedure used for P2, resulting in a red precipitate and finally gave a black colored solid. Yield: 98 %. mp > 300 ºC. ^{1}H NMR (500 MHz, $CDCl_3$+TFA): δ = 8.44(d, *J* = 5 hz, 2H), 8.29 (s, 1H), 7.78 (dd, *J* = 7 hz, 4 hz, 2H), 7.60 (s, 1H), 7.40-7.44 (m, 2H), 7.33 (dd, *J* = 11.5 hz, 4 hz, 3H),6.99-7.10 (m, 7H), 6.83-6.93 (m, 6H), 4.28 (d, *J* = 6.5 hz, 2H), 2.15-2.16 (m, 1H), 1.45-1.46 (m, 6H), 0.95-1.02 (m, 4H), 0.89-0.91 (m, 4H). FTIR (KBr, cm^{-1}): 2203.03 (C≡N), 1600.43 (C=O).

5.2.2.2.5.2 DSSC fabrication

A compact TiO_2 blocking layer was chemically deposited on the conducting surface of cleaned FTO by immersing it in a 0.04 M $TiCl_4$ aq. solution at 70 ºC for 30 minutes. Nanoporous TiO_2 films were created on the blocking layer by screen printing colloidal TiO_2

paste. The particle sizes for mesoporous transparent and scattering layers were 25 nm and 150 nm, respectively. The films were sintered up to 500 ºC for attaining better interfacial contact between the particles. The film thickness was set as 12 μm. Post $TiCl_4$ treatment was done before dye loading. Counter electrodes were made by depositing 4.8 mM chloroplatinic acid solution in ethanol on FTO followed by annealing at 450 °C for 15 minutes. A 25 μm thick surlyn spacer was used to club both the electrodes together. The cells were filled with electrolyte solution through a predrilled hole in the counter electrode and sealed by surlyn polymer and cover slip. Finally, the cells were soldered for external circuit connections. The cells made in such a way have an active area of 0.16 cm^2. TiO_2 films were soaked in 0.3 mmol solutions of all dyes made separately in DMSO for 12 hours at room temperature. Same procedure and composition was used for the electrolyte as used in other studies [68]. In order to analyze the amount of dye loading a solution of 0.1M $(CH_3)NOH$ in ACN and DI water in 1:1 ratio was used [69]. All the films were desorbed completely and the solutions of known concentrations of all dyes were made to calculate the adsorbed concentration of dyes in TiO_2 films.

5.2.3 COSENSITIZATION STUDY

5.2.3.1 Introduction

Ever since Grätzel and co-workers reported high solar cell efficiency of DSSCs based on ruthenium complex dye [2], DSSCs have been looked upon as a new era of sustainable, clean energy sources. Besides the low cost fabrication, DSSCs give opportunity for the flexibility and modulation in all the components involved which ensures enhancement in device performance. Among sensitizers, organic sensitizers offer much broader window in respect of optical and electrochemical tuning by structural modification than inorganic

sensitizers. This is the reason behind much interest shown towards the synthesis of novel organic sensitizers than for inorganic sensitizers, lately. There are some prerequisites for the organic dyes to be used in DSSCs. It should have higher molar extinction coefficient, with energy level of LUMO higher than the conduction band of TiO_2 and energy level of HOMO lower than I^-/ I_3^- redox potential [70].

It should posses at least one anchoring group to hold onto TiO_2 surface and the structure which originates the unidirectional flow of electron. Long term stability, resistance to aggregation and recombination are also desirable. Selections of anchoring group, donor moiety and linker moiety, addition of hydrophobic and bulky groups are done with precision for good performance of the DSSC devices. Although structural modulations through molecular engineering has been very effective in creating and combining all the required properties in order to give best possible efficiency by using organic sensitizers, it could not surpass the performance of Ru- based inorganic dyes. Owing to their strong and broad range absorption in visible region, Ru- based dyes, i.e., N-719, black dye etc., still lead in DSSCs [71]. To eliminate the limitation of coverage in visible region by organic sensitizers, the approach of co-adsorption of more than one dye has been adopted [72]. For the effective use of this strategy, it is important that the co-adsorbed dye rearranges the dye molecules of principal sensitizer on the surface and helps filling up the voids in order to give a compact packing and good coverage. It has been observed that the selection of cosensitizer is chosen on the basis of optical coverage only irrespective of the molecular structural correlation with the principal dye [72].

Recently, Chandraprakasham *et.al*. synthesized two D-π-A molecules, used as cosensitizers with Black dye and achieved a new record efficiency of 11.4 % with I^-/I_3^- redox

couple. Apart from higher molar extinction coefficient of these dyes than that of black dye, the dyes are designed in such a way that they reduce dye aggregation, restrict electron recombination and contribute enhancing the photocurrent. It is concluded that due to much smaller molecular sizes both the dyes fill up the voids by rearranging the dye molecules and intercalation in between the molecules of principal dye [73].

The selection of co-sensitizers is a crucial aspect and needs a careful investigation and analysis of optical characteristics. In order to cover most of the visible spectrum, the cosensitizer should be an analogue of the principal dye and must cover the part of the spectrum which is not absorbed by principal dye. In this way a broad range of visible region can be harvested by cosensitized DSSCs. Generally, the cosensitization can be done by one of the two approaches such as co-adsorption i.e. mixing the cosensitizers with the principal dye in an optimized ratio and the post adsorption which is a stepwise adsorption of cosensitizers over the principal dye or visa-versa [74]. Since this research work includes the synthesis and study of photovoltaic performance of cruciform tetra-anchoring carbazole based organic dyes, it is apprehended that the irregular molecular arrangement of dyes on the TiO_2 surface due to crowded periphery of the molecule, could be one of the reasons behind the below average performance of the DSSC devices fabricated. For enhancing the DSSC performance, a smaller dye molecule is thought to be inserted in between the dye molecules of dyes P1, P2, P3, P4 and P5 which can work as a filler and rearrange the dye molecules in order to approach the optimum dye loading and good coverage. A lot of work has been reported on the cosensitization strategy by organic as well as inorganic dyes i.e. D-131, D-205, SQ dyes, C-106, N-719 etc [75].

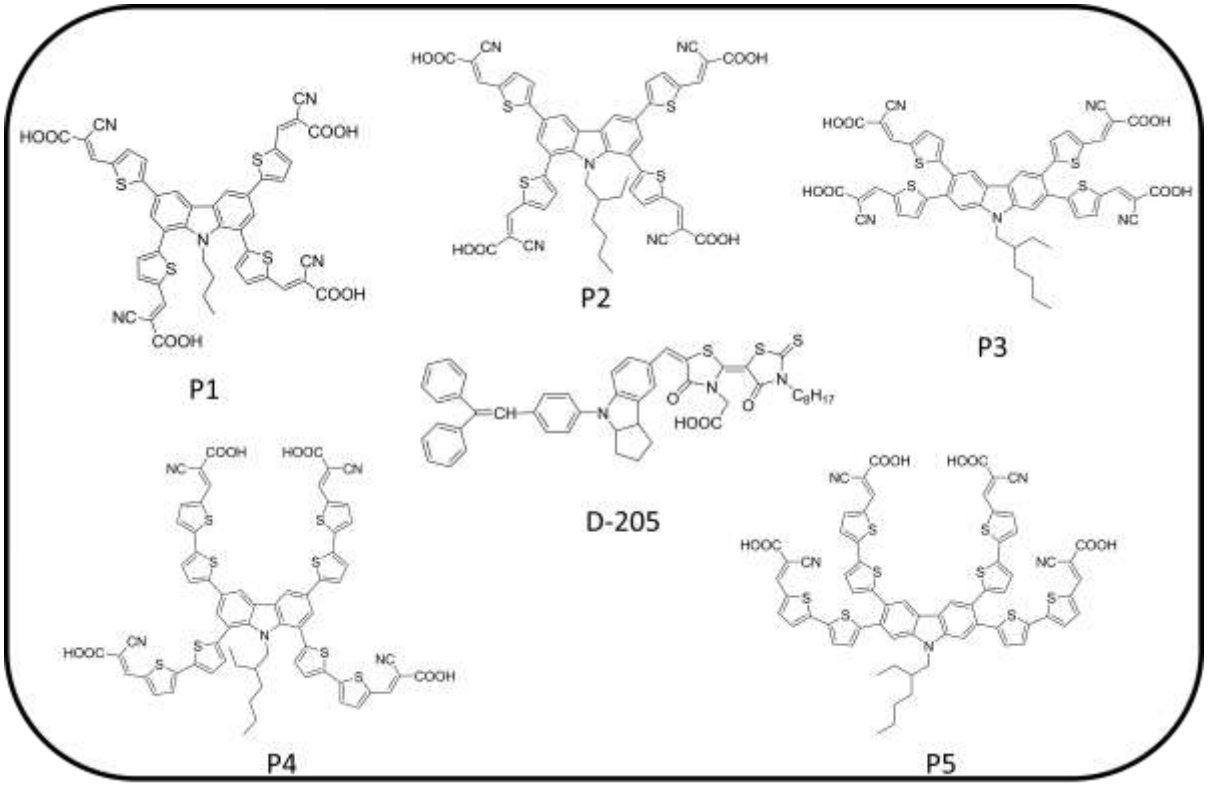

Figure 5.18: Molecular structures of principal dyes (P1-P5) and D-205 (Coadsorbed dye).

Organic dye, D-205 is judicially selected for the purpose of cosensitization in the current study. The molecular structure of D-205 along with principal dyes used in this study is given in figure 5.18. D-205 is an indoline based dye with high molar extinction coefficient of 72145 $L.mol^{-1}.cm^{-1}$ [76] and exhibits an absorption band centered at 525 nm which is complementary to the absorption bands of dyes P1, P2, P3, P4 and P5. D-205 consists of a rhodanine dimer as the acceptor and carboxylic acid as an anchoring group with an octyl chain attached to N of rhodanine. It is expected to contribute to limit the dye aggregation on TiO_2 film. The whole series of dyes was used in DSSC device fabrication with the cosensitizer, D-205. The effect of cosensitization is observed to be different, depending upon the orientation of anchoring arms in dyes (P1-P5).

5.2.3.2 Results and discussions

5.2.3.2.1 Photophysical properties

Figure 5.19 (a) depicts the UV-vis spectra of all the sensitized TiO_2 films pre and post co-adsorption of D-205. It is observed that the pattern of absorption spectra completely changed after the cosensitization. The dyes showed bathochromic shift in a consecutive manner from P1 to P5 which can be illustrated as P1=P2=P3<P4<P5 before cosensitization. Post co-adsorption all the dyes in conjunction with D-205 showed a considerable shift towards longer wavelength but dye P2 showed the largest shift of wavelength in visible region which is almost similar to that of D-205. Then it is P1 and P3 which also shifted near to P2. Dye P4 and P5 showed the least shift in wavelength. A hyperchromic shift is also seen in case of the post coadsorption of D-205 with dye P-5. The overall shift observed after co-adsorption of D-205 with all the dyes can be affirmed as P5<P4<P3<P1<P2=D-205. It is indicated by the optical studies of cosensitized TiO_2 films that the adsorption of D-205 could cause a reorientation of dye on TiO_2 surface to more upright configuration which reduces the aggregation on TiO_2 surface as a consequence of the steric repulsion resulting from the insertion of D-205 in between the dye molecules [77].

Figure 5.19 (b) shows the TiO_2 films before and after co-adsorption of D-205 with all the dyes (P1-P5). All the films exhibited much deeper color post co-adsorption which is consistent with the red shifted absorptions of all the films in Figure 15.19 (a).

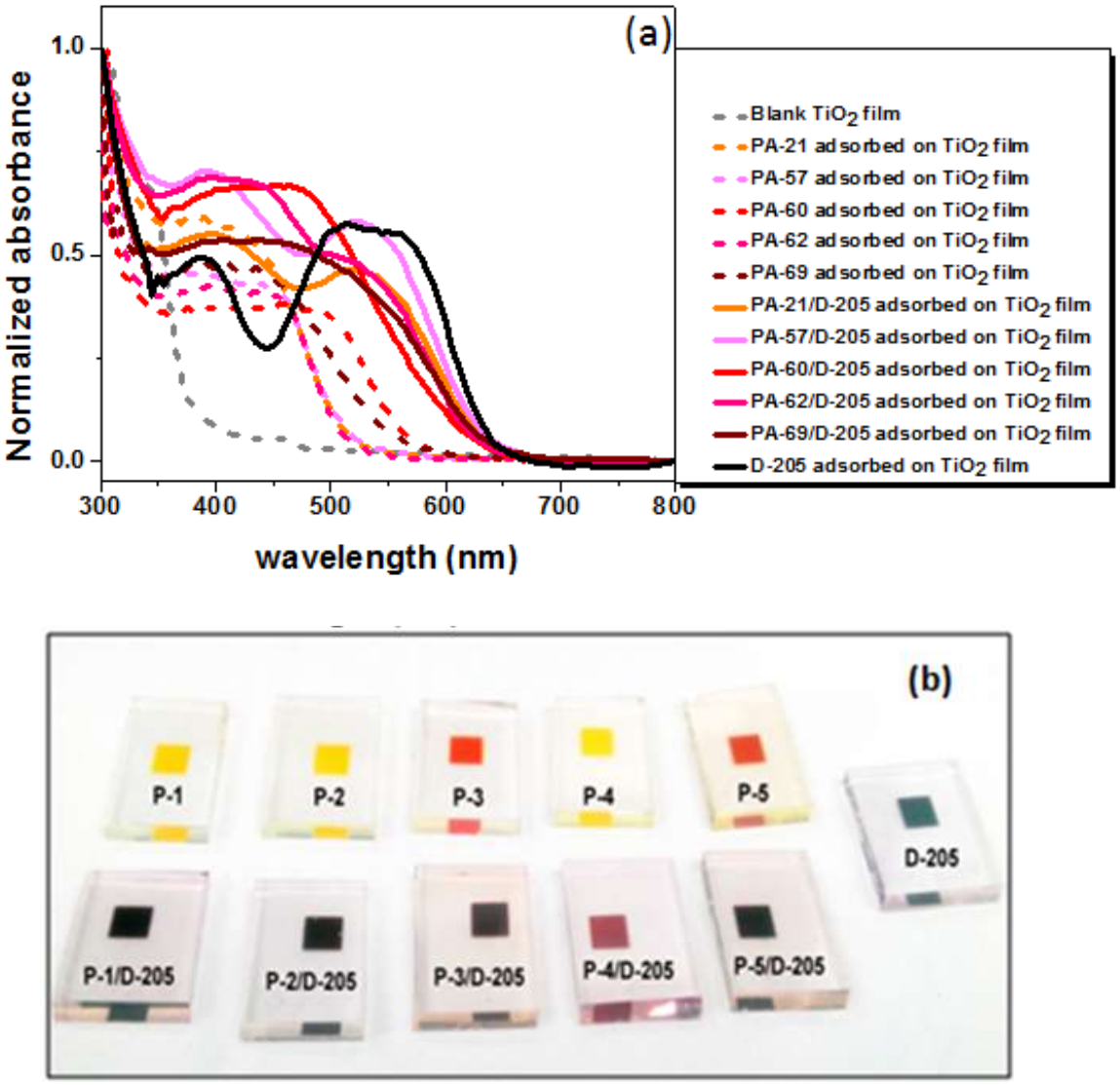

Figure 5.19: Optical properties of cosensitized TiO_2 films. (a) Absorbance spectra, (b) Pictures of TiO_2 films pre and post co adsorption of D-205.

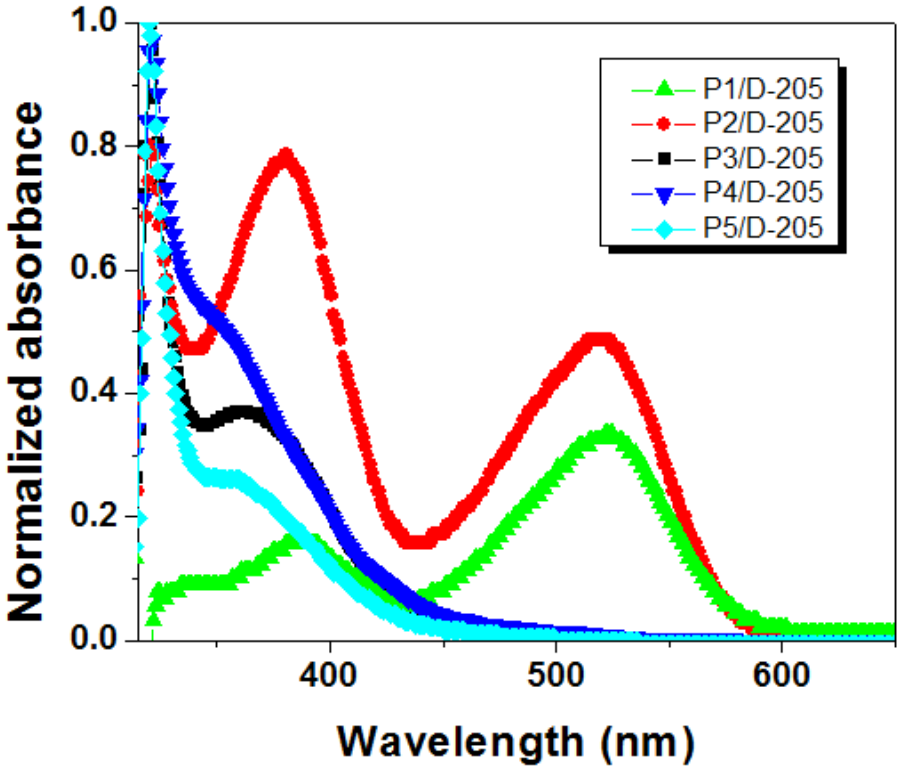

Figure 5.20: Absorption spectra of D-205 desorbed from cosensitized TiO_2 films.

Figure 5.20 shows the absorption spectra of dye D-205 after desorbing it from cosensitized films. The study was carried out by first desorbing principal dyes (P1-P5) in a solution of $(CH_3)NOH$ in ACN and DI water [78] and then by dipping the films in acetone. Since D-205 is found to be insoluble in $(CH_3)NOH$/DI water solution, acetone appeared to pull out D-205 from TiO_2 films very effectively. It is observed that the absorption range is broadened till 580 nm in case of cosensitization of P2 which is caused by good amount of post adsorption of D-205 in the film sensitized by dye P2. The coverage of spectrum from 430 nm to 580 nm is also seen in case of P1 cosensitized films, but the intensity of absorption peak dropped in shorter wavelength region of the UV- spectrum.

Cosensitized films of P3, P4 and P5 do not appear to absorb much amount of dye D-205 which is evident from absorption spectra of desorbed D-205 from these cosensitized TiO_2 films. There is no absorption beyond 450 nm in any of these cases. The information gathered by absorption spectra of D-205 desorbed from all cosensitized TiO_2 films affirms the findings of absorption spectra in Figure 5.19 (a).

5.2.3.2.2 Study of dye concentration in cosensitized TiO_2 films

Since cosensitization causes reorientation of dye molecules on the TiO_2 surface and filling of voids, it is expected to enhance the dye loading of principal dye in the TiO_2 films. To calculate the amount of loaded dye, dyes are desorbed in the solution of $(CH_3)NOH$ in ACN and DI water [78] which extracted only principal dye from the films. The amount of desorbed dyes from cosensitized films is compared with the amount of desorbed dyes from films sensitized by only principal dyes. Table 5.9 notifies the concentrations of all principal dyes (P1-P5) pre and post adsorption of D-205.

It is observed that except for the cosensitized films of dye P1, rest of the films adsorbed more amount of principal dyes on cosensitization. The amount of dye in the film is calculated as 0.015 mol L^{-1} before as well as after the cosensitization. For the cosensitized films of dyes P2 and P3 the amount of dye loading increased up to 0.02 mol L^{-1}. Cosensitized films of dye P4 and P5 also showed the moderate improvement of dye loading than in comparison with non cosensitized films. It is also noted that due to longer anchoring arms all around the carbazole moiety, the concentration of dyes P4 and P5 is already lesser than all the films sensitized by other dyes of this series. Figure 5.21 discloses the pictorial arrangement of organic dyes with bulky peripheries, which tend to reduce the concentration of dye molecules adsorbed on the TiO_2 surface.

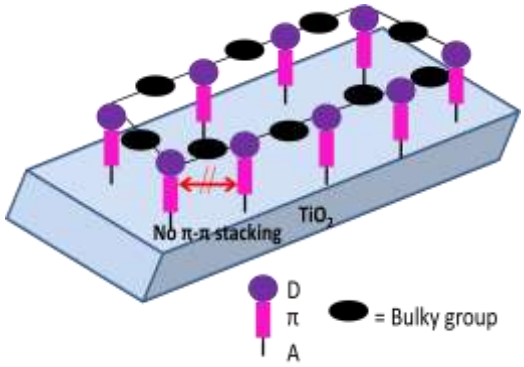

Figure 5.21: Pictorial arrangement of organic dyes with bulky periphery.

Table 5.9: Concentration of dye loaded in the TiO_2 films pre and post cosensitization.

Dye	Dye concentration in film (mol L^{-1})
P1	0.015
P1/D-205	0.015
P-2	0.015
P2/D-205	0.02
P3	0.0125
P3/D-205	0.02
P4	0.0075
P4/D-205	0.01
P5	0.0075
P5/D-205	0.0125

5.2.3.2.3 Effect of cosensitization on aggregation

Some solid state properties like self-assembly, morphology and aggregation are crucial aspects in deciding the fate of a solar cell based on organic dyes [79]. One of the

reasons of less photovoltaic performance of DSSCs in which organic sensitizers are used, is the intermolecular energy transfer due to dye aggregation on TiO_2 film [80] which is caused by planar or sterically less-hindered structures of organic dyes. The π-stacked dye aggregates stimulate nonradiative decays of the excited state to the ground state by allowing conduction-band electrons to recombine with I_3^- [81]. Aggregation causes filtering of absorbed light which affects the device performance adversely. Apart from structural modification [82], co-adsorption of fillers and additives like deoxycholic acid (DCA) and 4-tert-butylpyridine (TBP) has been taken into account to reduce aggragation caused quenching [83]. The modus operandi of coadsorption of DCA as well as cosensitizer for dissociation of π-stacked dye aggregates is shown in figure 5.22 which affirms that while reorganizing the dye molecules onto the surface, DCA insertion reduces the dye loading, which can affect the performance of the device if not optimized properly [84]. Cosensitization is an approach which proves to be more efficient than DCA addition in order to reduce the aggregation because it rearranges the dye molecules on the surface as well as complements the spectral absorption [85].

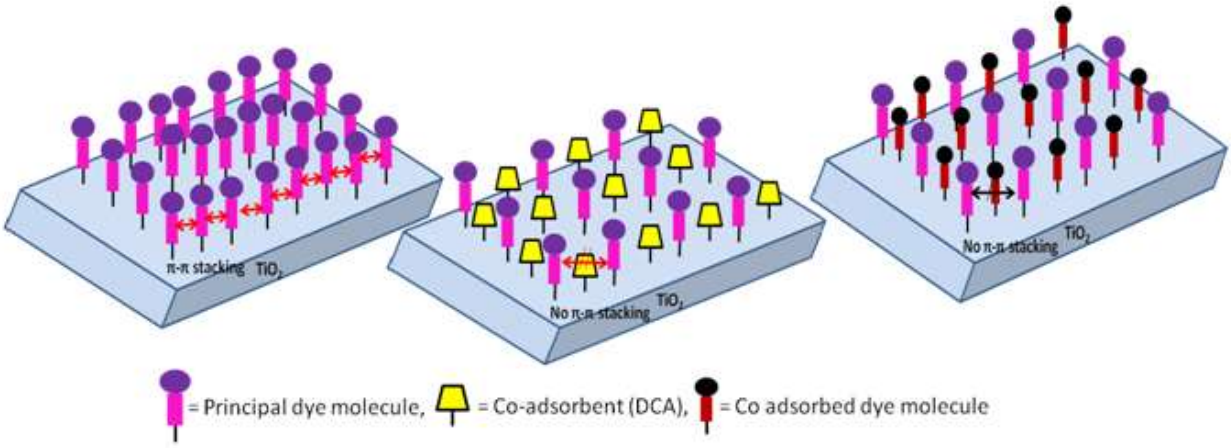

Figure 5.22: Schematic diagram of coadsorption of DCA as well as cosensitizer.

The effect of co sensitization on aggregation is studied by atomic force microscopy (AFM) in this study. Figure 5.23 shows the morphology of all the sensitized and co sensitized TiO_2 films. It has been observed that due to long and twisted anchoring arms of dye molecules, P4 and P5, the overall molecular geometry becomes reasonably non-planar with bulky periphery which assists in rearranging the dye molecules on the surface and prevents aggregation. The films are uniformly packed with the dye molecules and no aggregation is seen on these films before cosensitization. Since the films are compactly covered by principal dye molecules, it restricts the scope of co-adsorption of D-205 in these films which is evident by absorption graph of desorbed D-205 in Figure 5.20. Thus, cosensitization does not make any difference in the appearance of these films in AFM images (Figure 5.23).

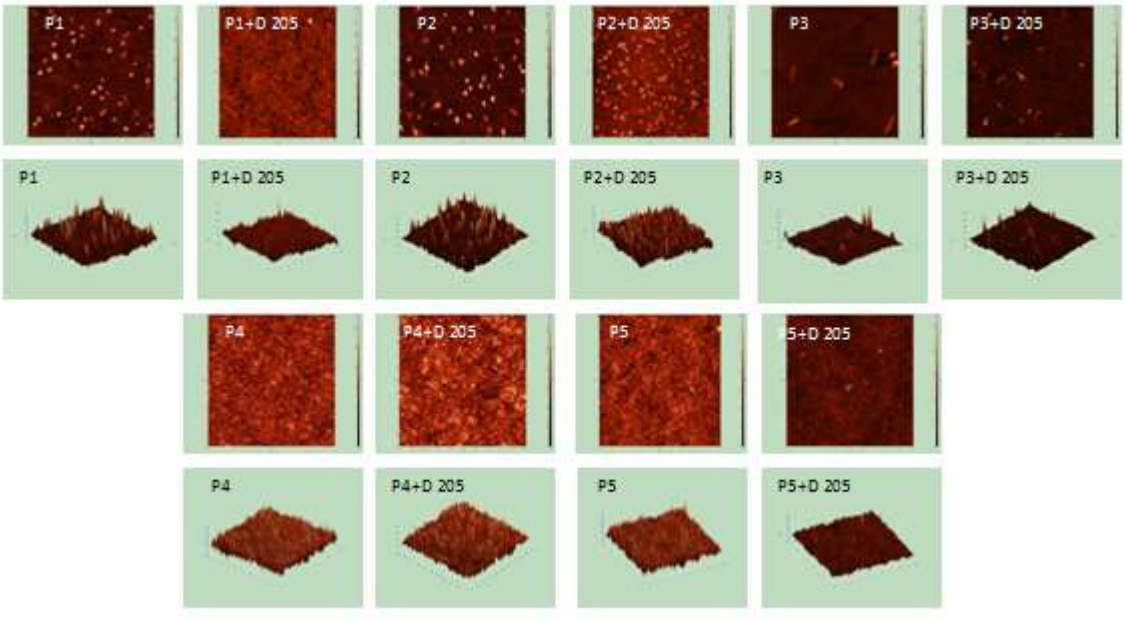

Figure 5.23: AFM images (2D and 3D) of sensitized and co sensitized TiO_2 films.

The aggregates are observed in the films sensitized by dyes P1, P2 and P3 (Figure 5.23). Since the substitution position of anchoring groups are same in case of dyes P1 and P2 (Figure 5.18) and leaves the structures more planar than in comparison with dye P3, causing the dye molecules to stacked together and aggregate. Adjacent substitutions of four anchoring groups in P3 twist the structure to some extent, reducing the formation of aggregates on the surface in comparison with P1 and P2. After co-sensitization with D-205, P1 film displayed complete vanishing of dye aggregates because of molecular rearrangement of dye molecules. Although the aggregates are very prominent post cosensitization in case of films P2 and P3, the aggregate size is reduced considerably. It is seen in the 3D images of P2 and P3 films in Figure 5.23 that aggregates are much smaller and more uniformly arranged onto the surface after cosensitization. The study of AFM images gives a new insight on the role of cosensitization in reducing the aggregation caused quenching in DSSC and being able to improve DSSC performance by enhancing optical as well as solid state properties of dye molecules on TiO_2 film.

5.2.3.2.4 Effect of co sensitization on photovoltaic performance of DSSCs

The *I-V* characteristics of DSSC devices fabricated by all the dyes (P1-P5), pre and post cosensitization, are depicted in figure 5.24 and *I-V* parameter are described in Table 5.10.

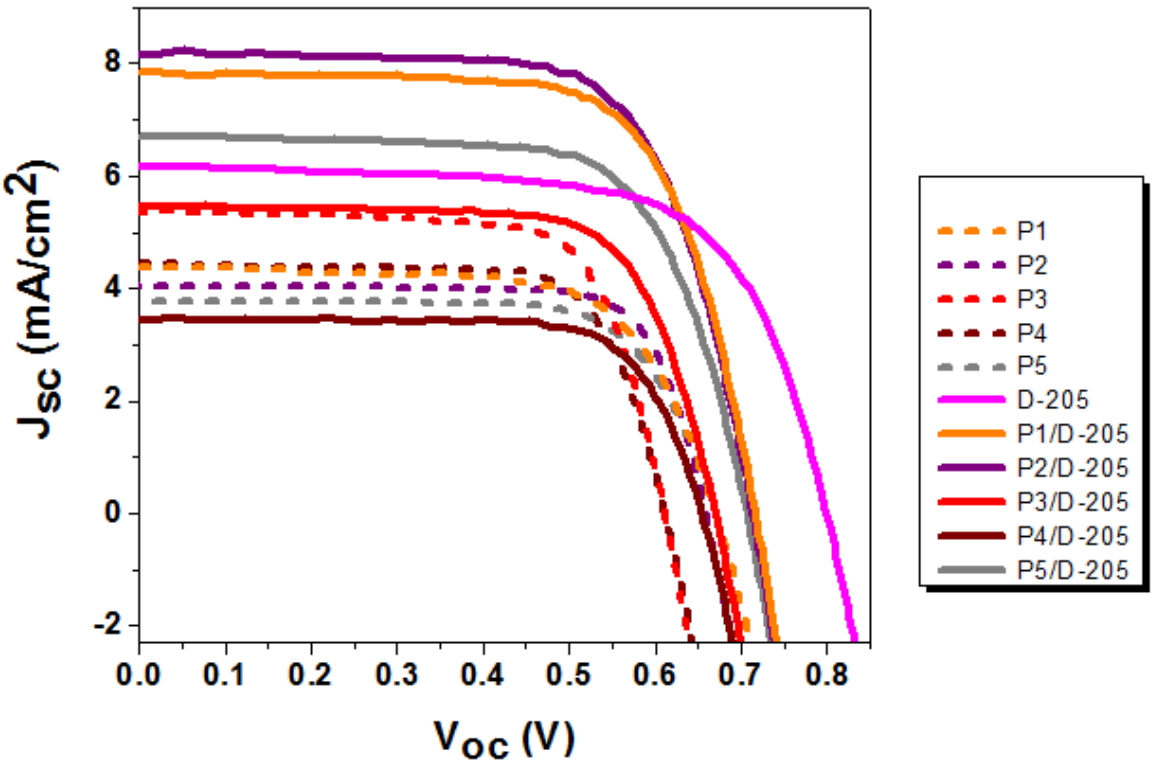

Figure 5.24: *I-V* characteristics of DSSC devices fabricated by all the dyes (P1-P5), pre and post cosensitization.

It can be observed that all the *I-V* parameters are improved in device P1/D-205 than that is in device P1. J_{sc}, V_{oc}, *FF* and efficiency increased from 5.45 mA/cm^2, 0.69 V, 70 % and 2.6 % to 8.03 mA/cm^2, 0.71 V, 71 % and 4.1 %, respectively, on cosensitization. The improvement in all the *I-V* parameters is due to complete eradication of aggragation post cosensitization in device P1/D-205. In DSSC device P2, V_{oc} and *FF* reduced from 0.66 V and 77 % to 0.54 V and 69 %, respectively on cosensitization. Since it is well studied and reported in literature that V_{oc} of DSSCs are affected by unfavorable back electron transfer caused by aggregation [86], it can be correlated by densely arranged small aggregates all over P2/D-205 film after cosensitization (Figure 5.23).

Table 5.10: *I-V* parameters of DSSC devices fabricated by all the dyes (P1-P5), pre and post cosensitization.

Dye	J_{sc} (mA/cm^2)	V_{oc} (V)	*FF*	η (%)
P1	5.45	0.69	70	2.6
P1/D-205	8.03	0.71	71	4.1
P2	4.05	0.66	77	2.1
P2/D-205	8.16	0.54	69	4.0
P3	3.78	0.67	72	1.8
P3/D-205	6.71	0.71	70	3.3
P4	4.44	0.61	74	2.0
P4/D-205	3.45	0.65	75	1.7
P5	5.37	0.61	72	2.4
P5/D-205	5.50	0.67	72	2.6
D-205	6.20	0.80	68	3.4

Due to major increase in J_{sc} of device P2/D-205 (8.16 mA/cm^2) than in comparison with device P2 (4.05 mA/cm^2) the overall device efficiency of 4.0 % could be achieved on cosensitization. Because of reduced aggregation in P3/D-205 films J_{sc}, V_{oc} and efficiency improved from 3.78 to 6.71 mA/cm^2, 0.67 to 0.71 V and from 1.8 to 3.3 %, respectively, in comparison with device P3. The J_{sc} decreased in P4/D-205 device than in comparison with device P4 and resulted in decreased conversion efficiency of the device on cosensitization. Since there is no considerable change in optical and morphological characteristics of cosensitized films, P4/D-205 and P5/D-205, all the I-V parameters of their devices remained almost the same as non cosensitized devices, i.e. P4 and P5. Device D-205 is fabricated as a control device with the dye loading time of 2 hours. The *I-V* parameters of device D-205

show a moderate performance with J_{sc}, V_{oc}, *FF* and efficiency of 6.20 mA/cm^2, 0.80 V, 68 %, 3.4 %.

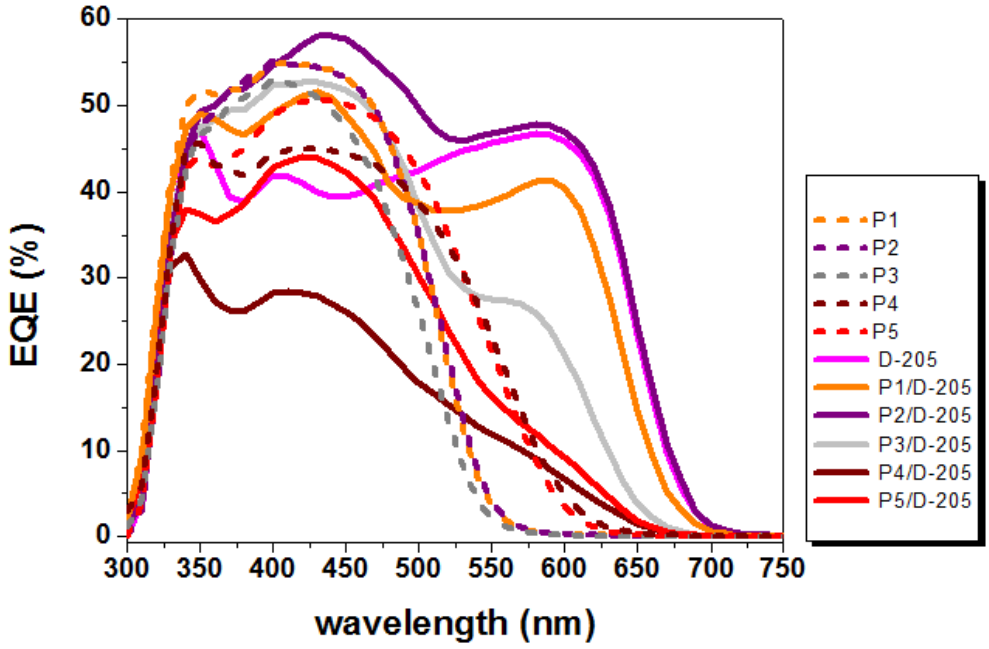

Figure 5.25: IPCE characteristics of DSSC devices fabricated by all the dyes (P1-P5), pre and post cosensitization.

Figure 5.25 shows the external quantum efficiency (EQE) of all the DSSC devices at the wavelength range of 300-750 nm. The IPCE graph patterns are observed to be well in support with the absorption spectra of sensitized and co sensitized TiO_2 films in Figure 5.19 (a). It is also in sync with the absorption profile of desorbed D-205 in Figure 7.3. The highest EQE of 59 % is observed at 430 nm in device P2/D-205. A broad coverage of 300-700 nm which was 300-550 nm prior to cosensitization of film P2, could be achieved. Device P1/D-205 also showed the similar spectra but with the lesser EQE. The EQE further decreased for the devices P3/D-205, P4/D-205 and P5/D-205 than in comparison with their

non cosensitized counter devices. The overall effect of co sensitization on DSSC efficiencies is illustrated in the bar diagram in Figure 5.26.

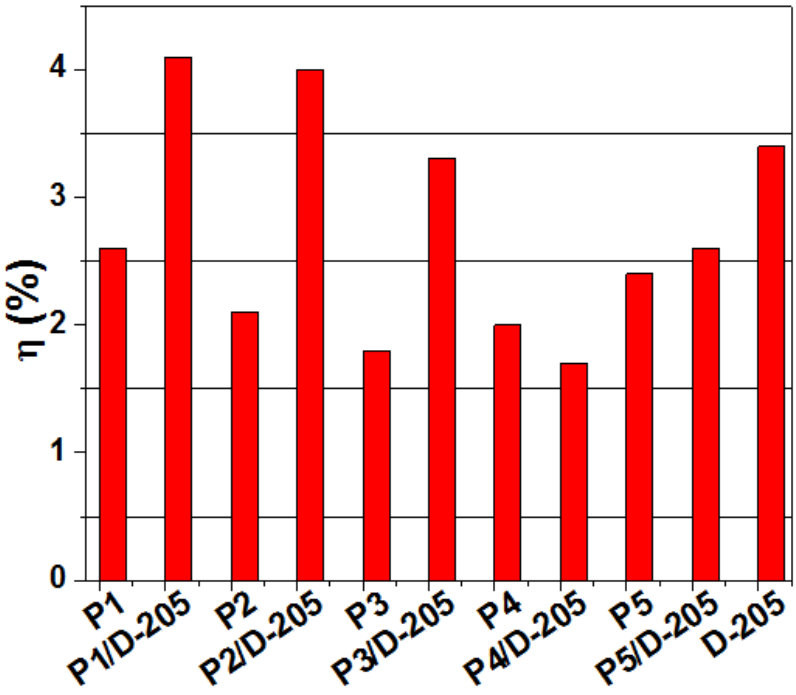

Figure 5.26: Effect of post adsorption of D-205 on efficiency of DSSCs.

5.2.3.3 Experimental

It is well-known that small molecules with alkyl chains tend to form densely packed monolayer due to the weak steric hindrance [87]. Furthermore, the post-adsorption of smaller molecules into the interstitial site of large-molecular layer would greatly increase the overall surface molecular coverage, thus impeding the I_3^- percolating to the TiO_2 surface [88].

Both the approaches of cosensitization have been attempted in the current study i.e. by mixing the dyes in the same solution and another includes post adsorption of dye. It is observed that cosensitization by former approach decreases the dye loading of this series of

molecules on TiO_2 film and affects the photovoltaic parameters adversely. So the work is preceded with the later approach. For the purpose of simplicity the results of simultaneous cosensitization study are not discussed here. A compact TiO_2 blocking layer was chemically deposited onto the conducting surface of pre-cleaned FTO (Nippon Sheet Glass10 Ohm/sq) by immersing it in a 0.04 M $TiCl_4$ aq. solution at 70ºC for 30 minutes. Nanoporous TiO_2 films were developed on the blocking layer by screen printing colloidal TiO_2 paste and sintered up to 500ºC. The films were rinsed with de-ionized water and annealed at 450ºC for 30 minutes, prior to dye loading. TiO_2 films were dipped in dye solutions of 0.3 mM in DMSO, separately in all the dyes (P1-P5) for 12 hours followed by 2 hours dipping in the 0.3 mM solution of D-205 in ACN. For making counter electrode 4.8 mM chloroplatinic acid solution was used in ethanol as platinum precursor, deposited on FTO by drop casting method and annealed at 450ºC for 15 minutes. Both the electrodes were clubbed together by a 25 µm thick surlyn spacer. The cells were filled with electrolyte solution through a predrilled hole in the counter electrode and the whole assembly was sealed with surlyn polymer and cover slip by hot pressing. Finally, the cells were soldered to connect to the external circuit. The cells made in such a way have an active area of 0.16 cm^2.

The amount of adsorbed dyes before and after the cosensitization was determined by desorbing completely in 0.1M $(CH_3)NOH$ in ACN and DI water solution in 1:1 ratio [78] followed by dipping in acetone to desorb D-205. The solutions of known concentrations of all dyes are made to calculate the adsorbed concentration of dyes in the TiO_2 films. The resulting dye solution was analyzed spectrophotometrically in a 1.00 cm^2 quartz optical cell. The concentration is determined by using fresh standard solutions, prepared by dissolving a

known amount of dye in 0.1M $(CH_3)NOH$ in ACN and DI water solution. The composition of electrolyte is taken as per previous studies [54].

5.3 LOW BAND GAP TiO_2 NANO PARTICLES FOR LIQUID STATE DYE SENSITIZED SOLAR CELLS (DSSCs)

5.3.1 Introduction

TiO_2 is a versatile material [89, 90] which is highly desirable in the field of sensors, paints, cosmetics, photocatalytic and photovoltaic applications. One of the best known applications of TiO_2 nanoparticles is the photo electronic conversion in dye-sensitized solar cells (DSSCs) where it acts as carriers [91, 92]. There are three crystalline forms of TiO_2: anatase, rutile and brookite. Rutile has a high chemical stability but is less active [93, 94]. Commercially available anatase particles have a band gap of 3.2 eV, corresponding to a UV wavelength of 385 nm. In contrast, the thermodynamically stable rutile phase has a smaller band gap of 3.0 eV with excitation wavelengths that extend into the visible range at 410 nm which affirms its suitability over anatase for effective light harvesting in visible region for DSSCs. The adsorptive affinity of anatase for organic compounds is higher than that of rutile [95] and it exhibits lower rate of recombination due to its 10-fold greater rate of hole trapping in comparison with rutile. Owing to the combined effect of lower rates of recombination and higher surface adsorptive capacity, metastable anatase phase is photo chemically more active phase of titania [96]. It is desirable to blend above discussed merits of anatase particles with reduced band gap of rutile to facilitate the visible light absorption by the formation of nanocomposites containing anatase and rutile phases.

Different approaches for narrowing the band gap of anatase particles have been pursued. The most common method is to dope TiO_2 with impurities [97]. It has been

observed recently that the visible light activity can be achieved effectively by using anion dopants such as nitrogen or carbon [98] but it generates lattice defects. These dopant-induced defects in the TiO_2 lattice have a degrading effect on photochemical activity due to the introduction of charge carrier trapping and recombination sites [97]. These degrading effects negate the increase in visible light absorption and cause a reduced photo activity in the doped TiO_2. Clearly, a dopant-free, pure TiO_2 phase with a band gap that matches the visible light energy would be ideal. Recently, it has been suggested that TiO_2 phases at high-pressure, might show such properties [99]. Unfortunately, these phases are not stable at atmospheric pressure, and are therefore not useful for photo activity.

In the past studies it was observed that TiO_2 with a large quantity of anatase and a small quantity of rutile exhibits a higher photochemical activity than in the pure anatase or rutile phases [100]. This is attributed, in part, to a wider optical absorption band and smaller electron effective mass of rutile than those of anatase, which promotes to higher mobility of charge carriers in rutile than in anatase [100]. When the size of TiO_2 is reduced to a few nanometers, the effect of the surface on their mechanical and electronic behaviors is amplified [101]. It has been found that the surface conditions strongly influence morphology, stability, and equilibrium shape of chemically prepared TiO_2 [102]. Understanding the relationship of structure, for example, size, orientation, and morphologies with the electronic properties of TiO_2 nano materials is essential for the possible exploitation of photosensitivity [103]. The bi-phase oxides with a high photochemical activity can be prepared by diverse routes, including phase alteration of amorphous or anatase TiO_2 into rutile at high temperatures [104] deposition of anatase onto rutile or visa-versa [105] and physical mixing of two oxides in a specific solvent [106]. Degussa P-25 is a mixture of anatase and rutile,

produced through flame hydrolysis of $TiCl_4$. This mixed oxide has an excellent photo activity and thus it is often used as a standard or reference for evaluation in new studies. Because anatase has a match able energy level with rutile, the charge transfer between two phases for the high activity of P-25 is proposed [107-109]. However, the direction of charge transfer from anatase to rutile, or from rutile to anatase, is still under debate [109].

In this investigation, the synergistic effect between anatase and rutile particles has been retraced for improving the photon absorption in visible region. Three TiO_2 nanocomposite samples with different proportions of anatase and rutile phases have been prepared and characterized. Further, these nanocomposites are analyzed for their absorptions in visible region and DSSC performance.

5.3.2 Results and discussions

5.3.2.1 Thermal analysis

The thermal analysis of the 'as synthesised' samples after milling for 2 hours was carried out to see the phase changes that are taking place during heating. Figure 5.27 shows the thermal analysis data from room temperature to 1000 ^oC.Three distinct exothermic peaks are seen at 270^oC, 500^oC and 673^oC, in DTA plot.

These exothermic peaks confirm the transformations where the energy is given out from the system. At 270^oC the peak denotes the release of adsorbed water molecules. At higher temperatures first phase transformation seems to take place from 400^oC to 538^oC, which shows the formation of anatase phase (corresponding to 2nd peak temperature 500^oC).

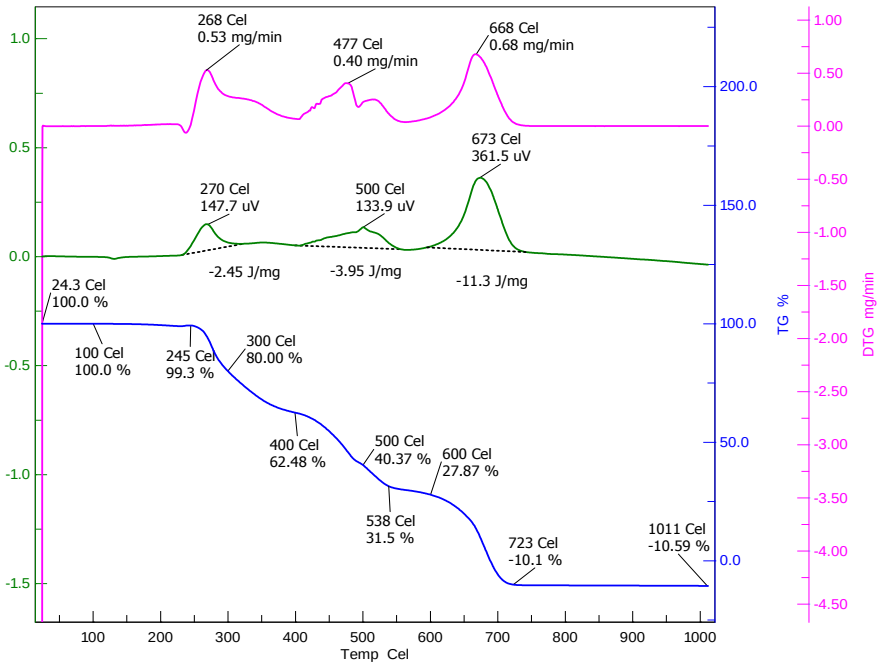

Figure 5.27: DTA/TG curve of dried TiO_2 powder room temperature to 1000^oC in air.

The 3rd peak which is between 600^oC to 723^oC with the peak temperature 673^oC corresponds to the phase transformation of rutile. All these three transformations give rise to the weight loss of about 19%, 22%, 17%, respectively. The first weight loss is due to the evaporation of water from the sample and the next two peaks are due to the phase transformations associated with weight losses. It is seen that the formation of anatase phase occurs below 500^oC and rutile phase below 673^oC. This is confirmed by the XRD analysis as given in Figure 5.33 when the samples are heat treated at 200, 400 and 600^oC it is observed different phase concentrations are present.

5.3.2.2 Field Emission Scanning Electron Microscopy (FESEM) images

The morphology of the TiO_2 synthesized and heat treated are examined by FESEM. No distinct particles could be identified before heat treatment. After heat treatment, due to structural and phase changes, distinct morphology of particles could be identified. FESEM micrographs shown in Figure 5.30 (a-c), illustrate that the grain sizes increase at higher heat treatment temperatures.

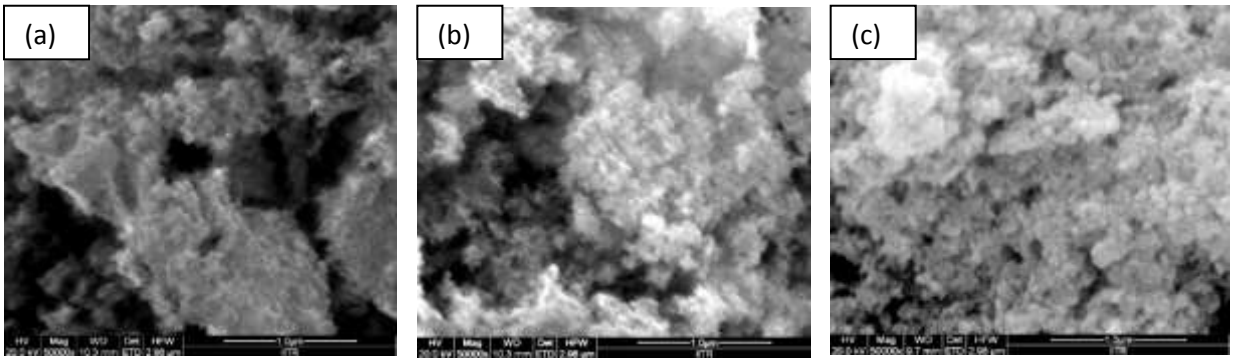

Figure 5.28: FESEM micrographs of heat treated TiO_2 for 2 h at different temperatures, (a) 200ºC, (b) 400ºC and (c) 600ºC.

The increase in grain size and density is particularly significant in samples heat treated at 400 and 600°C. Agglomeration is evident in all samples. A considerable amount of porosity is prevalent in all samples, with larger pores visible in the well strengthened agglomerates in the powders fired at 400 and 600°C. The samples exhibit less agglomeration, with a loosely packed porous structure retained after firing at 600°C (Figure 5.28 (c)). At higher magnification, (Figure 5.29) particles are seen to have different sizes of bigger nanoparticles. It could be due to Osward ripening and due to the different phases like anatese and rutile present in nanocomposite [110].

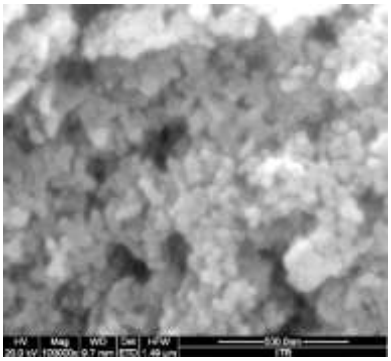

Figure 5.29: FESEM images of TiO_2 sample heat treated at 600^oC at higher magnification.

5.3.2.3 Transmission electron microscopy (TEM) analysis

TEM micrographs of TiO_2, heat treated for 2 hours at 600^oC are shown in Figures 5.30 (a and b). Some grains, as big as 20 nm where as others as small as 5 nm, are observed. The spectroscopic data are consistent with the HR-TEM data and indicate that unusually small rutile crystallites are interwoven with anatase crystallites to facilitate the efficient electron transfer at the anatase/rutile interface [110].

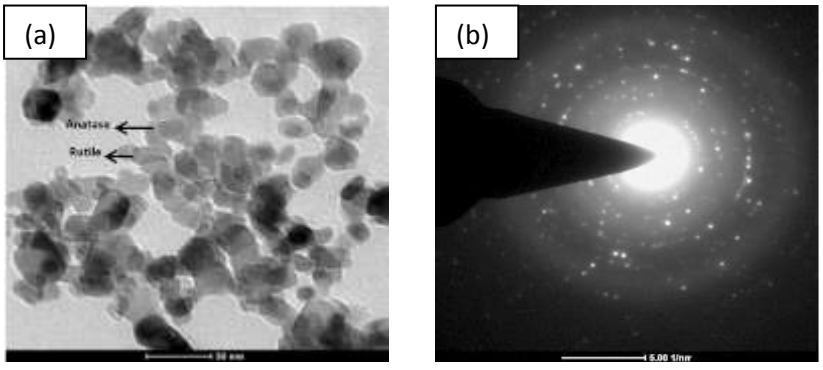

Figure 5.30: TEM images of TiO_2 sample heat treated for 2 h at 600^oC

(a) Micrograph, (b) SAD pattern.

The SAD pattern shown in Figure 5.30 (b) shows a number of ring patterns having various diameters corresponding to different interplanar distances corresponding to anatase and rutile phases. On firing at higher temperatures the grain size observed by FESEM is approximately consistent with the crystallite size observed by TEM. It is known that crystalline grains of anatase TiO_2 are spherical, while rutile ones are of rod structure [111]. Clusters of rutile crystallites are observed in between anatase which is evident from TEM images in figure 5.30 (a). Rutile crystallites are comparatively elongated yet smaller than anatase crystallites.

5.3.2.4 X-ray diffraction (XRD) analysis

Figure 5.31 shows the XRD patters of TiO_2 in the 'as synthesised' and heat treated conditions. The 'as synthesised' specimen prepared by chemical route is identified by XRD as dihydrogen trititanate, $H_2O_7Ti_3$ (ICSD collection code, no-245891) with monoclinic crystal structure.

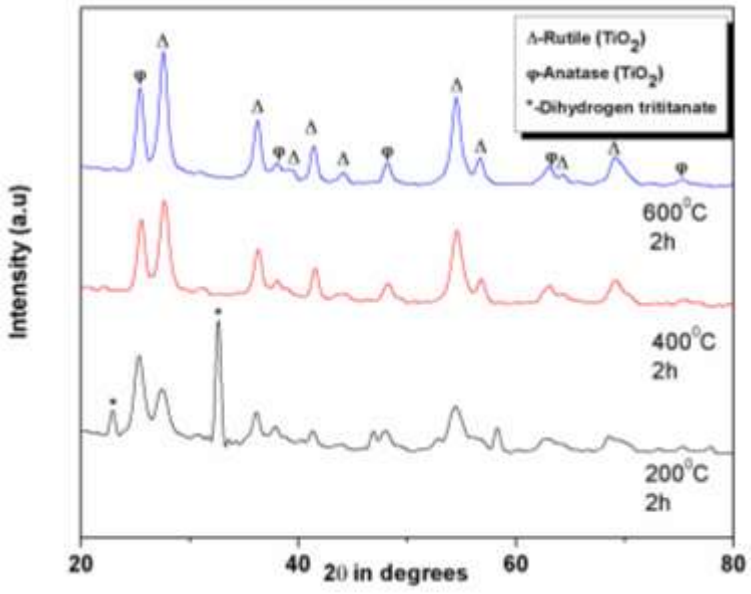

Figure 5.31: XRD patterns of heat treated TiO_2 powders for 2 h at 200, 400 and 600°C.

The highest peak at 32.66°C in plot of TiO_2 heat treated at 200°C confirms the presence of 88% of dihydrogen trititanate (Figure 5.31) and the grain size is calculated to be 52 nm. The remaining minor phases are identified as anatase ~2% and rutile ~10%. In plot of TiO_2 heat treated at 400°C the peak at 32.66°C diminished completely and phase transition of dihydrogen trititanate to titanium dioxide consisting rutile and anatase in a ratio of 50:50 was confirmed. From the third plot of TiO_2 heat treated at 600°C (Figure 5.31) the phases that could be identified are rutile and anatase. The mixture contained rutile (tetragonal) about 60% and anatase (tetragonal) about 40%. Rutile grains are of the size 15 nm which are calculated from the 2nd peak with 2Θ = 27.659, hkl = 110, (ICSD collection code no-202241) and the anatase (tetragonal) grains were found to have the size of 17 nm (calculated from the 1st peak at 2Θ = 25.504, hkl = 011, ICSD collection code no - 92363). The grain size that are calculated by Sherrer's formula from XRD data are smaller than the sizes seen from FESEM and TEM data in certain cases. This is because the grains (determined from XRD) are agglomerated to form particles which are observed under electron microscopes.

It is observed from XRD patterns that ratio of rutile to anatase crystallites increased consistently with increasing temperature. At 200°C rutile was 40% which increased to 50% at 400°C and became 60% at 600°C. Extended firing durations at narrower temperature intervals are required for a more accurate approximation of the phase transformation [112].

5.3.2.5 Optical absorption and optical band gap analysis

The UV-vis spectra of the nano-sized TiO_2 powders, shown in figure 5.32 were obtained to determine the relationship between the solar energy conversion efficiency and spectroscopic properties. The absorption band for the tetrahedral symmetry of Ti^{4+} normally appeared at approximately 300-700 nm. TiO_2 absorbed appreciably at wavelengths less than

700 nm which covers a wide range in visible region of spectra. The intensity of the absorption peaks are found to be increased with the increasing heat treatment temperatures.

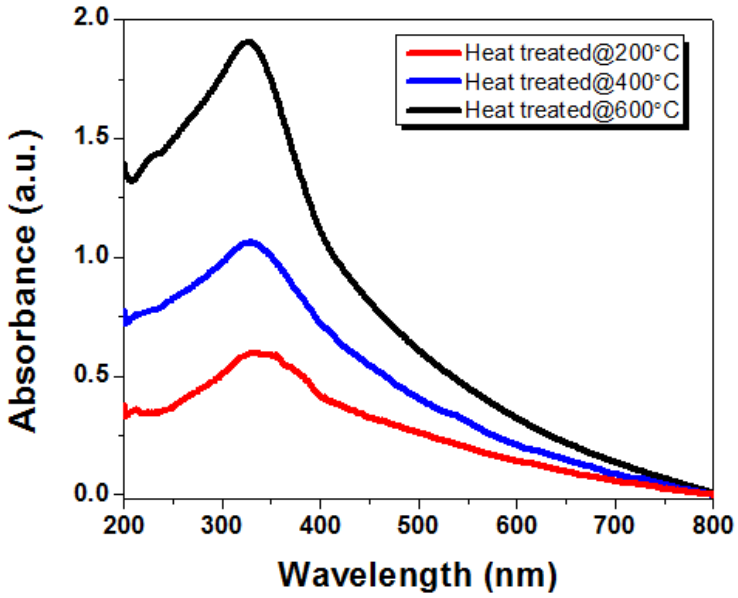

Figure 5.32: Optical absorption of TiO_2 samples heat treated for 2 hours at 200, 400 and 600°C.

Optical band gap energies of samples heat treated at 200, 400 and 600°C were calculated as 2.88, 2.81 and 2.59 eV, respectively. It is observed that with rise in firing temperature and consequently increased rutile to anatase ratio, the optical band gap energy decreased. Smaller band gap of rutile extends the useful range of photo-activity into the visible region due to the increase of rutile phase with a smaller band gap of 3.0 eV than that of anatase phase (3.2 eV). Contrary to this, Degussa P-25 has band-gap energy of 3.1 eV and crystallite sizes are in the range of 100-150 nm [113].

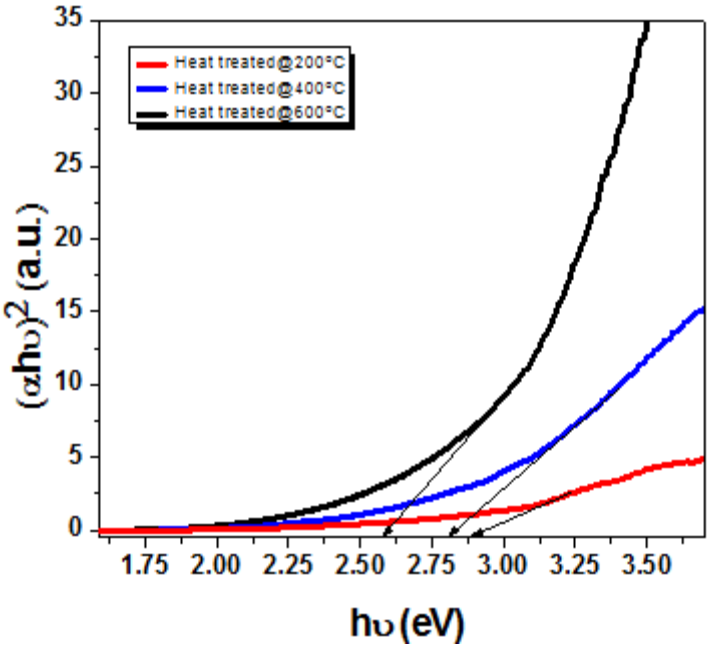

Figure 5.33: Optical band gap of TiO_2 samples heat treated for 2 hours at 200, 400 and 600°C.

The band gap energies are calculated by plotting $(\alpha h\upsilon)^2$ vs. $h\upsilon$ as in Figure 5.33. The band gaps in a semiconductor material are closely related to the wavelength range absorbed, where the absorption wavelength decreases with increasing band gap. It is well known that when light is absorbed by a dye molecule, electrons on the HOMO orbital are excited to an electronically excited state, LUMO orbital. The electrons are then transferred to the conduction band of TiO_2. With TiO_2 NPs having a short band gap, it is easier to move excited electrons from the valence band to the conduction band on the surface [114].

5.3.2.6 DSSC device

Three types of DSSC devices were prepared by TiO_2 nanoparticles heat treated at 200, 400 and 600°C and coded as D1, D2 and D3, respectively. Mixed-phase TiO_2 shows

greater photo-effectiveness due to smaller band gap of rutile nanoparticles and the stabilization of charge separation.

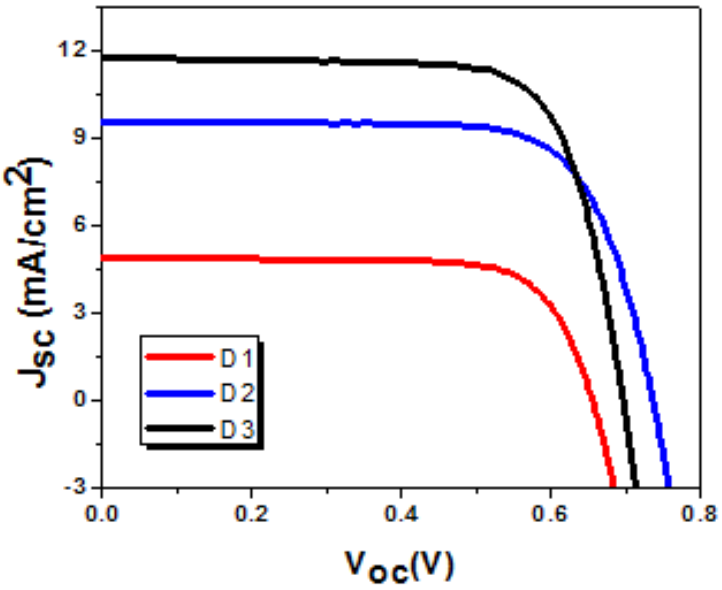

Figure 5.34: The current-voltage (*I-V*) characteristics of DSSCs fabricated by samples heat treated at 200ºC (D1), 400ºC (D2) and 600ºC (D3).

Table 5.11: *I-V* specific parameters of DSSC fabricated by TiO_2 heat treated at 200ºC, 400ºC and 600ºC for 2 hours each.

DSSC	J_{sc} (mA/cm^2)	V_{oc} (V)	*FF* (%)	η (%)
D1	4.85	0.73	76.03	2.69
D2	9.54	0.74	73.68	5.18
D3	11.76	0.70	74.31	6.08

Slow recombination due to electron transfer from rutile to anatase and active hot spots created at the rutile/anatase interface also play a significant part in the process [115].

The *I-V* curves of DSSCs prepared by TiO_2 nanoparticles heat treated at 200, 400 and 600ºC sensitized by N-719 are shown in Figure 5.34 and *I-V* parameters are given in Table 5.11. From the voltage and current intensity values recorded in the *I-V* curves the photovoltaic characteristics of the cells were calculated. The parameters calculated were open-circuit voltage (V_{oc}), short-circuit current density (J_{sc}), fill factor (*FF*) and efficiency (η). It is observed that there is a constant amplification in J_{sc} and η of the DSSCs fabricated by TiO_2 nanoparticles heat treated at higher temperatures. The J_{sc} has increased from 4.85 to 11.76 mA/cm^2 from device D1 to D3 and overall efficiency has improved from 2.69 to 6.08% from device D1 to D3. It can be credited to lower spatial confinement and much higher movements of free electrons in anatase due to which the chances of electrons returning to rutile once transferred to anatase are diminished [116]. The reduced probability of recombination of excited electrons and holes led to an increase in the short-circuit current (J_{sc}) since the stabilization of charge separation by electron shift from rutile to anatase slows recombination during the operation of the DSSCs [115].

The V_{oc} dropped considerably from 729 to 696 mV and *FF* from 76.03 to 74.31% from device D1 to D3 with the increase in rutile content in mixed phase DSSCs. Since the V_{oc} of DSSCs is dependent on the difference between the flat band potential of TiO_2 and the redox potential of the iodide-tri iodide couple [117] and decreases with decreased band gap of TiO_2, a sudden drop in V_{oc} was observed in device D3 which was fabricated by TiO_2 with the lowest band gap energy. This result was found to be in harmony with the calculated band gap energies. The incident photon to current conversion efficiency (IPCE) of the DSSC was plotted as a function of excitation wavelength which is shown in Figure 5.35. Three solar cells i.e. D1, D2 and D3, show strong photoelectric response to visible light ranged from 300

to 800 nm, and the highest External quantum efficiency (EQE) of 40.30% was obtained at 520 nm by the solar cell based on TiO_2 heat treated at 400ºC and 600ºC. The IPCE value in ultraviolet range is mainly caused by the strong absorption of TiO_2, since TiO_2 has an absorption peak around 350 nm for the direct band gap photo-electron excitation [118].

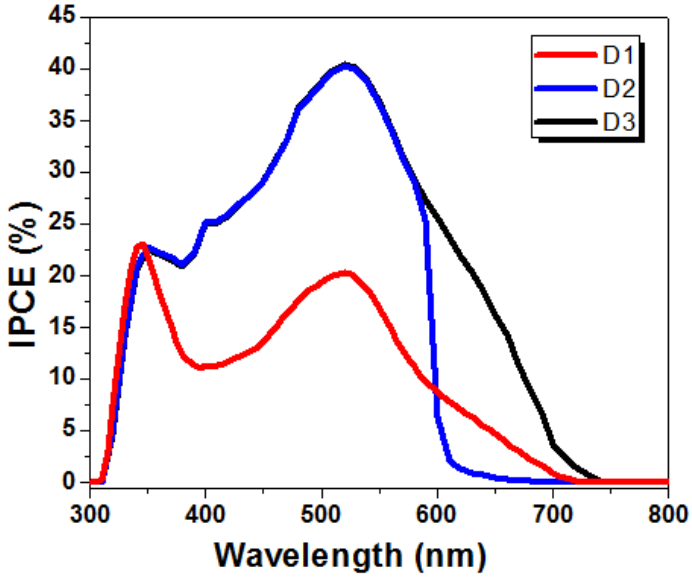

Figure 5.35: IPCE plots of DSSCs fabricated by samples heat treated at 200ºC (D1), 400ºC (D2) and 600ºC (D3).

The EQE was observed to be 20.18% at 525 nm in case of solar cell based on TiO_2 heat treated at 200ºC, i.e., D1, which is the lowest of all the devices fabricated. Devices D2 and D3 showed same EQE values but the absorption range covered in case of D2 is 300-630 nm which is less than the absorption range covered in case of D3 i.e. 300-720 nm. This 100 nm extension of wavelength in visible region is one of the reasons of better performance of device D3 over device D2. Li *et.al*. studied the effect of different quantity of rutile content mixed with anatase TiO_2 on the photovoltaic performance when used as photoanode in

DSSCs in conjunction with N-719. It was demonstrated by optical analysis of the sensitized photoanodes that the absorption edge was shifted more towards visible region as the concentration of rutile was increased. The specific surface area was found to be increased in the same manner, i.e., with increased amount of rutile, which ascertains the increased amount of dye adsorbed. Hence, rutile phase proved to be beneficial for higher dye loading when used in photoanode of DSSCs [116, 178].

5.3.3 Experimental

5.3.3.1 Synthesis of TiO_2 Nanocomposite powders

Nano particles of TiO_2 are synthesised by sol-gel method. The reagent titanium trichloride ($TiCl_3$), mixed in distilled water was subjected to stirring for 15 min at room temperature. Ammonia solution was added to the mixture drop wise to attain the pH of 7 at room temperature. The reaction mixture started forming a thick gel. After 16 hours of continuous stirring at room temperature more ammonia solution was added drop wise at room temperature. The initial purple colour of gel was converted into white colour. The white gel was dried at 100ºC for 24 hours to remove physically adsorbed water, followed by milling for 2 hours in high energy planetary ball mill at 200 rpm with balls to powder ratio of 5:1, which resulted in nanopowder.

5.3.3.2 Heat treatment

The dried and milled powder was placed in opaque alumina crucibles and calcined (atmosphere-air) in a muffle furnace in the temperature range of 200ºC to 600ºC. The heat treatment time was kept 2 hours and the temperatures identified for three different samples are, 200ºC, 400ºC and 600ºC.

5.3.3.3 Preparation of photo anode and Fabrication of DSSCs

10% of ethyl cellulose in ethanol and α-terpinol were added to TiO_2 powder, diluted by adding more ethanol and ultrasonicated, to avoid lumps formation. Solvent was evaporated at low pressure. After cleaning and drying FTOs, a compact TiO_2 blocking layer was chemically deposited onto the conducting surface of FTO by immersing it in a 0.04 M $TiCl_4$ aqueous solution at 70ºC for 30 mins. Nano-porous TiO_2 films were developed on the blocking layer by screen printing colloidal TiO_2 paste. Three consequent layers were screen printed followed by annealing each time. 'As coated' substrate was sintered on hot plate for 1 hour 45 mins. at different temperatures ranging from 125ºC to 500ºC, and cooled to 80°C. The TiO_2 film was opaque and the thickness was measured as 18 μm. After carrying out post $TiCl_4$ treatment, the film was annealed at 450ºC for 15 min. After cooling down to 80ºC, it was immersed into 0.3 mmol of N-719 dye solution in 1:1 acetonitrile and valeronitrile for overnight time period.

For making counter electrodes, conical holes were drilled on FTOs by sandblaster. Drilled FTOs were washed with 0.1 M HCl aqueous solution and ultrasonicated in acetone. Further 4.8 mM chloroplatinic acid solution in ethanol was used as platinum precursor and deposited on FTO by drop casting method. It was annealed at 450°C for 15 minutes to have better adhesion. Both the electrodes were clubbed together by a 25 μm thick surlyn spacer. The cells were filled with electrolyte solution through a predrilled hole in the counter electrode and the whole assembly was sealed with surlyn polymer and cover slip, by hot pressing. Finally, the cells were soldered to connect to the external circuit. The cells made in such a way have an active area of 0.16 cm^2.

5.4 CONCLUSION

In conclusion, a series of novel D-(π-A)$_4$ dyes with branched side chain substituted on nitrogen and elongated π-bridges at different substitution positions of carbazole, capped by cyanoacrylic acids were synthesized and applied on DSSCs effectively. Elongation of π-bridge explicitly shifted the absorption maxima from 384 nm to 465 nm and widened the coverage from 300 to 570 nm in visible spectrum. HOMO and LUMO levels of the all synthesized dyes (P1, P2, P3, P4 and P5) were observed well aligned for efficient electron injection and charge transportation in DSSCs. This chapter evidently reveals that the excessive thickness of the TiO_2 film is unfavorable for the DSSC performance owing of the electron recombination. Longer dye loading time can cause the formation of over layer of dye molecules which hinders the proper electron generation. Charge recombination and aggregation of dye on TiO_2 film are found to be restrained in the presence of binary additive and enhanced efficiency is achieved. Therefore, optimizing the cell efficiency requires close integration of every component within the DSSC system.

The surface morphologies of all sensitized films were analyzed by AFM and correlated with the photovoltaic performance of DSSCs fabricated by this series of tetra anchoring dyes. AFM images of sensitized TiO_2 thin films clearly indicate the reduction of aggregation caused by bulky periphery due to bithiophene linker present four sides of one carbazole core. The effect of step wise cosensitization on dye aggregation and optical properties of cosensitized TiO_2 film has been studied. The correlation of enhanced morphological and optical properties of photoanode with the photovoltaic performance of the DSSCs has been elaborated here. In this study five of the tetraanchoring organic dyes are used as principal dyes in conjunction with indoline dye D-205. It is observed that

cosensitization caused reduction of aggregates in all the films is the major influential factor for higher packing density of the dyes on the film surface which is responsible for the enhanced efficiencies of DSSCs. The highest efficiency achieved in this study is 4.1% which is more than the efficiencies obtained by separately sensitized photoanodes of principal dyes (P1-P5) and D-205 under the identical conditions.

This chapter also reveals the significance of different firing temperatures on the phase composition of TiO_2 NPs, effect of different composition of phases in bi phase semiconductor's optical band gap and consequent influence on the photovoltaic performance of DSSCs. The presence of rutile NPs is proved favorable in reducing the band gap of semiconductor. The optical band gap values are found to be in the range of 2.59-2.88 eV. The DSSCs fabricated by TiO_2 nanoparticles, heat treated at 600^{o}C show the energy conversion efficiency (η) of 6.08% with high photo current density (J_{sc}) of 11.76 mA/cm^2. The DSSC performance was found to be better than that of P-25 device [114] which is the similar mixed phase TiO_2 with a composition of 25% rutile and 75% anatase.

References

1. Zhang, G. L. B., Wang, H., Cheng, Y. M., Shi, D., Lv, X. J., Yu, Q. J., (2009), "High efficiency and stable dye-sensitized solar cells with an organic chromophore featuring a binary - conjugated spacer", P. Chem. Commun., pp. 2198-2200.

2. Ning, Z., Wu, W. J., Pei, H. C., Liu, B., Tian, H., (2008), "Starburst Triarylamine Based Dyes for Efficient Dye-Sensitized Solar Cells", J. Org. Chem., vol. 73, pp. 3791-3797.

3. Ooyama, Y., Yutaka, H., (2009), "Molecular Designs and Syntheses of Organic Dyes for Dye-Sensitized Solar Cells", Eur. J. Org. Chem., vol. 18, pp. 2903-2934.

4. Zeng, W. C., Wang, Y., Bai, Y., Wang, Y., Shi, Y., Zhang, M., Wang, F., Pan, C., (2010), "Efficient Dye-Sensitized Solar Cells with an Organic Photosensitizer Featuring Orderly Conjugated Ethylenedioxythiophene and Dithienosilole Blocks", P. Chem. Mater., vol. 22, pp. 1915-1925.

5. Thomas, K. R. J., Singh, P., Baheti, A., Ying-Chan, H., Kuo-Chuan, H., Jiann, T. L., (2011), " Electro-optical properties of new anthracene based organic dyes for dye-sensitized solar cells", Dyes and Pigments., vol. 91, pp. 33-43.

6. Jung-Kun, L. M., Lee, J. K., Yang, M., (2011), "Progress in light harvesting and charge injection of dye-sensitized solar cells", Materials Science and Engineering., vol. 176, pp. 1142- 1160.

7. Thavas, V. R., Jose, R., Ramakrishna, S., (2009), "Controlled electron injection and transport at materials interfaces in dye sensitized solar cells", Mater. Sci. Eng. R., vol. 63, pp. 81-99, (b) Mishra, A., Fischer, M. K. R., Bäuerle, P., (2009), "Metal-Free Organic Dyes for Dye-Sensitized Solar Cells: From Structure: Property Relationships to Design Rules", Angew. Chem., Int. Ed., vol. 48, pp. 2474-2499.

8. Teng, C. Y., Chunze, Y., Li, C., Chen, R., Tian, H., Li, S., Hagfeldt, A., Sun, L., (2009), "Two Novel Carbazole Dyes for Dye-Sensitized Solar Cells with Open-Circuit Voltages up to 1 V Based on Br^-/Br_3^- Electrolytes", Org. Lett., vol. 11(23), pp. 5542-5545.

9. Tian, H. A., Chen, R., Zhang, R., Hagfeldt, A., Sun, L., (2008), "Effect of Different Dye Baths and Dye-Structures on the Performance of Dye-Sensitized Solar Cells Based on Triphenylamine Dyes", J. Phys. Chem. C , vol. 112, pp. 11023-11033.

10. Srinivas, K. R., Ananth, R. M., Bhanuprakash, K., Jayathirtha, R. V., (2011), "D-π-A Organic Dyes with Carbazole as Donor for Dye-Sensitized Solar cells", Synth Met, vol. 161, pp. 96-105.

11. Venkateswararao, A., Thomas, K. R. J., Lee, C. P., Ho, K. C., (2013), "Synthesis and characterization of organic dyes containing 2, 7-disubstituted carbazole π-linker", Tetrahedron Letters, vol. 54, pp. 3985-3989.

12. Koumura, N. W., Wang, Z. S., Mori, S., Miyashita, M., Suzuki, E., Hara, K., (2006), "Alkyl-Functionalized Organic Dyes for Efficient Molecular Photovoltaics", J. Am. Chem. Soc., 128, 14256-14257.

13. Lai, H., Hong, J., Liu, P., Yuan, C., Li, Y., Fang, Q., (2012), "Multi-carbazole derivatives: new dyes for highly efficient dye-sensitized solar Cells", RSC Adv., vol. 2, pp. 2427-2432.

14. (a) Kim, M. S., Yang, H.S., Jung, D.Y., Kim, J.H., Han, Y. S., (2013), "Effects of the number of chromophores and the bulkiness of a nonconjugated spacer in a dye molecule on the performance of dye-sensitized solar cells", Colloids and Surfaces A: Physicochemical and Engineering Aspects, vol. 420, pp. 22-29. (b) Liu, D., Zhao, B., Shen, P., Huang, H., Liu, L. and Tan, S., (2009), "Molecular design of organic dyes based on vinylene

hexylthiophene bridge for dye-sensitized solar cells", Sci. China Ser. B-Chem., Vol. 52, pp. 1198-1209.

15. Gupta, V. D., Padalkar, V. S., Phatangare, K. R., Patil, V.S.; Umape, P. G., Sekar, N., (2011), "The synthesis and photo-physical properties of extended styryl fluorescent derivatives of N-ethyl carbazole", Dyes and Pigments, vol. 88, pp. 378-384.

16. Gupta, K. S. V., Suresh, T., Singh, S. P., Islam, A., Han, L., Chandrasekharam, M., (2014), "Carbazole based A-π-D-π-A dyes with double electron acceptor for dye-sensitized solar cell", Organic Electronics, vol. 15, pp. 266-275.

17. Heredia, D. N., Gervaldo, M., Otero, L., Fungo, F., Lin, C.Y., (2010), Organic Letters, vol. 1212(1), pp. 12-15.

18. Liu, Y. W., Niu, F. F., Lian, J. R., Zeng, P. J., Niu, H. B., (2010), "Synthesis and properties of starburst amorphous molecules: 1,3,5-Tris(1,8-naphthalimide-4-yl)benzenes", Synth.Met., vol. 160, pp. 2055-2060.

19. Duan, L. H., Lee, T. W., Qiao, J., Zhang, D. Q., Dong, G. F., Wang, L. D., Qiu, Y. J., (2010), "Solution processable small molecules for organic light-emitting diodes", Mater. Chem., vol. 20, pp. 6392-6407.

20. Ooyama, Y., Harima, Y., (2009), "Molecular Designs and Syntheses of Organic Dyes for Dye-Sensitized Solar Cells", Eur. J. Org. Chem., vol. 2009, pp. 2903-2934; (b) Koumura, N., Wang, Z., Miyashita, M., Uemura,Y., Sekiguchi, H., Cui, Y., Mori, A., Mori, S., Hara, K., (2009), "Substituted carbazole dyes for efficient molecular photovoltaics: long electron lifetime and high open circuit voltage performance", J. Mater. Chem., vol. 19, pp. 4829-4836.

21. Niu, F. N., Liu,Y., Lian, J., Zeng, P., (2011), "Synthesis, characterization and application of starburst 9-alkyl-1, 3, 6, 8-tetraaryl-carbazole derivatives for blue-violet to UV OLEDs", RSC Adv., vol. 1, pp. 415-423.

22. Fu, H., Wu, H., Hou, X., Xiao, F., Shao, B., (2006), "N-Aryl carbazole derivatives for non-doped red OLEDs", Synth Met, vol. 156, pp. 809-814.

23. Mishra, A., Fischer, M. K. R., Bäuerle, P., (2009), "Metal-Free Organic Dyes for Dye-Sensitized Solar Cells: From Structure: Property Relationships to Design Rules", Angew. Chem. Int. Ed., vol. 48, pp. 2474.

24. Srinivas, K., Ramesh, K. C., Ananth, R. M., Bhanuprakash, K., Jayathirtha, R. V., (2011), "D-π-A organic dyes with carbazole as donor for dye-sensitized solar Cells", Synth Met, vol. 161, pp. 96-105.

25. Yang, C. H., Liao, S. H., Sun, Y. K., Chuang, Y. Y., Wang, T. L., Shieh, Y. T. and Lin, W. C., (2010), J. Phys. Chem. C, Vol. 114, No. 49, pp. 21787.

26. Gupta, V. D., (2011), "The synthesis and photo-physical properties of extended styryl fluorescent derivatives of N-ethyl carbazole", Dyes and Pigments, vol. 88, pp. 378-384.

27. (a) Kim, S., Lee, J. K., Kang, S. O., Ko, J., Yum, J. H., Fantacci, S., De Angelis, F., Di Censo, D., Nazeeruddin, M. K., Grätzel, M., (2006), "Molecular Engineering of Organic Sensitizers for Solar Cell Applications", J. Am.Chem. Soc., vol. 128, pp. 16701- 16707. (b) Liang, M., Xu, W., Cai, F., Chen, P., Peng, B., Chen, J., Li, Z., (2007), "New Triphenylamine-Based Organic Dyes for Efficient Dye-Sensitized Solar Cells", J. Phys. Chem. C, vol. 111(11), pp. 4465-4472. (c) Xu, W., Peng, B., Chen, J., Liang, M., Cai, F., (2008), "New Triphenylamine-Based Dyes for Dye-Sensitized Solar Cells", J. Phys. Chem. C, vol. 112, pp. 874-880. (d) Hagberg, D. P., Yum, J. H., Lee, H., De Angelis, F., Marinado,

T., Karlsson, K. M., Humphry-Baker, R., Sun, L., Hagfeldt, A., Grätzel, M., Nazeeruddin, M. K., (2008), "Molecular Engineering of Organic Sensitizers for Dye-Sensitized Solar Cell Applications", J. Am. Chem. Soc., vol. 130, pp. 6259-6266.

28. Hara, K., Danoh, Y., Kasada, C., Shinpo, A., Suga, S., Arakawa, H., Sugihara, H., (2005), "Photophysical and (Photo) electrochemical Properties of a Coumarin Dye", J. Phys. Chem. B, vol. 109, pp. 3907-3914.

29. Hagfeldt, A., Grätzel, M., (1995), "Light-Induced Redox Reactions in Nanocrystalline Systems", Chem. ReV., vol. 95, pp. 49-68.

30. Guo, Y., Lee, N. H., Oh, H. J. (2008), "Preparation of titanate nanotube thin film using hydrothermal method", Thin Solid Films, vol. 516, 23, pp. 8363-8371.

31. Fitra, M., (2013), "Effect of TiO_2 Thickness Dye Solar Cell on Charge Generation", Energy Procedia, vol. 36, pp. 278-286.

32. Sayama, K., Tsukagoshi, S., Hara, K., Ohga, Y., Shinpou, A., Abe, Y., Suga, S., Arakawa, H., (2002), "Photoelectrochemical properties of J aggregates of benzothiazolemerocyanine dyes on a nanostructured TiO_2 film.Journal of Physical Chemistry", Vol. 106(6), pp. 1363-1371.

33. Kay, A., Gratzel, M., (1993), "Artificial photosynthesis- Photosensitization of titania solar cells with chlorophyll derivatives and related natural porphyrins", Journal of Physical Chemistry, Vol. 97, pp. 6272-6277.

34. Yamada, Y., Imahori, H., Nishimura, Y., Yamazaki, I., Fukuzumi, F., (2000), "Remarkable Enhancement of Photocurrent Generation by ITO Electrodes Modified with Self-Assembled Monolayer of Porphyrin", Chemical Communication, pp.1921-1922.

35. Imahori, H., Nishimura, Y., Yamazaki, I., Higuchi, K., Kato, N., Motohiro, T., Yamada, H., Tamaki, K., Arimura, M., Sakata, Y., (2000), "Chain Length Effect on the Structure and Photoelectrochemical Properties of Self-Assembled Monolayers of Porphyrins on Gold Electrodes", Journal of Physical Chemistry,Vol. 104, pp.1253-1260

36. Anikin, M., Tkachenko, N. V., Lemmetyinen, H., (1997), "Arrangement of Hydrophobically Shielded Porphyrin, 5, 10, 15, 20-tetrakis(3,5 di-tertbutylphenyl)porphyrin, in Octadecylamine L. B Multilayers", Langmuir, vol. 13 (11), pp. 3002-3008.

37. Wang, Z. S., Yamaguchi, T., Sugihara, H. and Arakawa, H., (2005), "Significant Efficiency Improvement of the Black Dye-Sensitized Solar Cell through Protonation of TiO_2 Films", Langmuir, American chemical society, Vol. 21, Issue.10, pp. 4272-4276.

38. Baxter, J. B. and Aydil, E. S., (2005), "Nanowire-based dye-sensitized solar cells", Applied Physics Letter, vol. 86, pp. 53114-53116.

39. Nazeetuddin, M. K., Grätzel, M., (1993), "Conversion of light to electricity by cis-X_2bis(2,2'-bipyridyl-4,4'-dicarboxylate)ruthenium(II) charge-transfer sensitizers (X = Cl-, Br-, I-, CN-, and SCN-) on nanocrystalline titanium dioxide electrode", Journal of American Chemical Society Vol. 115, PP. 6382-6390.

40. Kusama, H., Arakawa, H., (2004), "Influence of alkylaminopyridine additives in electrolyte on dye-sensitized solar cell performance", Solar Energy Materials & Solar Cells, Vol. 81, pp.87-99.

41. Kusama, H., Arakawa, H., (2004), Sol. Energy Mater. Sol. Cells, vol. 82, pp. 457.

42. Kusama, H., Arakawa, H., (2004), "Influence of aminotriazole additives in electrolytic solution on dye-sensitized solar cell performance", J. Photochemistry & Photobiology, A: Chem., vol.164, pp.103-110.

43. (a) Marinado, T., Hagberg, D. P., Hedlung, M., Edvinsson, T., Johansson, E. M. J., Boschloo, G., Rensmo, H., Brinck,T., Sun, L., Hagfeldt, A., (2009), "Rhodanine dyes for dye-sensitized solar cells : spectroscopy, energy levels and photovoltaic performance", Physical Chemistry Chemical Physics, Vol.11, pp.133-141.

44. Marinado, T., Hagberg, D. P., Hedlung, M., Edvinsson, T., Johansson, E. M. J., Boschloo, G., Rensmo, H., Brinck, T., Sun, L. and Hagfeldt, A., (2009), "Rhodanine dies for dies sensitized solar cell:spectroscopy, energy level and photovoltaic performance", Phys. Chem. Chem. Phys, Vol.11, pp.133-141.

45.Dembele, A., Rahman, M., MacElroy, J. M. D., Dowling, D. P., (2012), "Evaluation of Microwave Plasma Sintering for the Fabrication of Dye Sensitized Solar Cell (DSSC) Electrodes", Journal of Nanoscience and Nanotechnology, vol.12 (6), pp.4769-4774.

46. Alibabaei, L. K., Wang, M., Pootrakulchote, N., Teuscher, J., Di Censo, D., Humphry-Baker, R., Moser, J. E., Yu, Y. J., Kay, K. Y., Zakeeruddin, S. M., Grätzel, M., (2010), "Molecular design of metal-free D-π-A substituted sensitizers for dye-sensitized solar cells", Energy Environ. Sci, vol. 3, pp. 1757-1764.

47. Grätzel M, (2005), "Solar energy conversion by dye-sensitized photovoltaiccells.InorganicChemistry", Vol. 44, pp. 6841-6851.

48. Nazeeruddin, M. K., Péchy, P., Renouard, T., Zakeeruddin, S. M., Humphry-Baker, R., Comte, P., (2001), "Engineering of efficient panchromatic sensitizers for nanocrystalline TiO_2-based solar cells", Journal of American Chemcal Society, Vol. 123, pp.1613-1624.

49. Yella, A., Lee, H. W., Diau, E. W. G., Yeh, C. Y., Zakeeruddin, S. M., Grätzel, M., (2011), "Porphyrin-sensitized solar cells with cobalt (II/III)-based redox electrolyte exceed 12 percent efficiency", Science, Vol. 334, pp. 629-634.

50. Roncali, J., (2007), "Molecular Engineering of the Band Gap of π-Conjugated Systems: Facing Technological Applications.Macromolecular", Rapid Communication, Vol. 28, pp. 1761-1775.

51. Seo, K. D., You, B. S., Choi, I. T., Ju, M. J., Youb, M., Kang, H. S., Kim, H. K., (2013), "Dual-channel anchorable organic dye with triphenylamine-based corebridge unit for dye-sensitized solar cells", Dyes and Pigments, Vol. 99, pp. 599-606.

52. Namuangruk, S., Fukuda, R., Ehara, M., Meeprasert, J., Khanasa, T., Morada, S., Kaewin, T., Jungsuttiwong, S., Sudyoadsukand, T., Promarak, V., (2012), "D-D-π-A-Type Organic Dyes for Dye-Sensitized Solar Cells with a Potential for Direct Electron Injection and a High Extinction Coefficient: Synthesis, Characterization, and Theoretical Investigation", Journal of Physical Chemistry, Vol. 116, pp. 25653-25663.

53. Li, Q., Shi, J., Li, H., Li, S., Zhong, C., Guo, F., Peng, M., Hua, J., Qin, J. and Li, Z., (2012), "Novel pyrrole-based dyes for dye sensitized solar cells: from rod-shape to ''H'' type", Journal of Material Chemistry, Vol. 22, pp. 6689-6696.

54. Aljarilla, A., López-Arroyo, L., De la Cruz, P., Oswald, F., Meyer, T. B., Langa, F., (2012), "Organic Dyes Incorporating Oligothienylenevinylene for Efficient Dye-Sensitized Solar Cells", Organic Letter, 2012, Vol. 14, pp. 5732-5735.

55. Mba, M., D'Acunzo, M., Salice, P., Carofiglio, T., Maggini, M., Caramori, S., Campana, A., Aliprandi, A., Argazzi, R., Carli, S. and Bignozzi, C. A., (2013), "Sensitization of Nanocrystalline TiO_2 with Multibranched Organic Dyes and Co(III)/(II) Mediators: Strategies to Improve Charge Collection Efficiency", J. Phys. Chem. C, vol. 117, 19885-19896.

56. Ning, Z. J., Zhou, Y. C., Zhang, Q., Ma, D. G., Zhang, J. J., Tian, H., "Bisindolylmaleimide derivatives as non-doped red organic light-emitting materials", J. Photochem. Photobiol. A: Chem. 2007, vol. 192, pp. 8-16.

57. Koumura, N., Wang, Z. S., Mori, S., Miyashita, M., Suzuki, E., Hara, K., (2006), "Alkyl-Functionalized Organic Dyes for Efficient Molecular Photovoltaics", Journal of American Chemical Society, Vol. 128, pp. 14256-14257.

58. Chen, C.Y., Pootrakulchote, N., Wu, S. J., Wang, M., Li, J. Y., Tsai, J. H., Wu, C. G., Zakeeruddin, S. M., Grätzel, M., (2009), "New Ruthenium Sensitizer with Carbazole Antennas for Efficient and Stable Thin-Film Dye-Sensitized Solar Cells", Journal of Physical Chemistry C ,Vol. 113, pp. 20752-20757.

59. Samori, S., Tojo, S., Fujitsuka, M., Ryhding, T., Fix, A. G., Armstrong, B. M., Haley, M. M., and Majima, T., (2006), "Emission from regioisomeric bis(phenylethynyl)benzenes during pulse radiolysis", Journal of Organic Chemistry, Vol. 74, pp. 3776-3782.

60. Kauffman, J. F., Turner, J. M., Alabugin, I. V., Breiner, B. and Kovalenko, S. V., Badaeva, E. A., Masunov, A., Tretiak, S., (2006), "Two-photon excitation of substituted enediynes", Journal of Physical Chemistry, Vol. 110, pp. 241-251.

61. Stille, J. K., (1986), "The Mechanism of the Stille Reaction", Angew. Chem., Int. Ed, Vol. 25, pp. 508-524.

62. Knoevenagel, (1896), "Uebereine Dtarstellugwisedes Benzylidenecetessigesters", E. Chem. Ber, vol. 29, pp. 172-174.

63. Thomas, K. R. J., Hsu, Y. C., Lin, J. T., Lee, K. M., Ho, K. C., Lai, C. H., Cheng, Y. M., Chou, P. T., (2008), "Disubstituted Thiophene-Based Organic Dyes for Solar Cells", Chem. Mater. vol. 2, pp.1830-1840.

64. Yamaguchi, Y., Matsubara, Y., Ochi, T., Wakamiya, T., and Yoshida, Z. I., (2008), "How the π conjugation length affects the fluorescence emission efficiency", J. Am. Chem. Soc., vol. 130, pp.13867-13869.

65. J. M. Toussaint, J. L. Bredas, (1993), "Geometric and electronic structure of polydicyano methylene-cyclopenta-dicyclopentadiene, a conjugated polymer possessing a very small intrinsic band gap", Synth. Met. , vol. 61, pp. 103-106.

66. Hou, J., Park, M. H., Zhang, S., Yao, Y., Chen, L. M., Li, J. H. and Yang, Y., (2008), "Bandgap and energy level control of conjugate polymer photo voltaic material based on benzol", Macromolecules, Vol. 41, pp. 16.

67. Qu, S., Wu, W., Hua, J., Kong, C., Long, Y., Tian, H., (2010), "New diketopyrrolopyrrole (DPP) dyes for efficient dye-sensitized solar cells", J. Phys. Chem. C, vol. 114, pp. 1343-1349.

68. Dembele, A., Rahman, M., Mac Elroy, J. M., Dowling; D. P., (2012), "Evaluation of Microwave Plasma Sintering for the Fabrication of Dye Sensitized Solar Cell (DSSC) Electrodes", J Nanosci Nanotechnol, vol. 12(6), pp. 4769-4774.

69. Shelly, D., Shklover, B. V., Barbe, C., Comte, P., Arendse, F., Brooks, K., and Grätzel, M., (1998), "Self organization of TiO_2 nanoparticlesn thin films", Chem. Mater., vol. 10, pp. 2419-2425.

70. Chen, B. S., Chen, D. Y., Chen, C. L., Hsu, C. W., Hsu, H. C., Wu, K. L., Liu, S. H., Chou, P. T., Chi, Y., (2011), "Improvement of dye-sensitized solar cells toward the broader light harvesting of solar spectrum", J. Power Sources, vol. 196, pp. 4152 - 4161.

71. Nazeeruddin, M. K., Zakeeruddin, S. M., Humphry-Baker, R., Jirousek, M., Liska,

P., Vlachopoulos, N., Shklover, V., Fischer, C. H., Grätzel, M., (1999), "Acid-Base Equilibria of (2, 2'-Bipyridyl-4,4'-dicarboxylic acid)ruthenium(II) Complexes and the Effect of Protonation on Charge-Transfer Sensitization of Nanocrystalline Titania" , Inorg. Chem., vol. 38, pp. 6298-6305.

72. Agosta, R., Grisorio, R., De Marco, L., Romanazzi, G., Suranna, G. P., Giglia, G. and Manca, M., Name, J., (2014), "Iodopropyl-branched polysiloxane gelelectrolytes with improved ionic conductivity upon cross-linking", Chem. Commun.**,** vol. 50, pp. 13904-1390673.

73. Han, L., Islam, A., Chen, H., Malapaka, C., Chiranjeevi, B., Zhang, S., Yang, X., Yanagid, M., (2012), "High-efficiency dye-sensitized solar cell with a novel co-adsorbent", Energy Environ. Sci., vol. 5, pp. 6057-6060.

74. Bayliss, S. L., Cole, J. M., Waddell, P. G., McKechnie, S. and Liu, X., J., (2014), "Predicting Solar-Cell Dyes for Cosensitization", Phys. Chem. C, vol. 118 (26), pp. 14082-14090.

75. Zhanga, L., Yanga, Y., Fana, R., Wanga, P., Li, L., Zhang, L., (2012), "Enhance the performances of dye-sensitized solar cell by a new type of sensitizer to co-sensitize zinc oxide photoelectrode with ruthenium complex", Dyes and Pigments, Vol. 92, pp. 1314-13199

76. Magne, C., Urien, M., Pauportéa, T., (2013), "A highly efficient organic sensitizer for dye-sensitized solar cells", RSC Adv., vol. 3, pp. 6315-6318.

77. Hara, K., Dan-oh, Y., Kasada, C., Ohga, Y., Shinpo, A., Suga, S., Sayama K. and Arakawa, H., (2004), "Sensitizers of Dye-Sensitized Solar Cells", Langmuir, Vol. 20, pp. 4205-4210.

78. Shelly, D., Shklover, B. V., Barbe´, C., Comte, P., Arendse, F., Brooks, K. and Grätzel, M., (1998), "Self-Organization of TiO_2 Nanoparticles in Thin Films", Chem. Mater., Vol. 10, pp. 2419-2425.

79. Buerle, P., (2009), "Metal free organic dyes for dye sensitized solar cells", Angew. Chem. Int. Ed., vol. 48, pp. 2474-2499.

80. Hara, K., Dan-oh, Y., Kasada, C., Ohga, Y., Shinpo, A., Suga, S., Sayama, K., Arakawa, H., (2004), " A star-shaped sensitizer based on thienylenevinylene for dye-sensitized solar cells" , Langmuir, vol. 20, pp. 4205-4210.

81. Liu, D., Fessenden, R. W., Hug, G. L., Kamat, P. V., (1997), "Handbook of Nanostructured Materials and Nanotechnology", J. Phys. Chem. B, Vol. 3(101), pp. 2583.

82. Burfeindt, B., Hannappel, T., Storck, W., Willig, F., (1996), "Dye Sensitization of Nanocrystalline Tin Oxide by Perylene", J. Phys. Chem. , Vol. 100, pp. 16463-16465.

83. Hara, K., Dan-oh, Y., Kasada, C., Ohga, Y., Shinpo, A., Suga, S., Sayama, K., Arakawa, H., (2004), "A highly efficient organic sensitizer for dye-sensitized solar" , Langmuir, Vol. 20, pp. 4205-4210.

84. Luo, L., Lin, C., J., Tsai, C. Y., Wu, H. P., Li, L., Lo, C. F., Lin, C. Y. and Diau, E. W. G., (2010), "Effects of aggregation and electron injection on photovoltaic performance of porphyrin-based solar cells with oligo(phenylethynyl) links inside TiO_2 and Al_2O_3 nanotube arrays", Phys. Chem. Chem. Phys., Vol. 12, pp. 1064-1071.

85. Ooyama, Y. and Harima, Y., (2012), "Photophysical and Electrochemical Properties, and Molecular Structures of Organic Dyes for Dye-Sensitized Solar Cells", Chem Phys Chem, vol. 13, pp. 4032-4080.

86. Li, G., Jiang, K. J., Li, Y. F., Li, S. L., Yang, L. M., (2008), "Spirally configured cis-stilbene/fluorene hybrids as bipolar, organic sensitizers for solar cell applications", J. Phys. Chem. C., vol. 112, pp. 11591-11599.

87. Love, J. C., Estroff, L. A., Kriebel, J. K., Nuzzo, R. G. and Whitesides, G. M., (2005), "Electrochemical Sensors, Biosensors and their Biomedical Applications", Chem. Rev., Vol. 105, pp. 1103-1169.

88. Chappng, S., Wang, H., Hua, Y., Li, Q., Xiao, X., Wong, W. R., Zhu, X. and Chen, T., (2013), "Conformational engineering of co-sensitizers to retard back charge transfer for high-efficiency dye-sensitized solar cells", J. Mater. Chem. A, vol. **1**, pp. 11553-11558.

89. Fujishima, A., Honda, K., (1972), "TiO_2 photoelectrochemistry and photocatalysis" Nature, vol. 238, pp. 37.

90. Pardo, V., Pickett, W. E., (2009), "Half-Metallic Semi-Dirac-Point Generated by Quantum Confinementin", Phys. Rev. Lett., TiO_2/VO_2, Nano structures, vol. 102, pp. 166803.

91. Gratzel, M., (2001), "Photo electrochemical cells", Nature, vol. 414, pp. 338-344.

92. Li, Y., Somorjai, G. A., (2010), "Nano scale advances in catalysis and energy applications", Nano Lett., vol. 10, pp. 2289-2295.

93. Wang, G., (2007), "Hydrothermal synthesis and photocatalytic activity of Nanocrystalline TiO_2 powders in ethanol-water mixed solutions", Journal of Molecular Catalalyst A, Vol. 274, pp. 185-191.

94. Sahni, S., Reddy, B., Murty, B., (2007), "Influence parameters on the synthesis of nano-titania by sol-gel route", Mater Sci Eng A , vol. 452-453, pp. 758-62.

95. Riegel, G., Bolton, J. R., (1995), "Photocatalytic Efficiency Variability in TiO_2 Particles", J. Phys. Chem., vol. 99, pp. 4215-4224.

96. Deanna, C. H., (2003), "Explaining the enhanced photocatalytic activity of Degussa P25 mixed-phase TiO_2 using EPR", Journal of Physical Chemistry B., Vol. 107, No. 19, 4545-4549.

97. Choi, W., Termin, A. & Hoffmann, M. R. (1994), "The Role of Metal Ion Dopants in Quantum-Sized TiO_2: Correlation between Photoreactivity and Charge Carrier Recombination Dynamics", Journal of Physical Chemistry, vol. 98, pp. 13669-13679.

98. Khan, S. U. M., Al-Shahry, M., Ingler W. B., (2002), "Efficient photochemical water splitting by a chemically modified n-TiO_2", Jr. Science, vol. 297, pp. 2243-2245.

99. Mattesini, M., (2004), "Cubic TiO_2 as a potential light absorber in solar-energy conversion", Phys. Rev. B, vol. 70, pp. 115101.

100. Mo, S. D., Ching, W. Y., (1995), "Electronic and optical properties of three phases of titanium dioxide: Rutile, anatase, and brookite", Phys. Rev. B, Vol. 51, pp. 13023-13032.

101. Chen, C., Shi, Y., Zhang, Y., Zhu, J., Yan, Y., (2006), "Size Dependence of Young's Modulus in ZnO Nanowires", Phys. Rev. Lett., Vol. 96, pp. 075505.

102. Yang, H. G., Sun, C. H., Qiao, S. Z., Zou, J., Liu, G., Smith, S. C., Cheng, H. M., Cheng, H. M., Lu, G. Q. (2008), "Anatase TiO_2 single crystals with a large percentage of reactive facets", Nature, Vol. 453, pp. 638-641.

103. Yao, D., Zhang, G., Li, B., (2008), "A universal expression of band gap for silicon nanowires of different cross-section geometries", Vol. 8, pp. 4557-4561.

104. Sun, B., Vorontsov, A. V., Smirniotis, P. G., (2003), "Role of platinum deposited on TiO_2 in phenol photocatalytic oxidation", Langmuir, vol. 19, pp. 3135-3156.

105. Loddo, V., Marcì, G., Martín, C., Palmisano, L., Rives, V., Scalfani, (1999), "Preparation and characterization of TiO_2 (anatase) supported on TiO_2 (rutile) catalysts employed for 4-nitrophenol photodegradation in aqueous medium and comparison with TiO_2 (anatase) supported on Al_2O_3**"**, vol. 20, pp. 29-45.

106. Kim, S., Ehrman, S. H., (2009), "Photocatalytic activity of a surface-modified anatase and rutile titania nanoparticle mixture", J. Colloid and Interface Sci., vol. 338, pp. 304-307.

107. Hoffmann, M. R., Martin, S. T., Choi, W., Bahnemann, D. W., (1995), "Environmental Applications of Semiconductor Photocatalysis", Chem. Rev., vol. 95, pp.69-96.

108. Carp, O., Huisman, C. L., Reller, A. P., (2004), "Photoinduced reactivity of titanium dioxide", Solid State Chem, vol. 32, pp. 33-177.

109. Li, G., Gray, K. A., (2007), "The solid-solid interface: Explaining the high and unique photocatalytic reactivity of TiO_2 based nanocomposite materials", vol. 339, pp.173-187.

110. Hurum, D. C., Agrios, A. G., Gray, K. A., Rajh, T. and Thurnauer, M. C., (2003), "Explaining the enhanced photocatalytic activity of degussa P25 mixed-phase TiO_2 using EPR," Journal of Physical Chemistry B, vol. 107, no. 19, pp. 4545-4549.

111. Ding, (2013), "The influence of anatase-rutile mixed phase and ZnO blocking layer on dye-sensitized solar cells based on TiO_2 nanofiberphotoanode", Nanoscale Research Letters , vol.8, pp. 9.

112. Hanaor, D. A. H., Sorrell, C. C., (2011), "Review of the anatase to rutile phase transformation", Journal of Material Science, vol. 46(4), pp. 855-874.

113. Hegde, M. S., Nagaveni, K. and Roy, S., (2005), "Synthesis, structure and photocatalytic activity of nano TiO_2 and nano $Ti_{1-x}MxO_{2-\delta}$ (M=Cu, Fe, Pt, Pd, V, W, Ce, Zr)", J. Phys., Vol. 65(4), pp. 641-645.

114. Lee, Y., Kang, M., (2010), "The optical properties of nanoporous structured titanium dioxide and the photovoltaic efficiency on DSS", Materials Chemistry and Physics Vol. 122, pp. 284-289.

115. Hurum,D. C., el.al., (2003), "Explaining the enhanced photocatalytic activity of Degussa P25 mixed-phase TiO_2 using EPR", Journal of Physical Chemistry B, Vol.107 (19), pp. 4545-4549.

116. Li, G., Richter, C. P., Milot, R. L., Cai, L., Schmuttenmaer, C. A., Crabtree, R. H., Brudvig, G. W., Batista, V. S., (2009) "Synergistic Effect between Anatase and Rutile TiO_2 Nanoparticles in Dye-Sensitized Solar Cells", Dalton Transactions, pp.10078-10085.

117. Wang, Z. S., Yamaguchi, T., Sugihara, H., Arakawa, H., (2005), "Significant efficiency improvement of the black dye-sensitized solar cell through protonation of TiO_2 films", Langmuir, Vol. 21, pp. 4272-4276.

118. Senadeera, G., Kitamura, T., Wada, Y., Yanagida, S., (2005), "Photosensitization of nanocrystalline TiO_2 films by a polymer with two carboxylic groups, poly (3-thiophenemalonic acid)", Solar Energy Materials and Solar Cells, Vol. 83 (3), pp. 315-322.

Chapter 6: STUDY OF SOLAR CELLS BASED ON PEROVSKITE

6.1 CHAPTER OVERVIEW

Current chapter is focused on the study of thin film solid state solar cells based on perovskite. These are hybrid solar cells similar to dye sensitized solar cells in which the dye is replaced by a material perovskite. Perovskites are ambipolar semiconductors and can be used as electron as well as hole transporters. Mostly it works as a p-type semiconductor. The work carried out is focused on mesoporous layer of photoanode. For clear perceptive, the chapter has been classified in two parts:

- Effect of surface area of TiO_2 nanoparticles on perovskite based device performance.
- Effect of graphene oxide (GO) on charge transfer in perovskite based solar cells.

Former part of the chapter explains the effect of boiling point of solvent on the nucleation and growth of TiO_2 nanoparticles which affects the particle size and consequently the surface area and pore size. Two types of titanium dioxide (TiO_2) nanoparticles are synthesized by non-hydrolytic sol-gel method. The effect of variation of annealing temperatures along with the presence of different organic solvents during the synthesis is studied in respect with particle size, absorption in visible range and band gap. The organic solvents used in this study were ethanol and benzyl alcohol. The effect of different surface area and pore size has been further studied on the percolation of PbI_2, formation of perovskite and overall performance in perovskite based solar cells.

Later part of chapter reveals the influence of graphene oxide (GO) and different annealing temperatures of TiO_2/GO composite on the morphology and optical properties of photoanode. The devices are studied to analyze the effect of TiO_2/GO composite on the electron generation and transportation in perovskite based solar cells.

The materials synthesized in this study are well analyzed by DSC, X-Ray Diffraction (XRD) studies, Fourier Transform Infrared Spectroscopy (FTIR), Field Emission Scattering Electron Microscopy (FESEM), Atomic Force Microscope (AFM) and Ultra Violet Visible (UV-Vis) spectroscopic techniques. Surface area and pore size was analyzed by Brunauer-Emmett-Teller (BET). The results of device in this study have been validated by solar simulator for *I-V* characterization and IPCE for external quantum efficiency (EQE). In total around 60 solar cell devices have been fabricated in batches and characterized for this study. This chapter demonstrates the results obtained by best devices and are ascertained by checking the reproducibility of the results.

6.2 EFFECT OF SURFACE AREA OF TiO_2 NANOPARTICLES ON PEROVSKITE BASED DEVICE PERFORMANCE

6.2.1 Introduction

The very first evolution in solar cells based on organic and inorganic sensitizers was the replacement of liquid redox electrolyte with solid hole transporting materials (HTMs) in order to increase the stability and performance of solar cells [1]. Still the efficiency of such solvent-free solid state heterojunction dye sensitized solar cells is restricted to 7% [2, 3], while the use of perovskite ($CH_3NH_3PbI_{3-x}Cl_x$ (x = 0 or 1)) sensitizers have exceeded the PCEs of 17.6% [4].

$CH_3NH_3PbI_3$ is a material which exhibits a cubic crystal structure [5] in which the methylammonium ion ($CH_3NH_3^+$) is placed in a confined spot surrounded by four PbI_6 octahedra. Weak Van der Waals force exists among the organic components and hydrogen bonds bind the organic and inorganic components together for the interactions between the

amino group and the halide ions [6]. The orientation and occupation of the organic amino cations affect shapes and properties of the perovskite structure.

High quality films of $CH_3NH_3PbI_3$ with full coverage and crystallinity are very crucial for the photovoltaic performance and still remain a challenge [7]. Till now many deposition techniques have been applied to overcome the issues related to perovskites film quality. Initially one step solution based technique is applied but the efficiency of these devices was not satisfactory. It is deduced that because of high reaction rate between CH_3NH_3I and PbI_2, one-step solution-spun $CH_3NH_3PbI_3$film leaves pinholes which are detrimental for photovoltaic performance [8]. Later two steps sequential deposition is done in which PbI_2 is first spin coated on TiO_2 scaffold which is dipped in CH_3NH_3I solution [4]. Recently the technique of co deposition of PbI_2 and CH_3NH_3I by means of evaporation has been attempted which proved to produce the pin hole free film [9] and resulted in high efficiency. But this technique implies too many crucial aspects to take care for the controlled deposition. Till date the best conversion efficiency in observed by the sequential deposition method which is based on the penetration of $CH_3NH_3PbI_3$ inside the TiO_2 scaffold.

The results of sequential deposition are not found reasonable for planar solar cells due to absence of mesoporous layer. It leads to incomplete formation of $CH_3NH_3PbI_3$ in short period of dipping time, dissolution of PbI_2 in the solvent used for CH_3NH_3I for long time dipping and uncontrolled crystal growth [10-12].

During sequential deposition on the mesoporous layer of TiO_2, the crystal growth depends largely upon the morphological characteristics of the film. Unlike dye sensitized solar cells where the adsorption of sensitizer on high surface area semiconductor is one of the major contributing factors in the generation of photocurrent, perovskite assembly depends

upon the superior distribution of the material on the semiconductor. The surface area of the nanoparticles of semiconductor material would have little role to play in the sensitization process in perovskite based solar cells. If bigger particle size happens to assist the uniform allocation of material, the negative effect of overall decreased surface area would be encountered by high absorption coefficient of $CH_3NH_3PbI_3$ sensitizer [13, 14].

The different phases and crystal densities are the unique features of TiO_2 than other semiconductors which give more flexibility in tuning the optical and morphological properties of TiO_2. The fundamental characteristics of TiO_2 nanoparticles i.e., size, structure and morphology depend on pH of the solution, ratio of reagents in solvent, temperature of reaction and calcination temperature. All these parameters can only be controlled during the synthesis [15]. Microstructure and morphology of the product greatly depend upon selection of synthesis technique. In spite of many methods, the hassle free sol-gel method is always desired due to its efficacy in preventing co-precipitation and enabling atomic level mixing. The sol-gel technique is grouped into two methods, i.e., aqueous and non-aqueous sol-gel process. In aqueous method water is used as ligand and solvent. Its reactivity with metal oxide precursors makes the process a little complicated. Generally, non-aqueous sol gel processes are more in use for synthesis of TiO_2 nanoparticles [16].

In this study, the control of higher boiling point on the mechanism of nucleation and growth of nanoparticles has been addressed.TiO_2 nanoparticles in two different sizes (PA-1 and PA-2) are synthesized by non-aqueous sol-gel method by applying ethanol and benzyl alcohol separately in precursor solutions as solvents. These TiO_2 nanoparticles are applied on the solar cells based on perovskites material as a mesoporous scaffolds at heterojunction to evaluate their photovoltaic properties.

6.2.2 Results and discussions

6.2.2.1 Investigation of PA-1 and PA-2 nanoparticles

6.2.2.1.1 Thermal analysis

Figures 6.1 (a) and (b) show the DSC data of PA-1 and PA-2, respectively. Blue graph represents weight loss and the reaction thermodyanamics is shown by green graph. PA-1 shows only exothermic reaction and no endothermic reactions are observed. On increasing the temperature, exothermic reaction observed in PA-2 converts into the endothermic reaction. A constant weight loss is observed in case of PA-1 with increasing temperature up to 500°C. Weight loss is gradual in case of PA-2 from 100-1400°C.

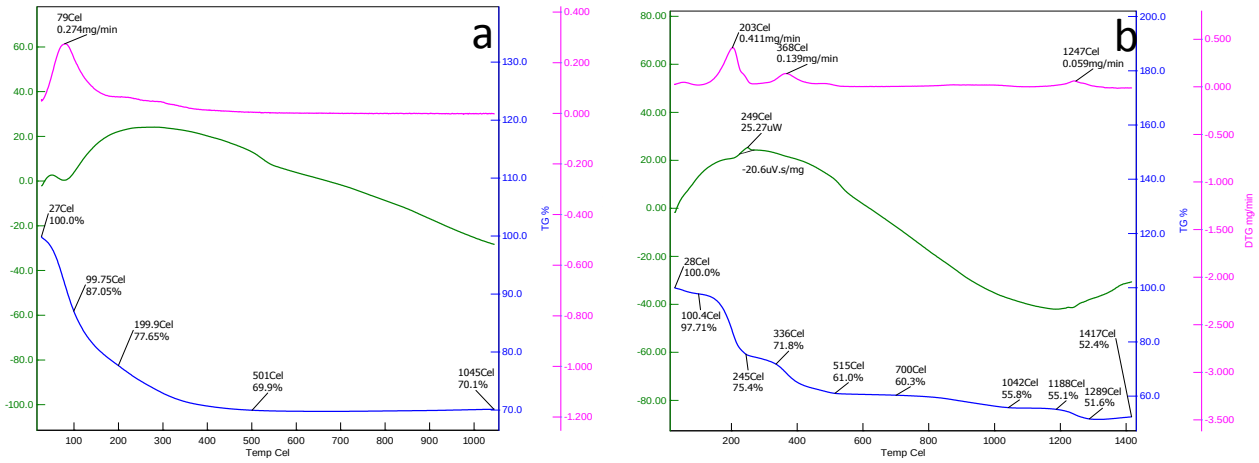

Figure 6.1: DSC analysis of TiO_2 nanopowders (a) PA-1 and (b) PA-2.

6.2.2.1.2 Phase and surface area analysis

Figure 6.2 depicts the XRDs of PA-1 and PA-2. The smaller particle size of PA-1 is suggested by broader peaks of PA-1 than that of PA-2. Much lower boiling point of ethanol (78.37°C) in comparison with benzyl alcohol (205°C) impedes the nucleation and growth of nanoparticles because of shorter duration for the reaction to complete. This could be the

reason for the larger particle size of PA-2 than that of PA-1. In case of PA-1, the presence of pure anatase structure is confirmed by the characteristic peak of anatase at 25.24° (JCPDS-01-071-1167) of TiO_2 [17]. The similar pattern of XRD graph is observed after calcination of TiO_2 powder for 5 hours at 450°C, in case of PA-2 which ensured the presence of pure anatase phase (JCPDS-00-001-0562) [18].

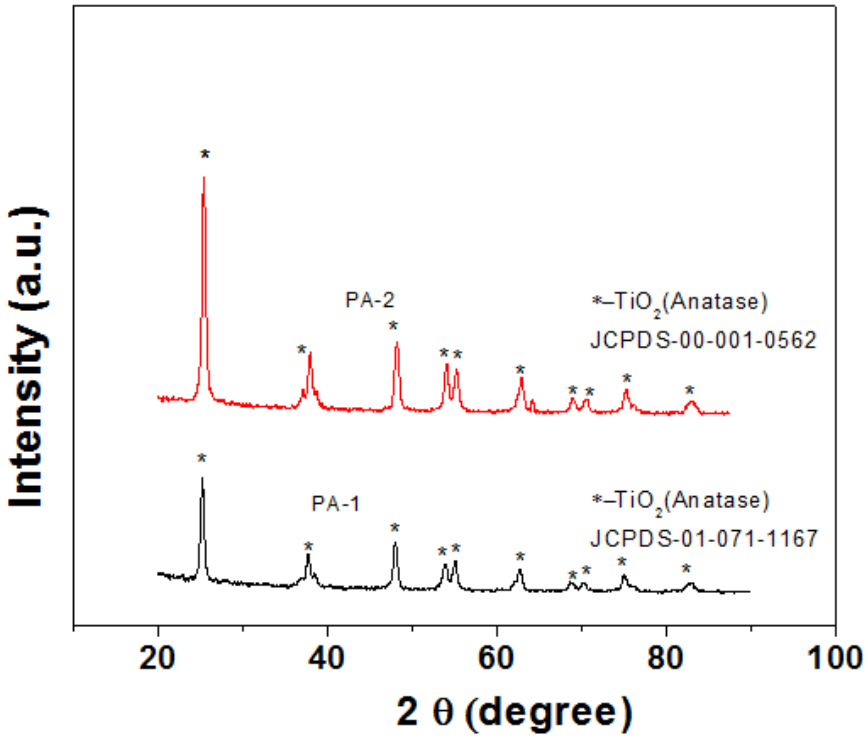

Figure 6.2: XRD analysis of TiO_2 nanopowder PA-1 and PA-2.

More intense peaks and clearer baseline in PA-2 XRD graph portrays higher purity of anatase phase in PA-2 than PA-1. This could be due to longer annealing of PA-2 than of PA-1 which helps removing organic impurities.

Figure 6.3 shows the IR spectra of TiO_2 nanoparticles synthesized by both types of alcohols and observed to be very similar. Being the characteristic bands of Ti-O bond, 548

$cm^{-1}$and 555 cm^{-1} bands in PA-1 and PA-2, respectively, declare the synthesis of TiO_2 nanoparticles. Absorption bands in the region of 600-400 cm^{-1} in case of PA-1 and PA-2 clearly indicate the formation of anatase phase. Annealing for longer period of time led to significant sharpening of absorption bands in the region of 600-400 cm^{-1} in case of PA-2, supports the purity of anatase phase.

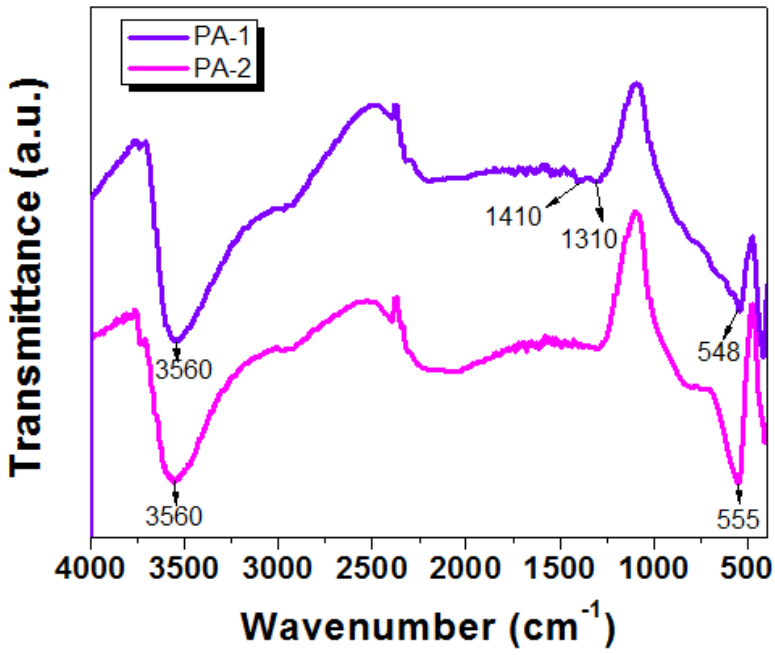

Figure 6.3: IR spectra of PA-1 and PA-2.

The absorptions at 1310 and 1410 cm^{-1} are observed in IR spectra of PA-1 (Figure 6.3). These peaks represent asymmetrical and symmetrical vibration of M-O-C groups [19, 20] and alkyl groups [21]. Since the above-mentioned absorptions are not observed in case of PA-2, it substantiates the finding of XRD data (Figure 6.2) of being relatively pure TiO_2 due to the longer calcination of PA-2. The restrained atmospheric water or alcohol used during

synthesis process is demonstrated by bands at 3560 cm^{-1} in case of both types of TiO_2, which is narrower in PA-2. It shows the removal of water on longer annealing of PA-2 [22].

The surface area and pore volume of both the synthesized nanoparticles are analyzed by BET surface analyzer. It is observed that BET surface area of PA-1 (66.6200 m^2/g) is higher than that of was found in PA-2 (40.0879 m^2/g). Pore size of PA-1 and PA-2 is 107.1184 Å and 74.1372 Å, respectively. Since the particle size of PA-2 is much bigger than that of PA-1, its surface area and pore size is observed to be much lower in comparison with PA-1.

6.2.2.1.3 Morphological analysis

The pictures of the thin films prepared by spin coating the suspension of PA-1 and PA-2 on FTO substrates are shown in Figure 6.4, which demonstrate an opaque and a relatively transparent film made by PA-1 and PA-2, respectively.

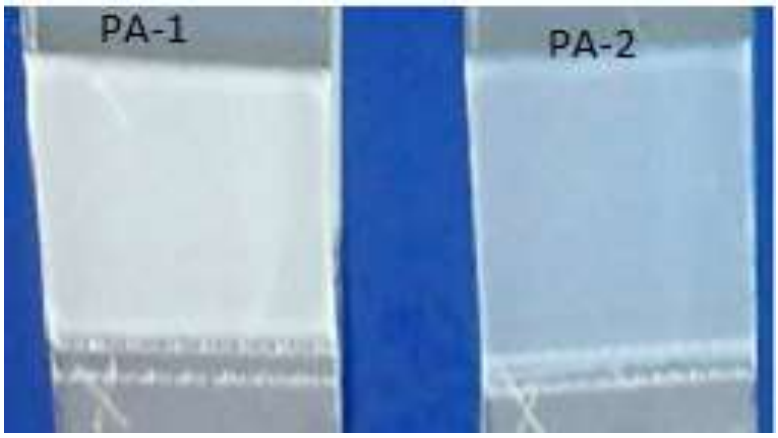

Figure 6.4: Pictures of spincoated films of PA-1 and PA-2.

The FESEM images of the films spin coated by both types of nanoparticles (PA-1 and PA-2) at the same magnification are shown in Figures 6.5 (a) and (b). Both the nanoparticles

(PA-1 and PA-2) are spherical in shape with average size of 20-30 nm for PA-1 and 40-60 nm for PA-2 nanoparticles. In case of PA-1 a significant agglomeration is observed as big clusters of nanoparticles which are unevenly present all over in the film. This could be one of the reasons behind opaque appearance of the film PA-1. In contrast with PA-1 the films prepared by PA-2 are uniform with compact packaging of particles on the surface.

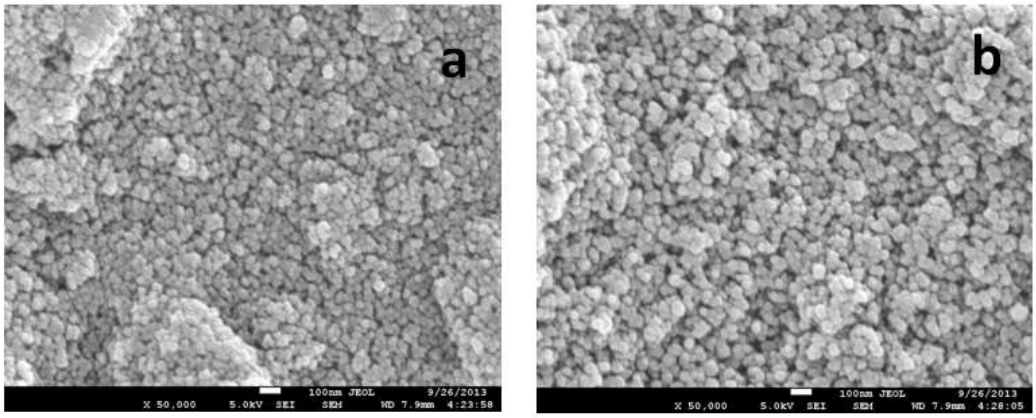

Figure 6.5: FESEM images of (a) PA-1 and (b) PA-2 nanoparticles.

6.2.2.1.4 Optical property analysis

Figure 6.6 (a) shows the absorption spectra of PA-1 and PA-2 in which a red shifted absorption band of PA-2 is observed in comparison with PA-1. The coverage of spectra is also broadened from 350 nm in PA-1 to 400 nm in case of PA-2. Direct band gap of the samples are calculated by plotting $(\alpha hv)^2$ vs. hv as in literature [23]. The calculated band gap energies are 3.54 eV and 3.37 eV for PA-1 and PA-2, respectively (Figure 6.6 (b)). Increased band gap of PA-1 can be explained on the basis of effective mass model (EMM) of small semiconductor particles which is observed to increase as the particle size decreases [24, 25].

6.2.2.2 Investigation of perovskite solar cells based on PA-1 and PA-2

Spun coated TiO_2 films (PA-1/PbI_2, Pa-2/PbI_2) and perovskite films (PA-1/$CH_3NH_3PbI_3$ andPA-2/$CH_3NH_3PbI_3$) formed during the study are thoroughly examined by XRD, UV-vis and FESEM for the property-performance correlation in the study. Figure 6.7 shows the XRD plots of films PA-1 and PA-2 spincoated by PbI_2. Sharp peaks at $2\theta = 12.23°$ which corresponds to (001) lattice plane of crystallized PbI_2 [26] confirms the presence of PbI_2 in the films.

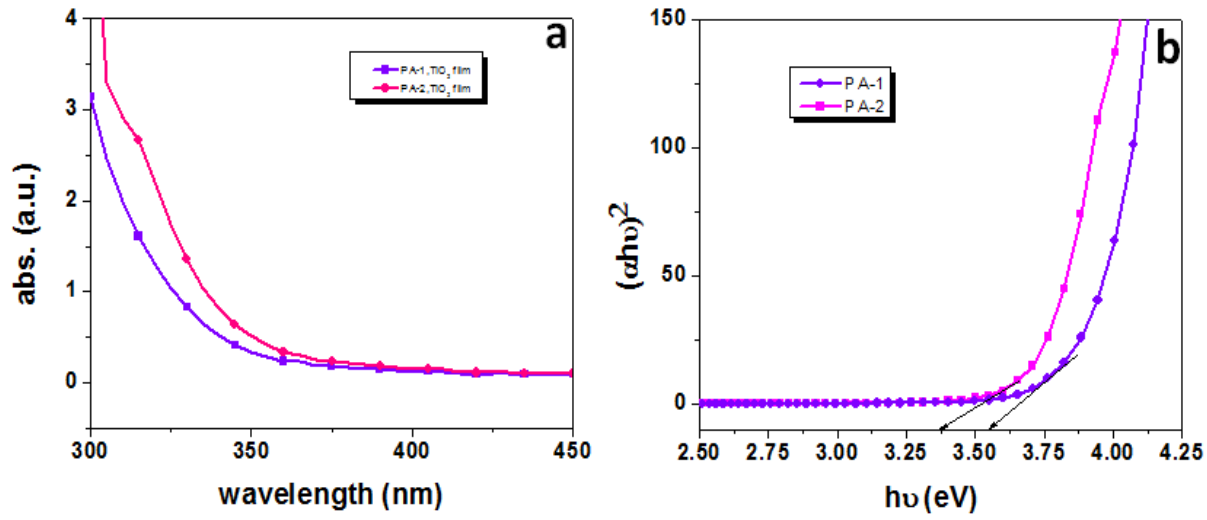

Figure 6.6: Optical properties of PA-1 and PA-2 nanoparticles. (a) Absorption spectra and (b) Band gap energies.

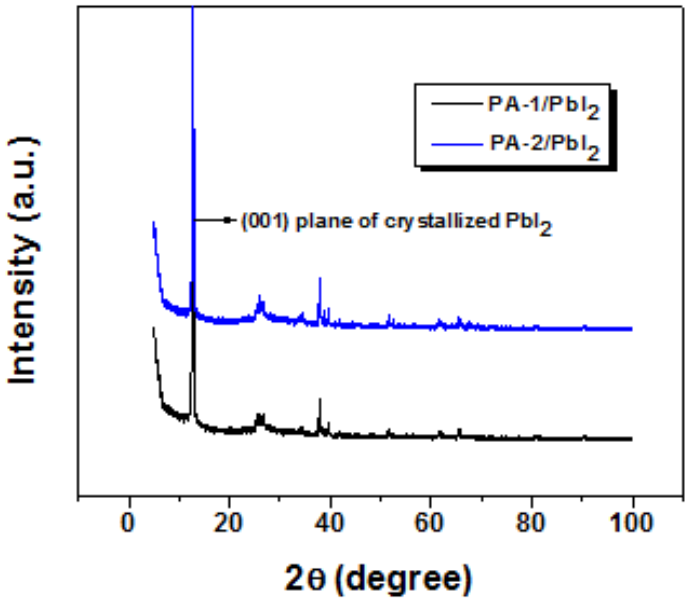

Figure 6.7: XRD spectra of PA-1/PbI_2 and PA-2/PbI_2 film.

The FESEM images of PA-1/PbI_2 and PA-2/PbI_2 films are compared in Figure 6.8 for their surface morphologies. It is clearly observed that PbI_2 formed layered crystals on the surface of PA-1 while on PA-2 it is distributed very uniformly which looks more like an amorphous layer than crystalline. This vast difference in crystal sizes is correlated with the large BET surface area (66.6200 m^2/g) of PA-1 than that of PA-2 (40.0879 m^2/g). It can be concluded that because of large available surface area and bigger pore size, the infilteration of PbI_2 into PA-1 is much more than that of PA-2. This led to uncontrolled growth of crystals on PA-1/PbI_2. While in case of PA-2/PbI_2, smaller pore size hindered the infilteration of PbI_2 into PA-2 film and restricted the crystal growth.

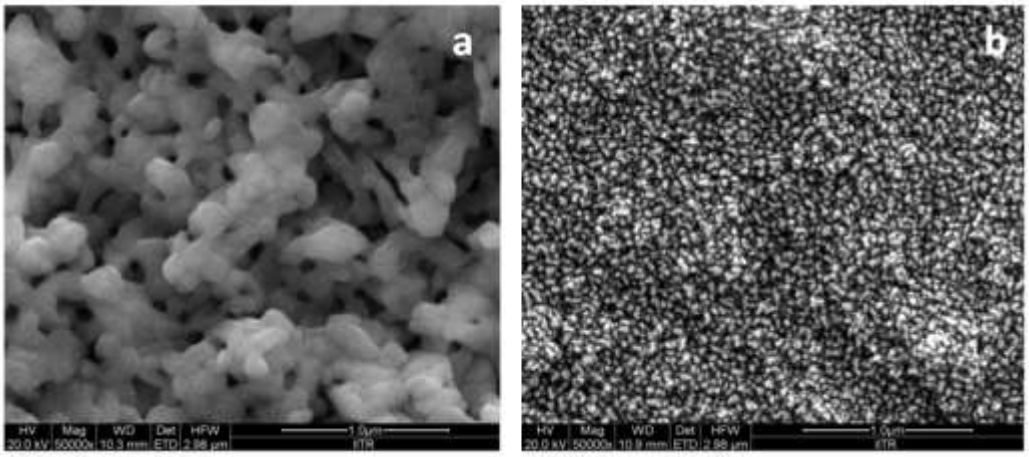

Figure 6.8: FESEM images of (a) PA-1/PbI_2 and (b) PA-2/PbI_2 film surface.

To analyze the effect of the thickness of mesoporous layer both the TiO_2 nanoparticles (PA-1 and PA-2) are spin coated in two different thicknesses (~ 370 and ~ 580 nm).

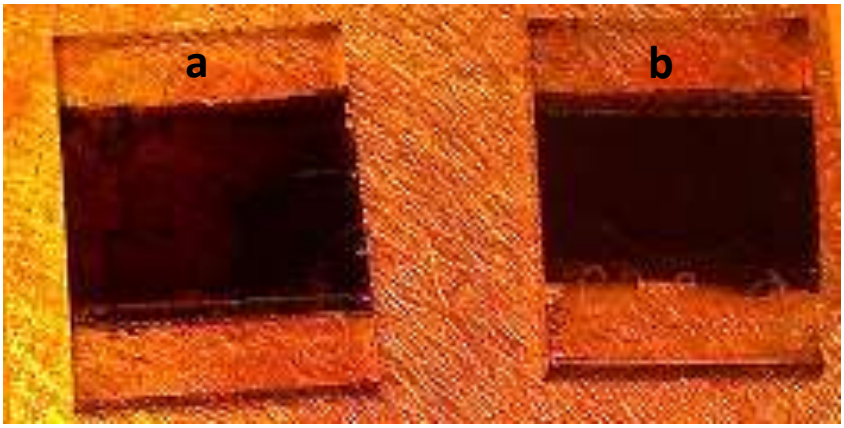

Figure 6.9: Pictures of perovskite films (a) PA-1/$CH_3NH_3PbI_3$ and (b) PA-2/$CH_3NH_3PbI_3$.

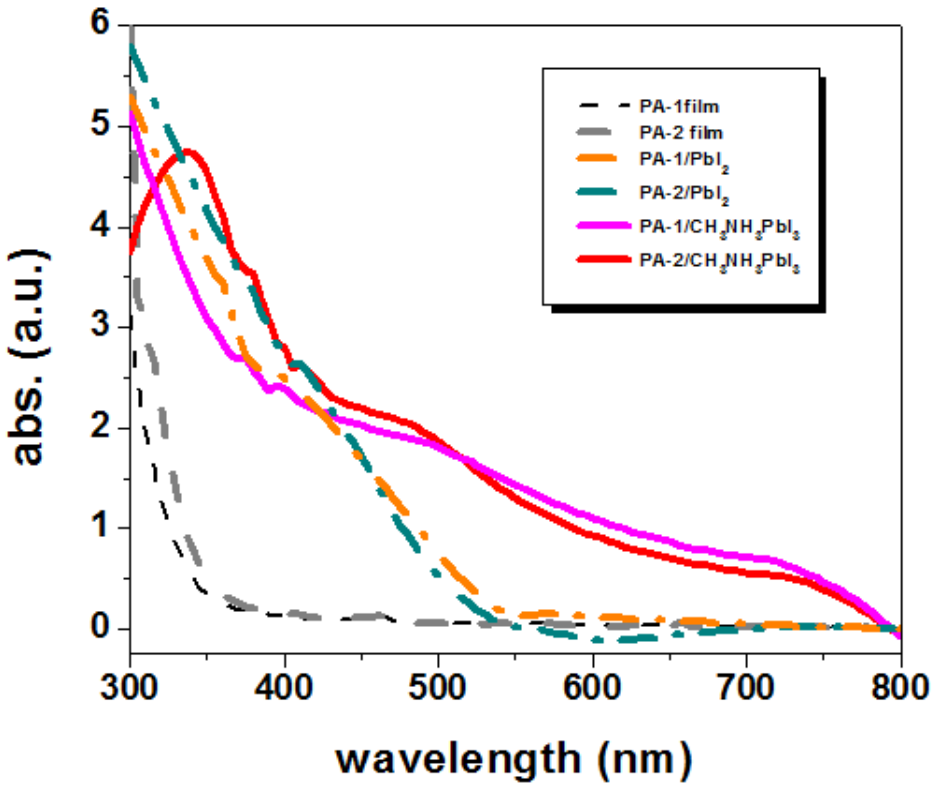

Figure 6.10: Absorption spectra of bare PA-1, PA-2 films, PA-1/PbI_2, PA-2/PbI_2 films and PA-1/$CH_3NH_3PbI_3$ and PA-2/$CH_3NH_3PbI_3$ films.

On dipping the films of PA-1/370/PbI_2, PA-1/580/PbI_2, PA-2/370/PbI_2 and PA-2/580/PbI_2 in solution of CH_3NH_3I all yellow coloured films turned into dark brown (Figure 6.9) irrespective of the particle size and thickness of the mesoporous films, indicates the perovskite formation in all the films. The red shifted absorption in case of PA-1/PbI_2 and PA-2/PbI_2 after the dipping in CH_3NH_3I also substantiates the perovskite formation in the films (Figure 6.10).

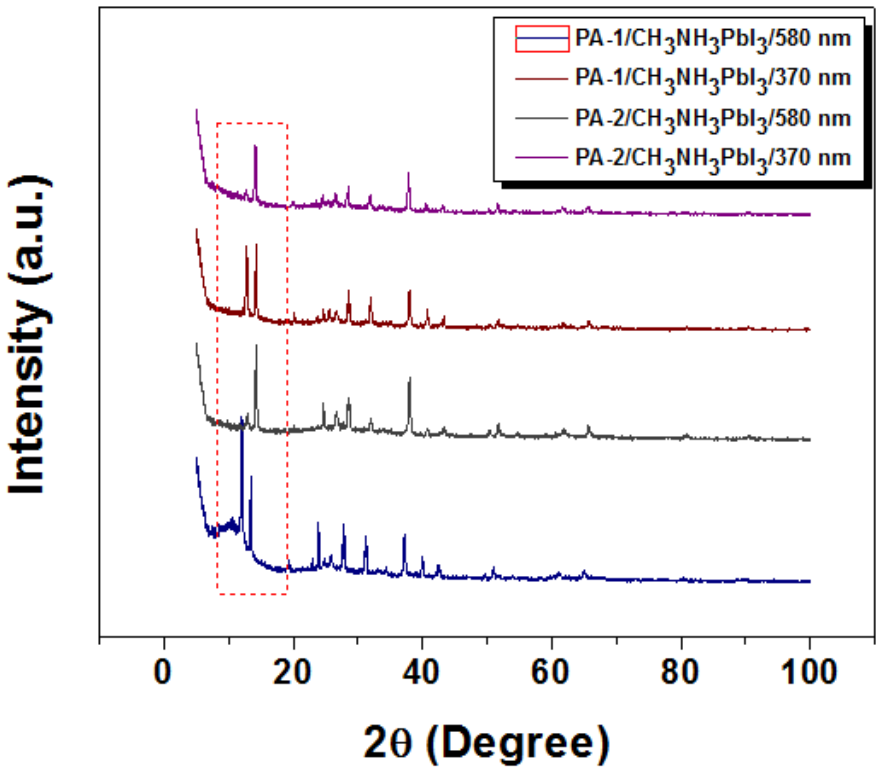

Figure 6.11: XRD spectra of PA-1/$CH_3NH_3PbI_3$ and PA-2/$CH_3NH_3PbI_3$ with different thicknesses.

These films are further analyzed by XRD to confirm the conversion of PbI_2 and CH_3NH_3I into $CH_3NH_3PbI_3$. Figure 6.11 shows the XRD graphs of PA-1/$CH_3NH_3PbI_3$/370 nm, PA-1/$CH_3NH_3PbI_3$/580 nm, PA-2/$CH_3NH_3PbI_3$/370 nm and PA-2/$CH_3NH_3PbI_3$/580 nm. All the films display a set of diffraction peaks at 13.6°, 28° and 31.7° which validate the tetragonal structure of perovskite in all the films [26]. A sharp peak at 12.23° has been noticed in case of PA-1/$CH_3NH_3PbI_3$/580 nm and PA-2/$CH_3NH_3PbI_3$/580 nm which explains the presence of unreacted PbI_2 in the film. Peak representing PbI_2 is intense only at the thickness of 580 nm in both types of films (PA-1 and PA-2). The peak shoots as high as more than double the height of the diffraction peak at 13.6° representing $CH_3NH_3PbI_3$ in case of

PA-1/$CH_3NH_3PbI_3$/580 nm. It shows that only around one-third of PbI_2 could be exhausted for the perovskite formation in PA-1 film thickness of ~580 nm. XRD results observed for the film PA-2/$CH_3NH_3PbI_3$/580 nm show that half of the PbI_2 is still not converted into perovskite. Although the results at ~580 nm are similar for both the perovskite films, the deep penetration of PbI_2 into the PA-1 mesoporous film owing to high surface area and large pore size of PA-1 nanoparticles, resulted in most of the PbI_2 remaining unreacted at 15 min of dipping time. The same explanation may be valid for the PbI_2 peak which is more intense in case of PA-1/$CH_3NH_3PbI_3$/370 nm than that of PA-2/$CH_3NH_3PbI_3$/370 nm. With the bigger particle size and smaller pore area most of the PbI_2 in the PA-2/370/PbI_2 film is expected to be on the sites where it can be easily reacted and converted into perovskite. Most of the PbI_2 is observed to get converted into perovskite in PA-2/370/$CH_3NH_3PbI_3$ films (Figure 6.11 violet graph) at 15 min of dipping time. It has been emphasized that the uncontrollable amount of PbI_2 is detrimental for the device performance as well as for the reproducibility of the results [26].

Figure 6.12 shows the FESEM images of PA-1/$CH_3NH_3PbI_3$ and PA-2/$CH_3NH_3PbI_3$ films at the same magnifications. The uncontrolled crystal growth is observed in both the films (inset) which is an outcome of sequential deposition of perovskite via dipping PbI_2 coated PA-1 and PA-2 films in CH_3NH_3I solution. The uncontrolled crystal growth is also evident in 3D AFM images of PA-1/$CH_3NH_3PbI_3$ and PA-2/$CH_3NH_3PbI_3$ films at the same magnifications (Figures 6.13 (a) and (b)).

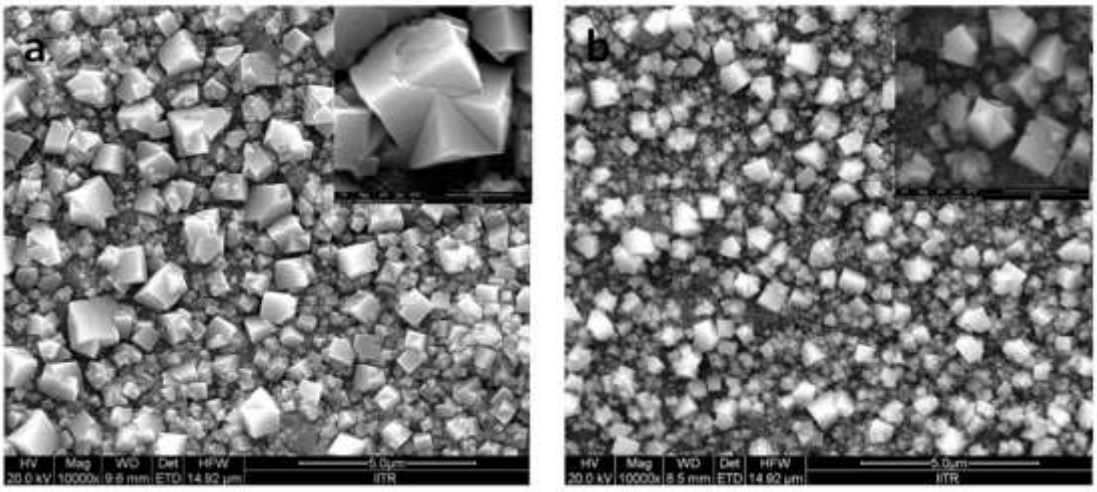

Figure 6.12: FESEM images of (a) PA-1/$CH_3NH_3PbI_3$, (b) PA-2/$CH_3NH_3PbI_3$ films and (inset) crystal growth at higher magnification.

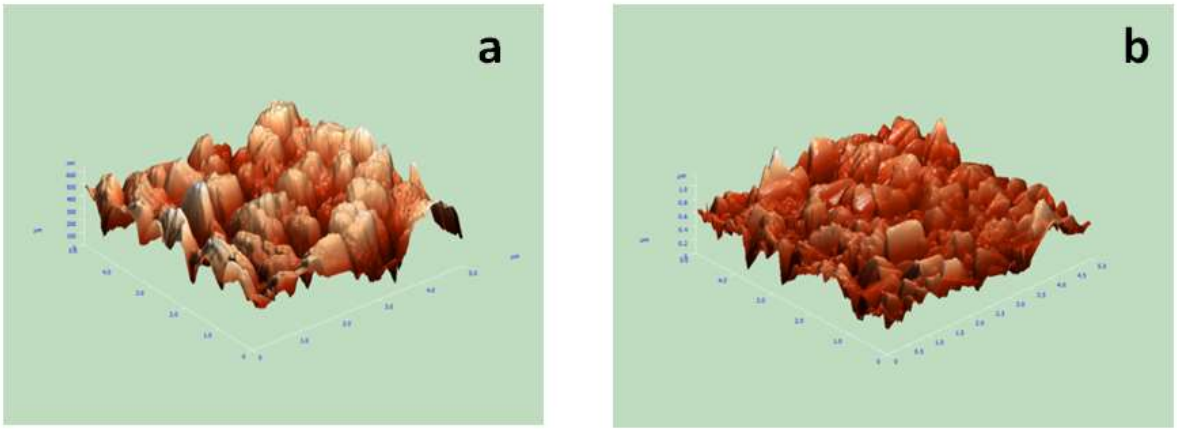

Figure 6.13: AFM images of (a) PA-1/$CH_3NH_3PbI_3$ and (b) PA-2/$CH_3NH_3PbI_3$ films.

The cross sectional FESEM images of the devices PA-1 and PA-2 are shown in Figures 6.14 (a) and (b). The device compositions are FTO/blTiO_2/PA-1/$CH_3NH_3PbI_3$/SpiroOMeTAD/Gold and FTO/blTiO_2/PA-2/$CH_3NH_3PbI_3$/SpiroOMeTAD/Gold. Both the devices are fabricated by restricting the thickness of TiO_2 film around 370 nm. The separation of infilterated HTM layer and gold

electrode from the back contact via photoanode region is very evident in device PA-2. No such separation is observed in PA-1 device which deduces the possibility of dark current generation in PA-1 device when it is illuminated.

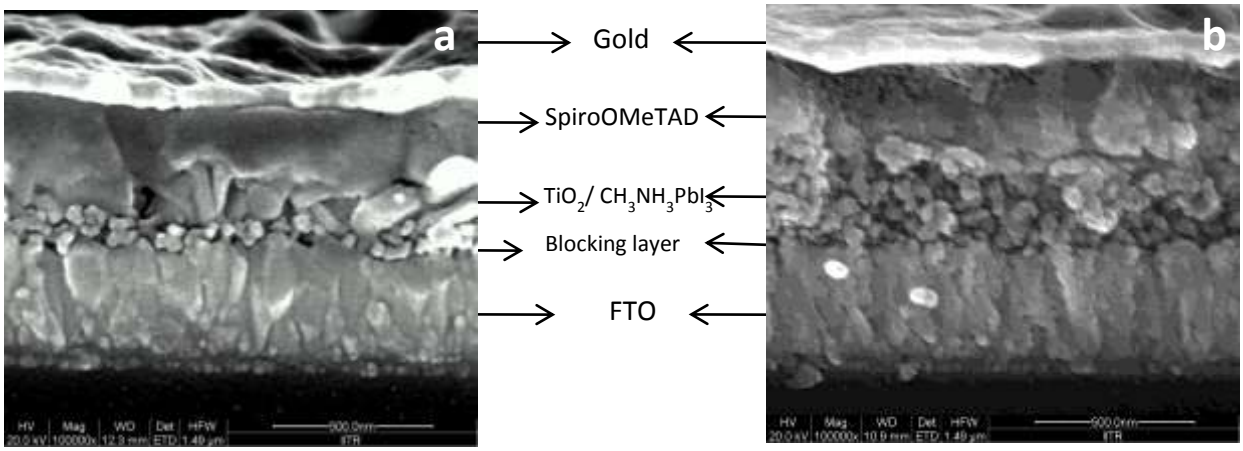

Figure 6.14: FESEM images cross section of (a) PA-1 and (b) PA-2 devices.

Figures 6.15 and Figure 6.16 show the *I-V* and EQE measurements of PA-1 and PA-2 devices fabricated with thicknesses ~370 and ~580 nm. Device P-25 is fabricated as a control by using commercial TiO_2 nanopowder, P-25 in photoanodes. The highest J_{sc} and V_{oc} of 16.29 mA/cm^{2}and 0.98 V has been observed from device PA-2 (~370 nm) with highest overall efficiency of 8.56% and surpassed the efficiency of 6.51 % obtained by device P-25 (~370 nm). Device parameters are discussed in Table 6.1 and found to be better than that of device P-25 in case of both PA-1 and PA-2 when the thickness has been taken as ~370 nm. The highest EQE of 58% is observed for the device PA-2 (~370 nm). The device data in this study is found to be in agreement with the compositional, optical and morphological data of PA-1 and PA-2 films.

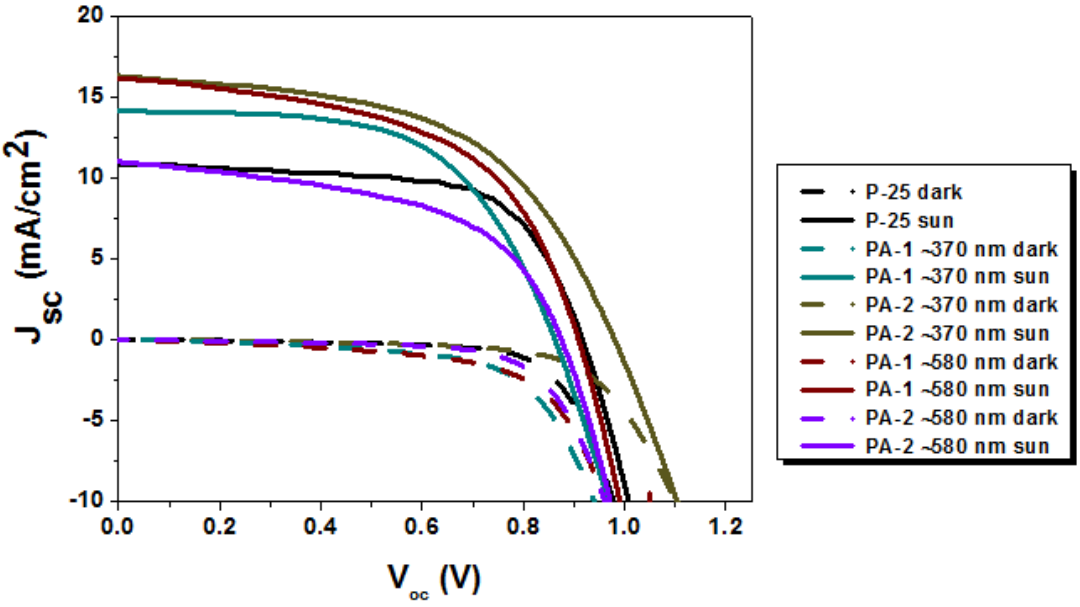

Figure 6.15: *I-V* characteristics of PA-1 and PA-2 device with different thicknesses of mesoporous layer.

Table 6.1: *I-V* parameters of device PA-1 and PA-2 at different thickness of mesoporous layer.

TiO_2	J_{sc}(mA/cm²)	V_{oc} (V)	*FF*	η (%)
P-25 (~370 nm)	10.825	0.916	65.66	6.51
PA-1 (~580 nm)	11.014	0.875	52.45	5.10
PA-1 (~370 nm)	14.148	0.862	59.02	7.20
PA-2 (~580 nm)	16.167	0.909	54.03	7.94
PA-2 (~370 nm)	16.289	0.980	53.62	8.56

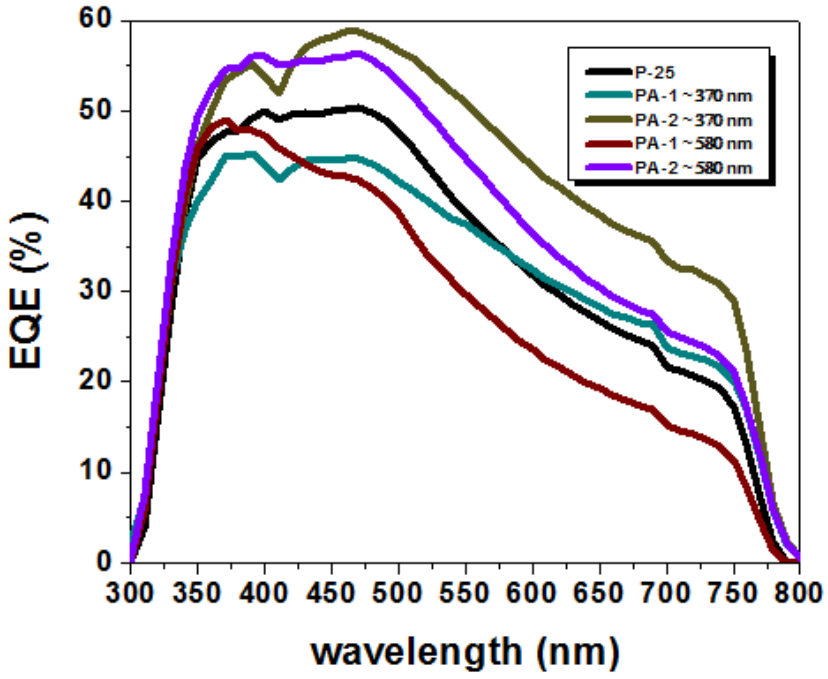

Figure 6.16: IPCE characteristics of PA-1and PA-2 device with different thicknesses of mesoporous layer.

6.2.3 Experimental

6.2.3.1 Synthesis of nanoparticles

During the synthesis $TiCl_4$ reacts with alcohols and $TiCl_2(OH)_{4-X}$ is generated with the exhaustion of a large quantity of HCl gas. Some amount of water in absorbed from atmospheric moisture by $TiCl_2(OH)_{4-X}$, which resulted into Ti-OH and …-Ti-O-….-Ti-OH strings are produced. On heating $Ti(OH)_4$ converts into TiO_2 (equation (6.1)) [27, 28].

$$Ti(OH)_4 \rightarrow TiO_2 + 2H_2O \quad (6.1)$$

$TiCl_4$ (Merck) is added in ethanol (Merck) and benzyl alcohol (Merck) drop wise separately at room temperature with continuous stirring in the ratio of 1:10. With ethanol the

reaction produced a clear yellow solution and with benzyl alcohol a bright orange solution was observed with white puffs which dissolved later on aging. Reactions are left at 70-85°C under constant stirring for aging. After hours (~ 36 hours) of aging the colors of the reaction mixtures turned to off white. In case of ethanol based synthesis, a white amorphous powder was obtained and calcined at 500°C for 1 hour. Benzyl alcohol mediated synthesis turned into a white dispersion which was kept inside the oven at 80°C for 12 hours after filteration. The recovered powder was calcined at 450°C for 5 hours in furnace. As synthesized nanopowders are coded as PA-1 (synthesized via ethanol) and PA-2 (synthesized via benzyl alcohol) in the current study.

6.2.3.2 Fabrication of solar cells

TiO_2 paste was made by 10% of ethyl cellulose in ethanol and α terpinol (2 g) added to TiO_2 powder (1 g), diluted by adding more ethanol to avoid lump formation and ultrasonicated. Solvent was evaporated at low pressure for 3-4 hours to make more homogeneous paste. TiO_2 paste was further diluted by ethanol in 1:3.5 ratios and stirred overnight. A 60 nm thick dense blocking layer of TiO_2 (bl-TiO_2) was deposited onto a FTO by spray pyrolysis deposition carried out using a 20 mM titanium diisopropoxide bis(acetylacetonate) solution at 450°C. It prevents direct contact between FTO and the hole-conducting layer. Thick mesoporous TiO_2 films were spin coated onto the bl-TiO_2/FTO substrate. PA-1 and PA-2 NPs were spincoated at 4500 rpm for 30 sec to achieve the thickness of ~ 370 nm and at 3000 for 30 sec to achieve the thickness of ~ 580 nm. Films were then calcined at 500°C for 1 hour to remove the organic part. CH_3NH_3I was synthesized as per the reported method [29]. The mesoporous TiO_2 films were infiltrated with PbI_2 by spin coating at 6,500 rpm for 5 sec and dried at 70°C for 30 min. For the solution preparation

of PbI_2, 462 mg ml^{-1} (1 M) solution of PbI_2 in *N*, *N*-dimethylformamide (DMF) was kept at 70°C. After cooling down to room temperature, the films were pre-wetted in 2-propanol and dipped in a solution of CH_3NH_3I in 2-propanol (10 mg mL^{-1}) for 15-20 min, rinsed with 2-propanol and dried at 70°C for 30 min. The HTM (SpiroOMeTAD) was deposited on the perovskite layer by spin coating at 4,000 r.p.m. for 30 sec. The spin coating formulation of HTM was prepared as per the reported method [30]. Finally, 80 nm of gold was thermally evaporated on top of the device to form the back contact. The device fabrication was carried out under controlled atmospheric conditions. The active area of the cells was 0.20 cm^2.

In this study the effect of different particle size and thickness of TiO_2 film on the charge transportation and performance of solar cells based on perovskites sensitizer is studied. Two types of device architectures have been fabricated in this study, i.e., FTO/bl-TiO_2/meso-TiO_2(~370nm)/$CH_3NH_3PbI_3$/HTM/Gold and FTO/bl-TiO_2/meso-TiO_2(~580 nm)/$CH_3NH_3PbI_3$/HTM/Gold, by taking PA-1 and PA-2 as meso-TiO_2 layers at both the thicknesses.

6.3 EFFECT OF GRAPHENE OXIDE (GO) ON CHARGE TRANSFER IN PEROVSKITE BASED SOLAR CELLS

6.3.1 Introduction

Research in the field of perovskite based solar cells has taken decades leap and surpassed the best efficiency obtained by dye sensitized solar cells within merely 2-3 years [31-34]. It has been categorized as a novel type of solar cell with a record efficiency of 16.2 % and is expected to provide PCE of around 20 % given 1.1 V of voltage [35, 36]. The emphasis has been given to improve the perovskite layer [37-39], mesoporous layer [40, 13] and hole transporting layer [41, 42].

Charge recombination is the major blockage which impedes the efficiency enhancement even after continuous research on all the components of perovskite solar cells. For the effective charge transfer across semiconductor interfaces in solar cell a lot of attempts have been made by modifying semiconducting layer. The designing of solar cells wherein there are interactions of two types of semiconductors or the interactions of semiconductor with metal [43-45] have been attempted. Some of the new studies showed the influence of graphene content on TiO_2 which leads to the improved performance of the solar cell due to increased recombination resistance of the device [46, 13].

Graphene is a unique class of 2D carbon configurations with a work function of 4.7 eV to 4.9 eV and possess an exceptional quality of high mobility for both, holes as well as electrons [47]. Superior electron mobility of graphene is due to delocalized network of π electrons in graphene sheets. Other attractive properties exhibited by graphene are high thermal conductivity, high intrinsic carrier mobility, high optical transmittance in the UV-Visible region and large specific surface area. Graphene oxide (GO) is a form of heavily oxygenated graphene which is exfoliated in water in order to yield single layer sheets [48]. Amphiphilic nature of GO facilitates its dispersion in the solvents of different polarities which makes it versatile in several applications [49-53].

Based on all the desirable properties of GO, it is expected to act as an electron acceptor which can be used with the semiconductors for enhancing the electron transfer in solar cells. On illumination the electrons are transferred into GO from semiconductor where they can be stored inside the C-C network. In this way, GO withTiO_2 promotes the charge carriers separation efficiently and reduces the charge recombination. TiO_2/GO nanocomposites seem very promising for overcoming electron-hole recombination, which

makes them desirable to be successfully employed in dye degradation, sensors, photocatalysis and photovoltaics [51, 54].

The surface states and surface morphologies of semiconductors tend to affect the performance of a solar cell. The nanocrystalline TiO_2 contains many trap states and haphazard pathway morphologies because of which around 90 % of electrons are reported to be trapped while in working condition. The overall effect is the lowering down the electron transport in solar cells [55-57]. It has been reported that incorporation of GO into TiO_2 constructs links among TiO_2 nanoparticles which work as a bridge and augments charge collection and transfer within the solar cell [58]. Graphene based semiconductors have been used in a wide range of applications and the synthetic methods are classified into four types, i.e., hydrothermal and/or solvothermal methods [59], sol-gel [51, 54], solution mixing and in situ growth [60].

This chapter throughs light on the effect of GO incorporation with TiO_2 semiconductor and the influence of sintering temperatures on the optical, electrochemical, morphological and photovoltaic properties of TiO_2/GO composite. The composite has been used in the solar cells based on organo halide perovskite as sensitizer. The composition of perovskite has been kept constant as $CH_3NH_3PbI_3$, throughout this study. The technique of perovskite growth adopted in this work is solution based sequential deposition. Appropriate characterization tools have been used for the authentication of the results in this study which support the enhancement of electron transportation and reduced recombination of charges in the solar cells based on TiO_2/GO composite.

6.3.2 Results and discussions

6.3.2.1 Compositional analysis of TiO_2/GO composites

Figure 6.17 shows the IR spectra of TiO_2, TiO_2/GO/150 and TiO_2/GO/450 where TiO_2/GO/150 is the composite annealed at 150°C and TiO_2/GO/450 is the composite annealed at 450°C.

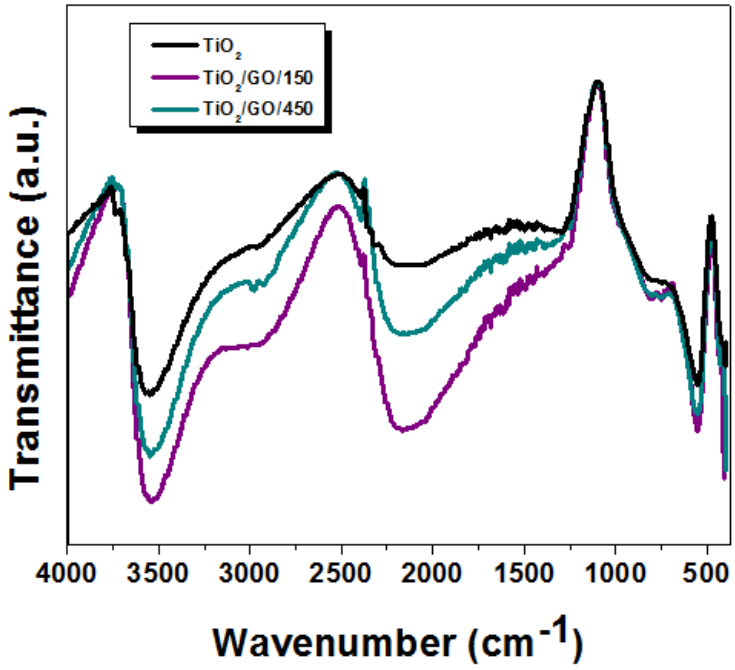

Figure 6.17: Comparison of FTIR spectra of TiO_2 and GO composites.

IR spectra of TiO_2 films demonstrate the characteristic peak at 500-729 cm^{-1} which is originated in crystalline TiO_2 from the stretching vibrations of Ti-O-Ti bonds [61]. The presence of -OH stretching group is observed as absorption peak at 3550 cm^{-1}.

For the TiO_2/GO composites the strong absorption peaks which represent various functional groups, i.e., CH_2 and alcoholic C-OH stretching are observed at 2940 and 1460 cm^{-1}, respectively. The absorption peak below 1000 cm^{-1} observed in case of IR spectra of TiO_2 turns more intense in case of TiO_2/GO composites which are attributed to the existence

of Ti-O-C vibrations (810 cm^{-1}) along with the Ti-O-Ti [61]. Although peaks in IR spectra of both the composites (TiO_2/GO/150 and TiO_2/GO/450) demonstrate the presence of GO in both the composites, it is more intense in TiO_2/GO/150. The decreased intensity of absorption peaks of TiO_2/GO/450 can be due to the alterations in oxygen containing groups (OCG) of GO on heating at high temperature. It has been demonstrated in earlier studies that heating above 200°C breaks down OCGs of GO and as a result GO starts getting decomposed which is apparent by disappearing of most of the corresponding peaks [62].

Figure 6.18 illustrates the XRD plots of TiO_2 and both TiO_2/GO composite films. A sharp peak at 11.8 (2θ value) validates the presence of GO in TiO_2/GO/150 [62]. On heating the composite at 450°C the intensity of the peak reduces and a broad peak is observed. Since the peak is still noticeable after annealing at 450°C, it is suggested that even if the structure of GO is disturbed, the OCGs are still present in TiO_2/GO/450 composite.

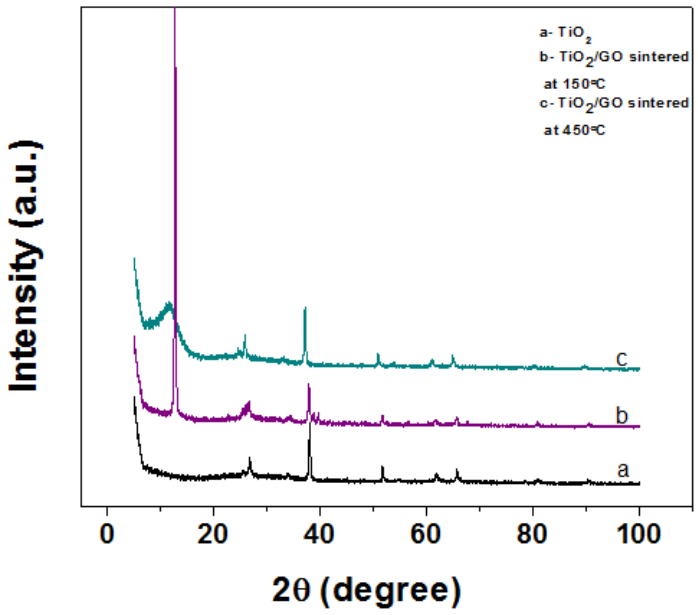

Figure 6.18: XRD plots of TiO_2, TiO_2/GO/150 and TiO_2/GO/450 films.

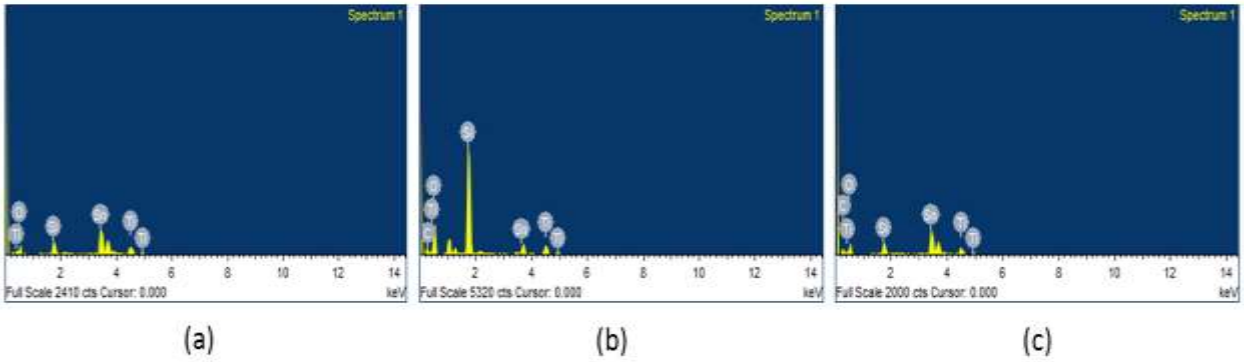

Figure 6.19: EDX analysis of (a) TiO_2, (b) TiO_2/GO/150 and (c) TiO_2/GO/450 films.

The compositional analysis of all films was further carried out by energy dispersive X-ray spectroscopy (EDX). The EDX spectra of pure TiO_2, TiO_2/GO/150 and TiO_2/GO/450 are shown in Figures 6.19 (a), (b) and (c). The presence of elements Sn and Si is due to FTO coated glass substrate which is been used for the film deposition. Peaks at 4.5 and 4.9 KeV of Ti element and at 0.5 KeV of O substantiate the TiO_2 crystallites in all the film. Peak of element carbon which is observed only in TiO_2/GO composites must have come from the GO component. The elemental microanalyses (wt%) of the films are listed in Table 6.2. Since elements Si and Sn come from the substrates used in all the films and do not have much relevance with the main study here, their elemental wt% is not included in the table. O element is highest in the TiO_2/GO/150 composite due to TiO_2 and GO components. Reduced amount of O in TiO_2/GO/450 composite shows the partial reduction of GO into graphene because of higher temperature of annealing of TiO_2/GO/450 film.

Table 6.2: Compositional analysis wt % of TiO_2, TiO_2/GO/150 and TiO_2/GO/450 films.

Element	TiO_2	TiO_2/GO/150	TiO_2/GO/450
C	-	17.39	11.91
O	41.20	46.91	40.76
Ti	9.13	5.45	6.05

6.3.2.2 Optical Absorption

The absorption spectra of TiO_2/GO composites are shown in Figure 6.20 which explicitly demonstrates the influence of GO incorporation on the optical behavior of TiO_2. Both the absorption edges of TiO_2/GO composites show a red shifted absorption than in comparison with TiO_2 absorption band. The absorption threshold shifted from 375 nm of TiO_2 to 550 nm for the composite TiO_2/GO/450 and to 680 nm for TiO_2/GO/150. The effectiveness of introduction of GO in semiconductor on its visible light response has been reported earlier in enhancing the photocatalytic activity of semiconductor [63-65].

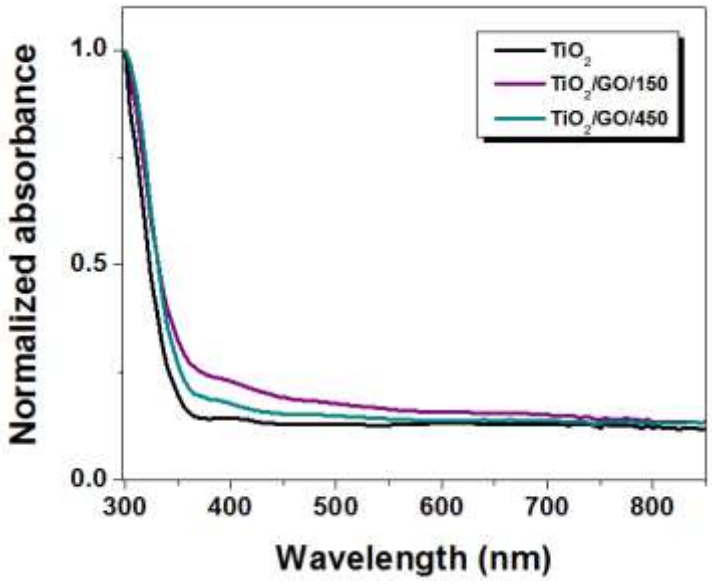

Figure 6.20: Normalized absorbance of TiO_2, TiO_2/GO/150 and TiO_2/GO/450 composites.

Similar observations in this study evidence close interactions among GO and semiconductor in a TiO_2/GO composite which facilitates the visible light absorption and charge separation effectively. Since the intercalated bonds of GO are intact in case of TiO_2/GO/150, it shows the most red shifted absorption edge and better optical behavior than that of composite TiO_2/GO/450.

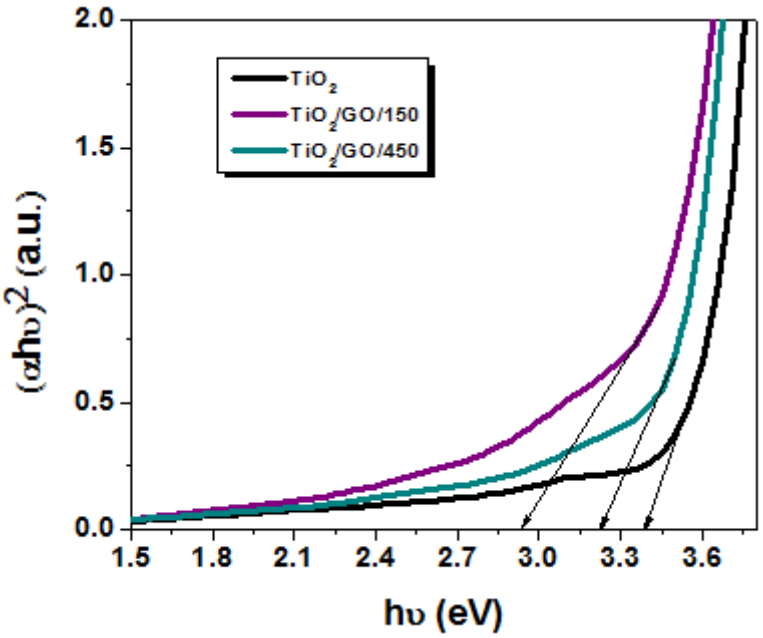

Figure 6.21: Band gap energies of TiO_2, TiO_2/GO/150 and TiO_2/GO/450 composites.

The energy band gap is calculated as 3.4 eV, 3.25 eV and 2.9 eV for TiO_2, TiO_2/GO/450 and TiO_2/GO/150, respectively by the method described in the literature [66] (Figure 6.21). It has been observed that the bang gap energy decreases by the effect of GO present in TiO_2 and is the least for the composite TiO_2/GO/150. It is supposed that Ti-O-C bonds which are formed by the unpaired π-electrons moving free on the TiO_2 surface resulted in up shifted valance band edge and reduced band gap [67].

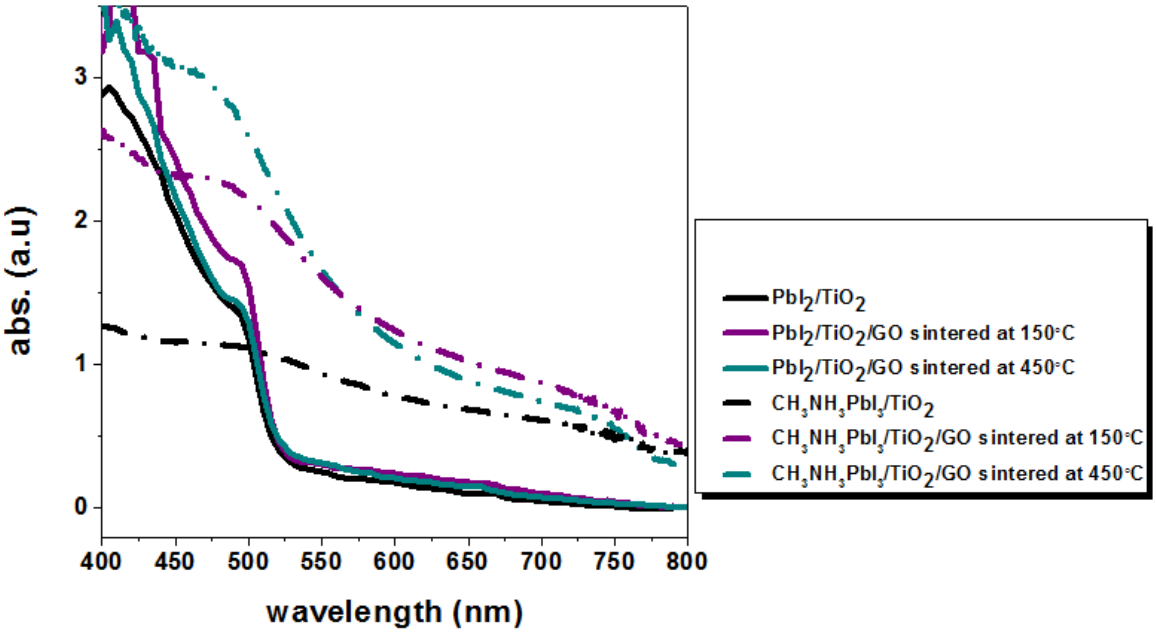

Figure 6.22: Absorption spectra of Sensitized TiO_2, TiO_2/GO/150 and TiO_2/GO/450 composites.

The dense, uniform and fine quality layer of perovskite developed over TiO_2/GO/150 is further analyzed by UV-vis spectroscopy to see the optical property enhancement of the films. Figure 6.22 shows a comparative analysis of the absorbance of PbI_2/TiO_2, PbI_2/TiO_2/GO and $CH_3NH_3PbI_3/TiO_2$, $CH_3NH_3PbI_3/TiO_2$/GO films in visible region of solar spectra. All the perovskite films spectra are evidently red shifted than in comparison with PbI_2 films. PbI_2/TiO_2/GO/150 film showed the most red shifted absorption edge than that of PbI_2/TiO_2/GO/450 and PbI_2/TiO_2. Although all of the perovskite films are covering the whole area in visible region of spectra, $CH_3NH_3PbI_3/TiO_2$/GO/150 films demonstrated a huge exposure in the region between 550-800 nm.

6.3.2.3 Morphological analysis

Figures 6.23 (a) and (b) show the morphology of films prepared by TiO_2/GO annealed at 450°C and 150°C, respectively, at the same magnification. There is an apparent morphological difference in both the films due to the variation of annealing temperatures. Since the phase change from anatase to rutile happens only beyond 600°C, it is certain that no phase transition has taken place in TiO_2/GO films annealed at 450°C. It is observed from the surface images of both composites that grain boundaries are clearer and particles are visibly spherical in the film annealed at 450°C. Whereas the boundaries and particle shapes are not clear in the film annealed at 150°C. It is observed that porosity of film TiO_2/GO/450 is far better than that of TiO_2/GO/150 film but it looks more compact.

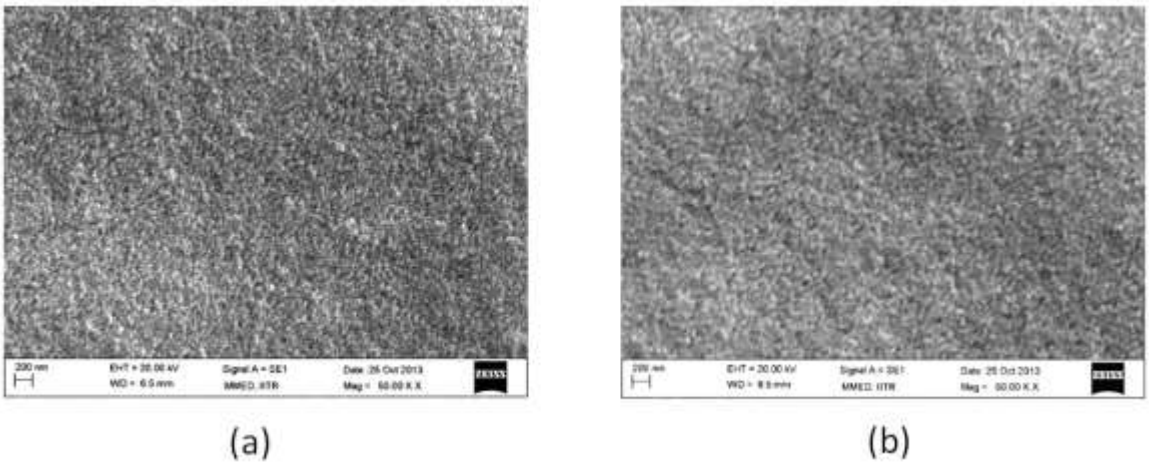

Figure 6.23: FESEM images of films prepared by TiO_2/GO annealed at (a) 450°C and (b) 150°C.

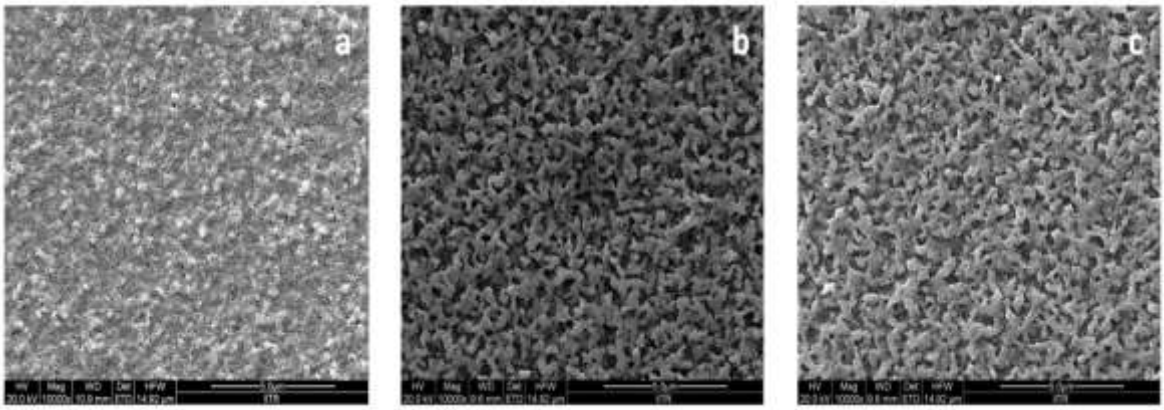

Figure 6.24: FESEM images of films after spin coating with PbI_2. $PbI_2/TiO_2/GO$ annealed at (a) 150°C, (b) 450°C and (c) PbI_2/TiO_2 annealed at 450°C.

Figures 24 (a), (b) and (c) show FESEM images at same magnificationof all the films ($PbI_2/TiO_2/GO$ annealed at 150°C, $PbI_2/TiO_2/GO$ annealed at 450°C and PbI_2/TiO_2 annealed at 450°C) after deposition of PbI_2 at same magnification. The coverage is good in all the films but more compact layer of PbI_2 over TiO_2 is observed in the films sintered at 150°C. It has been studied that surface chemistry of TiO_2 films depend on the sintering temperatures [68]. Due to higher temperature sintering the films of TiO_2/GO/450 incorporates a lot of voids. The solvents used in colloidal paste of TiO_2 nanoparticles are removed at higher temperatures, cause shrinkage of surface boundaries. This restricts the direct connection between TiO_2 nanoparticles in the film sintered at higher temperature and creates bridges type structures on PbI_2 deposition. The films sintered at low temperature are uniformly packed and show the homogeneous percolation of PbI_2 into the TiO_2/GO network (Figure 6.24 (a)).

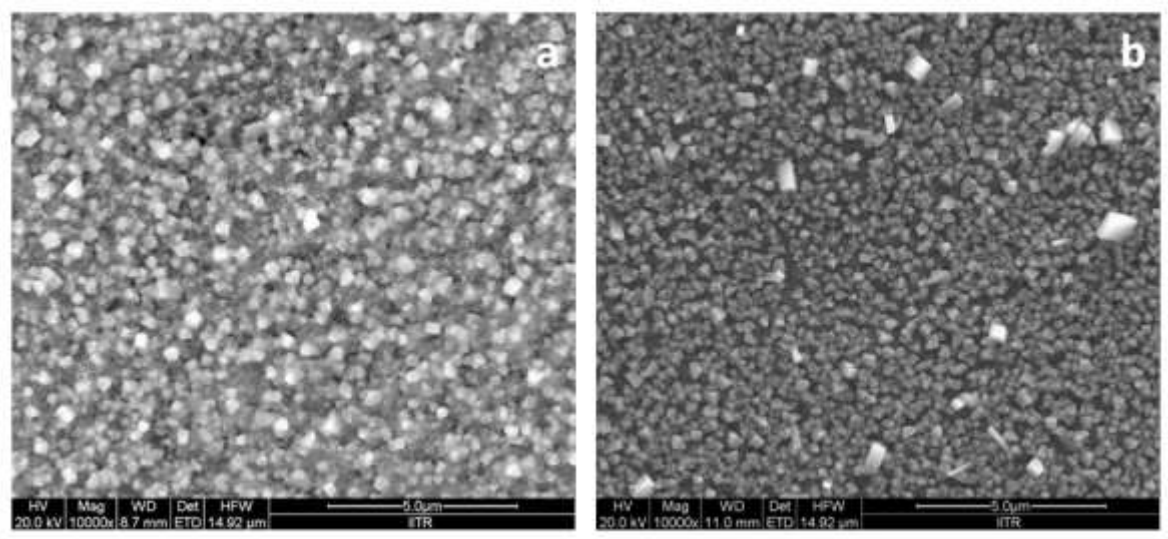

Figure 6.25: FESEM images of (a) $CH_3NH_3PbI_3/TiO_2$/GO/150 and (b) $CH_3NH_3PbI_3/TiO_2$/GO/450.

The similar distribution of perovskite is observed in $CH_3NH_3PbI_3/TiO_2$/GO films sintered at 150°C and 450°C which are shown in Figures 6.25 (a) and (b). Perovskite crystals are more closely packed in $CH_3NH_3PbI_3/TiO_2$/GO/150 than that of $CH_3NH_3PbI_3/TiO_2$/GO/450. Better coverage of TiO_2 film by perovskite substantiates better distribution and better optical properties, which is evidenced by absorption profile of the films (Figure 6.22).

Further the morphological properties of films are analyzed by Atomic Force Microscopy (AFM). Figures 6.26 (a) and (b) show 3D images of surface of TiO_2/GO, PbI_2/TiO_2/GO and $CH_3NH_3PbI_3/TiO_2$/GO films sintered at 150°C and 450°C, respectively. The uniformity of films sintered at 150°C is more apparent in the 3D images.

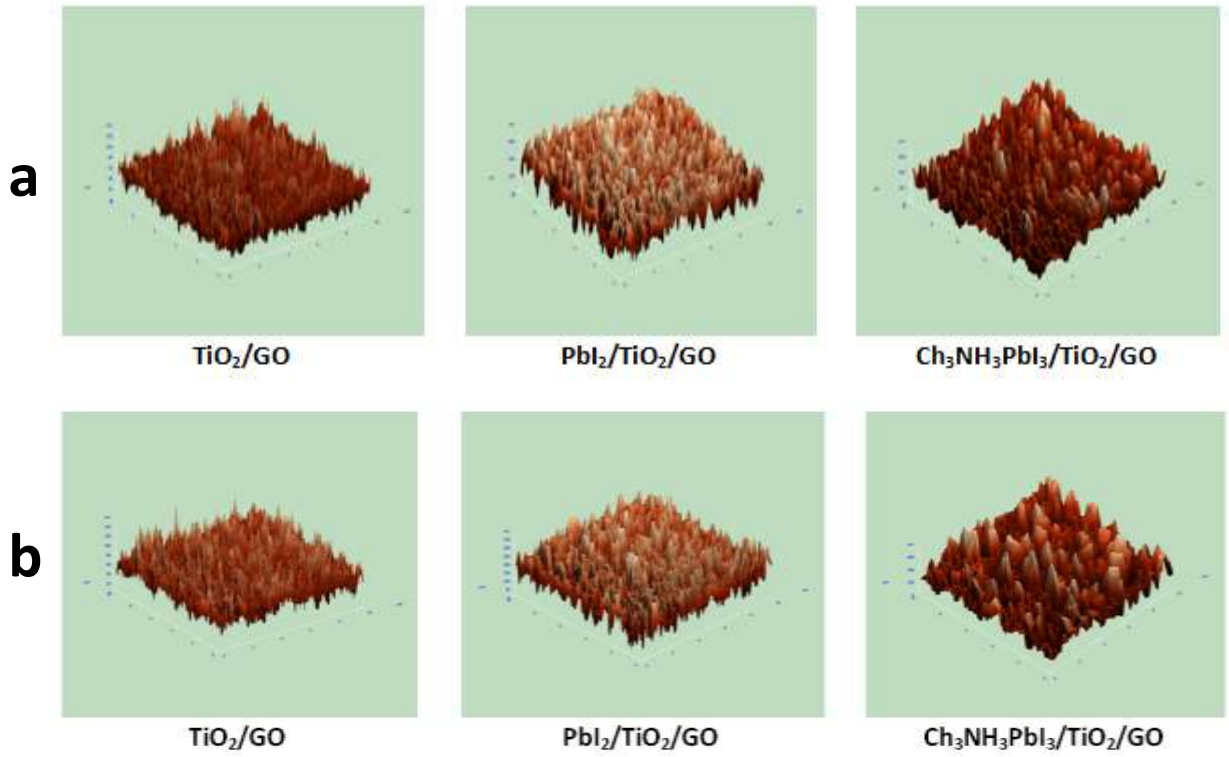

Figure 6.26: AFM (3D) images of TiO_2/GO, PbI_2/TiO_2/GO and $CH_3NH_3PbI_3/TiO_2$/GO after sintered at (a) 150°C and (b) when sintered at 450°C.

6.3.2.4 Analysis of perovskite based solar cell performance:

I-V curves in Figure 6.27 are showing the dark current of the devices (TiO_2, TiO_2/GO/150 and TiO_2/GO/450). The essential information which can be extracted from the dark current-voltage (*I-V*) characteristics are series resistance and shunt resistance which have the direct influence on fill factor (*FF*) of the solar cell [69]. The reduced *FF* of solar cell TiO_2/GO/450 affirms a rise in series resistance and a declined shunt resistance of the device. Device TiO_2 exhibits the lowest V_{oc}. The *J-V* characteristic and parameters of devices fabricated are shown in Figure 6.28 and Table 6.3. Device TiO_2/GO/150 shows the best *FF* yet the best J_{sc} is demonstrated by device TiO_2/GO/450. The highest J_{sc} of about 18.29

mA/cm^2 is exhibited by device TiO_2/GO/450 but the overall efficiency of device TiO_2/GO/150 was observed to be the best as 10.23%.

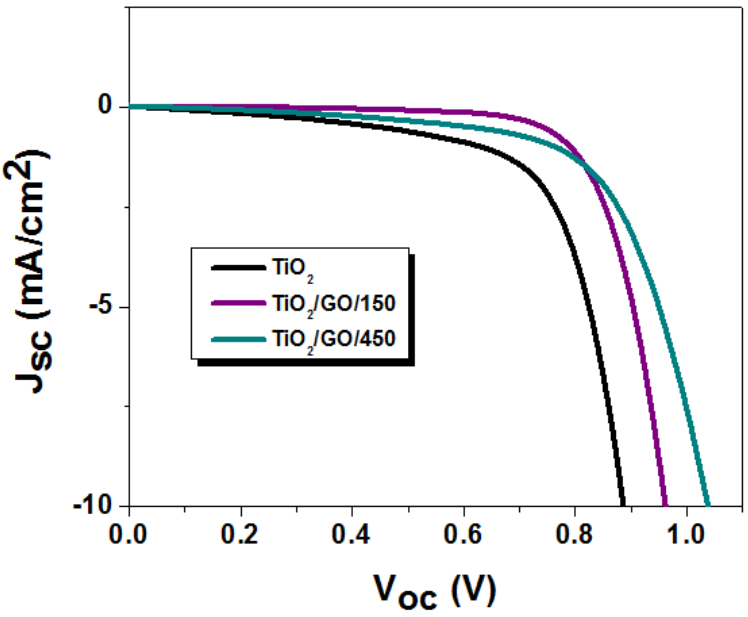

Figure 6.27: Dark current *I-V* characteristics of device TiO_2, TiO_2/GO/150 and TiO_2/GO/450.

The highest efficiency of device TiO_2/GO/150 is the outcome of all the parameters (J_{sc}, V_{oc}, *FF*) being fairly moderate in respect with devices TiO_2 and TiO_2/GO/450. The biggest drawback of perovskite based devices is the low *FF* which might arise due to unfavorable electronic contact between perovskite-FTO interfaces. The low temperature processed electron collection layer in device TiO_2/GO/150 is expected to be the reason behind high *FF* of this device.

A fair efficiency of 9.85% is realized by device TiO_2/GO/450 which is higher than the device TiO_2. Since both the devices are made by the films sintered at same temperature, i.e., 450°C, the raise in photovoltaic parameters in TiO_2/GO/450 is due to the incorporation

of GO. Although the *FF* of device TiO_2 is higher than device TiO_2/GO/450, the elevated V_{oc} and J_{sc} of later are the reason for its better performance. It has been studied that an efficient electron transfer takes place from TiO_2 nanoparticles to GO in TiO_2/GO composites so it is assumed that the majority of electrons are located in GO [70]. In this way TiO_2 is left with very less density of electrons and the chances of charge recombination at the perovskite-TiO_2 interface is reduced effectively, which finally contribute in increasing the photocurrent while in working condition [70].

Table 6.3: *I-V* parameters of device TiO_2, TiO_2/GO/150 and TiO_2/GO/450.

Device	J_{sc}(mA/cm^2)	V_{oc}(V)	*FF*	η (%)
TiO_2	14.90	0.889	61.16	8.11
TiO_2/GO/150	16.77	0.960	63.52	10.23
TiO_2/GO/450	18.29	0.958	56.23	9.85

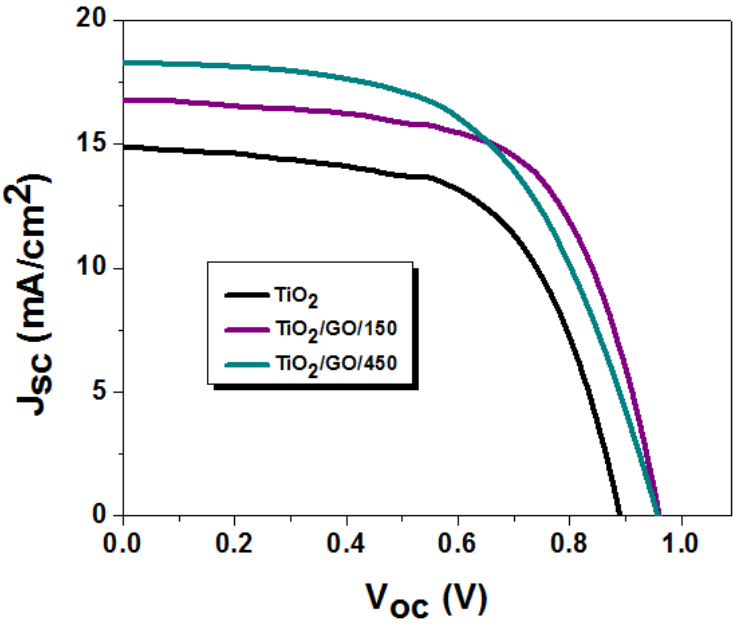

Figure 6.28: *I-V* characteristics of device TiO_2, TiO_2/GO/150 and TiO_2/GO/450 in 1 sun.

The cross sectional images of device TiO_2/GO/150 and TiO_2/GO/450 are shown in Figures 6.29 (a) and (b), which display a mesoporous structure wherein poly crystalline perovskite layer and spiroOMeTAD as a HTM layer are clubbed between TiO_2 and gold. It has been already studied in the dye sensitized solar cells that the GO incorporation does not affect the dye adsorption in the TiO_2film; it only enhances the visible light absorption [13, 71, 72]. Thus, it can be concluded that the higher efficiency of device TiO_2/GO/150 is due to the uniform and compact surface morphology of photoanode which influenced the charge generation and GO content increased the charge collection efficiency of the device [58].

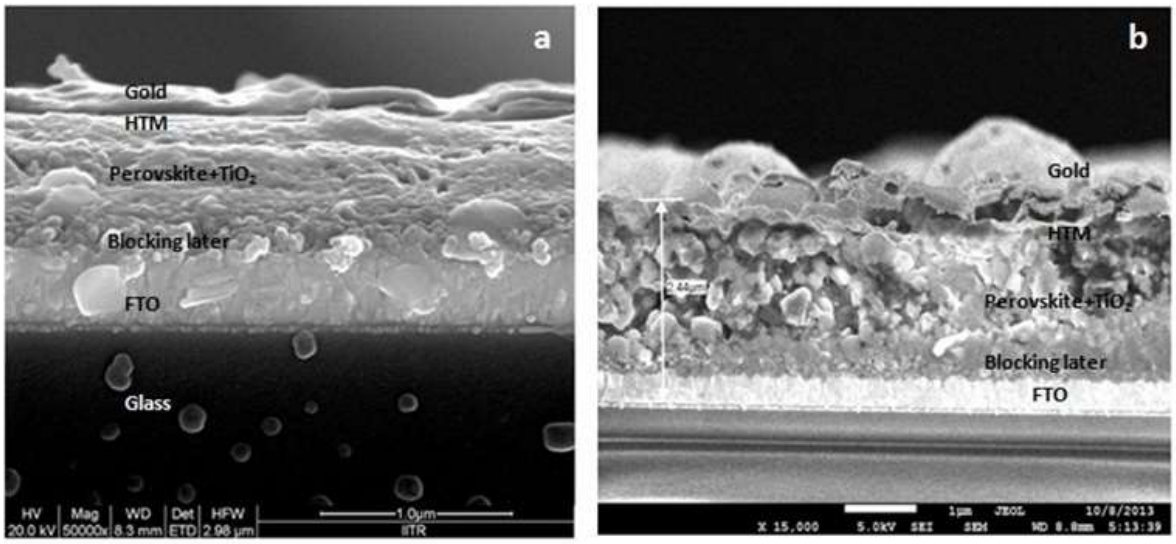

Figure 6.29: Cross sectional FESEM images of devices (a) TiO_2/GO/150 and (b) TiO_2/GO/450.

The external quantum efficiency (EQE) of devices TiO_2, TiO_2/GO/150 and TiO_2/GO/450 are observed as 49%, 62% and 76%, respectively (Figure 6.30). Apart from the superior charge mobility of GO than that of TiO_2, its work function lies in between FTO and

TiO_2 conduction band. So it may facilitate a better charge collection by reducing the energy barriers [73]. The enhancement of EQE from 49 to 76% reflects the enormous improvement in charge collection efficiency due to GO incorporation in TiO_2. The huge jump in EQE in visible light region in case of device TiO_2/GO/450 is in accordance with the hyperchromic shift of absorption spectra of film $CH_3NH_3PbI_3/TiO_2$/GO/450 in Figure 6.22.

6.3.3 Experimental

6.3.3.1 Synthesis of TiO_2/GO composite

GO used in this study is prepared by Hummers method [74] and stored in DI water after removal of aggregates by washing and centrifugation several times. GO is washed, sonicated and centrifuged in ethanol for several times, in order to wash away water content completely.

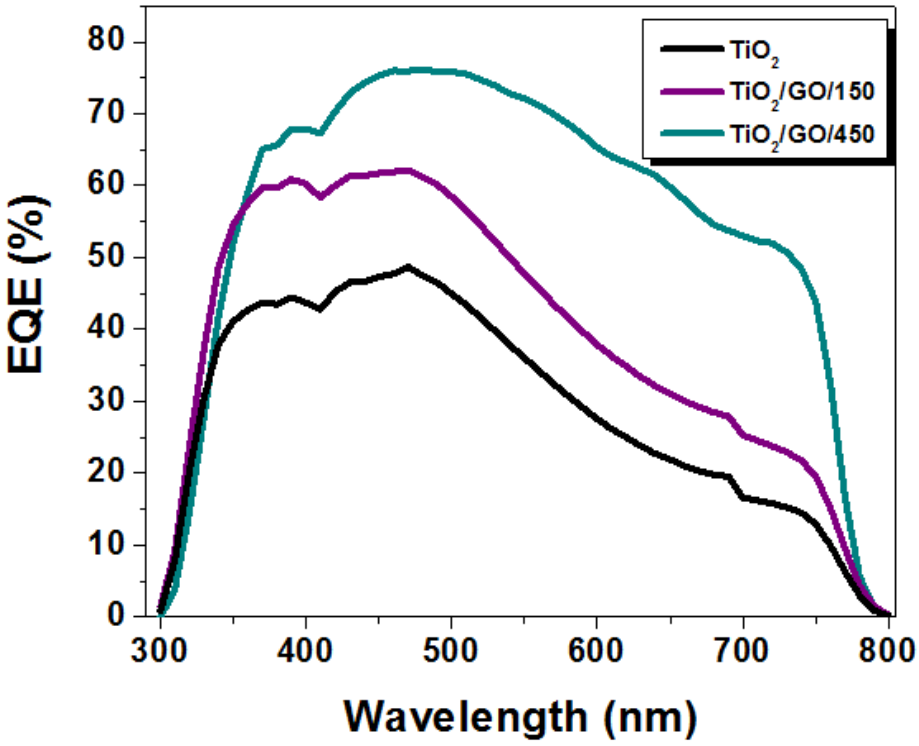

Figure 6.30: IPCE of devices TiO_2, TiO_2/GO/150 and TiO_2/GO/450.

Supernatant liquid is carefully discarded every time in order to collect GO in ethanol. TiO_2/GO composite is produced by physical mixing of both the contents in a fixed ratio. TiO_2 paste with 19 nm particle size is used in this study. GO is added to the paste in 0.1 wt% of total quantity. Mixture is further diluted by ethanol taken as five times of TiO_2 paste. The mixture is subsequently ultrasonicated and aged for 20-24 hours with constant stirring resulted in TiO_2/GO composite. The color of the composite is observed to be darker than the initial color of TiO_2.

6.3.3.2 Fabrication of solar cells

Solar cells were fabricated in the same way as discussed in earlier section of this chapter (sec. 6.2.3.2). The thickness was kept almost the same 380-420 nm throughout the study by restricting the rpm to 4500 for 30 sec. Since the study is based on different heat treatment temperatures on the properties of TiO_2/GO composite, the films produced are annealed at two temperatures, i.e., 150°C for half an hour and 450°C for two hours.

6.4 CONCLUSION

Present chapter justifies the effect of boiling points of different organic solvents used for the synthesis of TiO_2 nanoparticles. This work deliberates the effect of high boiling point of benzyl alcohol in comparison with the low boiling point of ethanol on TiO_2 nanoparticle size and other properties. The nanoparticles are formed in the particle size range of 20-30 nm and 40-60 nm with ethanol and benzyl alcohol, respectively. The BET surface area of the particles synthesized in this study is calculated as 66.6200 m^2/g and 40.0879 m^2/g with ethanol and benzyl alcohol, respectively. The pore size of 107.1184 Å and 74.1372 Å was observed. Both types of synthesized TiO_2 nanoparticles are used in perovskite solar cell fabrication. It has been observed that contrasting to DSSCs large surface area of

nanoparticles and more thickness of mesoporous layer may not be very beneficial for the perovskite based solar cell performance.

This chapter also elaborates the role of GO in enhancing charge transportation and charge collection efficiency of the solar cell. GO works as a charge collection layer in TiO_2/GO composite which facilitates in restricting the charge recombination. The best device results in the efficiency as high as 10.23%. It also elaborates the effect of low temperature annealing on film properties and distribution of perovskite crystals on the TiO_2 surface.

References:

1. Bach, U., Lupo, D., Comte, P., Moser, J. E., Weissörtel, F., Salbeck, J., Spreitzer, H., Grätzel, M., (1998), "Solid-state dye-sensitized mesoporous TiO_2 solar cells with high photon-to-electron conversion efficiencies", Nature, vol. 395, pp. 583-585.

2. Chang, J. A., Im, S. H., Lee, Y. H., Kim, H. j., Lim, C. S., Heo, J. H., Seok, S. I., (2012), "Panchromatic photon-harvesting by hole-conducting materials in inorganic-organic heterojunction sensitized-solar cell through the formation of nanostructured electron channels", Nano Lett. Vol. 12, pp. 1863-1867.

4. Martin, A. G., Baillie, A. H. and Snaith, H. J., (2014), "The emergence of perovskite solar cells", Nature Photonics, vol. 8, pp. 506-514.

5. Yukihiko, K., Hiroyuki, M. and Katsuhiko, H., (2002), "Structural Study on Cubic-Tetragonal Transition of $CH_3NH_3PbI_3$", J. Phys. Soc. Jpn, vol. 71(7), pp. 1694-1697.

6. Covaliu, C. I., Chioaru, L. C., Craciun, L., Oprea, O. and Jitaru, I., (2011), "Electrical properties of new organo-inorganic layered perovskites", Optoelectron. Adv. Mater., vol. 5, pp. 1097-1102.

7. Kim, H. S., Im, S. H. and Park, N. G., (2014), "Fabrication of semi-transparent perovskite films with centimeter-scale superior uniformity by the hybrid deposition method", J. Phys. Chem. C, vol. 118, pp. 5615-5625.

8. Burschka, J., Pellet, N., Moon, J., Humphry-Baker, S. R., Gao, P., Nazeeruddin, M. K. and Gratzel, M., (2013), "Sequential deposition as a route to high-performance perovskite-sensitized solar cells", Nature, vol. 499, pp. 316-319.

9. Malinkiewicz, O., Yella, A., Lee, Y. H., Espallargas, G. M., Gratzel, M., Nazeeruddin, M. K. and Bolink, H. J., (2014), "Perovskite solar cells employing organic charge-transport layers", Nature Photon., vol. 8, pp. 128-132.

10. Chen, Q., Zhou, H., Hong, Z., Luo, S., Duan, H., Wang, H., Liu, Y., Li, G. and Yang, Y., Am, J., (2013), "Planar heterojunctionperovskite solar cells via vapor-assisted solution process", Chem. Soc.,Vol. 136, pp. 622-625

11. Burschka, J., Pellet, N., Moon, S., Humphry-Baker, R., Gao, P., Nazeeruddin, M. K. and Grätzel, M., (2013), "Sequential deposition as a route to high-performance perovskite-sensitized solar cells", Nature, vol. 499, pp. 316-319.

12. Yella, A., Heiniger, L., Gao, P., Nazeeruddin, M. K. and Grätzel, M., (2014), "Nanocrystalline Rutile Electron Extraction Layer Enables Low-Temperature Solution Processed Perovskite Photovoltaics with 13.7% Efficiency", Nano Lett., Vol. 14, pp. 2591-2596.

13. Kim, H. S., Lee, J. W., Yantara, N., Boix, P. P., Kulkarni, S. A., Mhaisalkar, S., Grätzel, M., Park, N. G., (2013), "High Efficiency Solid-State Sensitized Solar Cell-Basedon Submicrometer Rutile TiO_2 Nanorod and$CH_3NH_3PbI_3$ Perovskite Sensitizer", Nano Letters, vol. 13 , pp. 2412-2417.

14. Im, J. H., Lee, C. R., Lee, J. W., Park, S. W., Park, N. G., (2011), "6.5% efficient perovskite quantum-dot-sensitized solar cell", Nanoscale , vol. 3, pp. 4088-4093.

15. Niederberger, M., Bart, H. M., Stucky, D. G., (2002), "Benzyl Alcohol and Titanium Tetrachloride- A Versatile Reaction System for the Nonaqueous and Low-Temperature Preparation of Crystalline and Luminescent Titania Nanoparticles", Chem. Mater., vol. 14, pp. 4364-4370.

16. Niederberger, Markus,Pinna, Nicola, (2009), “Metal Oxide Nanoparticles In Organic Solvents, Aqueous and Non Aqueous Sol-GelChemistry”, (Chapter-2), Springer London, pp 7-18.

17. Azizia, R., Rasouli, S., Ahmad, N. P., Jafarijafarkola, A. and Azizi, M., (2012), “A systematic investigation of experimental conditions on the particle size and structure of TiO_2 nanoparticles synthesized by a sol-gel method”, Journal of Ceramic Processing Research, vol. 13(2), pp. 164-169.

18. PDF Card #00-001-0562 PCPDFWIN Version 2 JCPDS-ICDD 2009.

19. Burgos, M. and Langlet, M., (1999), “The Sol-Gel Transformation of TIPT Coatings: A FTIR Study”, Thin Solid Films, Vol. 349, No. 1-2, pp. 19-23.

20. Harizanov, O., Harizanova, A., (2000), "Development and investigation of sol-gel solutions for the formation of TiO_2 coatings", Sol En Met., vol. 63(2), pp. 185-195.

21. Djaoued, Y., Taj, R., Brüning, R. S., Badilescu, P. V., Ashrit, G. Bader, Vo-Van, T., (2002), ”Study of the phase transition and the thermal nitridation of nanocrystalline sol-gel titania films”, Non-Cryst. Solids, Vol. 297, pp. 55-66.

22. Jiang, X., Wang, Y., Herricks, J. and Xia, Y., (2004), “Ethylene glycol-mediated synthesis of metal oxide nanowires”, J. Mater Chem., Vol. 14, pp. 695-703.

23. Pathak, C. S., Agarwala, V., (2013), “Synthesis and characterization of zinc sulphide nanoparticles prepared by mechanochemical route”, Superlattices and Microstructures, vol. 58, pp. 135-143.

24. Efros, A. L., (1982), “Interband absorption of light in a semiconductor sphere”, Fiz. Tekh. Poluprovodn, vol. 16, pp. 1209-1214.

25. Brus, L. E. J., (1984), "Electron-electron and electron-hole interactions in small semiconductor crystallites: The size dependence of the lowest excited electronic state", Chem. Phys., vol. 80, pp. 4403-4409.

26. Wu, Y., Islama , A., Yang, X., Qin, C., Liu, J., Zhang, K., Peng, W. and Han, L., (2014), "Retarding the crystallization of PbI_2 for highly reproducible planar-structured perovskite solar cells via sequential deposition", Energy Environ. Sci., vol. 7, pp. 2934-2938.

27. Zhu, Y., Zhang, L., Gao, C., Cao, L., (2000), "The senthesis of nanosized TiO_2 powder using a solgel method $TiCl_4$ as a precursor", J. Math. Sci., vol. 35, pp. 4049-4054.

28. Shahruz, N., Hossain, M. M., (2011), "Synthesis andsize-control of TiO_2photocatalyst nanoparticles preparation using sol-gel method", World Appl. Sci. J., vol. 12 (11), pp. 1981-1986.

29. Noh, J. H., Joong Jeon, N., Choi, Y. C., Nazeeruddin, M. K., Seok, M. G. S., (2013), "Nanostructured $TiO_2/CH_3NH_3PbI_3$ heterojunction solar cells employing spiro-OMeTAD/Co-complex as hole-transporting material", J. Mater. Chem. A, vol. 1, pp. 11842-11847.

30. Burschka, J., Pellet, N., Moon, S. J., Humphry-Baker, R., Gao, P., Nazeeruddin, M. K. and Grätzel, M., (2013), "Sequential deposition as a route to high-performance perovskite-sensitized solar cells", Nature, vol. 499, pp. 316-319.

31. Lee, J. W., Seol, D. J., Cho, A. N. and Park, N. G., (2014), "High-Efficiency Perovskite Solar Cells Based on the Black Polymorph of $HC(NH_2)_2PbI_3$", Adv. Mater, vol. 26, pp. 4991-4998.

32. Burschka, J., Pellet , N., Moon , S. J., Humphry-Baker , R., Gao, P., Nazeeruddin, M. K., Grätzel, M., (2013), "Sequential deposition as a route to high-performance perovskite-sensitized solar cell", Nature, vol. 499 (7458), pp. 316-319.

33. Liu, M., Johnston, M. B., Snaith, H. J., (2013), "Efficient planar heterojunctionperovskite solar cells by vapour deposition", Nature, vol. 501, pp. 395-398.

34. Science News, (2013), "Breakthrough of the Year-Newcomer Juices Up the Race to Harness Sunlight", Science, vol. 342, pp. 1438.

35. Park, N. G., (2013), "Organometal perovskite light absorbers towards a 20% efficiencylow-cost solid-state mesoscopic solar cell", J. Phys. Chem. Lett., vol. 4, pp. 2423-2429.

36. Snaith, H. J., (2013), "The emergence of a new era for low-cost, high-efficiency solar cells", J. Phys. Chem. Lett., vol. 4, pp. 3623-3630.

37. Noh, J. H., HyukIm, S., Heo, J. H., Mandal, T. N. and Seok, S., (2013), "Chemical Management for colorful, efficient, and stable inorganic-organic hybrid nanostructured solar cells", Nano Lett, vol. 13, pp. 1764-1769.

38. Ahmad, S., Hanmandlu, C., Kanaujia, K. P. and Prakash, G. V., (2014), "Direct deposition strategy for highly ordered inorganic organic perovskite thin films and their optoelectronic applications", Optical Material Express, vol. 14(7), pp. 1313-1323.

39. Samuel, D. S., (2013), "Electron-hole diffusion lengths exceeding 1 micrometer in an organometal trihalide perovskite absorber", Science, vol. 342, pp 341.

40. Qin, P., Domanski, Anna L., Chandiran, A. K., Berger, R., Butt, J., Dar, M. I., Moehl, T., Tetreault, N., Gao, P., Ahmad, S., Nazeeruddin, M. K. and Gr¨atzel, M., (2014), "Yttrium-substituted nanocrystalline TiO_2 photoanodes for perovskite based heterojunction solar cells", Nanoscale, vol. 6, pp. 1508-1514.

41. Christians, J. A., Fung, R. C. M. and Kamat, P. V., (2014), "An inorganic hole conductor for organo-lead halide perovskite solar cells improved hole conductivity with copper iodide", J. Am. Chem. Soc, vol. 136, pp. 758-764.

42. Bi, D., Yang, L., Boschloo, G., Hagfeldt, A. and Johansson, E. M. J., (2013), "Effect of different hole transport materials on recombination in $CH_3NH_3PbI_3$ perovskite-sensitized mesoscopic solar cells", J. Phys. Chem. Lett., vol. 4, pp. 1532-1536.

43. Choi, W., Termin, A. & Hoffmann, M. R., (1994), "The role of metal ion dopants in quantum-sized TiO_2: correlation between photoreactivity and charge carrier recombination dynamics", J. Phys. Chem., vol. 98, pp. 13669-13679.

44. Sahi, R., Morikawa, T., Ohwaki, T., Aoki, K. & Taga, Y., (2001), "Visible-light photocatalysis in nitrogen-doped titanium oxides", Science, vol. 293, pp. 269-271.

45. Khan, S. U. M., Al-Shahry, M. & Ingler, W. B., (2002), "Efficient photochemical water splitting by a chemically modified n-TiO_2", Jr. Science, vol. 297, pp. 2243-2245.

46. Kim, H. S., Mora-Sero, I., Gonzalez-Pedro, V., Fabregat- Santiago, F., Juarez-Perez, E. J., Park, N. G., Bisquert, (2013), "Mechanism of carrier accumulation in perovskite thin-absorber solar cells", J. Nat. Commun., vol. 4, pp. 2242.

47. Jung, M. H., Chu, M. J., (2014), "Comparative experiments of graphene covalently and physically binding CdSe quantum dots to enhance the electron transport in flexible photovoltaic devices", nanoscale, vol. 7; 6(15), pp. 9241-9249.

48. Stengl, V., Bakardjieva, S., Grygar, T. M., Bludská, J. and Kormunda, M., (2013), "TiO_2-graphene oxide nanocomposite as advanced photocatalytic materials", Chemistry Central Journal, vol. 7(41), pp. 1-12.

49. Kamat, P. V., (2010), "Graphene-based nanoarchitectures, anchoring semiconductor and metal nanoparticles on a two-dimensional carbon support", Journal of Physical Chemistry Letters, vol. 1, (2), pp. 520-527.

50. Kamat, P. V., (2011), "Graphene-based nano assemblies for energy conversion", Journal of Physical Chemistry Letters, vol. 2, (3), pp. 242-251.

51. Lightcap, I. V., Kosel, T. H., Kamat, P. V., (2010), "Anchoring semiconductor and metal nanoparticles on a two-dimensional catalyst mat. storing and shuttling electrons with reduced graphene oxide", Nano Letters ,vol. 10, (2), pp. 577-583.

52. Krishnamurthy, S., Kamat, P. V., (2012), "Galvanic exchange on reduced graphene oxide: designing a multifunctional two-dimensional catalyst assembly", The Journal of Physical Chemistry, vol 117, (1), pp. 571-577.

53. Krishnamurthy, S., Lightcap, I. V., Kamat, P. V., (2011), "Electron transfer between methyl viologen radicals and graphene oxide: reduction, electron storage and discharge", Journal of Photochemistry and Photobiology a-Chemistry, vol. 221(2-3), pp. 214-219.

54. Zhang, X. Y., Li, H. P. and Cui, X. L., (2009), "Preparation and photocatalytic activity for hydrogen evolution of TiO_2/graphene sheets composite", chin J Inorg. Chem., vol. 25(11), pp. 1903-1907.

55 Lightcap, I. V., Kosel, T. H. & Kamat, P. V., (2010), "Anchoring semiconductor and metal nanoparticles on a two-dimensional catalyst mat. Storing and Shuttling Electrons with Reduced Graphene Oxide", Nano Lett., vol. 10, pp. 577-583.

55. Zhu, P., Nair, A. S., Shengjie, P., Shengyuan, Y., Ramakrishna, S., (2012), "Facile fabrication of TiO_2-graphene composite with enhanced photovoltaic and photocatalytic properties by electrospinning", ACS Appl. Mater. Interfaces, Vol. 4, pp. 581-585.

56. Sun, S., Gao, L., Liu, Y., (2010), "Enhanced dye-sensitized solar cell using graphene-TiO 2 photoanode prepared byheterogeneous coagulation", Appl. Phys. Lett., Vol. 96, pp. 0831131-0831133.

57. Tang, Y. B., Lee, C. S., Xu, J., Liu, Z. T., Chen, Z. H., He, Z. B., Cao, Y. L., Yuan, G. D., Song, H. S., Chen, L. M., Luo, L. B., Cheng, H. M., Zhang, W. J., Bello, I., Lee, S. T., (2010), "Incorporation of graphenes in nanostructured TiO_2 films via molecular grafting for dye-sensitized solar cell application", ACS Nano, Vol. 4, pp. 3482-3488.

58. Kim, H. N., Yoo, H., Moon, J. H., (2013), "Graphene-embedded 3D TiO_2 inverse opal electrodes for highly efficient dye-sensitized solar cells: morphological characteristics and photocurrent enhancement", Nanoscale, Vol. 5, pp. 4200-4204.

59. Zhang, H., Lv, X. J., Li, Y. M., Wang, Y., Li, J. H., (2010), "P25-Graphene Composite as a High Performance Photocatalyst", ACS Nano, Vol. 4, pp. 380-386.

60. Li, N., Liu, G., Zhen, C., Li, F., Zhang, L., Cheng, H. M., (2011), "TiO_2 Nanospheres/Graphene composites by template free self assembly", Adv. Funct. Mater. Vol. 21, pp. 1717-1722.

61. Liu, Y., Cheng, Y., Shu, W., Peng, Z., Chen, K., Zhou, J., Chen, W., Zakharovab, G. S., (2014), "Formation and photovoltaic performance of few-layered graphene-decorated TiO_2 nanocrystals used in dye-sensitized solar cells", Nanoscale, Vol. 6, pp. 6755-6762.

62. Hu, Z., Chen, Y., Hou, H., Yin, R., Liu, F., Chena, H., (2012), "Characterization of graphite oxide after heat treatment", New J. Chem., Vol. 36, 1373-1377.

63. Fan, W., Lai, Q., Zhang, Q., Wang, Y., (2011), "Nanocomposites of TiO_2 and Reduced Graphene Oxide as Efficient Photocatalysts for Hydrogen Evolution", J. Phys. Chem., Vol. 115, pp. 10694-10701.

64. Jia, L., Wang, D. H., Huang, Y. X., Xu, A. W., Yu, H. Q., (2011), "Highly Durable N-Doped Graphene/CdS Nanocomposites with Enhanced Photocatalytic Hydrogen Evolution from Water under Visible Light Irradiation", J. Phys. Chem., Vol. 115, pp. 11466-11473.

65. Bell, N. J., Ng, Y. H., Du, A., Coster, H., Smith, S. C., Amal, R., (2011), "Understanding the Enhancement in Photoelectrochemical Properties of Photocatalytically Prepared TiO_2-Reduced Graphene Oxide Composite", J. Phys. Chem., Vol. 115, pp. 6004-6009.

66. Pathak, C.S., Mandal, M. K., Agarwala, V., (2013), "Synthesis and characterization of zinc sulphide nanoparticles prepared by mechanochemical route", Superlattices and Microstructures, Vol. 58, pp. 135-143.

67. Zhang Y, Pan C., (2011), "TiO_2/graphene composite from thermal reaction of graphene oxide and its photocatalytic activity in visible light", J Mater Sci., Vol. 46, pp. 2622-2626.

68. Pichot, F., Pitts, J. R., Gregg, B. A., (2000), "Low-Temperature Sintering of TiO_2 Colloids: Application to Flexible Dye-Sensitized Solar Cells", Langmuir, Vol. 16, pp. 5626-5630.

69. Jenny Nelson (2003), "The Physics of Solar Cells", Imperial College Press. ISBN 978-1-86094-340-9.

70. Yang, N., Zhai, J., Wang, D., Chen, Y., Jiang, L., (2010). "Two-dimensional graphene bridges enhanced photoinduced charge transport in dye-sensitized solar cells", ACS Nano, Vol. 4, pp. 887-894.

71. Barea, E. M., Shalom, M., Gimenez, S., Hod, I., Mora-Sero, I., Zaban, A., Bisquert, J., (2010), "Design of Injection and Recombination in Quantum Dot Sensitized Solar Cells", J. Am. Chem. Soc., Vol. 132, pp. 6834-6839.

72. Barea, E., Xu, X. Q., Gonzalez-Pedro, V., Ripolles-Sanchis, T., Fabregat-Santiago, F., Bisquert, J., (2011), "Origin of efficiency enhancement in Nb_2O_5 coated titanium dioxidenanorod based dye sensitized solar cells", Energy Environ. Sci., Vol. 4, pp. 3414-3419.

73. Kim, H. S., Mora-Sero, I., Gonzalez-Pedro, V., Fabregat-Santiago, F., Juarez-Perez, E. J., Park, N. G., Bisquert, J. (2013), "Mechanism of carrier accumulation in perovskite thin-absorber solar cells", Nat. Commun., Vol. 4, Article 2242.

74. Hummers, W. S., Offeman, R. E. (1958), "Preparation of graphitic oxide",J. Am. Chem. Soc. Vol. 80, pp. 1339-1339.

Chapter 7: CONCLUSION

Present work represents the modulation of organic dye structure and development of TiO_2 semiconductor and establishes a coherent relationship between material properties and the performance of solar cells. The optimization of organic dye and perovskite based solar cells is the main focus of this study. Structural, optical, electrical, and transportation properties of the synthesized materials, i.e., organic dyes and TiO_2 nanoparticles, are analyzed thoroughly by different characterization tools. The initial part of the thesis includes a review on the materials and solar cells which elaborates the previous work done in this direction and the results obtained. The techniques used for material and device characterizations are also briefed.

In conclusion four studies have been carried out on solar cells,

- Designing, synthesis and application of tetra anchoring organic dyes in DSSCs and their cosensitization studies.
- Synthesis and application of mixed phase TiO_2 nanoparticles to analyze the effect of phase ratios on optical and DSSC performance.
- Effect of solvent boiling point on synthesis of TiO_2 nanoparticles by sol-gel method and their performance on perovskite based solar cells.
- Effect of graphene oxide (GO) on charge transfer in perovskite based solar cells.

7.1 DESIGNING, SYNTHESIS AND APPLICATION OF TETRA ANCHORING ORGANIC DYES IN DSSCs AND THEIR COSENSITIZATION STUDIES

Five carbazole cruciform derivative, functionalized at its 1, 3, 6, 8-positions and 2, 3, 6, 7-positions with thiophene and bi thiophene moieties were synthesized and applied on DSSCs successfully. Designing of organic dyes is done by taking carbazole unit as a donor

with four activated sites where bridging groups can be substituted in order to connect to the acceptor. The elongation of π-bridge helps in shifting the absorption towards longer wavelength. It has been evidenced that apart from molecular structure of dye and properties of semiconductors, DSSC performance depends upon some of the device fabrication parameters such as thickness of mesoporous TiO_2 film, dye loading time, presence of binary additives and cosensitization. Excessive thickness of mesoporous layer causes electron recombination which is detrimental for DSSC performance. Over layers can be developed due to longer dye loading and binary additives help in restraining charge recombination and aggregation of dye on TiO_2 film. The effect of aggregation on TiO_2 film seemed to dominate the optical behavior of the dyes with four anchoring dyes due to direct correlation of aggregation caused quenching with the dark current and consequently with electron lifetime and J_{sc}.

Cosensitization is found to be advantageous in order to reducing the dye aggregation and enhancing dye concentration in films, by rearranging the dye molecules on the TiO_2 surface. The surface morphologies of all sensitized and cosensitized films are analyzed by AFM. The overall efficiency has been improved to 4.1% from 2.6% by cosensitization. It is suggested that higher packing density of the dyes on film surface as a result of cosensitization is the major factor responsible for enhanced cell performance.

7.2 SYNTHESIS AND APPLICATION OF MIXED PHASE TiO_2 NANOPARTICLES TO ANALYZE THE EFFECT OF PHASE RATIOS ON OPTICAL AND DSSC PERFORMANCE

TiO_2 NPs which are synthesized and used in DSSC photoanodes are biphasic nanoparticles (mixture of anatase and rutile phases) which proved to have different properties

from their monophasic counterparts, i.e., anatase and rutile. It has been revealed by this study that different annealing temperatures are very significant in controlling the ratios of both the phases in biphasic TiO_2 nanoparticle. The existence of rutile NPs is proved to be superb way in reducing the band gap of semiconductor without doping. The optical band gap values are found to be in the range of 2.59-2.88 eV with increasing rutile component in the mixture of biphasic TiO_2. The increased ratio of rutile to anatase is beneficial for photovoltaic performance. The presence of rutile nanoparticles can be set to reduce the probability of recombination of excited electrons and holes which increases the short-circuit current (J_{sc}). An optimum current conversion efficiency of 6.08% has been achieved in this study.

7.3 EFFECT OF SOLVENT BOILING POINT ON SYNTHESIS OF TiO_2NANOPARTICLES BY SOL-GEL METHOD AND THEIR PERFORMANCE ON PEROVSKITE BASED SOLAR CELLS

In another study elaborated in this thesis the effect of boiling points of different organic solvents used for the synthesis of TiO_2 nanoparticles is described. The effect of high boiling point of benzyl alcohol in comparison with the low boiling point of ethanol on TiO_2 nanoparticle size and other properties has been elaborated. High boiling point of solvent offers longer time for nucleation and growth of nanoparticles and favors increased particle size. Both types on nanoparticles are optimized for solar cells based on perovskite material. The nanoparticles are formed in the particle size range of 20-30 nm and 40-60 nm with ethanol and benzyl alcohol, respectively. The BET surface area of the particles synthesized in this study is calculated as 66.6200 m^2/g and 40.0879 m^2/g with ethanol and benzyl alcohol, respectively. The pore size of 107.1184 Å and 74.1372 Å was observed. Both types of synthesized TiO_2 nanoparticles are used in perovskite solar cell fabrication. It has been

observed that contrasting to DSSCs large surface area of nanoparticles and more thickness of mesoporous layer may not be very beneficial for the perovskite based solar cell performance.

7.4 EFFECT OF GRAPHENE OXIDE (GO) ON CHARGE TRANSFER IN PEROVSKITE BASED SOLAR CELLS

The role of GO in enhancing charge transportation and charge collection efficiency of the solar cell has also been explored on perovskite based solar cells. It is substantiated that GO works as a charge collection layer in TiO_2/GO composite which restricts the charge recombination. The low temperature annealing of mesoporous layer is also studied and observed to be more suitable for perovskite based solar cell performance. The best device gave the efficiency as high as 10.23%.

Although this work does not present a final solution for energy crisis, some of the vital points are concluded for the betterment of conversion efficiency of solar cells which will be useful in future studies.

SUPPORTING INFORMATION

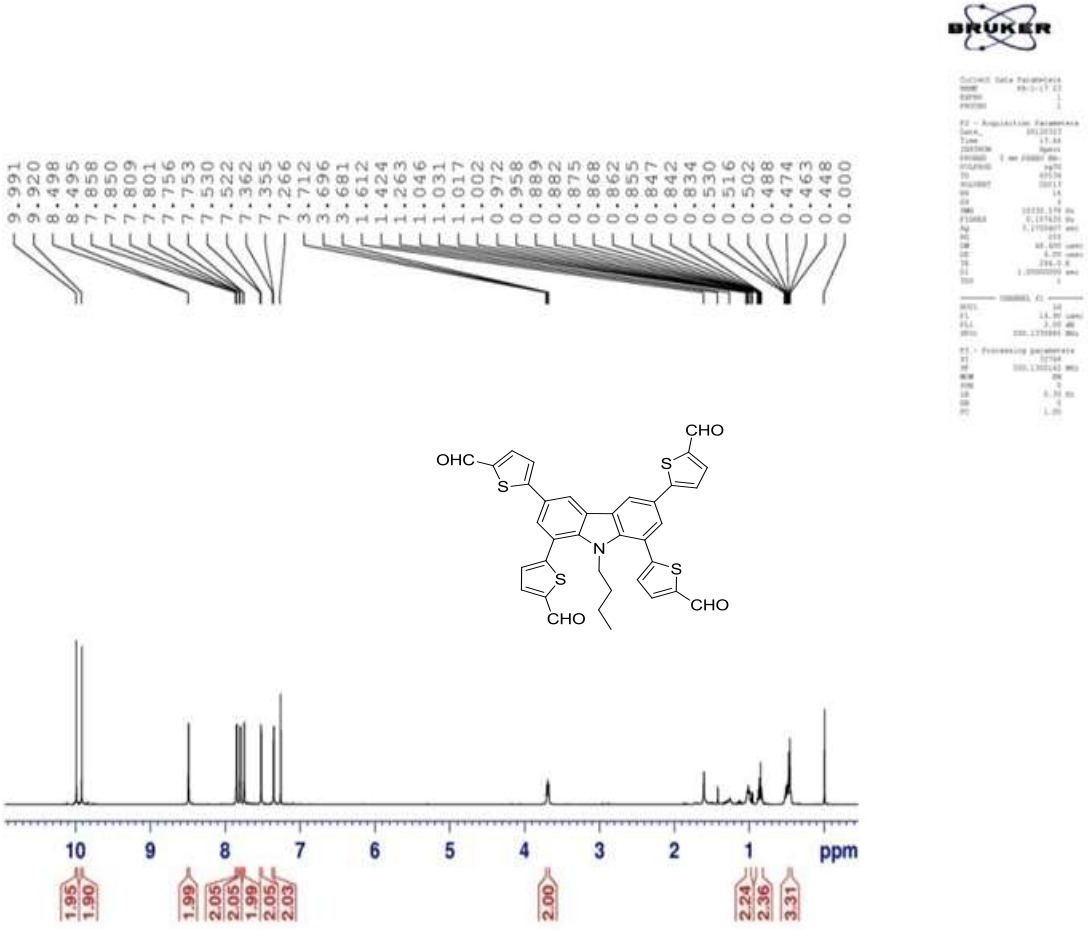

Figure S1: ^{1}H NMR of compound 1b recorded in $CDCl_3$

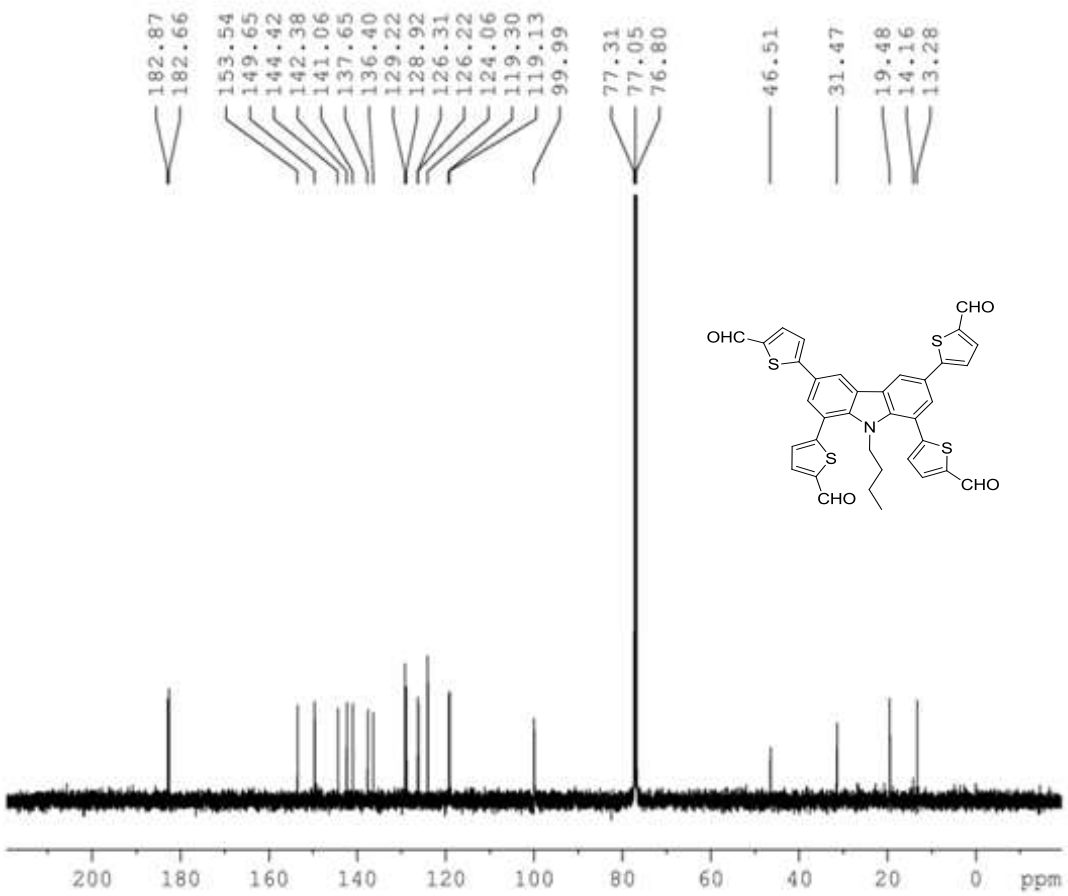

Figure S2: ^{13}C NMR of compound 1b recorded in $CDCl_3$

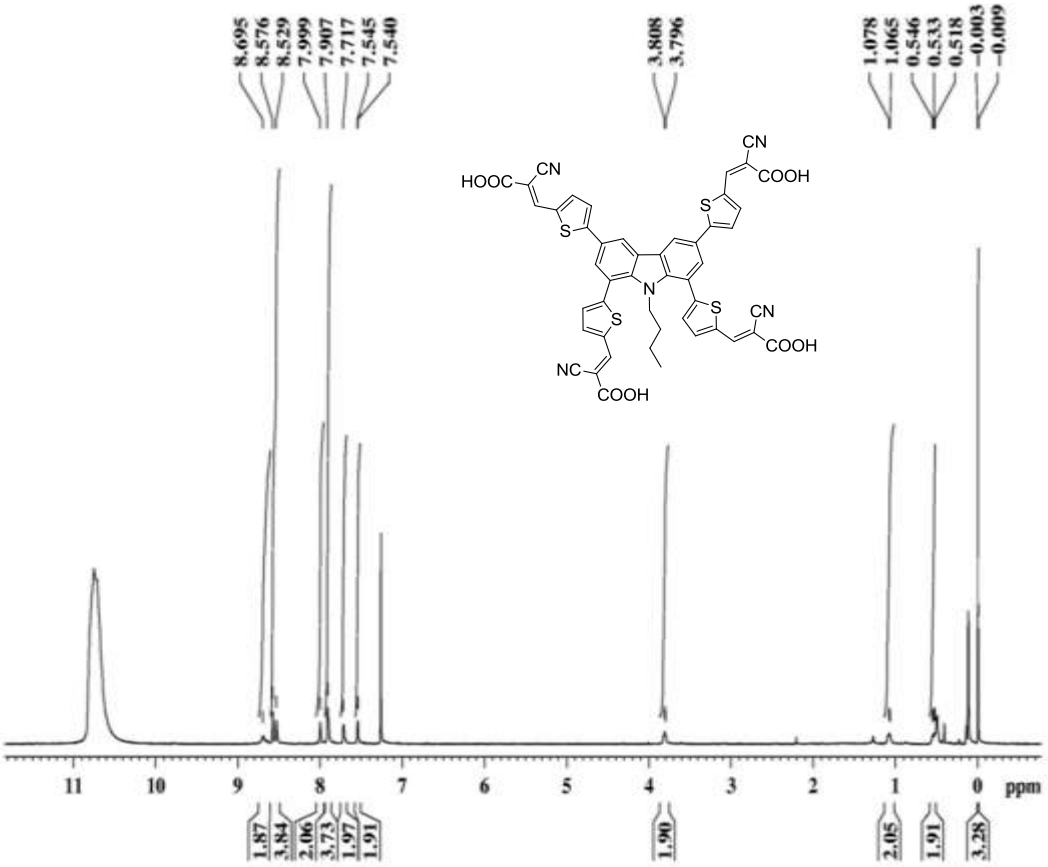

Figure S3: ^{1}H NMR of compound P1 recorded in $CDCl_3$+TFA

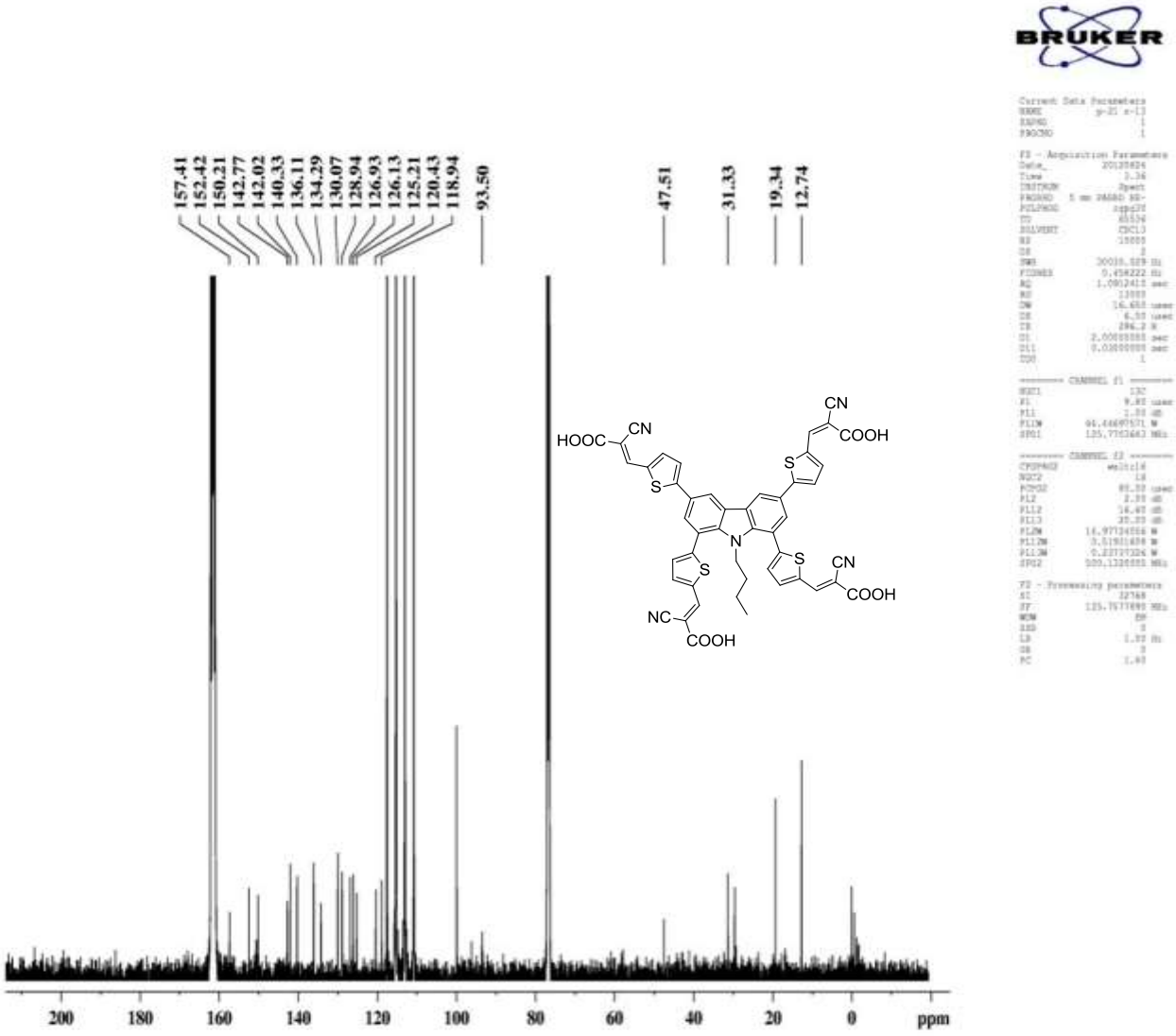

Figure S4: ^{13}C NMR of compound P1 recorded in $CDCl_3$+TFA

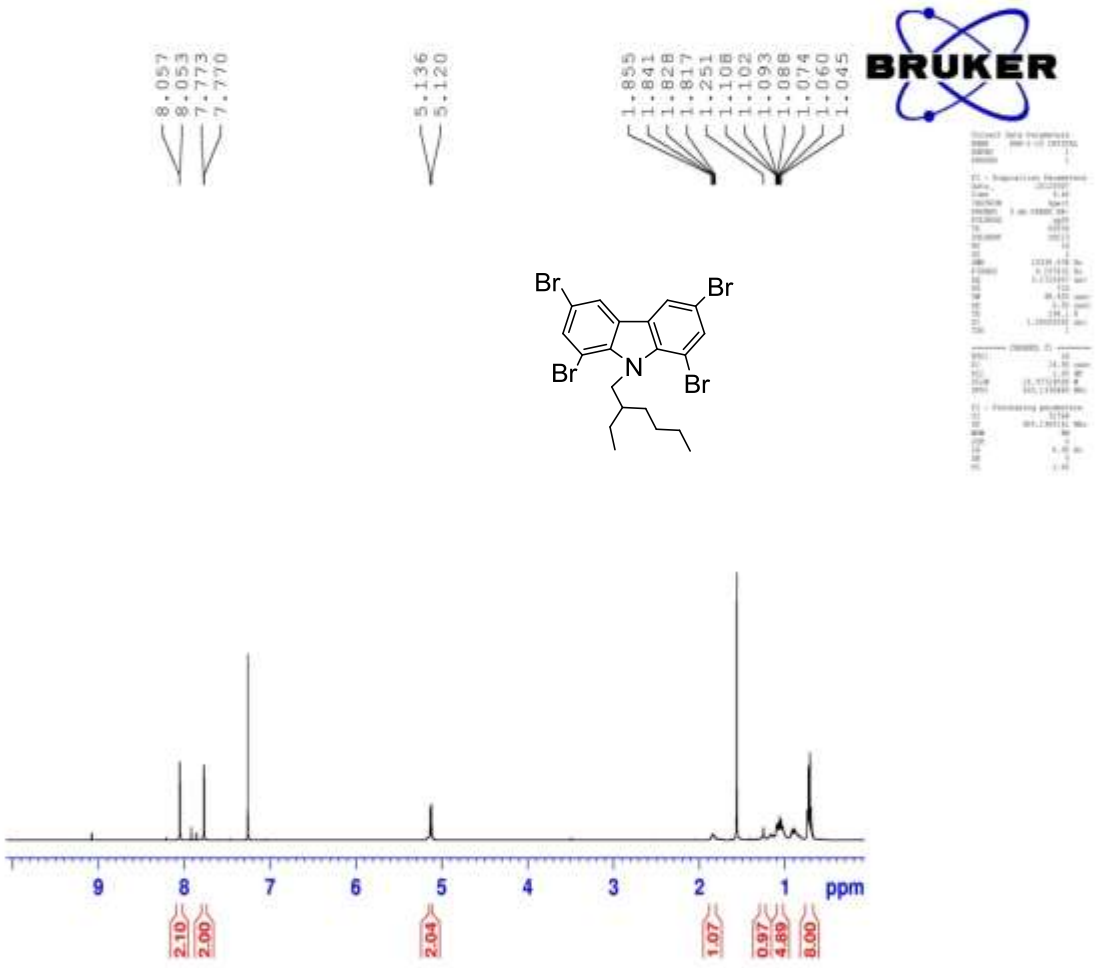

Figure S5: ^{1}H NMR of compound 2a recorded in $CDCl_3$.

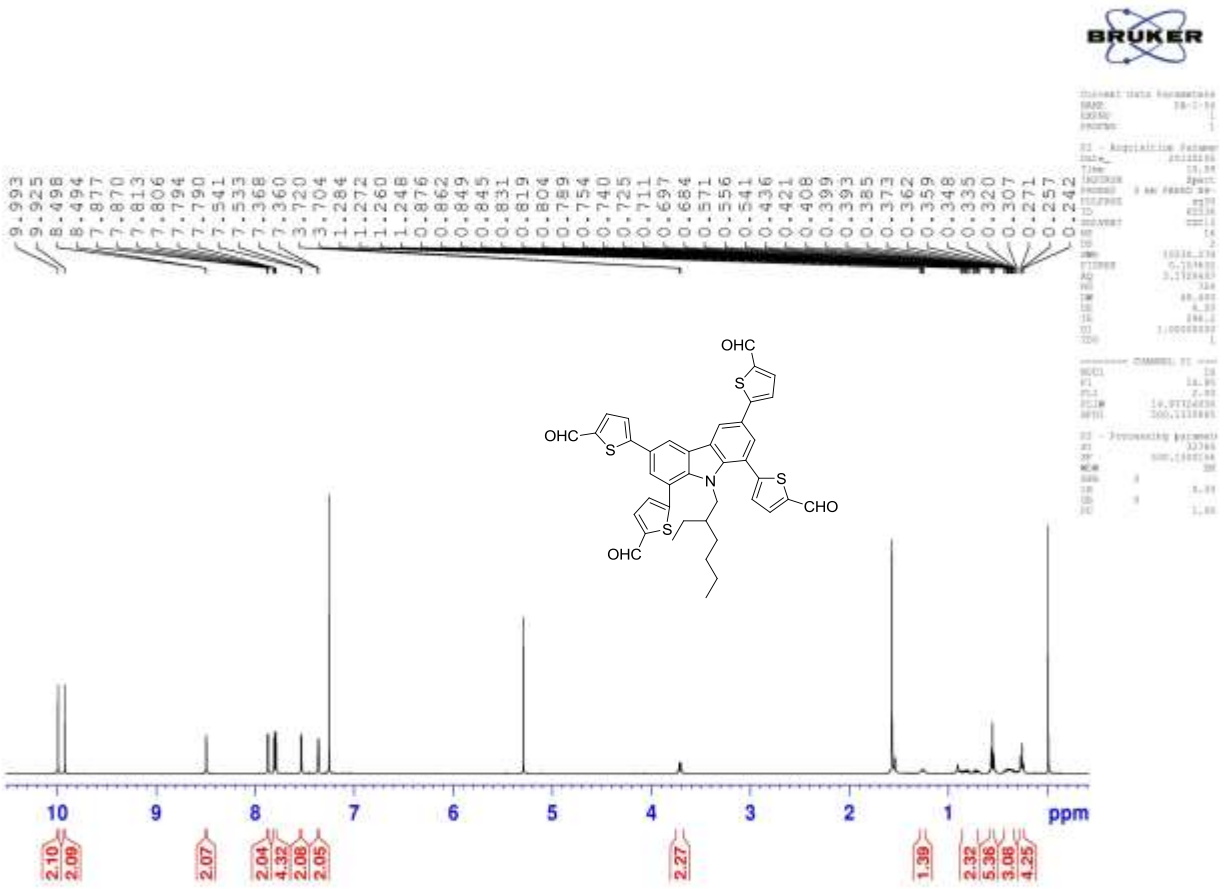

Figure S6: ^{1}H NMR of compound 2b recorded in $CDCl_3$.

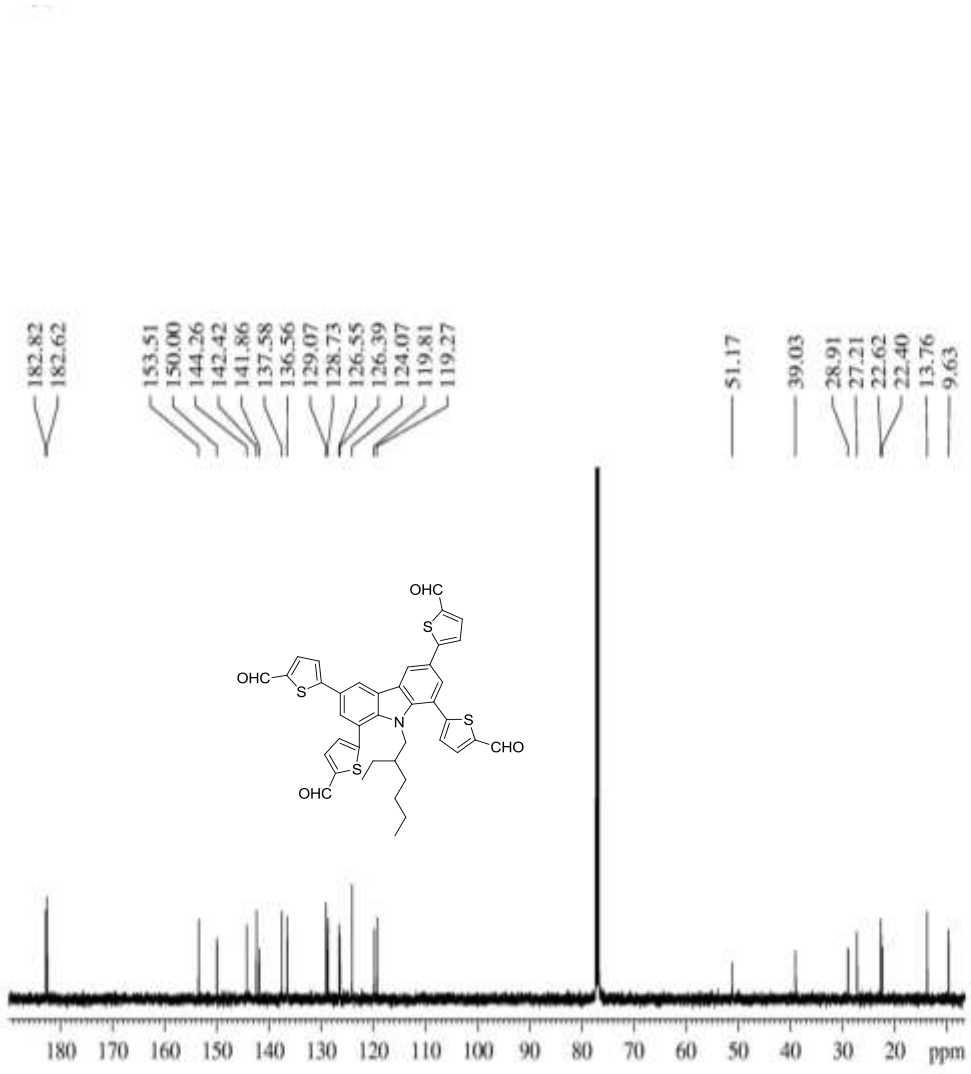

Figure S7: ^{13}C NMR of compound 2b recorded in $CDCl_3$

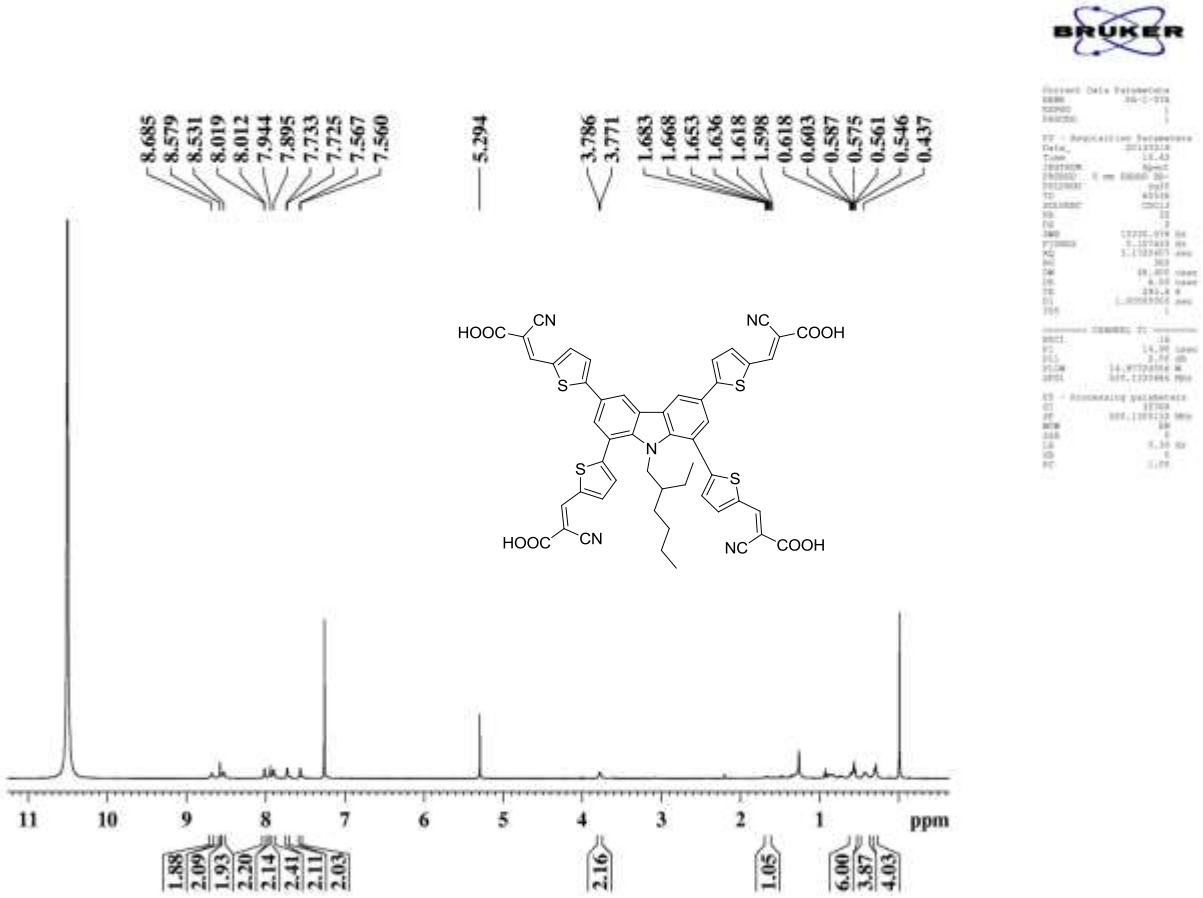

Figure S8: ^{1}H NMR of compound P2 recorded in $CDCl_3$+TFA.

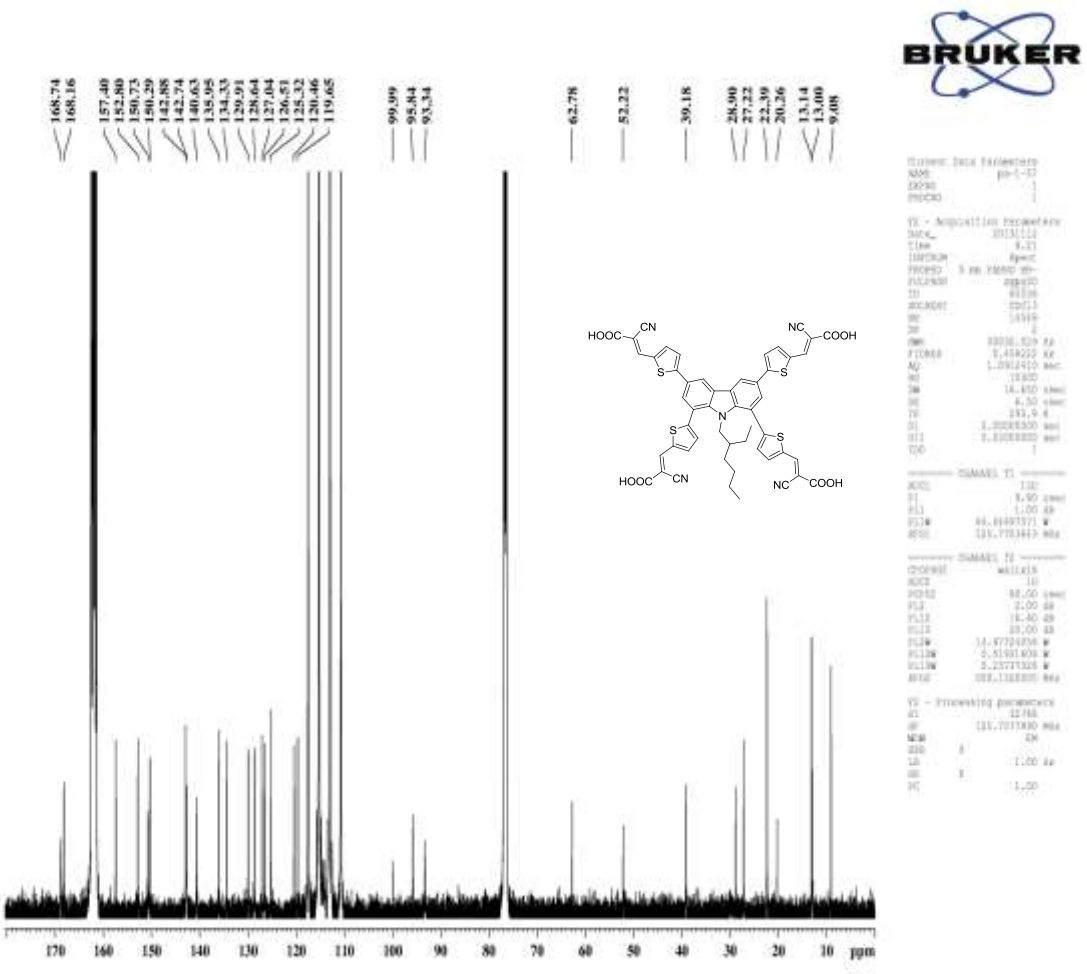

Figure S9: ^{13}C NMR of compound P2 recorded in $CDCl_3$+TFA.

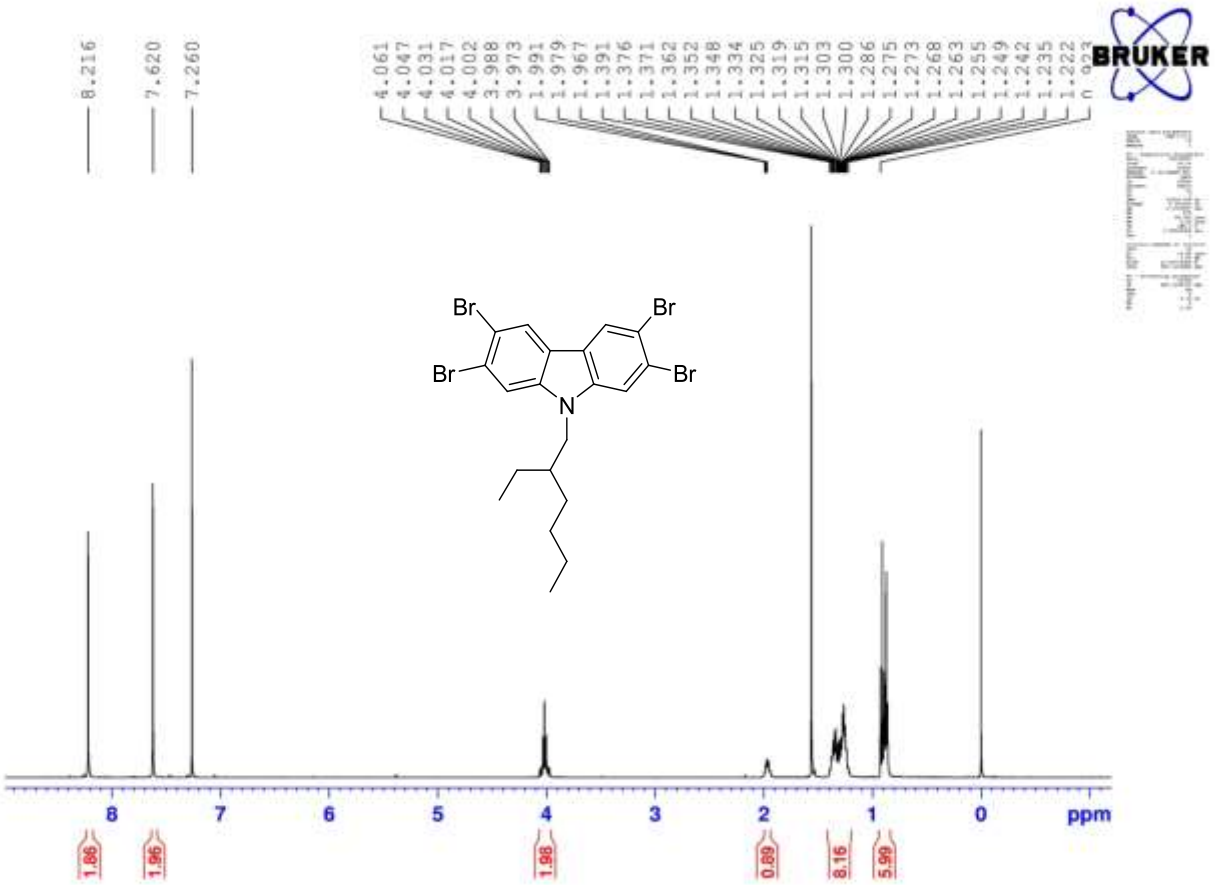

Figure S10: ^{1}H NMR of compound 3a recorded in $CDCl_3$.

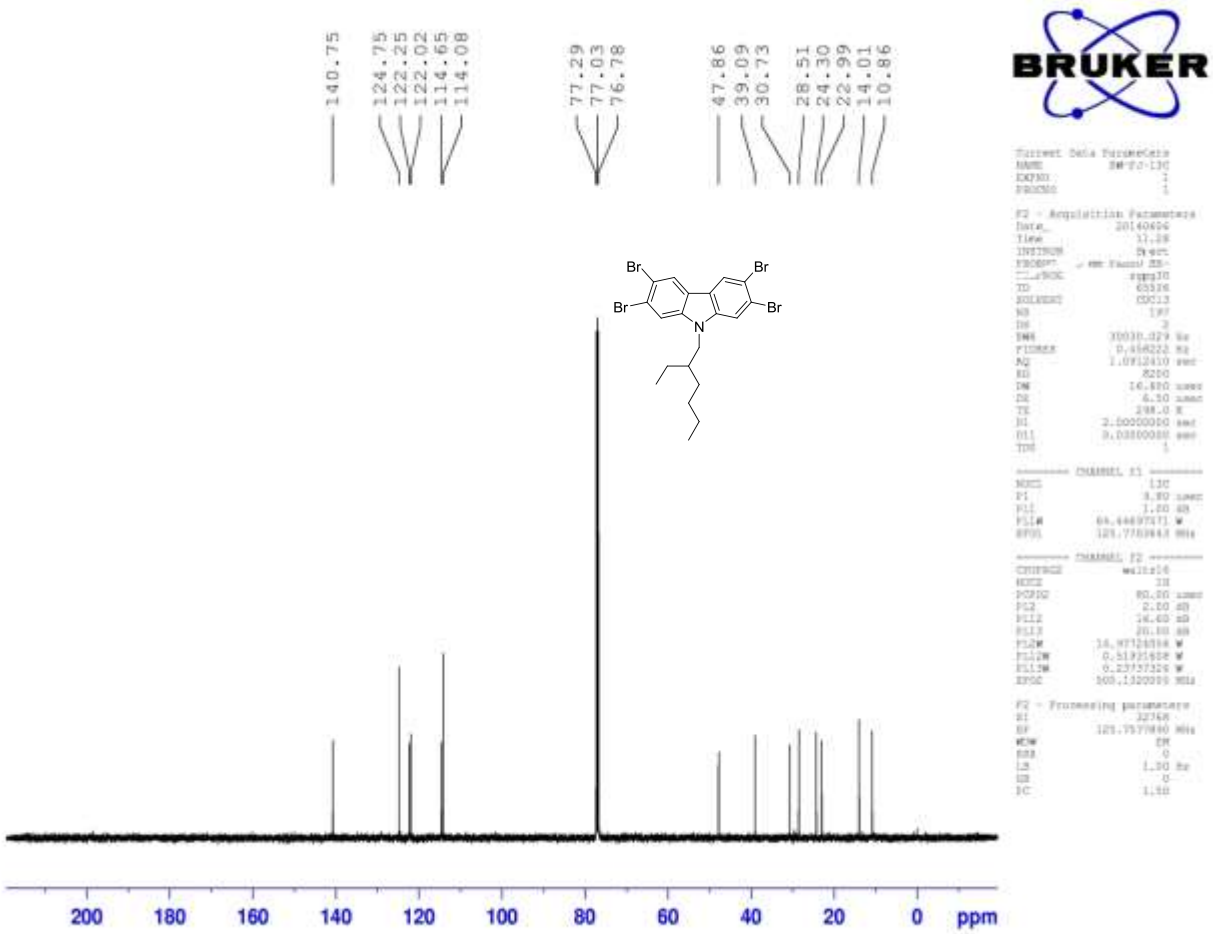

Figure S11: ^{13}C NMR of compound 3a recorded in $CDCl_3$.

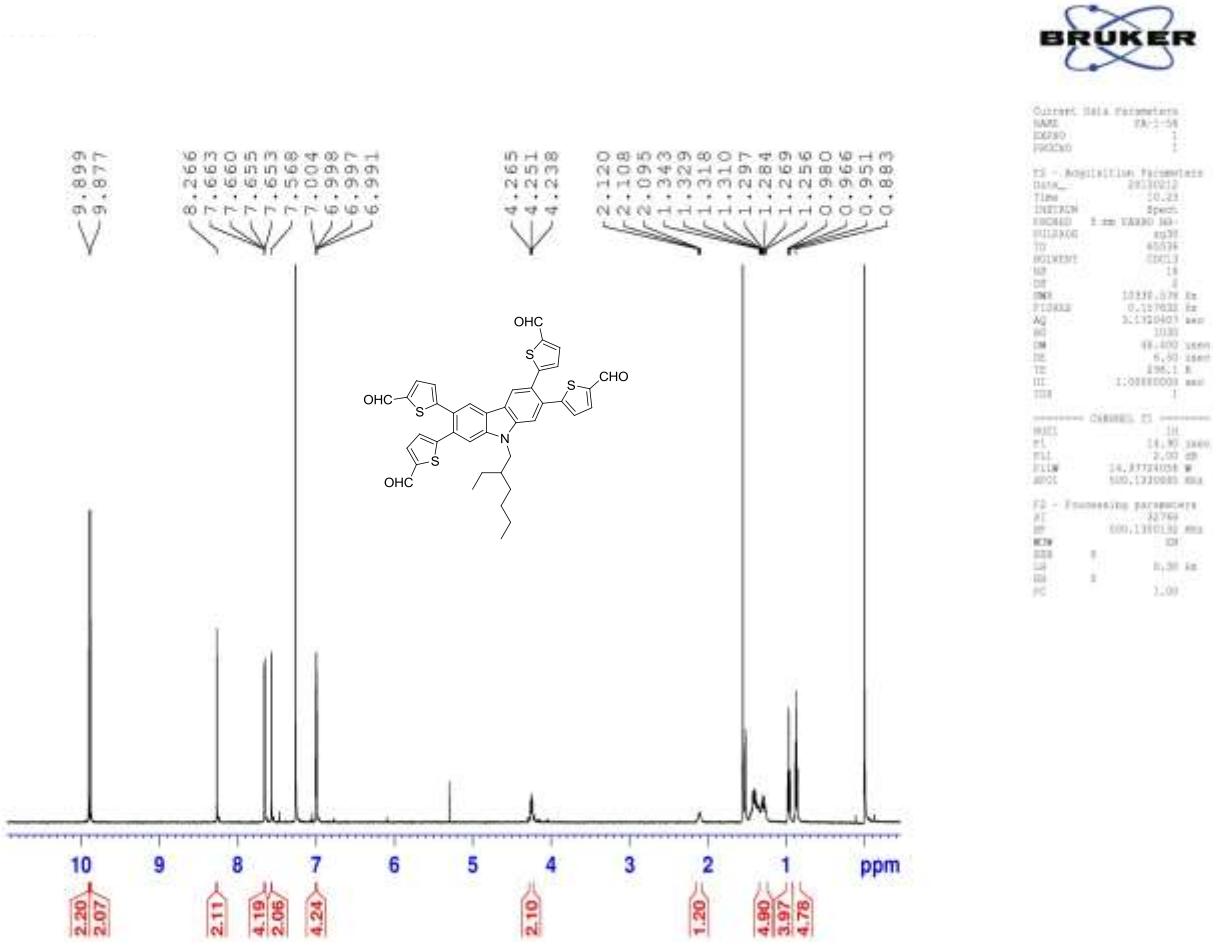

Figure S12: ^{1}H NMR of compound 3b recorded in $CDCl_3$.

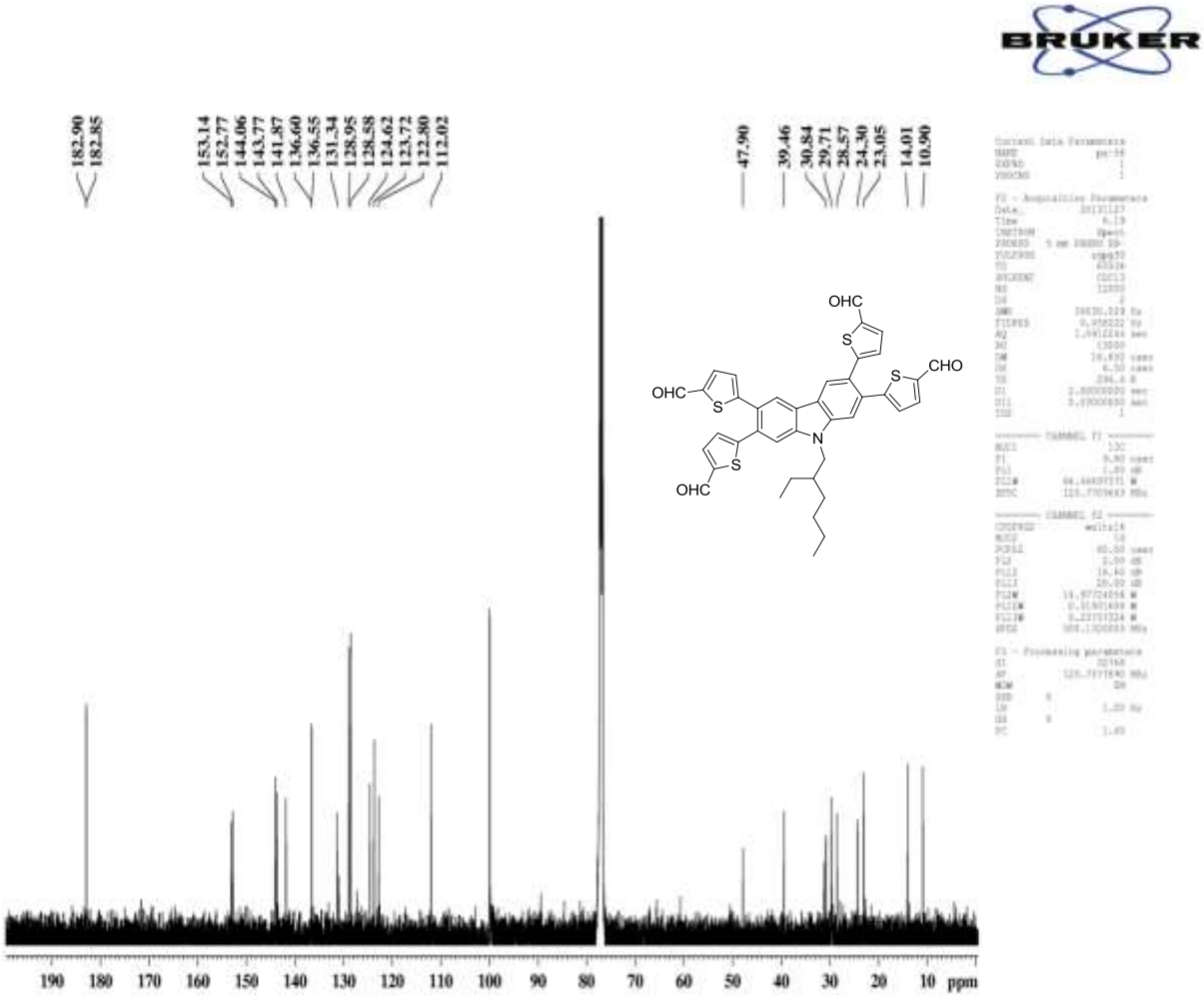

Figure S13: ^{13}C NMR of compound 3b recorded in $CDCl_3$.

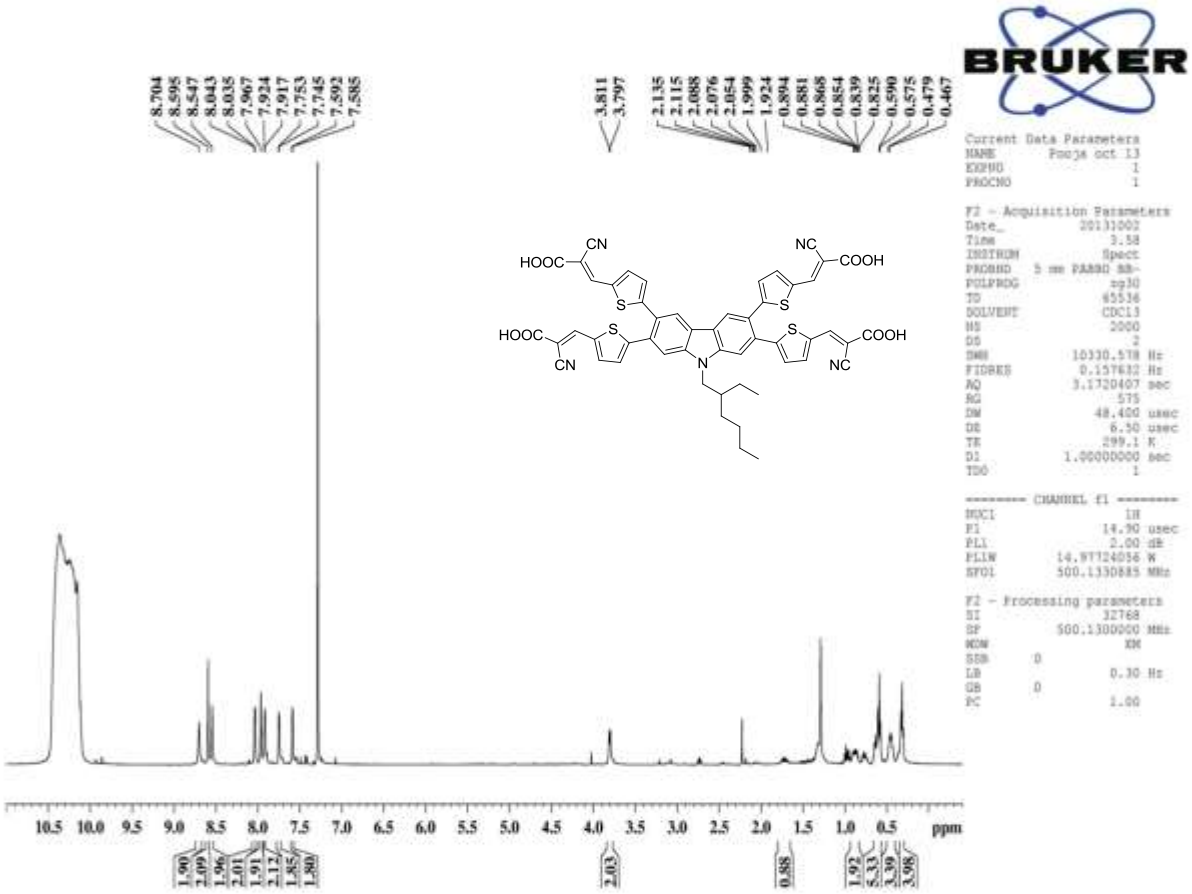

Figure S14: ^{1}H NMR of compound P3 recorded in $CDCl_3$+TFA.

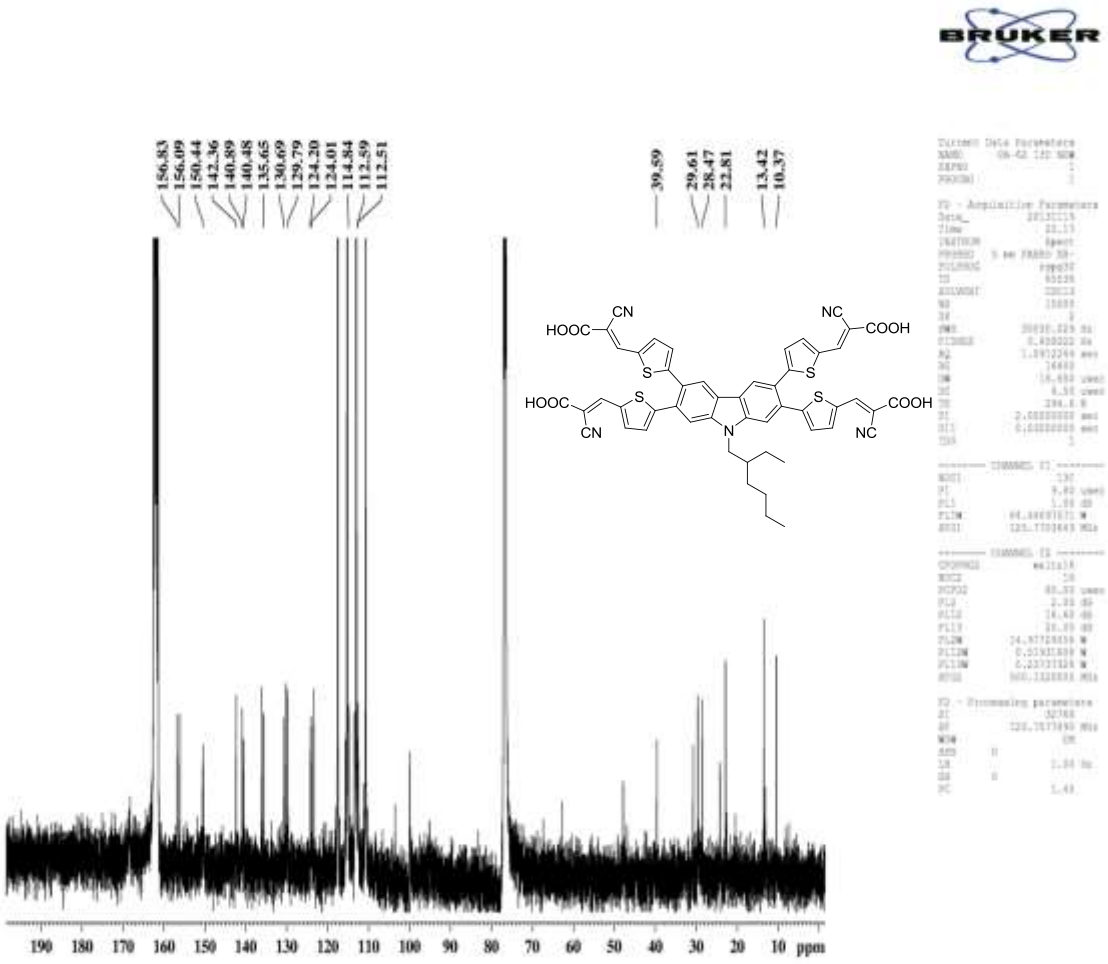

Figure S15: ^{13}C NMR of compound P3 recorded in $CDCl_3$+TFA.

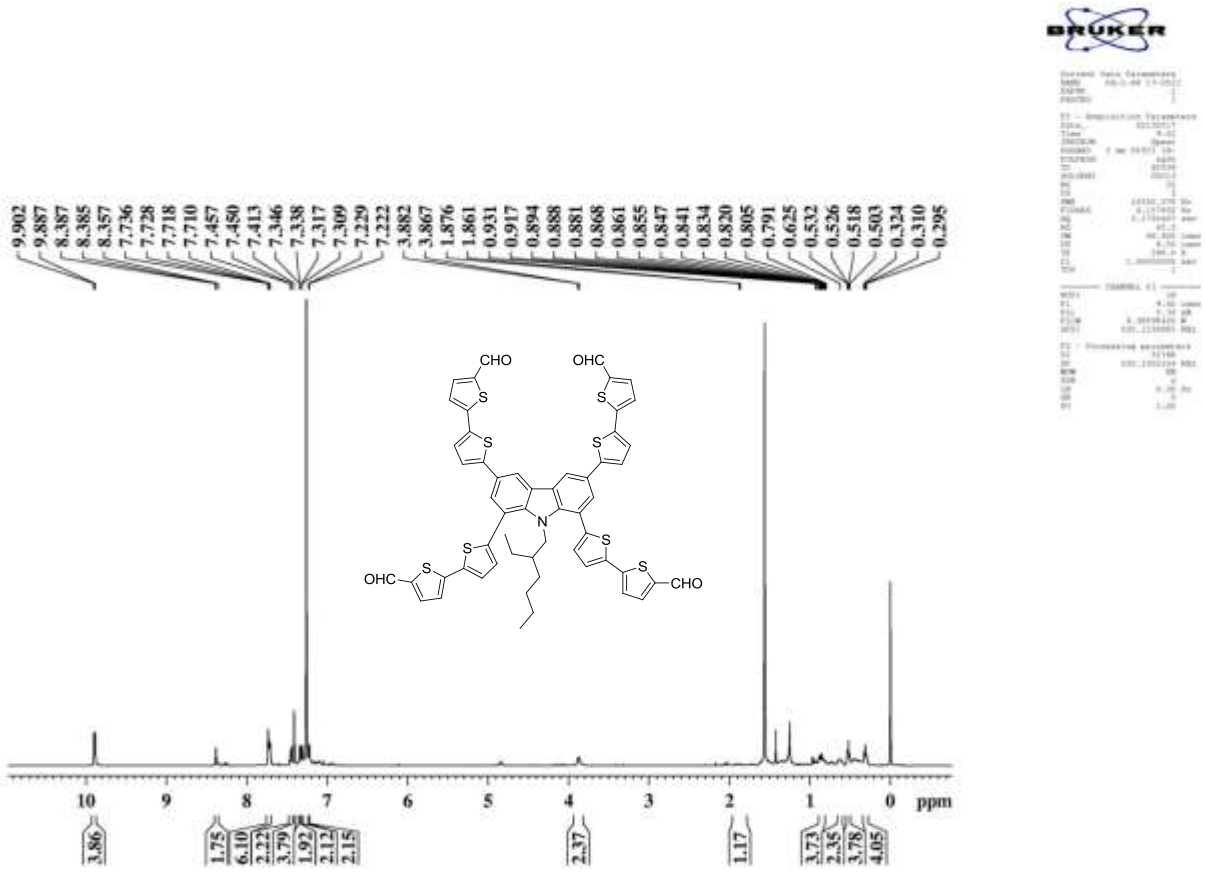

Figure S16: ^{1}H NMR of compound 4b recorded in $CDCl_3$

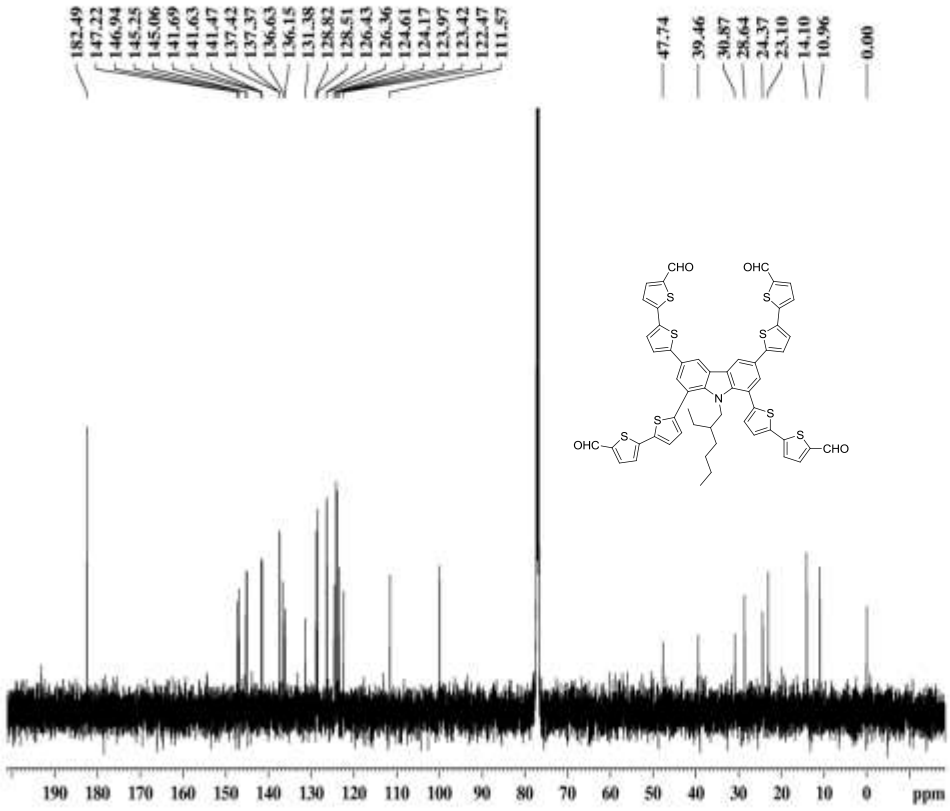

Figure S17: ^{13}C NMR of compound 4b recorded in $CDCl_3$

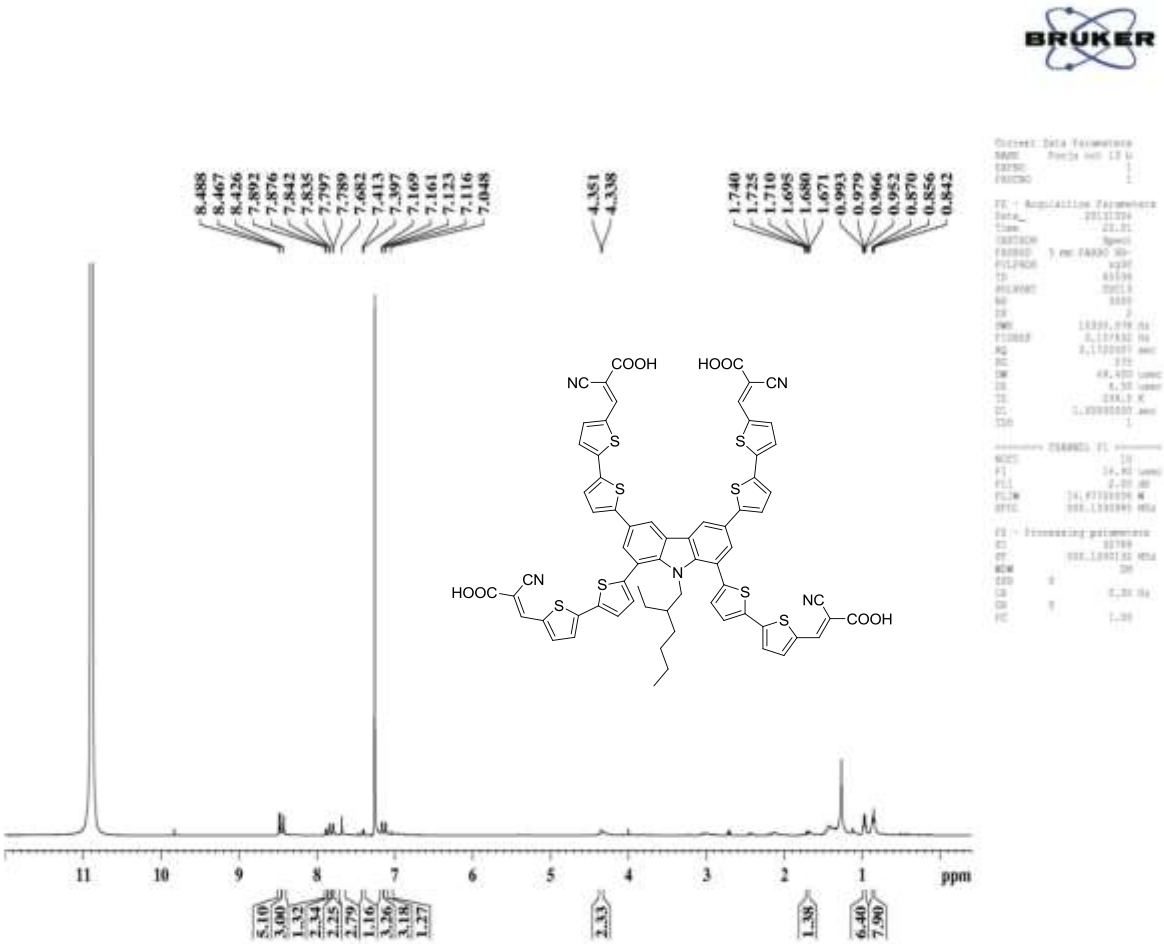

Figure S18: ^{1}H NMR of compound P4 recorded in $CDCl_3$+TFA

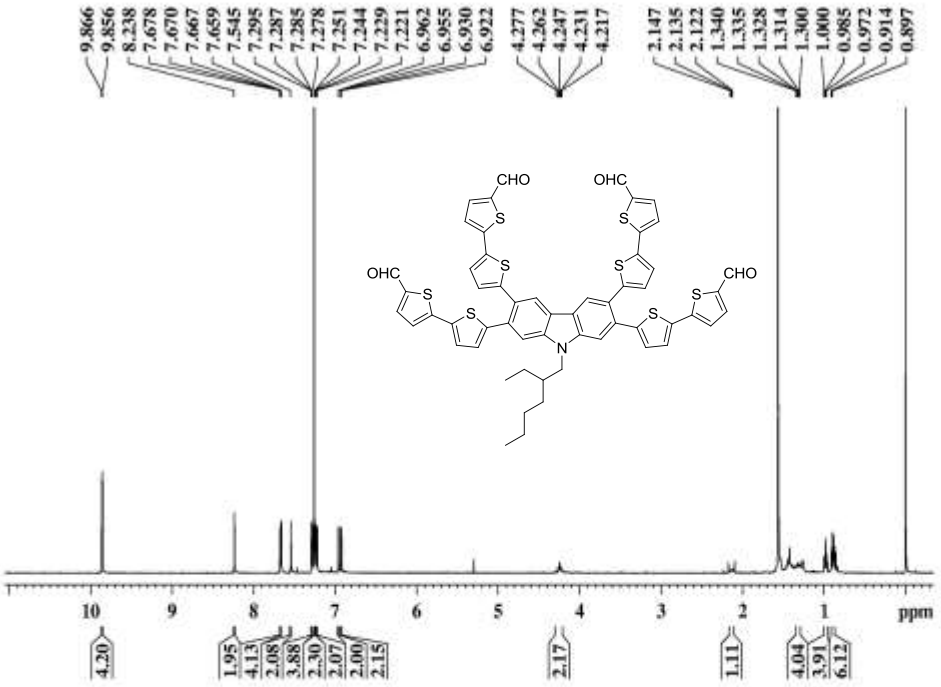

Figure S19: ^{1}H NMR of compound 5b recorded in $CDCl_3$.

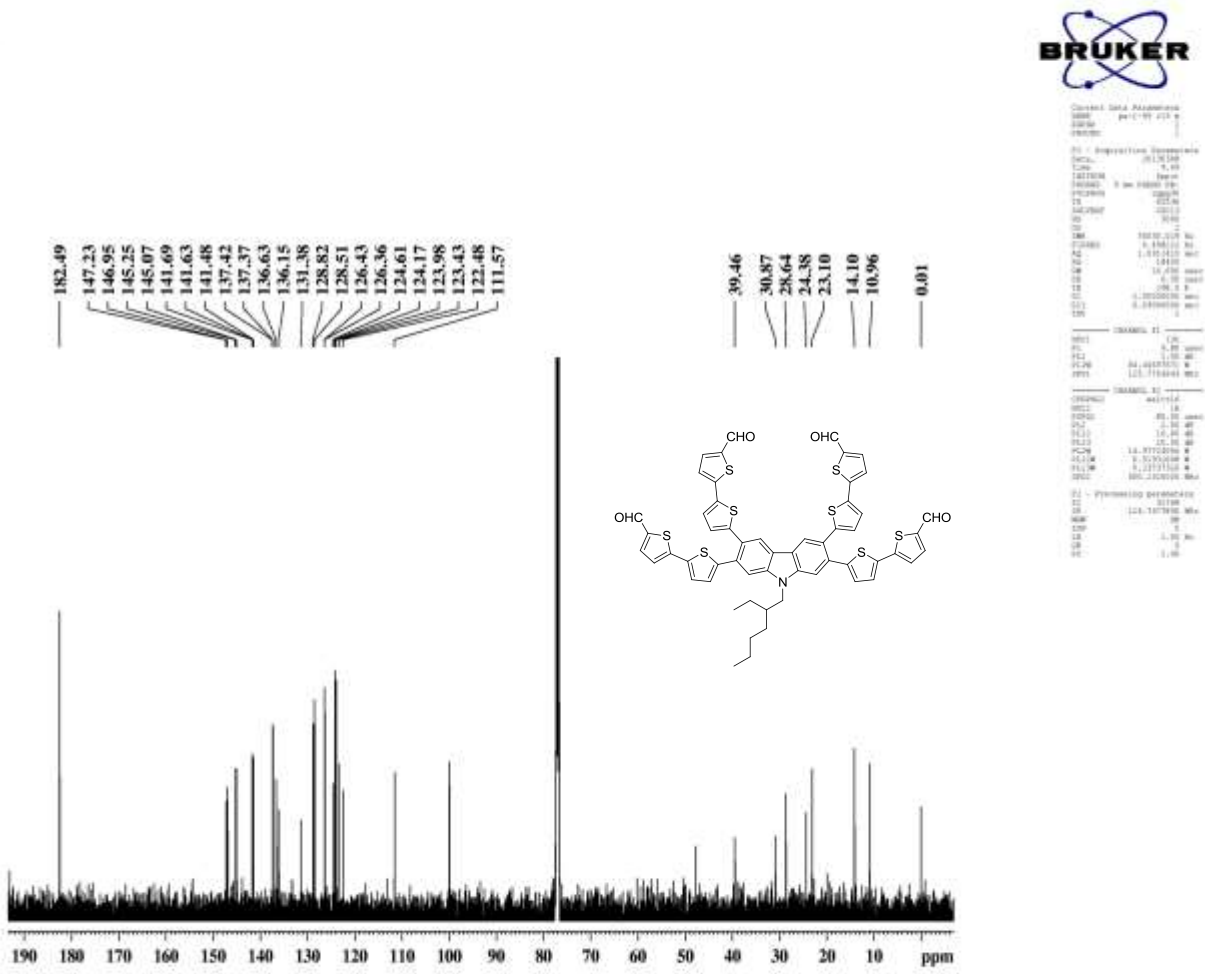

Figure S3: ^{13}C NMR of compound 5b recorded in $CDCl_3$.

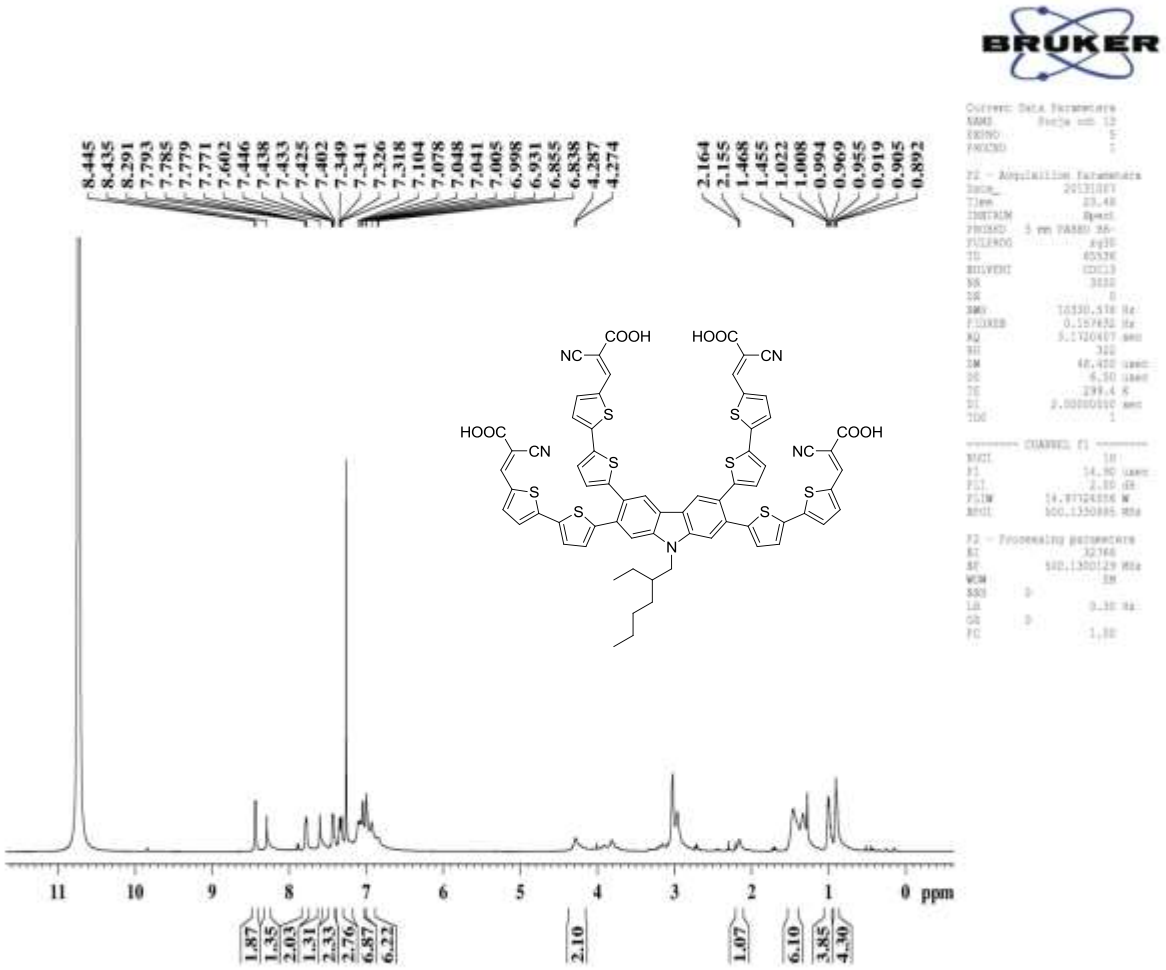

Figure S3: ^{1}H NMR of compound P5 recorded in $CDCl_3$+TFA.